Power system integration of VSC-HVDC connected offshore wind power plants

Zeni, Lorenzo; Sørensen, Poul Ejnar; Hansen, Anca Daniela; Hesselbæk, Bo; Kjær, Philip Carne

Publication date:
2015

Document Version
Publisher's PDF, also known as Version of record

DTU Wind Energy
PhD Thesis 2015

Power system integration of VSC-HVDC connected offshore wind power plants

Control principles, power system services, clustering of wind power plants

Lorenzo Zeni, March 2015

Report: DTU Wind Energy PhD-0053 (EN)

DTU Vindenergi
Institut for Vindenergi

POWER SYSTEM INTEGRATION OF VSC-HVDC CONNECTED WIND POWER PLANTS

Control principles, power system services, clustering of wind power plants

Ph.D. Thesis

Lorenzo Zeni

March 2015

Power system integration of VSC-HVDC connected wind power plants

Control principles, power system services, clustering of wind power plants

Author:	Lorenzo Zeni	
Supervisors:	Prof. Poul E. Sørensen	DTU Wind Energy
	Dr. Anca D. Hansen	DTU Wind Energy
	Bo Hesselbæk	DONG Energy Wind Power
	Dr. Philip C. Kjær	Dept. of Energy technology, AAU

Project:	Top-level Research Initiative TFI PK-int 02 (OffshoreDC)
Funding:	DONG Energy Wind Power Nordic Energy Research

Department of Wind Energy
Technical University of Denmark
Frederiksborgvej 399
4000, Roskilde, Denmark
www.vindenergi.dtu.dk
bcar@dtu.dk
+45 46 77 50 24

DONG Energy Wind Power
Engineering – Electrical Systems
Kraftværksvej 53
Skærbæk, 7000, Fredericia, Denmark
www.dongenergy.com
+4599551111

Submitted on:	March 31st, 2015
Class:	1 (public)
Edition:	1st
Comments:	This report was written to partially fulfil the requirements to obtain a Ph.D. degree at the Technical University of Denmark
Rights:	Lorenzo Zeni
DTU report number:	DTU Wind Energy PhD-0053 (EN)
ISBN:	978-87-93278-45-5

…a mia sorella Mariangela,

e a Claudio Tomaselli…

Preface

The work described along this report represents the core of Work Package 3 in the project co-funded by Nordic Energy Research entitled "DC grids for integration of large scale offshore wind power – OffshoreDC" (www.offshoredc.dk). The project is within the Top-level Research Initiative frame and has project number TFI PK-int 02.

The work was conducted as a Ph.D. project. During the Ph.D. studies, the author was firstly employed at Vestas Wind Systems and then at DONG Energy Wind Power, who was the main co-funder of the project, and enrolled at the Ph.D. school of the Technical University of Denmark, Department of Wind Energy.

The present thesis was written in partial fulfilment of the requirements to obtain the Ph.D. degree at the Technical University of Denmark, other requirements having been met along the project. The Ph.D. study started on October 1st, 2011 and this report was submitted for review to the examination committee on March 31st, 2015.

Lorenzo Zeni

Risø, Roskilde

March 31st, 2015

Abstract

This report presents an overview of challenges and solutions for the integration into the power system of offshore wind power plants (WPPs) connected to onshore grids through a voltage-source converter based high voltage direct current (VSC-HVDC) transmission system. Aspects that are touched upon are (i) principles for the control of offshore alternating current (AC) networks behind offshore VSC-HVDC converters, (ii) power system services that could be featured by VSC-HVDC connected WPPs and (iii) clustering of multiple WPPs to co-ordinately provide desired control actions.

After a brief introduction to justify the study, describe the state-of-art and formulate the project's objectives, the report is essentially divided into three parts, as follows.

Control principles of offshore AC networks

The control of offshore AC networks relies purely on power electronics, especially if Type 4 wind turbine generators (WTGs) are used. Assuming the WTGs are controlled in a "standard" way (based on established literature), two state-of-art control strategies for the offshore HVDC converter are compared in different operational scenarios: (Option 1) nested voltage-current control scheme based on vector control and (Option 2) direct AC voltage control with addition of active damping.

The design of controllers at no-load is discussed, after which Option 2 appears superior. Recommendations for enhanced performance with Option 1 are given.

Further analysis is performed when a WPP is connected to the network, highlighting the fact that Option 2's performance is less dependent on the control parameters than Option 1's. This could be an advantage, since it may allow for independent design of other elements in the network. On the other hand, it may be disadvantageous, since small room for performance improvement is left.

The latter point is somehow confirmed by scenarios where multiple HVDC converters are sharing the control of the network. In this situation, Option 1 with proper active and reactive power droop loops appears superior at a first glance. However, Option 2 seems more easily adaptable to different scenarios. Anyhow, a more complete assessment is necessary for a final conclusion on the absolutely best control scheme.

Power system services

First among the power system services under focus is the control of the AC voltage at the onshore HVDC station. In particular, interesting results are derived in terms of AC voltage control for connection to weak AC networks as well as of long-term voltage stability. New illustrative diagrams in the reactive power – AC voltage plane are drawn for connection to weak grids, shedding light on some peculiarities such as the non-linearity of the continuous short circuit power contribution from the HVDC station and the importance of using AC voltage control when connecting to weak grids. In terms of long-term voltage stability, the focus is on the HVDC converter behaviour when reaching its current limitation while the network approaches its voltage

stability limit. The benefits of not prioritising active power during current-limited operation are demonstrated on a simple system and the possible implications on the control of a WPP potentially connected behind the HVDC converter are discussed.

Active power balance control is the second service being analysed in this report. In AC-DC grids, this is linked to the control of AC frequency and DC voltage. The two control services are treated one by one. Since the former has already widely been discussed in literature, focus is on formulating recommendations for real-life implementation of the service, by comparing a communication-based scheme with a communication-less one on a point-to-point VSC-HVDC connection of WPP. For most of the cases, use of communication may be considered the best solution. Other inherent limitations that are observed in WPPs are discussed. DC voltage control is briefly analysed from the standpoint of WPPs, once again taking into account their realistic limitations and their implications for the other players in the control of the DC network.

Power oscillation damping (POD) is the last service within the scope of this report. Aspects related to its implementation are analysed. In particular, a deeper assessment of the robustness of POD with active and reactive power is made, emphasising the better performance of active power based POD as opposed to reactive power, mainly due to the presence of voltage regulators. Furthermore, a better understanding of which information should be exchanged between manufacturers, utilities and transmission system operators is gained. Crucial information is for example (i) the active power and voltage sensitivity of synchronous generators to injection of active and reactive power from the HVDC converter, (ii) the voltage regulation characteristics of the network in the vicinity of the HVDC station and (iii) limiting characteristics of WPPs such as inherent control and communication delays, presence of mechanical resonances at the same frequency as POD and active power ramp-rate limitations.

Clustering of wind power plants

The proof of concept of clustering significantly different WPPs is conducted in the last part of the report, demonstrating the possibility of implementing coordinated and synchronised active power control. An experimental validation is used to corroborate part of the results, which also provides support for the validity of some of the simulation results provided earlier. Furthermore, the characteristics of the test devices allow supporting some of the recommendations that are proposed earlier in the report, predominantly with regard to the implementation of POD.

Resumé på dansk

Denne rapport giver et overblik over udfordringer og løsninger i forbindelse med integration af offshore vindkraftværker, som er tilsluttet el-nettet på land gennem ene jævnstrømsforbindelse med moderne spændingsstyrede konvertere (Voltage-Source Converter – High Voltage Direct Current, VSC-HVDC). Rapporten omhandler (i) principper for styring af offshore vekselstrømssystemet bag konverteren, (ii) systemydelser til el-systemet som kan leveres af vindkraftværket og (iii) koordineret styring af en klynge af vindkraftværker med henblik på samlet leverance af systemydelser.

Rapporten indledes med en kort introduktion, som indeholder motivation for PhD studiet, beskrivelse af det aktuelle udviklingsniveau og en formulering af formålet med PhD studiet. Resten af rapporten er opdelt i følgende tre hovedafsnit:

Styringsprincipper for offshore vekselstrømssystemet

Styringen af offshore vekselstrømssystemet bag konverteren afhænger helt og holdent af effektelektronikken, især hvis der anvendes type 4 vindmøller (dvs. møller med fuldskala frekvensomformere). To forskellige standard styringsstrategier for offshore konverteren undersøges og sammenlignes. Begge styringsstrategier er baseret på standard metoder, som er beskrevet i litteraturen. Den første styringsstrategi er en integreret strøm – spænding metode, som er baseret på vektorkontrol. Den anden styringsstrategi er baseret på direkte spændingsstyring suppleret med aktiv dæmpning.

Indledningsvis undersøges de to styringsstrategier under tomgangsdrift, dvs. offshore konverter uden tilslutning af vindkraftværket. Denne undersøgelse tyder på at den anden styringsstrategi er den bedst egnede. Derefter gives anbefalinger for forbedring af den første styringsstrategi.

Derefter undersøges de to styringsstrategier med vindkraftværket tilsluttet offshore konverteren. Den undersøgelse viser at den anden styringsstrategi er mere robust over for styringsparametre end den første styringsstrategi. Det kan være fordelagtigt fordi det giver flere frihedsgrader for design af andre elementer i systemet. På den anden side kan det være begrænsende fordi der omvendt ikke er særlig gode muligheder for forbedringer af den anden styringsstrategi.

Denne begrænsning bekræftes af studier af et mere kompleks scenarie hvor der tilsluttes flere HVDC konvertere, som derfor skal koordinere styringen af systemet. For dette scenarie synes den første styringsstrategi umiddelbart at være bedst egnet såfremt den implementeres med passende statik til fordeling af såvel aktiv som reaktiv effekt mellem konverterne. Omvendt er den anden styringsstrategi lettere at tilpasse forskellige scenarier. Derfor er det nødvendigt med yderligere undersøgelser for at kunne konkludere på hvilken strategi som er bedst egnet.

Systemydelser til el-nettet på land.

Den første ydelse som undersøges er bidraget til styring af vekselstrømsspændingen i tilslutningspunktet for den landbaserede HVDC station. Her er der lagt vægt på at undersøge tilslutning til svage net og på spændingsstabilitet med lange tidshorisonter. Vedrørende tilslutning

til svage net anvendes sammenhængen mellem reaktiv effekt og spænding til at illustrere specielle egenskaber så som ulineariteter i konverternes langvarende bidrag til kortslutningseffekten samt vigtigheden af at anvende spændingsstyring. Vedrørende spændingsstabilitet fokuserer undersøgelserne på strømbegrænsningen i konverteren når der opereres tæt på spændingsstabilitetsgrænsen. I den forbindelse illustreres fordelene ved at prioritere reaktiv effekt frem for aktiv effekt, og de implikationer som det har på driften af vindkraftværket diskuteres.

Derefter undersøges aktiv styring af effektbalancen. Aktiv effektstyring sammenkæder frekvensreguleringen i vekselstrømssystemet med spændingsstyring i jævnstrømssystemet. I den forbindelse sammenlignes to forskellige styringsstrategier, hvor den første kræver et kommunikationssystem, mens den anden ikke gør. Den første strategi er baseret på at frekvensen af vekselspændingen på land måles og kommunikeres til offshore vindkraftværkets styringssystem, mens den anden strategi spejler frekvensen på land i jævnstrømsspændingen, som efterfølgende spejles i frekvensen offshore. Den kommunikationsbaserede løsning er sandsynligvis bedst i de fleste tilfælde. Desuden diskuteres andre begrænsninger i vindkraftværket, herunder hvorvidt vindkraftværket er egnet til at deltage i styringen af jævnstrømsspændingen.

Dæmpning af resonanssvingninger i elsystemet er den sidste service som undersøges. Dæmpningen kan enten baseres på aktiv effekt eller reaktiv effekt. Det konkluderes af undersøgelsen at den mest robuste løsning er at anvende aktiv effekt til at dæmpe svingningerne, først og fremmest pga. påvirkningen fra hurtige spændingsregulatorer. Desuden giver disse studier en bedre forståelse af hvilke informationer der skal udveksles mellem fabrikanter, operatører og netselskaber. Blandt disse informationer er (i) følsomheden af synkrongeneratorer over for injektion af aktiv og reaktiv effekt, (ii) karakteristiske egenskaber af spændingsreguleringen nær konverterstationen og (iii) begrænsninger i vindkraftværket så som styrings- og kommunikationsforsinkelser, mekaniske resonanser og begrænsede reguleringshastigheder.

Klyngestyring af vindkraftværker

Til sidst undersøges koordineret styring af klynger af vindkraftværker af væsentligt forskellige typer. Først belyses muligheden for at koordinere og synkronisere reguleringen af den aktive effekt fra de involverede vindkraftværker. Der er anvendt eksperimenter til validering af dele af en sådan koordination, hvilket også øger værdien af tidligere simuleringsresultater. Det anvendte testudstyr har desuden gjort det muligt direkte at underbygge tidligere anbefalinger, primært vedrørende dæmpning af resonanssvingninger.

Sommario in italiano

Questa tesi presenta le maggiori problematiche e relative soluzioni per la connessione e la conseguente efficiente integrazione nel sistema elettrico di centrali eoliche offshore tramite un apparato di trasmissione in alta tensione in corrente continua basato su convertitori a transistori (cosiddetti sistemi VSC-HVDC). I seguenti aspetti sono trattati: (i) principi di controllo di reti in correnti alternata (AC) situate a valle del convertitore HVDC offshore, (ii) servizi ausiliari che possono essere offerti da suddette installazioni e (iii) raggruppamento di centrali eoliche con caratteristiche diverse e loro conseguente coordinamento per garantire i summenzionati servizi.

Dopo una breve introduzione che giustifica lo studio qui sintetizzato, ne descrive il punto di partenza in base alla letteratura disponibile e ne definisce gli obiettivi, la tesi è essenzialmente divisa in tre parti, in accordo con quanto descritto di seguito.

Principi di controllo per reti AC offshore

Il controllo di reti AC offshore avviene puramente avvalendosi di convertitori elettronici di potenza, in particolar modo quando le turbine installate siano di Tipo 4 e cioè facenti uso di convertitore elettronico dimensionato per l'intera potenza generata. Assumendo che le turbine siano controllate secondo principi consolidati ed ampiamente descritti in fonti bibliografiche, due possibili controllori per il convertitore HVDC sono selezionati dalla letteratura e messi a confronto in una varietà di condizioni di lavoro: (Opzione 1) è basata su controllori di tensione e corrente in cascata e poggiantisi su controllo vettoriale, mentre (Opzione 2) fa uso di un controllo diretto della tensione accompagnato da un anello di smorzamento supplementare.

La discussione del progetto dei due controllori operanti sulla rete a vuoto porta alla conclusione che l'Opzione 2 risulti vantaggiosa. Di conseguenza alcune proposte per il miglioramento delle prestazioni dell'Opzione 1 vengono indicate.

L'analisi della rete con centrale eolica connessa e producente potenza mette in luce, nel caso dell'Opzione 2, una minore dipendenza delle prestazioni dai vari parametri di controllo. Se da un lato questo può permettere un maggior disaccoppiamento nel progetto dei vari controllori agenti nella rete, ciò lascia d'altro canto minore spazio per azioni correttive nel caso in cui delle instabilità sorgano in seno alla rete stessa.

Proprio quest'ultima considerazione sembra confermata dai risultati ottenuti impiegando due convertitori HVDC. In tal caso, infatti, l'Opzione 1 opportunamente espansa con controllo proporzionale di potenza attiva e reattiva appare migliore dopo una prima valutazione. Nonostante ciò, l'Opzione 2 sembra offrire una maggior adattabilità alle condizioni di lavoro ed in ogni caso è necessaria una valutazione più completa per raggiungere una conclusione definitiva.

Servizi ausiliari

Il primo tra i servizi ausiliari presi in considerazione è il controllo della tensione alternata da parte del convertitore HVDC onshore. Degli interessanti risultati discendono dal calcolo delle caratteristiche nel piano tensione – potenza reattiva, soprattutto nel caso di connessione ad una

rete debole. Le caratteristiche, per esempio, mettono in risalto la non-linearità del contributo che la stazione HVDC fornisce alla potenza di corto circuito equivalente ai suoi terminali, oltre ad evidenziare la generica importanza del controllo di tensione in connessioni a sistemi deboli. Inoltre, viene illustrata una prima analisi del comportamento del convertitore HVDC quando operante in limitazione di corrente in un sistema che si sta avvicinando al limite di stabilità della tensione, dimostrando gli effetti deleteri del porre la priorità sulla potenza attiva. In tal senso, si discutono altresì le conseguenze che ciò può avere sulla filosofia di controllo di centrali eoliche con connessione in HVDC.

Il controllo della potenza attiva è il secondo servizio descritto. In reti miste AC-DC, ciò si riconduce allo studio del controllo di frequenza (in AC) e tensione (in DC). Siccome il primo è stato ampiamente trattato in precedenti studi, l'attenzione in questa tesi è posta sulla discussione di aspetti prettamente legati alla sua realizzazione in pratica, focalizzandosi su un confronto tra due schemi facenti o meno uso di comunicazione e suggerendo l'utilizzo di quest'ultima nella maggior parte dei casi. Altri possibili fattori che entrano in gioco in centrali eoliche commerciali e che potrebbero limitarne il potenziale sono poi discussi. Il controllo della tensione DC è trattato solo brevemente, ancora una volta principalmente concentrandosi su fattori che potrebbero limitarne il contributo da parte delle centrali eoliche, discutendone pure le conseguenze per gli altri dispositivi che partecipano al controllo e per i sistemi ad essi connessi sul lato AC.

In ultima istanza viene trattato lo smorzamento di oscillazioni di potenza tra generatori, discutendone in special modo aspetti legati alla sua realizzazione in pratica su installazioni del tipo qui considerato. In particolare, si analizza la solidità di tale servizio quando sia fornito tramite modulazione di potenza attiva o reattiva, concludendo che la potenza reattiva comporta una maggior dipendenza dalle caratteristiche dei regolatori di tensione in seno alla rete. Altro importante aspetto che viene discusso è il genere di informazioni che devono essere scambiate tra il gestore della rete di trasmissione, l'installatore ed i fornitori di turbine ed HVDC in modo da realizzare un progetto adeguato del servizio. A titolo di esempio, è cruciale che sufficiente conoscenza sui seguenti aspetti sia condivisa: (i) l'influenza che la modulazione di potenza attiva e reattiva da parte del convertitore HVDC ha sulla potenza attiva e la tensione dei generatori le cui oscillazioni devono essere smorzate, (ii) le caratteristiche dei regolatori di tensione e (iii) alcune caratteristiche della centrale eolica, come per esempio gli inevitabili ritardi dovuti a controllo e comunicazione, la presenza di risonanze sul lato meccanico delle turbine e possibili limitazioni nel gradiente della potenza attiva.

Raggruppamento di centrali eoliche

L'ultima parte della relazione si focalizza sulla dimostrazione sperimentale della possibilità di controllare in modo coordinato centrali eoliche con caratteristiche anche di gran lunga differenti, utilizzando come esempio il controllo della potenza attiva. La verifica sperimentale permette anche di guadagnare confidenza sui modelli utilizzati in altre fasi dello studio. Inoltre, le conclusioni derivanti dalla verifica sperimentale corroborano ampiamente le raccomandazioni avanzate in precedenza, in maniera più speculativa, in merito alla partecipazione allo smorzamento delle oscillazioni di potenza.

Acknowledgement

At the end of this three and a half years' journey, it is time to spend a few trivial, yet most honest, words, to acknowledge the pillars upon which I could rely for finding the motivation to conduct the Ph.D. project towards its end.

I wish to express deep gratitude to my supervisors. To Poul Ejnar Sørensen and Anca Daniela Hansen I am thankful for their academic, professional and personal support which dates far back in time, way before I started this Ph.D. project. DONG Energy Wind Power and Bo Hesselbæk in particular are warmly thanked for allowing me to pursue the Ph.D. and give it an industrial character, which I hope is reflected in this report. I am also truly indebted with Philip Carne Kjær, whose skills, love and dedication for the discipline I honestly envy. Finally, I would like to acknowledge the support received from Troels Stybe Sørensen who, although not being my supervisor, has certainly been a precious mentor.

I am thankful to all my colleagues at DONG Energy Wind Power, Electrical Systems Analysis department, as well as to my former colleagues at Vestas Wind Systems and to my academic comrades at the Wind Energy Systems section, Department of Wind Energy at DTU. I would also like to express my appreciation to Nordic Energy Research and the OffshoreDC consortium for the financial contribution and for being an interesting group of research partners respectively.

Authors and co-authors of the publications that have academically shaped my Ph.D. project have been crucial sources of dialogue and support. I wish to acknowledge more warmly Yanis Margaris, Til Kristian Vrana, Michal Sztykiel, Rodrigo da Silva, Torsten Lund, Hjörtur Jóhannsson and Robert Eriksson, as well as Jakob Glasdam, who also had, together with Mikkel Gryning, an important role in sharing knowledge and concerns in our periodical industrial Ph.D.s meetings in DONG Energy. I cannot forget, then, to thank Vahan Gevorgian and Robb Wallen from NREL as well as John Bech from Siemens Wind Power for the good collaboration during my stay in Colorado.

There is no way I can express enough gratitude to all my family in Tesero, for their unceasing encouragement and support, as well as for being the roots upon which I have grown the core of who I am.

It would surely turn out to be unfair, then, to try and give a thank shout to each one of my friends without unjustly forgetting anyone. Thank you, friends in Denmark, for making my life far from home and the mountains truly enjoyable and as personally rich as I could imagine. Thank you, friends in Tesero and all over Italy and the world, for being a firm lighthouse despite the distance and the sporadic contacts. And thank you all, for continuously being a source of joy and inspiration and a trigger for new passions out of the technical world, and for patiently understanding my being up and down.

Lastly and most sincerely, I want to thank Eleftheria, whose presence and love have sweetened the last two years of this adventure.

List of abbreviations

AC	Alternating Current
AVR	Automatic Voltage Regulator
BW	BandWidth
CC	Cluster Controller
CGI	Controllable Grid Interface
DC	Direct Current
DFIG	Doubly-Fed Induction Generator
DSL	DIgSILENT Simulation Language
EMT	ElectroMagnetic Transient
ES	Excitation System
EWEA	European Wind Energy Association
FRT	Fault-Ride-Through
FSC	Full-Scale Converter
GPS	Global Positioning System
GSC	Grid Side Converter
HV	High Voltage
HVDC	High Voltage Direct Current
IEC	International Electrotechnical Commission
IEEE	Institute of Electrical and Electronics Engineers
IG	Induction Generator
IGBT	Insulated Gate Bipolar Transistor
IR	Inertial Response
LAN	Local Area Network
LCC	Line Commutated Converter
LHP	Left Half Plane
LP	Low-Pass
MI	Mass-Impregnated
MMC	Modular Multilevel Converter
MPPT	Maximum Power Point Tracking
MSC	Mechanically Switched Capacitor
MV	Medium Voltage
NREL	National Renewable Energy Laboratory
OEM	Original Equipment Manufacturer
OLTC	On-Load Tap Changer
PCC	Point of Common Coupling
PE	Power Electronic
PFC	Primary Frequency Control
PI	Proportional-Integral
PLL	Phase-Locked Loop
PM	Phase Margin
PMSG	Permanent Magnet Synchronous Generator
POD	Power Oscillation Damping
PSS	Power System Stabiliser
PWM	Pulse Width Modulation
PXI	PCI eXtenstion for Instrumentation
RES	Renewable Energy Sources
RMS	Root Mean Square
ROCOF	Rate Of Change Of Frequency

RSC	Rotor Side Converter
SCP	Short Circuit Power
SCR	Short Circuit Ratio
SCRAMNet	Shared Common Random Access Memory Network
SG	Synchronous Generator
SRF	Synchronous Reference Frame
STATCOM	STATic COMpensator (transistor-based)
SVC	Static Var Compensator (thyristor-based)
TSO	Transmission System Operator
VSC	Voltage Sourced Converter
WPP	Wind Power Plant
WPPC	Wind Power Plant Controller
WTG	Wind Turbine Generator
XLPE	Crossed-Linked Polyethylene

List of figures

Figure 1	Annual and cumulative offshore wind power installations in Europe – source EWEA [12].
Figure 2	Overview of European offshore wind projects by distance to PCC and capacity – sources [13],[14].
Figure 3	Simplified sketch of Type 4 WTG – inspired by [22].
Figure 4	Summary of offshore grid configurations.
Figure 5	Generic layout of wind power installation.
Figure 6	Qualitative minimum modelling requirements for main blocks, chapter by chapter.
Figure 7	Single machine model for active power balance and POD studies.
Figure 8	Modified IEEE 12-bus system used for POD studies [109].
Figure 9	Converter station electrical model, valid for EMT and RMS.
Figure 10	Generic converter control model.
Figure 11	Example of implementation of onshore station outer controller.
Figure 12	Option 1 for offshore station outer controller – see Chapter 4.
Figure 13	Option 2 for offshore station outer controller – see Chapter 4.
Figure 14	WPPC: active power controller.
Figure 15	Average MMC model [102] for model adequacy study.
Figure 16	DC side dynamic performance dependence on MMC active power.
Figure 17	Response of average MMC model to i_d current reference steps and POD signal.
Figure 18	Generic simplified offshore HVDC converter control layout.
Figure 19	Offshore AC network configuration with single HVDC converter and lumped WPP converters.
Figure 20	Offshore AC network configuration with two HVDC converters and lumped WPP converters.
Figure 21	Offshore network admittance as seen from the HVDC converter.
Figure 22	Laplace domain block diagram for standard design of current controller.
Figure 23	Open- and closed-loop transfer functions for current control problem with $Z_d = 0$.
Figure 24	Time domain response of current controller with $Z_d = 0$.
Figure 25	Open-loop transfer function for current control problem with voltage feed-forward with perfect measurement: non-ideal and ideal VSC behaviour.
Figure 26	Effect of time delay on numerator and denominator of Eq. (10).
Figure 27	Step response of current controller for the design cases described above.
Figure 28	Nyquist diagram for current control design at positive and negative frequencies.
Figure 29	Open-loop transfer function for HVDC converter voltage control problem.
Figure 30	Voltage reference step response and sensitivity to capacitance variation.
Figure 31	Voltage reference step response and sensitivity to capacitance variation using current feed-forward.
Figure 32	Laplace domain block diagram for voltage control design in the *d*-axis.
Figure 33	Transfer functions for voltage control design in Option 2.
Figure 34	Response to voltage reference step for Option 2.
Figure 35	Option 1: Effect of WPP active power production on eigenvalues with default control parameters.
Figure 36	Option 1: Effect of WPP active power production on eigenvalues with modified voltage control parameters according to Table 8.
Figure 37	Option 1: Effect of export cable length on system eigenvalues with modified voltage control parameters.
Figure 38	Option 1: Effect of control proportional gain on system eigenvalues.
Figure 39	Disturbance rejection and reference tracking response for Option 1 augmented with

current feed-forward at the WPP power production levels.
Figure 40 Time domain verification of linear analysis for Option 1.
Figure 41 Time domain verification of linear analysis for Option 2.
Figure 42 Time domain validation of aggregation methodology.
Figure 43 Study case results for Option 1.
Figure 44 Study case results for Option 2.
Figure 45 Active power droop controller for HVDC converters.
Figure 46 Reactive power droop controller for HVDC converters.
Figure 47 Simulation results for Case A.
Figure 48 Simulation results for Case B.
Figure 49 Simulation results for Case C.
Figure 50 Network model for derivations in Section 5.2.
Figure 51 Q-V_{AC} plots of network constraint and VSC-HVDC limits.
Figure 52 Q-V_{AC} characteristics with droop control from HVDC station.
Figure 53 SCP improvement from droop control VSC: influence of P and Q_L.
Figure 54 Steady-state model of VSC-HVDC converter feeding isolated load.
Figure 55 PV curves on load fed by isolated VSC-HVDC: influence of rated power factor pf_N.
Figure 56 Electrical model for PQ exchange between converter and AC grid.
Figure 57 PQV diagrams for power exchange between VSC-HVDC and grid.
Figure 58 Electrical model of three-bus system.
Figure 59 Constant equivalent voltage circles and intersection with converter current locus.
Figure 60 PV curves for three-bus system in ideal normal operation and current-limited mode (IN = 0.4 pu) with two different current angles.
Figure 61 Load PV curves from dynamic simulation in ideal unlimited case, Id-priority and vector limitation.
Figure 62 Complex and SRF converter current locus for two current limited cases.
Figure 63 Time plot of converter active and reactive power in pu of converter ratings.
Figure 64 Sketch of candidates for frequency control provision.
Figure 65 *P Droop* block for onshore and offshore converter in Candidate 2.
Figure 66 Onshore power production: base case and Candidates 1A vs 2A.
Figure 67 Onshore and offshore frequency and DC voltage for base case and Candidate 2A.
Figure 68 Onshore power production: base case and Candidates 1B vs 2B.
Figure 69 Onshore and offshore frequency and DC voltage for base case and Candidate 2B.
Figure 70 Response for Candidate 2B and DC line voltage drop compensation.
Figure 71 Influence of communication delays on response with IR.
Figure 72 Effect of ramp-rate limiter on WPP active power reference for Candidate 2B.
Figure 73 Simplified DC network configuration for DC voltage control study.
Figure 74 DC voltage controller on WPPC.
Figure 75 Open-loop simulation of DC voltage control contribution from WPP.
Figure 76 Time domain simulation results for DC voltage control test.
Figure 77 Single-machine model for POD studies.
Figure 78 PSS-like control scheme for POD implementation.
Figure 79 Steady-state phasor diagram of single-machine system.
Figure 80 Variation of target eigenvalue's damping factor at two initial power transmission values and varying AVR control gain.
Figure 81 Pole position variation for ideal POD controller.
Figure 82 Target eigenvalue movement for real POD controller and varying POD gain.
Figure 83 Phasr-like diagram of induced electrical torques on SG.
Figure 84 Possible block diagram implementation of *Freeze logic* block.
Figure 85 Non-linear simulation results on IEEE 12-bus system.
Figure 86 AVR gains' effect on critical pole of IEEE 12-bus system.
Figure 87 Generalised diagram of POD closed-loop system.
Figure 88 Generic Bode diagrams for open-loop transfer function with ideal G_{ACT}.
Figure 89 Example of Bode plot for open-loop POD transfer function: description of cases above.

Figure 90	Time domain simulation of selected cases.
Figure 91	Influence of communication delay on POD performance for varying eigenfrequency.
Figure 92	Shaft's system resonance frequency and damping ratio for varying mechanical model parameters.
Figure 93	Experimental setup – courtesy of NREL.
Figure 94	Overal model diagram.
Figure 95	Cluster controller block diagram – only active power path.
Figure 96	WPPC 2 active power control block diagram.
Figure 97	Functional sketch of implementation on PXI.
Figure 98	Validation of reference step for WPPC 2.
Figure 99	Validation of frequency control event for WPPC 2 and CC: produced power.
Figure 100	Validation of frequency control event for WPPC 2 and CC: reference power to WPPC 2.
Figure 101	Bode diagram of G_{WPP2} for estimation of compensation for three values of communication delay.
Figure 102	Validation of 100 mHz POD event for CC and WPPC 2.
Figure 103	Validation of power reference step to WTG 1.
Figure 104	Validation of power reference step for WPPC 1.
Figure 105	Validation of frequency control event for WPPC 1.
Figure 106	Validation of 200 mHz POD emulation for WPPC 1.
Figure 107	Response of cluster of WPPs to frequency control event.
Figure 108	Response of cluster of WPPs to POD event.
Figure 109	Generic governing system model: PowerFactory block diagram.
Figure 110	ES and AVR model: PowerFactory block diagram.
Figure 111	ES and AVR model used in IEEE 12-bus system: PowerFactory block diagram.
Figure 112	Standard PLL - EMT simulations [125]: PowerFactory block diagram.
Figure 113	Current controller: PowerFactory block diagram.
Figure 114	Current prioritisation.
Figure 115	Reference WPP: HVDC system model in PowerFactory.
Figure 116	Reference WPP: export system model in PowerFactory.
Figure 117	Reference WPP: section WPP1 model in PowerFactory.
Figure 118	Reference WPP: section WPP2 model in PowerFactory.
Figure 119	Reference WPP: section WPP3 model in PowerFactory.
Figure 120	Simplified block diagram for design of DC voltage controller.
Figure 121	Example of step response for DC voltage controller.
Figure 122	Example of open-loop Bode diagram for DC voltage controller.
Figure 123	Electrical and control diagram for small-signal derivations.
Figure 124	Equivalent small-signal electrical diagram of simple system.
Figure 125	Decoupled equivalent circuit.
Figure 126	Block diagram for calculation of DC system approximated transfer function.
Figure 127	Option 1: Effect of export cable length on system eigenvalues with default voltage control parameters.
Figure 128	Option 2: Effect of WPP active power production on system eigenvalues.
Figure 129	Option 2: Effect of export cable length on system eigenvalues.
Figure 130	Option 2: Effect of voltage control gain K_e on system eigenvalues.
Figure 131	Option 2: Effect of WPP active power production on system eigenvalues with power-frequency droop.
Figure 132	Option 2: Effect of export cable length on system eigenvalues with power-frequency droop.
Figure 133	Option 2: Effect of voltage control gain K_e on system eigenvalues with power-frequency droop.
Figure 134	Time domain verification of linear analysis for Option 2 with power-frequency droop.
Figure 135	Case A with K_{pV} = 1.0 pu.

Figure 136	Case A with halved converter transformer impedance.
Figure 137	Case B with halved converter transformer impedance.
Figure 138	Case A with halved converter transformer impedance and additional derivative droop.
Figure 139	Case A with longer interlink cable (L = 20 km).
Figure 140	Case B with longer interlink cable (L = 20 km).
Figure 141	Case A with different power sharing.
Figure 142	Case B with different power sharing.
Figure 143	Validation of 500 mHz POD emulation for WPPC 1.
Figure 144	Validation of 500 mHz POD emulation, generated with frequency modulation for WPPC 1.
Figure 145	Validation of frequency control event for WPPC 2 and CC: frequency.

List of tables

Table 1	Overview of VSC-HVDC projects for offshore WPP connection.
Table 2	Summary of offshore WPPs with VSC-HVDC connection.
Table 3	List of calculations and simulation studies to be performed.
Table 4	Option 1: HVDC converter current control parameters.
Table 5	Option 1: HVDC converter voltage control parameters.
Table 6	Option 2: Parameters for active damping block.
Table 7	Option 2: Control parameters for terminal voltage control.
Table 8	Option 1: Re-tuned voltage control parameters.
Table 9	Control of AC network with multiple HVDC converters: list of study cases.
Table 10	Parameter settings for droop controllers.
Table 11	Modified parameters for Option 1 voltage controller in Case A and C.
Table 12	Relevant control parameters for frequency control simulations.
Table 13	Nomenclature of Candidates compared.
Table 14	Relevant data for coordinated DC voltage control simulations.
Table 15	Control settings for ideal POD controller.
Table 16	Per-unit SG's power and voltage sensitivities to P,Q injection at Bus 2.
Table 17	Control settings for real POD controller.
Table 18	Calculated needed angle correction and results achieved for K_{POD} = 0.5 pu.
Table 19	Example of phase compensation parameters for k_L = 0 and accounting for corrections from Table 18.
Table 20	Derived POD phase shift and gain for test on IEEE 12-bus system and achieved linear results.
Table 21	Sample parameters for governing system model.
Table 22	Sample parameters for ES and AVR model.
Table 23	Sample parameters for ES and AVR models in IEEE 12-bus system.
Table 24	Sample parameters for HVDC converter electrical model.
Table 25	Sample parameters for standard PLL.
Table 26	Sample parameters for current controller.
Table 27	Sample parameters for active power control of WTG model Type 4B.
Table 28	Sample parameters for WPPC model.
Table 29	Sample parameters for mechanical two-mass model.
Table 30	Sample parameters for export cables.
Table 31	Sample parameters for WTG converter current controller for simulations of detailed model.
Table 32	Sample parameters for aggregated WTG converter current controller when synchronised at HV side of AC substation transformer.
Table 33	Sample parameters for aggregated WTG converter current controller when synchronised at LV side of AC substation transformer.
Table 34	Modbus communication parameters.
Table 35	Experimental setup model: WTG 1 parameters.
Table 36	Experimental setup model: WTG 2 parameters.
Table 37	WPPC 1 active power control parameters.
Table 38	WPPC 2 active power control parameters.
Table 39	Time delay for communication channels models.
Table 40	Parameters for CC.
Table 41	Parameters varied for frequency control with cluster.
Table 42	Parameters varied for POD with cluster.

Table of contents

Preface ..... **I**

Abstract ..... **III**

Resumé på dansk ..... **V**

Sommario in italiano ..... **VII**

Acknowledgement ..... **IX**

List of abbreviations ..... **XI**

List of figures ..... **XIII**

List of tables ..... **XVII**

Table of contents ..... **XIX**

Chapter 1 Introduction **1**

1.1 Background **1**

1.2 Project objectives and limitations **2**

1.3 Contributions **3**

1.4 Outline of the thesis **4**

1.5 List of publications **5**

1.5.1 Conference and journal publications related to the study 5

1.5.2 Other relevant publications 6

Chapter 2 State-of-art: VSC-HVDC and wind power **7**

2.1 Introduction **7**

2.1.1 Integration of RES in power systems 7

2.1.2 Why offshore wind power and VSC-HVDC? 8

2.1.3 Overview of VSC-HVDC projects for offshore WPPs 10

2.2 Wind power plants **11**

2.2.1 Wind turbine generator technology 11

2.2.2 Control of wind power plants 12

2.3 VSC-HVDC **13**

2.3.1 VSC technology for HVDC 13

2.3.2 Control of VSC-HVDC converters 14

2.4 VSC-HVDC connected WPPs **15**

2.4.1 General aspects 16

2.4.2 System services 16

2.4.3 System configurations 17
2.4.4 Thesis problem formulation and limitations 19
Chapter 3 Modelling for simulation 23
3.1 Introduction 23
3.1.1 Target studies 23
3.1.2 Modelling requirements 25
3.2 Simulation models 27
3.2.1 Power system 27
3.2.2 VSC-HVDC 29
3.2.3 Wind power plant 31
3.3 Model adequacy 32
3.3.1 VSC-HVDC model evaluation 33
3.4 Summary 36
Chapter 4 Offshore AC network control 37
4.1 Introduction 37
4.1.1 State-of-art control candidates 38
4.1.2 Offshore AC network configurations 39
4.1.3 Network impedance aggregation 41
4.2 No-load operation 42
4.2.1 Introduction 42
4.2.2 Design of HVDC converter controller at no-load 43
4.3 Operation with WPP 54
4.3.1 Introduction 54
4.3.2 Linear analysis of performance 55
4.3.3 Time domain verification 59
4.3.4 Verification of aggregation validity 61
4.3.5 Example study case 62
4.3.6 Discussion and recommendation 64
4.4 Operation with multiple HVDC converters 66
4.4.1 Active and reactive power droop 66
4.4.2 Description of study cases 67
4.4.3 Time domain simulations, discussion and recommendations 69
4.5 Summary 71
Chapter 5 Onshore AC voltage control 73
5.1 Introduction 73

5.2 Continuous AC voltage control **74**
5.2.1 Main VSC-HVDC limitations 75
5.2.2 Combination with network equations 75
5.2.3 Droop contribution to voltage regulation 76
5.3 Long-term voltage stability **79**
5.3.1 Modelling of VSC-HVDC for long-term voltage stability 79
5.3.2 Study on simple three-bus system 82
5.3.3 Discussion: influence on WPP control 87
5.4 Summary **88**
Chapter 6 Power balance control **89**
6.1 Introduction **89**
6.2 AC frequency control **90**
6.2.1 Candidate 1: communication-based scheme 90
6.2.2 Candidate 2: communication-less scheme 91
6.2.3 Comparison of control candidates 92
6.3 DC voltage control **97**
6.3.1 Contribution of HVDC converters to DC voltage control 98
6.3.2 Contribution of WPPs to DC voltage control 99
6.3.3 Coordinated DC voltage control 101
6.4 Summary **103**
Chapter 7 Power oscillation damping **105**
7.1 Introduction **105**
7.2 Contribution of VSC-HVDC to POD **107**
7.2.1 Simple case study: single-machine system 107
7.2.2 Implementation of POD controller 108
7.2.3 Practical considerations for tuning of parameters 109
7.2.4 Discussion 116
7.3 Combined POD from WPP and VSC-HVDC **117**
7.3.1 Implementation of POD controller on WPP 117
7.3.2 Demonstration of combined POD from VSC-HVDC and WPP 119
7.3.3 Closed loop stability and performance limitations 122
7.3.4 Sensitivity to communication and control delays 126
7.3.5 Ramp-rate limiters 128
7.3.6 Collateral effects on WTGs 129
7.4 Summary **131**

Chapter 8 Experimental verification of clustering of WPPs 133
8.1 Introduction – Clustering of wind power plants 133
8.1.1 Why clustering WPPs? 133
8.1.2 Challenges in clustering of WPPs 134
8.1.3 Assumptions and limitations 134
8.2 Experimental setup 135
8.3 Modelling and implementation 136
8.3.1 Overview 136
8.3.2 Cluster controller 137
8.3.3 Wind power plant controllers 138
8.3.4 Wind turbine generators 139
8.3.5 Communication delays 139
8.3.6 Implementation 139
8.4 Model validation 140
8.4.1 WTG 2 and Cluster controller 140
8.4.2 WTG 1 and WPPC 1 144
8.4.3 Discussion 147
8.5 Simulation of cluster of WPPs 148
8.5.1 Frequency control 148
8.5.2 Power oscillation damping 149
8.6 Summary and recommendation 149
Chapter 9 Conclusion and outlook 151
9.1 Summary 151
9.1.1 Chapter 3 151
9.1.2 Chapter 4 151
9.1.3 Chapter 5 152
9.1.4 Chapter 6 153
9.1.5 Chapter 7 154
9.1.6 Chapter 8 154
9.2 Future work 155
9.2.1 Chapter 4 155
9.2.2 Chapter 5 155
9.2.3 Chapter 6 155
9.2.4 Chapter 7 155
9.2.5 Chapter 8 156

Bibliography **157**
Appendix 1 Simulation models: description **169**
Appendix 2 Simulation models: data **177**
Appendix 3 Control parameter tuning **181**
Appendix 4 Mathematical derivations **185**
Appendix 5 Additional figures **197**
Appendix 6 Experimental setup: data **209**

Chapter 1 Introduction

This chapter briefly introduces motivation and content of this thesis. Background information is given at the beginning, which justifies why a Ph.D. study in this field is needed at a general level. Following that, a list of high-level project objectives is proposed, which provides the foundation for the whole study. The chapter continues by summarising the main techno-scientific contributions of this report and outlining the content of the next chapters. As a conclusion, the publications upon which this thesis is based are listed, accompanied by other relevant material authored or co-authored by the student.

1.1 Background

Among the options for transforming energy systems into more sustainable and independent ones are both VSC-HVDC technology and offshore WPPs. Chapter 2 gives a more detailed description of such technologies and more solidly addresses the particular aspects this study is concerned with. Here, it suffices to say that both massive deployment of offshore WPPs and HVDC systems for interconnection of energy markets are foreseen by political authorities, regulating bodies, TSOs and research institutes, particularly in Europe – a non-exhaustive list of references being [1]-[5].

The most advanced references in the field are mainly dedicated to conception and implementation of so-called super-grids, where a mixture of AC and DC technologies will serve as transmission backbone in order for the future European power system to function efficiently and accommodate high amounts of RES.

However, looking at a shorter term, several challenges exist on less complex systems that are being deployed as of now across power systems, and are hence particularly relevant for the industrial community. An example of such systems is the connection to land of offshore WPPs through VSC-HVDC technology in a point-to-point configuration. While, as said, a more complete description of state-of-art and challenges is the subject of Chapter 2, three preliminary, high-level, aspects to be more deeply looked at are pointed out here to motivate the scope of the study:

- Implementation of VSC-HVDC connection of offshore WPPs has encountered delays and the industry is climbing a steep part of the learning curve. More widespread and confident

understanding of the basic problems is crucial to capitalising on the experience gained, eventually reducing costs, mitigating risks and standardising solutions.

- VSC-HVDC, WPPs and their combination offer great controllability and possess inherent limitations. What this means to the power system in terms of its control and operation still gives room for research. More specifically, and from an applicative perspective, better understanding of facets that could positively fuel the dialogue between different parties involved in the development of such systems (OEMs, TSOs, utilities,…) is of paramount importance for the industrial community.
- Large WPPs may in the future be consisting of WTGs supplied by different manufacturers, thereby forming so-called clusters of WPPs. Since the size of VSC-HVDC connected WPPs is usually very large, the clustering of WPPs is particularly relevant in this case. Very little literature is available on the topic and no commercial installation to date is based on such a layout.

The above items are looking at the development from the standpoint of the power engineering world. One should not forget, though, that the learning effort should proceed in parallel within other realms too. Moreover, the three bullets above are intended to look at the problem from an industrial and reasonably short-term perspective, narrowing down the scope to challenges that are encountered presently or will be encountered shortly rather than extending the focus to several lustra or decades.

1.2 Project objectives and limitations

The general objectives above can be particularised to more thoroughly formulate requirements for the present study. This is done in more detail throughout Chapter 2. Here, only a set of chosen project objectives is listed:

- Control of the offshore AC island networks behind VSC-HVDC converters must be analysed in more detail. Small-signal stability with and without WPP is to be assessed for different state-of-art control strategies of the VSC-HVDC converter station. Moreover, stability and performance against larger disturbances must also be assessed. As a conclusion, recommendations in terms of which control philosophy performs better should derive from the analysis.
- Better understanding of AC voltage control capabilities of onshore VSC-HVDC stations is to be achieved, taking into account limitations and their interaction with more or less strong power systems.
- The behaviour of the system VSC-HVDC/WPP in heavily stressed power systems approaching long-term voltage collapse must be characterised. Limitations imposed by power electronics have to be accounted for, as well as interdependence with the control of WPPs connected behind the HVDC system.
- Participation of VSC-HVDC connected WPPs to the active power balance control of AC-DC networks must be analysed, focussing on realistic control and communication limitations.
- Participation of VSC-HVDC connected WPPs to POD of onshore AC systems must be analysed. Once again, the focus must be on realistic limitations. Moreover, a practical approach is to be used, that allows to derive conclusions which are positively propelling discussions accompanying real-life implementation of the service on such systems.

- The proof of concept for clustering of WPPs must be performed, taking as example the services mentioned above and on which all this work is based. An experimental setup is to be used for validation of models and related simulation results.

The main high-level limitations of the study are:

- Transient phenomena are completely discarded, together with all characteristics which have an influence only in their assessment.
- Harmonic emission from and other non-linearities of PE converters and their interaction with other elements are discarded too. Only resonance phenomena inherent to the impedances will be touched upon.
- Except for the descriptive analysis of long-term voltage stability, long-term power system phenomena are discarded too, limiting the focus to stability issues spanning from milliseconds to several seconds.
- Wind variability is not taken into account along this report.
- Largely disturbed operation such as faults, outages, etc… is only partly considered in this study, where it is functional to illustrating the concepts.

1.3 Contributions

The contributions of this work can be summarised as follows:

- Better knowledge of the control of offshore AC islands was developed. Theoretical analysis and time domain simulations of an offshore AC island excited by an HVDC converter and hosting a WPP were conducted, resulting in:
    - Recommendation of preferred HVDC control strategy
    - Insight of control and circuit parameters influencing stability and performance
- Better understanding of the challenges faced when implementing AC islands with multiple HVDC converters and WPPs was gained, through the use of time domain study cases. Preliminary recommendations in terms of control setup were derived.
- Better characterisation of steady-state AC voltage control capabilities of an onshore VSC-HVDC station taking into account its main limitations has been done. The superimposition of such characteristics with those of an external grid modelled with Thevenin equivalent gave interesting insights on (i) most important factors affecting the VSC-HVDC capability and (ii) the non-linear SCP contribution an HVDC station gives when operating in AC voltage droop control mode and connecting to a weak external network.
- The behaviour of VSC-HVDC during potentially long-term voltage unstable conditions has been analysed through a simple example. The possible detrimental effect of VSC-HVDC current limitation on the voltage stability of a three-bus system was demonstrated. Looking more closely at the axis prioritisation during current limitation, conclusions were drawn in terms of which control strategy is most beneficial to voltage stability. The implications these conclusions have on the operation of a WPP possibly connected behind the VSC-HVDC have been discussed.
- The contribution WPPs connected by point-to-point VSC-HVDC transmission can give to frequency control was analysed. Two control schemes with and without long-distance fast communication were compared. A recommendation as for which one of them should be

used was formulated, accounting for realistic technical limitations and different power system characteristics.

- The performance offered by WPPs for DC voltage control in multiterminal HVDC networks was assessed. Based on the different dynamic requirements with respect to frequency control, a recommendation for preferred communication setup was derived. The consequences of WPP limitations on other converters/power systems contributing to DC voltage control were discussed. The direction for necessary future research in the field was suggested.
- A better practical understanding of POD implementation on VSC-HVDC-connected WPPs was developed, in particular focussing on (i) assessment of most important physical factors influencing a real-life implementation of POD and (ii) understanding of main WPP limitations and derivation of related requirements. Both aspects help a possible dialogue between utilities, TSOs and OEMs when deploying the feature on real installations. Furthermore, other interesting issues related to the most robustly stable implementation of POD through a classical PSS-like scheme are illustrated.
- The proof of concept for clustering of WPPs was performed, relying upon a simple, but real-scale, experimental setup. Focus was upon coordinated provision of active power control and services related to it (frequency control and POD).

1.4 Outline of the thesis

This Ph.D. thesis is organised in 9 chapters as follows:

- Chapter 1 provides an introduction by motivating the study, briefly outlining the scope, summarising the contributions and listing the publications related to the study.
- Chapter 2 is dedicated to justifying the study in more detail by giving an overview of the state-of-art and pointing out the main gaps that this report tries to fill.
- Modelling requirements and model adequacy are discussed in Chapter 3, based on the scope of work outlined in the previous chapters.
- Chapter 4 concerns the control of offshore AC islands connected behind VSC-HVDC converter(s). Small-signal stability and a number of time domain study cases are used to illustrate the results.
- The topic of the first part of Chapter 5 is onshore AC voltage control. The steady-state contribution a VSC-HVDC station can give to AC voltage control is analysed by overlapping VSC-HVDC converter limitations and external grid constraints. The second part of the chapter is dedicated to illustrating the influence of the VSC-HVDC behaviour during current limitation on a power system approaching its long-term voltage stability limit.
- The attention in Chapter 6 is shifted to the active power balance control in AC-DC networks, i.e. to the control of AC frequency and DC voltage. The behaviour of WPPs, VSC-HVDC and their combination is focussed on.
- POD from VSC-HVDC and WPPs is the subject of Chapter 7. A practical approach is used to emphasise the main factors that are determining choices for implementation of POD on real units, from AC grid characteristics to WPP limitations. Furthermore, a few interesting issues regarding POD closed-loop stability are touched upon.
- Chapter 8 describes the experimental verification of the concept of clustering of WPPs. In the same chapter, the experimental model validation is presented too, which allows building confidence on some of the models used throughout this report.

- Finally, Chapter 9 summarises the main conclusions and draws the lines for future work.

1.5 List of publications

1.5.1 Conference and journal publications related to the study

The following publications have been used as a basis for this report:

1. L. Zeni, T. Haileselassie, G. Stamatiou, A.G. Eriksen, J. Holbøll, O. Carlsson, K. Uhlen, P. Sørensen and N.A. Cutululis, "DC grids for integration of large scale wind power", in *EWEA Offshore 2011,* Amsterdam, December 2011.
2. J. Glasdam, L. Zeni, M. Gryning, J. Hjerrild, L. Kocewiak, B. Hesselbæk, K. Andersen, T. Sørensen, M. Blanke, P.E. Sørensen, A.D. Hansen, C.L. Bak and P.C. Kjær, "HVDC Connected Offshore Wind Power Plants: Review and Outlook of Current Research", in *12th Wind Integration Workshop,* London, October 2013.
3. N.A. Cutululis, L. Zeni, W.Z. El-Khatib, J. Holbøll, P. Sørensen, G. Stamatiou, O. Carlsson, V.C. Tai, K. Uhlen, J. Kiviluoma and T. Lund, "Challenges Towards the Deployment of Offshore Grids: the OffshoreDC Project", in *13th Wind Integration Workshop,* Berlin, November 2014.
4. J. Glasdam, L. Zeni, J. Hjerrild, L. Kocewiak, B. Hesselbæk, P.E. Sørensen, A.D. Hansen, C.L. Bak and P.C. Kjær, "An Assessment of Converter Modelling Needs for Offshore Wind Power Plants Connected via VSC-HVDC Networks", in *12th Wind Integration Workshop,* London, October 2013.
5. M. Sztykiel, R. da Silva, R. Teodorescu, L. Zeni, L. Helle and P.C. Kjær, "Modular Multilevel Converter Modelling, Control and Analysis under Grid Frequency Deviations", in *EPE Joint T&D and Wind Chapters*, Aalborg, June 2012.
6. L. Zeni, T. Lund, A. Hansen, P. Sørensen, P. Kjær, B. Hesselbæk and J. Glasdam, "Coordinated system services from offshore wind power plants connected through HVDC networks", in *Cigré session 2014,* Paris, August 2014.
7. L. Zeni, H. Jóhannsson, A.D. Hansen, P.E. Sørensen, B. Hesselbæk and P.C. Kjær, "Influence of Current Limitation on Voltage Stability with Voltage Sourced Converter HVDC", in *ISGT Europe Conference,* Lyngby, October 2013.
8. L. Zeni, B. Hesselbæk, P.E. Sørensen, A.D. Hansen and P.C. Kjær, "Control of VSC-HVDC in offshore AC islands with wind power plants: comparison of two alternatives", accepted for publication *in PowerTech 2015,* Eindhoven, June 2015.
9. L. Zeni, I. Margaris, A. Hansen, P. Sørensen and P. Kjær, "Generic Models of Wind Turbine Generators for Advanced Applications in a VSC-based Offshore HVDC Network", in *The 10th IET Conference on AC/DC Power Transmission,* Birmingham, December 2012.
10. L. Zeni, S. Goumalatsos, R. Eriksson, M. Altin, P. Sørensen, A. Hansen, P. Kjær and B. Hesselbæk, "Power Oscillation Damping from VSC-HVDC connected Offshore Wind Power Plants", under revision in *IEEE Transactions on Power Delivery,* 2015.

1.5.2 Other relevant publications

Other relevant publications in the field authored and co-authored by the author of this report are the following:

11. V. Mier, P.G. Casielles, J. Coto and L. Zeni, "Voltage margin control for offshore multi-use platform integration", in *International Conference on Renewable Energies and Power Quality*, Santiago de Compostela, March 2012.
12. T.K. Vrana, L. Zeni and O.B. Fosso, "Active Power Control with Undead-Band Voltage and Frequency Droop for HVDC Converters in Large Meshed DC Grids", in *European Wind Energy Conference*, Copenhagen, April 2012.
13. T.K. Vrana, L. Zeni and O.B. Fosso, "Active Power Control with Undead-Band Voltage And Frequency Droop Applied to a Meshed DC Grid Test System", in *Energycon 2012*, Firenze, September 2012.
14. L. Zeni, A.J. Rudolph, J. Münster-Swendsen, I. Margaris, A.D. Hansen and P. Sørensen, "Virtual inertia for variable speed wind turbines", *Wind Energy*, DOI:10.1002/we, 2012.
15. T.K. Vrana, L. Zeni and O.B. Fosso, "Dynamic Active Power Control with Improved Undead-Band Droop for HVDC Grids", in *The 10th IET Conference on AC/DC Power Transmission*, Birmingham, December 2012.
16. A.G. Laukhamar, L. Zeni and P.E. Sørensen, "Alternatives for Primary Frequency Control Contribution from Wind Power Plants Connected to VSC-HVDC Intertie", in *European Wind Energy Conference*, Barcelona, March 2014.
17. J. Glasdam, L.H. Kocewiak, J. Hjerrild, C.L. Bak and L. Zeni, "Comparison of Field Measurements and EMT Simulation Results on a Multi-Level STATCOM for Grid Integration of London Array Wind Power Plant", in *Cigré session 2014*, Paris, August 2014.
18. W.Z. El-Khatib, D. Schwartzberg, I. Arana Aristi, J. Holbøll and L. Zeni, "Transients in VSC-HVDC connected offshore wind power plants", in *The 11th IET Conference on AC/DC Power Transmission*, Birmingham, February 2015.

Moreover, the student has contributed as a corresponding author to the following technical brochures published by Cigré:

19. Cigré WG B4-55, "Technical Brochure DRAFT – HVDC Connection of Offshore Wind Power Plants", *to be published in 2015.*
20. Cigré WG B4-57, "Technical Brochure 604 – Guide for the Development of Models for HVDC Converters in a HVDC grid", *published by Cigré*, Paris, December 2014.

Chapter 2 State-of-art: VSC-HVDC and wind power

The aim of this chapter is to give an overview of the state-of-art in VSC-HVDC connection of WPPs. By describing where academia and industry stand, it helps justify the scope of the present study and formulate high-level requirements for the analysis conducted in subsequent chapters. The chapter starts out by providing state-of-art and outlook of challenges for modern power systems, in the context of the current predicted development of RES, particularly in Europe. After discussing the reasons for installing WPPs with VSC-HVDC connection, a summary of wind power projects with VSC-HVDC is given. The chapter then addresses state-of-art and current challenges in the power system integration of WPPs, VSC-HVDC and their combination. Finally, it concludes by considering a set of possible system configurations and, after selecting which of them are relevant for this work, derives high-level requirements for the rest of the study. This chapter's topic was the subject of Publications 1, 2 and 3 [6]-[8].

2.1 Introduction

The technical aspects touched upon in this study fall within a larger pool of challenges of diverse nature, all stemming from the eagerness society has shown in the last few decades to try and revolutionise the energy system [3], [9]. Deep socio-economic, political and environmental reasons exist to take this direction, such as energy independence, security of supply, climate change attenuation, pollution reduction, etc. It is therefore important to briefly describe how VSC-HVDC connection of WPPs finds room within this scenario.

2.1.1 Integration of RES in power systems

As the entire energy system undergoes significant changes, a large part of it is represented by the power system, which can thus contribute significantly to reaching the chosen objectives in terms of e.g. energy independence and decarbonisation. One of the pathways to the above objectives is certainly the conversion of the power production facilities to more widely available and sustainable resources, and RES are one of the options to achieve such transformation. RES have therefore gained public favour and are being deployed massively across power systems. As a result, conventional power stations based on fossil fuels are progressively being replaced by units based on RES, such as wind, sun and biomass.

In conducting such transformation, however, a number of challenges are encountered. Among them, as an incomplete list, one could mention:

- A peculiarity of some RES is their intermittent nature. Since the power system control paradigm is based on matching both energy *and* power production and consumption, the volatility of RES calls for means to always make up for the difference between power production and consumption, be it positive or negative.
- Energy yield and public acceptance reasons often push RES installations far from load centres, calling for new expensive transmission infrastructure.
- Substitution of conventional generation is financially challenging for utilities. Investments on power stations are planned over a temporal span of at least 20 years and reduced energy production due to replacement by RES negatively impacts the business case.
- From a TSO perspective, the reduction in number of conventional units partly deprives the transmission system of services that have historically been tapped from them.

All the mentioned items, at the end of the day, yield a high cost for society. Such cost may be outweighed by long term socio-economic benefits. Nevertheless, if the transformation is to be achieved, it is desirable to minimise the cost. This study, from a general perspective, is concerned mostly with the first two and the last of the above items.

2.1.2 Why offshore wind power and VSC-HVDC?

A leading role among RES has been taken, historically, by wind power. Wind turbine installations for power production are dated as far back as the late 19th century, in the US, UK and Denmark [10]. However, only during the last twenty years has wind power spread swiftly and globally [11]. Even more recent is the emergence of offshore wind power (the object of this study), the development of which has just started, as shown in Figure 1, where annual and cumulative installed capacity in Europe up to 2014 is reported [12]. Commercial installations out of Europe still amount to a negligible capacity.

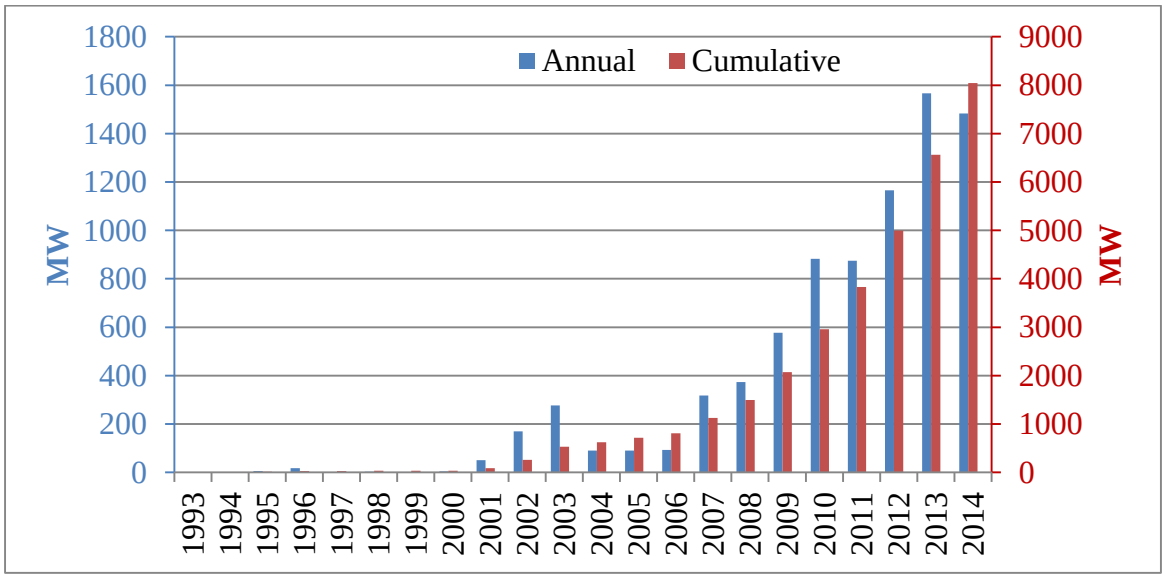

Figure 1 - Annual and cumulative offshore wind power installations in Europe – source EWEA [12].

Due to technological immaturity, the cost per MWh of offshore wind power is still not competitive and must be lowered if the technology is to have a future. A way to bring it down is technological development, achieving economies of scale and standardisation. Furthermore, higher energy yields can also be a driver for cost reduction. When benefits in terms of produced energy outweigh added costs due to transmission distance and water depth, installing WPPs farther from shore reduces cost of electricity. Usually, hence, larger distance to the onshore PCC requires a larger WTG and WPP capacity to improve the economics. In addition to this, local factors such as public acceptance and other restrictions (protected areas, telecommunications, naval routes, etc…) influence the sizing and positioning of offshore WPPs. All aspects above are exemplified by Figure 2, where European offshore WPPs with capacity over 30 MW, in operation or in the construction phase, are reported divided by country and showing their distance to the onshore PCC and installed capacity. Data are updated to November 2014 according to [13], [14].

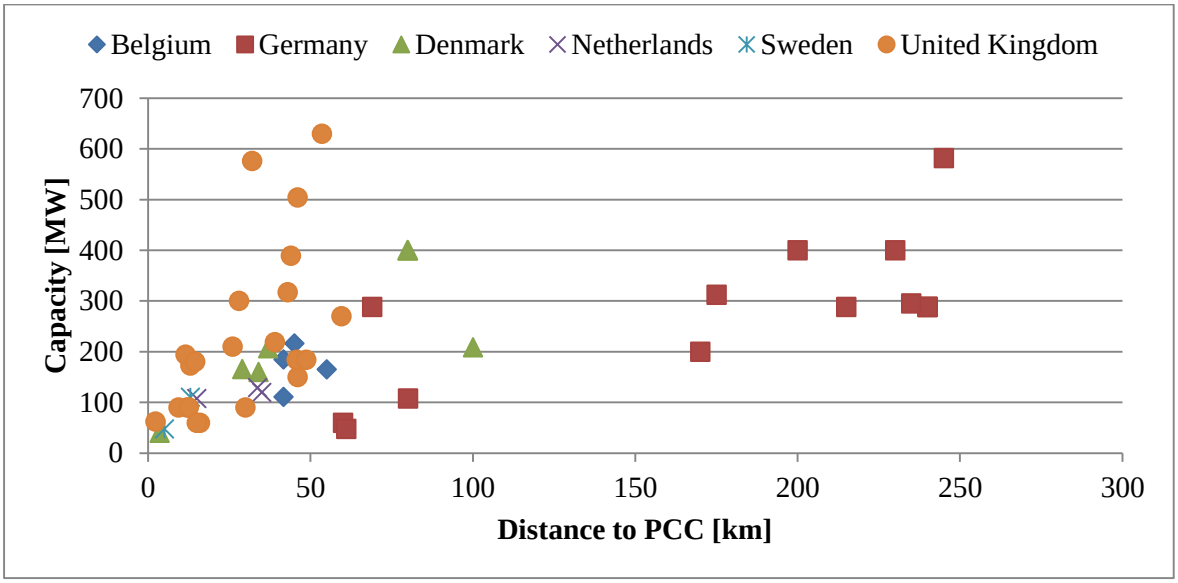

Figure 2 - Overview of European offshore wind projects by distance to PCC and capacity – sources [13], [14].

As far as the electrical transmission infrastructure is concerned, the impact of the distance on the transmission technology used is also seen clearly by Figure 2. The German clusters with distance greater than 150 km are all VSC-HVDC-connected, while the rest of the WPPs are all provided with classical AC connection. As exemplified for instance in [15], uncompensated AC transmission has technical constraints which limit the transmittable power through a sea cable, depending on its length, ampacity and voltage level. For various reasons it is not absolutely clear, however, what the *economic* break-even length is. And this too is somehow apparent from the clear split in Figure 2. German North Sea clusters are HVDC-connected due to (i) their large distance from shore and (ii) the clustering of multiple WPPs behind the same HVDC converter. Both reasons may not necessarily derive from purely technical or economic arguments but are the result of more holistic top-down decisions. All other WPPs make use of AC connection and do indeed show a limit distance. A number of alternatives are proposed to increase the reachable distance with AC technology, such as intermediate compensation platforms [16] or low-frequency (50/3 Hz in Europe) transmission, borrowed from traction applications [17]. On the other hand, the feasibility of VSC-HVDC transmission at lower distances will become reality if actual costs and lead times for VSC-HVDC are reduced. It should not be forgotten, though, that other concepts making use of LCC-HVDC have also been proposed for the purpose of connecting WPPs [18]. In order to limit the scope of the study, however, the attention is here limited to VSC

technology. Therefore, in the remainder of this report, VSC-HVDC and HVDC will be considered equivalent unless differently specified.

In light of the above, and considering further technical challenges – part of which will be described below – posed by VSC-HVDC, it is clear that HVDC technology for offshore WPPs still is in embryo and the community is climbing up its learning curve. However, it is true that (i) German wind clusters are already being connected with HVDC and (ii) elsewhere, as valuable sites close to shore get depleted and foundation technology evolves allowing for greater water depths more remote locations will become economical. Therefore, HVDC is still expected to play a major role for WPP connection. Moreover, looking further ahead, the development of so-called offshore grids may happen in the future. Such a concept is based on integrated massive deployment of interconnectors between countries and offshore wind power and could give birth to a real large meshed HVDC grid based on VSC technology [1], [2], [4], [19].

2.1.3 Overview of VSC-HVDC projects for offshore WPPs

An overview of the commercial VSC-HVDC projects expected to provide a path for transmitting offshore wind power to shore is reported in Table 1. Data are taken from [20] and are updated to November 2014, when all commercial projects decided upon were in German North Sea waters.

Table 1 - Overivew of VSC-HVDC projects for offshore WPP connection.

Project	Rating [MW]	Conv. technology	DC voltage [kV]	DC cable length [km]	Year
BorWin 1	400	HVDC Light®	± 150	200	2012
DolWin 1	800	HVDC Light® CTL	± 320	165	2014
BorWin 2	800	HVDC Plus MMC	± 300	200	2014
HelWin 1	576	HVDC Plus MMC	± 250	130.5	2014
SylWin 1	864	HVDC Plus MMC	± 320	199.5	2014
DolWin 2	900	HVDC Light® CTL	± 320	135	2015
HelWin 2	690	HVDC Plus MMC	± 320	130.5	2014
DolWin 3	900	MaxSine® Converter	± 320	161	2017
BorWin 3	900	HVDC Plus MMC	± 320	160	(2019)

Table 2 - Summary of offshore WPPs with VSC-HVDC connection.

Project	Capacity [MW]	P_{WTG} [MW]	HVDC station
Amrumbank West	288	3.6	HelWin 2
BARD Offshore 1	400	5.0	BorWin 1
Borkum Riffgrund 1	312	4.0	DolWin 1-3
Borkum West 2 (Trianel)	200	5.0	DolWin 1
Butendiek	288	3.6	SylWin 1
DanTysk	288	3.6	SylWin 1
Global Tech 1	400	5.0	BorWin 2
Gode Wind 1+2	582	6.0	DolWin 2
Meerwind Süd und Ost	288	3.6	HelWin 1
Nordsee Ost	295	6.15	HelWin 1

Public information regarding which WPP is connected to which HVDC converter station is less certain and temporary connections to one station are also happening, to then switch to another.

Moreover, multiple HVDC stations may actually be connected on the offshore AC side, giving birth to AC islands consisting of multiple HVDC converters and WPPs. Only WPPs completed or being commissioned are considered here, and reported in Table 2 along with their rated capacity, WTG rated power and respective HVDC converter station, all according to [13].

More installations are expected to take place and be allocated to the available transmission capacity that will be commissioned before 2020. More commercial projects are being planned and several research or demonstration projects are operating or planned worldwide.

2.2 Wind power plants

An overview of WPPs is given in this section. According to the scope of the study, the focus is restricted to the characteristics that are relevant for electrical phenomena, discarding unnecessary details. Brief reference to literature on WTG technology is done. Thereafter, an overview of state-of-art control features at WTG and WPP level is given, with special attention to so called power system (or ancillary) services. In the same terms, a summary and outlook of further possibly desired control features are also presented.

2.2.1 Wind turbine generator technology

From an electrical standpoint, WTG technology has evolved from being based on fixed-speed electric machines directly coupled to the grid to relying on more modern variable-speed concepts provided with variable resistor or PE converter. The latter can be (i) rated for a fraction of the turbine power and coupled to the rotor of a DFIG or (ii) rated for full power (FSC) and coupled to the stator of an IG, SG or PMSG [21]. The second side of the converter (GSC) is always coupled to the grid. The qualitative classification above has nowadays been adopted in a more official fashion by industrial community and standardisation bodies. For example, the draft IEC standard [22] classifies the above technologies into Type 1 to Type 4. Different concepts have been proposed but have not spread commercially yet.

The efficiency and controllability featured by Type 3 and Type 4 WTGs combined with ever stricter grid connection requirements have essentially ruled other WTG types out of markets with widespread wind power production. Since offshore wind power is typically deployed in large scale and in systems with an already relevant share of onshore wind and is as such usually subject to demanding grid codes, focus in this work is restricted to WTGs provided with PE converter, and in particular to those based on FSC (Type 4), a sketch of which is illustrated in Figure 3, based on [22].

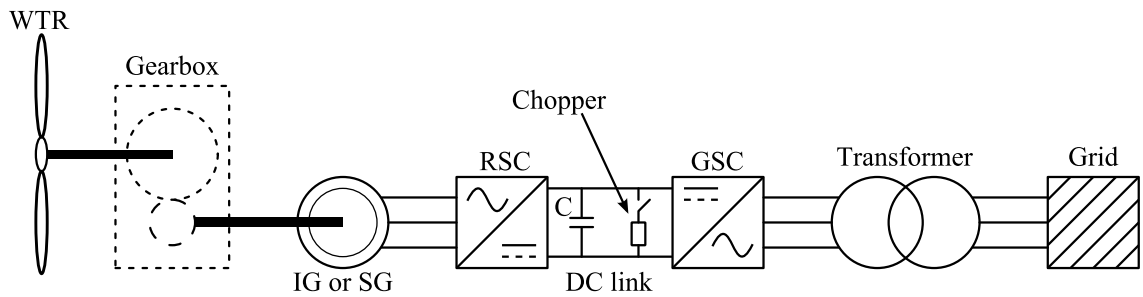

Figure 3 - Simplified sketch of Type 4 WTG – inspired by [22].

The electromechanical energy conversion is, in Type 4 WTGs, fully decoupled from the grid by a back-to-back AC-AC converter, consisting of a RSC acting as rectifier and a GSC operating as

inverter, connected to each other by a DC link with energy storage capacitor. The control objective is usually power reference tracking to maintain constant DC voltage for the GSC. The RSC, on the other hand, may be called to simply control torque so as to maximise or limit the power. In average terms, the power injected into the DC link by the RSC is evacuated to the grid by the GSC. Control of the latter has been widely described in literature – e.g. generally in [23] and more specifically in [24]. Further features are usually superimposed on these basic ones, such as damping of mechanical resonances (e.g. shaft) or FRT [21]. For the latter, a supplementary chopper is often employed at the DC link.

Type 3 WTGs based on DFIG are also being installed with VSC-HVDC connection [13] and are hence also relevant within the present scope. However, they are discarded here. In many cases, from a power system perspective, their characteristics are similar to those of Type 4 machines. Where they are not, it will be pointed out. Moreover, one should not forget other concepts that have been proposed more specifically for VSC-HVDC connected WPPs, making use of fixed speed machines whose power output is controlled by the offshore HVDC converter – see e.g. [25]-[28]. These concepts too are discarded here.

2.2.2 Control of wind power plants

(a) Normal operation and state-of-art services

Abundant literature is available on control of WTGs, e.g. [21], [29] and related references. The control of single WTGs is a well-established discipline, as it had to be performed satisfyingly since the first wind power installations. The basic control principles of Type 4 WTGs have been outlined above.

As WPPs become more and more spread across power systems and grid code requirements more demanding [30]-[32], additional control features at a WTG level and further control actions at an overall plant level become important too. In general, steady-state set-point tracking for both active and reactive power (or power factor or voltage) at the PCC is guaranteed at a WPP level by a dedicated controller. The latter, depending on specific application and requirements, may also require additional equipment (e.g. MSCs, SVC, STATCOM). So called power system services such as frequency control, dynamic voltage (reactive power) control and FRT are also demanded by current grid codes. FRT is typically provided at WTG level due to needed fast response times, while voltage control at PCC is usually performed at WPP level, due to the needed coordination. On the other hand, a service like frequency control gives more freedom and may be implemented as a mixed solution like in [33], where IR was implemented on the WTGs and PFC[1] on the plant controller, but alternative approaches can also be chosen.

The above mentioned features are commercially installed in WTGs and WPPs. However, research is still ongoing to refine some of the aspects. Concerning FRT, attention is especially paid to control during unbalanced faults [24] and other phenomena such as PLL loss of synchronism [34]. As for frequency control, most recent research has been mainly directed to evaluation of control alternatives [33], [35], [36], the influence of wind power variability and distribution on the available power [37] and frequency control provision by WPPs through HVDC connection and HVDC networks [38]-[41].

[1] The definition of *primary frequency control* (PFC) may be ambiguous. In the context of this study, it is meant to include the control action usually performed by governors and proportional to the frequency deviation. IR is thus distinguished from PFC, throughout this report.

The last point is of special interest for this study. Robust applicable solutions must be devised to provide adequate frequency control. Attention has been paid mostly to avoiding communication [38], [40], but the desired amount of communication must also consider particular application (electrical topology, HVDC ownership and operation, etc…) and reliability of communication links, as well as other limitations presently imposed by WPPs. More emphasis will be put on this topic in Chapter 6.

(b) Advanced services

More advanced services are being focussed on by current literature and are not featured yet by commercial WPPs. Among these, one could mention synchronising torque, POD, DC voltage control in HVDC grids, etc… Based on the scope of work, the last two are discussed here.

POD provision from WPPs has recently gained interest and TSOs are already proposing its requirement in legally binding documents [42], [43]. The subject has found room in several recent publications, such as [44]-[54]. Criteria to select and design controllers as well as their inputs and outputs have been proposed, mainly through modal analysis – the most renowned approach for small-signal stability analysis – and robust control theory. However, with the exception of [48] and partly [44], real limitations imposed by WPPs have not been accounted for, and all the above sources could more generically refer to controllable power sources rather than WPPs and could go along with other studies such as [55]-[58]. Moreover, the discussion of which power system characteristics are crucial to the implementation of POD could still be enriched. Particularly AVRs are very often neglected when studying POD from PE converters. Finally, more certainty is needed on understanding which solutions are really the most robust and applicable on commercial installations. This knowledge would be particularly precious for utilities, TSOs and OEMs. This topic is treated in more detail in Chapter 7.

DC voltage control in HVDC networks is the equivalent of frequency control in AC networks, i.e. linked to the active power balance. However, there are significant differences between the two, mainly related to the very different time constants involved [59] and to the fact that DC voltage, contrary to AC frequency, is not exactly a global measure of power balance [60], [61]. Recent publications have regarded DC voltage control in HVDC grids and its coordination with nearby AC grids and their frequency control [62]-[66]. Once again, though, WPPs' real limitations have hardly been considered by any of the cited references. When the share of wind power connected to a HVDC grid is significant, such constraints become crucial to the effective control of the DC voltage. Chapter 6 is dealing in more detail with this issue.

2.3 VSC-HVDC

A summary on VSC-HVDC is given in this section, again solely focussing on aspects that are important in the context of this study. General characteristics are discussed first, then moving to control aspects, making a distinction between control of onshore and offshore stations for WPP connection.

2.3.1 VSC technology for HVDC

VSC technology has found commercial application in HVDC since 1999 [67]. Despite being far more expensive than LCC technology, it offers advantages for instance if the following aspects are important [68]:

- Compactness

- Black-start capability
- Connection to weak networks
- Independent control of active and reactive power
- Fast reversibility of active power flow

Based mainly on the first two items above, VSC-HVDC has been considered the only possible solution for connection of remote offshore WPPs, although more innovative concepts may be explored in the future too. For this reason, the focus in this thesis is solely on VSC-HVDC. LCC technology and other more immature concepts are discarded.

The VSC-HVDC market has for many years been a monopoly based on two- or three-level converters [68]. However, the recent advent of more complex MMCs [69]-[72] has brought new players into the scene. Additional hardware and control complexity of MMCs are outweighed by advantages in terms of waveform quality (elimination of filters), reduced switching losses, modularity, and absence of accurate gate firing control for IGBT stacks.

Use of VSC for most typical HVDC applications (long distance high power transmission) is prevented by (i) higher cost per MW and losses than for LCC [73] and (ii) immaturity of XLPE cable technology, limiting reachable DC voltage and hence power levels (± 525 kV have been reached only recently [74], compared to voltages as high as ± 800 kV for LCC with MI cables [75]). For other technical reasons VSC is considered the only feasible solution to date for HVDC connecting WPPs, but both the above points eventually result in high cost.

Multiterminal HVDC systems have been implemented with LCC [76] and pilot projects are being deployed with VSC too. However, very large systems have so far been prevented from appearing by the lack of easy power reversal for LCC and the lack of a proven and affordable solution for selective DC current breaking for VSC [1], [77], [78].

The flexibility and controllability featured by VSC-HVDC and their possible benefits to power system control and stability were firstly highlighted in [79]. The role of the research community is now to explore all the actual opportunities and limitations, also considering the specific application to WPP connection.

2.3.2 Control of VSC-HVDC converters

(a) Grid connection of VSC-HVDC converters

State-of-art control of VSC-HVDC converters connected to conventional AC grids[2] resembles common schemes for generic VSCs (renewable generation, STATCOMs, etc…). Valuable sources in this respect are for example [23], [24], while a good summary for specific application to HVDC can be found in [80].

VSC-HVDC systems are more likely to be connected to weak grids[3] than LCC systems, where further control challenges appear. Reference [80] and related articles offer a good treatment of the

[2] A *conventional* AC grid is here meant to be a grid where a sufficiently strong voltage is present independently of the connection of the VSC-HVDC, due to other voltage sources. As importantly, the frequency of the AC grid voltage is also sufficiently stiff. In the context of this study, *conventional* essentially means *onshore*.

[3] The definition of *weak* grid is not a clear one, but it is here assumed to be one with SCR < 3, where SCR is the ratio between the SCP at the PCC and the converter rated apparent power.

topic. So does [81], while [82] discusses in particular the effect of PLL tuning for weak grid connections.

Depending on the particular application and requirements, the basic control features of a grid connected HVDC station can vary. Additional control services may be added if necessary, similarly to what is done in WPPs – see Section 2.2.2. An interesting aspect which has not been widely treated in the literature yet is related to the behaviour of VSC-HVDC during current limitation and its relation to long-term voltage stability. Since the HVDC station may be operated by a different party than the TSO, this matter is of importance to both TSOs and operators. Chapter 5 touches upon this.

(b) VSC-HVDC converters connection to offshore AC islands

When a VSC-HVDC converter is connected to offshore AC islands, differences may arise with respect to typical grid connected applications. No stiff voltage source is in principle present in the system and the HVDC converter may have to be the main element to keep the voltage constant. Even more interestingly, the average frequency may not be bound to any rotating mass and the network may be effectively inertia-less. This changes the control paradigm for the grid, and VSCs must adapt to it.

Considering the simplest configuration where a single HVDC converter is controlling voltage and frequency of an offshore WPP, two approaches have been proposed in literature:

- Reference [83] adopts a voltage control scheme with nested current controller, both of them based on well-known vector control and essentially already described in [23].
- Reference [15], instead, makes use of a simpler open-loop voltage-angle control, which is actually a particular – “uncontrolled” – case of that presented in [84].

None of the above references, however, presented a complete analysis of the topic and a firm justification for choosing either of the control approaches. Further interesting material has been published in the field (see e.g. [85]-[87]), but a solid theoretical explanation of the phenomena and assessment of the stability are still somewhat missing. More attention is dedicated to this subject in Chapter 4.

Extension of the problem to a more variegated AC island with multiple HVDC converters, offshore WPPs and possibly other elements makes it even more interesting and a generic approach such as those suggested in [23], [87] would be preferable. However, [23] does not consider some peculiarities of offshore WPP networks and [87] does not provide sufficient theoretical insight.

Besides the normal operation, then, faults in AC islands are also of high interest from different perspectives (post-fault stability, component ratings, protection system design, etc…). However, literature is scarce in the field. Reference [88] attempts a first treatment, but more work is definitely needed in the area.

2.4 VSC-HVDC connected WPPs

A brief summary of the state-of-art in VSC-HVDC connection of WPPs is given in this section, partly recalling what mentioned above and adding further details when necessary.

2.4.1 General aspects

First studies for VSC-HVDC connection of offshore WPPs were done in [15], [83], where the proof of concept was conducted, addressing basic challenges for normal and disturbed operation. Further research should thus be aiming at (i) deeper investigation of the most interesting issues, raising the level of detail, (ii) improvement of confidence in the results, possibly pointing out new challenges, (iii) more precise and solid robustness assessment of the existing configurations and (iv) proposal of new more innovative solutions.

With regard to normal operation, the main gaps in currently available literature are probably related to the control of offshore AC islands. As mentioned in Section 2.3.2(b), although research has touched upon the subject already – e.g. [85]-[87] – satisfyingly solid conclusions are still missing. This will be partly covered by Chapter 4. Adding on this, other interesting phenomena may be observed when considering offshore WPPs with Type 3 WTGs (out of scope here). Even in this case, preliminary work has been done on the topic [89], but more exhaustive assessments should stem from future research.

As for disturbed operation and in particular faults in offshore AC grids, much research is still needed, as hinted above. DC faults gain interest especially in multiterminal HVDC configurations, while onshore AC faults have been treated quite extensively already [15], [83], and Publication 6 [90], but room for research may be left in terms of participation of WPPs in case of permanent onshore faults [81].

2.4.2 System services

Concerning power system services, as mentioned in Sections 2.2 and 2.3, several investigations have been conducted on WPPs and VSC-HVDC separately, and some of them considered their coordination. Services like AC voltage control and frequency control have reached a certain maturity, but may still leave room for research. In the context of this study:

- With regard to AC voltage control, the influence of current limitation of VSC-HVDC and/or WPPs in extreme situations such as proximity to long-term voltage collapse still needs to be investigated. Connection to weak AC networks also provides room for derivation of interesting results. Chapter 4 is concerned with these matters.
- As for frequency control, its dependence on wind power variability as well as its provision in combination with HVDC voltage control in multiterminal DC grids are interesting subjects for current research. For simpler HVDC network configurations, realistic assessment of communication needs and limitations must be conducted, to derive requirements for real-life implementation. The last point is touched upon in Chapter 6.

Research on more advanced services such as POD and participation of WPPs in HVDC voltage control is still in its infancy.

In particular, although literature on POD from static power sources is abundant – see Section 2.2.2(b), the combination of VSC-HVDC and WPPs has not been looked at so closely. More importantly, (i) real performance limitations imposed by modern WPPs are usually not taken into account and (ii) theoretical results on POD from VSCs have not been accompanied by practical considerations regarding which elements are crucial in determining robustness and effectiveness of the service. Both gaps are important when the service must be implemented in reality, and Chapter 7 mainly regards exactly such issues.

Since participation of WPPs to HVDC voltage control becomes a real problem only in multiterminal DC grids, research in the subject is even more in embryo. Several publications have generically regarded power balance control in AC/DC grids, but again possible real inherent limitations of WPPs have traditionally been neglected. The second part of Chapter 6 is dedicated to this.

2.4.3 System configurations

In this section, a set of possible simplest configurations for both offshore network and wind power installation is outlined, then selecting the layouts that are relevant throughout this document.

(a) Offshore grid

The simplest possible layouts of the offshore grid can be obtained by different permutations of the switches in the simplified drawing in Figure 4. Four VSC-HVDC converters and two wind power installations are shown. Two converters are positioned onshore and connected to one or two power systems. Two offshore converters are connected to two wind power installations.

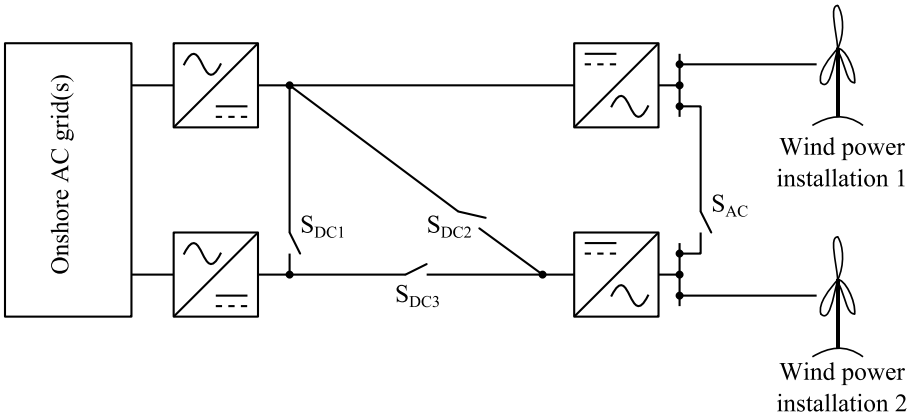

Figure 4 - Summary of offshore grid configurations.

The following combinations can be considered as basic configurations:

1. **Point-to-point HVDC connection**: it is implemented by closing switch S_{DC3} and leaving all other switches open and it is the only commercial configuration nowadays – excluding Nan'ao multiterminal in China, for which available information is still limited [91]. Each wind power installation is transmitting power to land by a single VSC-HVDC link.
2. **Parallel HVDC connection**: switches S_{DC3} and S_{AC} are closed, the others being open. This is analogous to the above layout, but the switch on the offshore AC side is closed. Advantages and challenges of this solution compared to the previous one were discussed in [92]. Such configuration may become reality quite soon with small incremental changes, for example in the German North Sea.
3. **Radial multiterminal connection**: switch S_{DC1} (or S_{DC2}) is closed, while all other switches are open. The DC part of the network effectively becomes multiterminal, but the path for power to travel between any two points in the network is still unique:
    a. With S_{DC1} closed, wind power is injected into a DC system that connects two onshore points, e.g. an interconnector between countries. This configuration is particularly interesting from a market [93] and active power control perspective [94] – Publication 16. A slightly more complex configuration of the same kind (so-called H grid with S_{DC1} and S_{DC3} closed) was analysed for example in [95].

b. With S_{DC2} closed, wind power is transmitted to a single onshore point from two different offshore locations. This does not add many interesting features to configuration 1., if the onshore HVDC station is rated for the total wind power.

4. **Meshed multiterminal connection:** when all S_{DCi} switches are closed the simplest meshed DC grid configuration takes place. Besides being multiterminal, the DC network allows for power to flow between two points through two different paths. As it becomes larger, the meshed layout brings in all issues that are typically encountered in nowadays AC systems and additional ones. Several references make use of such a layout or more complex ones and effort is being put into devising systems that can capture all relevant phenomena for research and development in the area [59].

A more detailed and generalised discussion of the configurations above can be found e.g. in [96].

(b) Wind power installation

A generic layout for each wind power installation in Figure 4 is depicted in Figure 5 for the special case of two WPPs – generalisation to more than two is immediate. It is assumed here that each WPP is provided with dedicated WPPC, as this is a commonly established practice in WPPs, particularly if large and offshore.

Nowadays, each WPP runs independently. Future development may, however, lead to so called *clustering* of multiple WPPs, running with machines of different size, technology and manufacturer. Obtaining the desired lumped response from a cluster of WPPs may be achieved in different ways, for instance:

1. Eliminating WPPCs and deploying a dedicated overall cluster controller (CC).
2. Developing a CC that operates in open-loop and dispatches references to each WPPC.
3. Developing a CC that operates in closed-loop, calculates the references for each WPPC and dispatches them. This option is depicted in Figure 5.

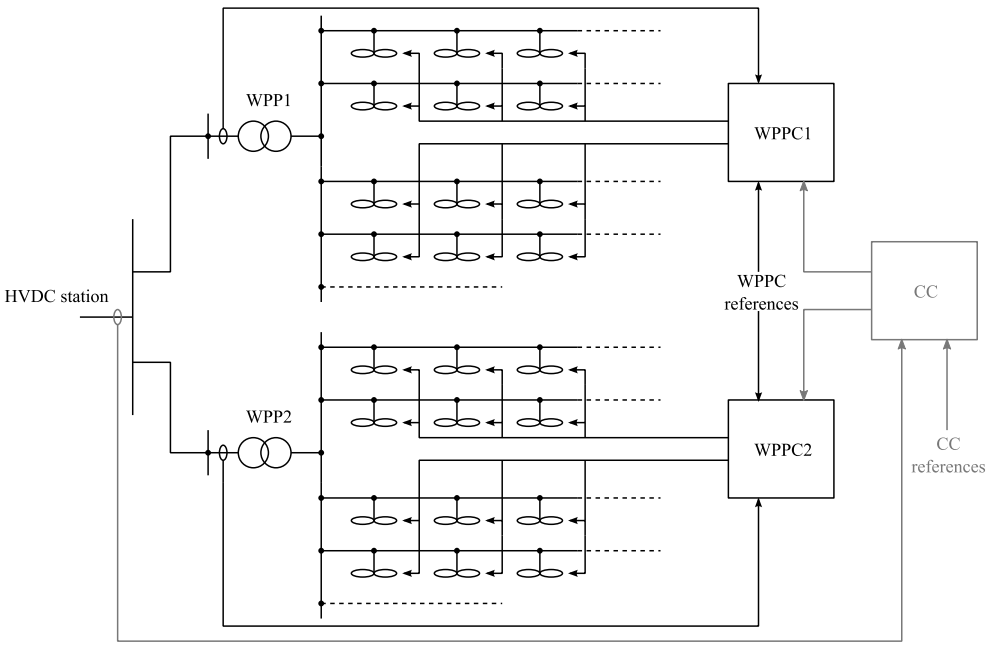

Figure 5 - Generic layout of wind power installation: (black) WPPCs operating independently, (grey) closed-loop CC driving parallel WPPCs.

(c) Relevant configurations for this study

In the course of this study, only a few of the above mentioned configurations for offshore grid and wind power installation have been looked at. Specifically:

- In terms of offshore grid layout – Section 2.4.3(a):
  - The default configuration is 1., i.e. a point-to-point VSC-HVDC connection.
  - Some of the findings reported in Chapter 4 are valid for configuration 2., although they do not regard the whole system but only its offshore AC part. A slightly more detailed illustration of the configurations relevant for Chapter 4 is given in Figure 19 and Figure 20.
  - Configuration 3.a is used in Section 6.3 to treat HVDC voltage control contribution from WPPs, since such service becomes interesting only in multiterminal HVDC grids.
- In terms of wind power installation layout – Section 2.4.3(b) – only a single WPP solution with dedicated WPPC is relevant in this study – only black part of the drawing in Figure 5. However, in Chapter 8, a cluster of WPPs is taken into consideration, i.e. the structure as depicted in Figure 5, except for the fact that the measurement feedback to the CC will not be included (grey arrow from HVDC station to CC).

2.4.4 Thesis problem formulation and limitations

According to the state-of-art, some of its pending points and the configurations outlined in Sections 2.2 to 2.4, the following high-level objectives can be formulated for the investigations through the next chapters:

- The problem of controlling offshore AC island networks is to be investigated in more detail to enrich present knowledge.
- VSC-HVDC and WPPs offer opportunities and pose limitations in terms of participation in power system control, which need be more deeply understood:
  - As for onshore AC voltage control, connection to weak networks and behaviour in stressful power system situations can be further investigated.
  - Participation of VSC-HVDC and WPPs to frequency control may shortly have to be ensured by real installations. Aspects related to a real implementation are thus interesting to look at.
  - Inclusion of WPPs in DC voltage control schemes in DC grids must consider intrinsic WPP limitations if it is ever to be taking place.
  - Delivery of POD from VSC-HVDC-connected WPPs in real installations must start from firm understanding of power system physics, practical crucial influencing factors and real performance limitations.
- Verification of the concept of clustering of WPPs is to be made utilising an experimental setup, considering active power control and services related to it, such as frequency control and POD. Experimental validation of the models shall also boost confidence on the results achieved throughout the report.

The high-level objectives above have been particularised along the study, resulting in a more detailed scope of work, which is structured into different chapters of this thesis as follows:

- Chapter 4 – Offshore AC network control:
  - State-of-art controllers for offshore VSC-HVDC converters must be selected.

    - Their performance in terms of control of the passive WPP network must be assessed by using control theory tools.
    - Their performance in terms of control against another converter must be assessed by using control theory tools.
    - Effect of aggregating the WPP network and converters must be assessed through time domain simulations of the complete model.
    - A thorough discussion of the comparison must be proposed, resulting in a recommendation as for which controller performs best based on following criteria:
        - Stability
        - Robustness and independence of operating conditions
        - Applicability to clusters containing multiple WPPs and HVDC converters
        - Simplicity
- Chapter 5 – AC voltage control:
    - Steady-state behavioural characterisation of AC voltage controlling HVDC converters must be derived, both for operation within and at the VSC limits.
    - The influence of current limitation strategy on long-term voltage stability of a simple system must be analysed to understand the implications for both the power system and the control of active and reactive power of the HVDC station.
    - A discussion of the implications the previous bullet has on the control of what lies behind the HVDC converter, particularly a WPP, must be made.
- Chapter 6 – Power balance control:
    - Frequency control:
        - Selection and implementation of alternatives for provision of the service on a point-to-point VSC-HVDC connection of WPP must be made. Focus is on IR and PFC.
        - Assessment of realistic limitations imposed by long distance communication must be made.
        - Further limiting factors for efficient provision of the service must be pointed out.
        - Recommendation of most reasonable solution for delivery of frequency control onshore must be proposed.
    - DC voltage control:
        - DC voltage control service must be implemented on a WPP, namely a droop kind of control.
        - The control must be tested on a simple three-terminal HVDC network and its performance must be verified.
        - The impact realistic control and communication delays have on the efficacy of the service and the consequences for the system must be assessed.
- Chapter 7 – Power oscillation damping:
    - A controller for provision of POD must be installed on onshore VSC-HVDC station and offshore WPP, considering a point-to-point connection. Test of the control on simple and more complex systems must be conducted.
    - AVRs' effect must be included and thoroughly analysed. Conclusions in terms of robustness of POD service depending on network's voltage regulation capability must be drawn.

- Practical guidelines for approximate tuning of control parameters must be put forward, accounting for the above objective too.
- Assessment of potentially detrimental factors must be conducted, focussing on:
  - Delays: communication, WPPC, HVDC control.
  - WPP's power ramp-rate limitation.
- Other collateral effects on WPPs must be discussed:
  - Mechanical resonances.
  - WTGs' rotor speed stability.

- Chapter 8 – Experimental verification of clustering of WPPs:
  - Develop a CC that can dispatch signals to WPPCs with different characteristics.
  - Validate the simulation models with experimental facility.
  - Use the validated models to simulate and verify technical feasibility of clustering of WPPs for active power control and services related to it (frequency control and POD).
  - Use additional experimental measurements to validate the simulations above.
  - Provide recommendation for real implementation of such multi-WPP configuration.

Chapter 3 Modelling for simulation

In this chapter, modelling requirements for this study are discussed. Due to the different nature (temporal range, level of detail) of the studies to be performed, such an assessment cannot but start from a list of simulations to be conducted, which naturally yields modelling requirements. Afterwards, an overview of the simulation models is given, while the reader is referred to literature or Appendix 1 and Appendix 2 for further details. Average MMC models' adequacy is discussed with more emphasis at the end of the chapter. This chapter's subject was touched upon in Publications 4 and 5 as well [97], [98].

3.1 Introduction

The kind and level of detail of models for simulations and numerical computations is defined by the studies the models are used for, their purpose and desired level of detail. Discarding important facets during the conception and development of a model deprives the results of their validity and may lead to wrong conclusions. On the other hand, excessively accurate models may not add any significant value to the studies, though most likely requiring a much larger development effort. For this reason, this chapter starts out by listing the target simulation studies and formulating modelling requirements.

3.1.1 Target studies

The nature of the studies to be performed varies significantly from chapter to chapter in this thesis. Hence, the list of numerical calculations and simulation studies is divided by chapter in this section, listing their purpose too. Table 3 presents such list, while Section 3.1.2 will derive, from it, modelling requirements for each specific case. The description is kept generic, while the particular simulation setup will be detailed in the dedicated chapters.

Table 3 - List of calculations and simulation studies to be performed.

Chapter	Study	Purpose
3	Dynamic simulations of detailed, average and RMS MMC model, connected to DC line and stiff AC voltage source	Determination of adequacy of simplified models for the different kinds of studies (Chapters 4-7)
4	Bode and Nyquist plots for design of offshore HVDC converter controllers at no-load	Provide frequency domain visualisation of design, identify theoretical obstacles to optimal design, assess achievable performance
	Dynamic simulation of offshore HVDC converter connected to stiff DC voltage source and passive offshore AC network, controlling voltage and frequency	Verify design conducted in the calculations above
	Eigenvalue analysis of offshore AC network control with HVDC converter and lumped WPP converter, with different controllers and varying relevant parameters (operational scenario, electrical and control parameters)	Identify important factors influencing the control performance, compare control strategies
	Dynamic simulation of the system above, subject to variation of P and Q from WPP and/or voltage and frequency variations from HVDC converter or larger disturbances (outages)	Verify eigenvalue analysis through non-linear simulation and study large signal behaviour
	Dynamic simulation comparing results from aggregated and detailed WPP model	Assess to which extent the results from the above simulation can be extrapolated to a detailed setup
	Dynamic simulation of AC offshore network with multiple HVDC and WPP converters	Verification of applicability of control techniques to generalised offshore AC island and assessment of their performance
5	HVDC station capability curves and steady-state intersection between AC voltage droop provision and grid characteristics for varying SCR and operational point (P,Q)	Geometrical determination of equivalent SCR improvement provision from HVDC station for varying grid strengths
	Dynamic simulation of HVDC station connected to AC grid of varying strength and stiff DC voltage source, subject to a reactive power demand step at different P levels	Demonstration of concepts illustrated by the calculation above and quantitative assessment of equivalent SCR improvement
	Steady-state calculation of long-term voltage stability during converter current limitation	Illustrate the effect of different current vector prioritisation strategies on voltage stability
	Dynamic simulation of three bus system with load increase	Prove the correctness of the results from static calculation above
6	Dynamic simulations of VSC-HVDC link and WPP contributing to onshore frequency control (IR and PFC) with two different control schemes	Verification of capability for frequency control provision, assessment of impact of communication delay and other factors depending on control scheme
	Dynamic simulation of three-terminal HVDC grid with one WPP during loss of converter, with focus on DC voltage control	Verification of capability for WPP contribution to DC voltage control. Assessment of the implications its limited capability has on the rest of the system.
7	Modal analysis of simple and more complex system with VSC-HVDC and WPP contributing to POD	Determination of potential HVDC-connected WPP contribution to small signal stability. Support of parameter tuning guidelines. Illustration of effect of relevant parameters.
	Bode diagrams of closed loop form of POD from VSC-HVDC connected WPP	Illustration of influence of measurement feedback, DC link dynamics and other delays on stability and performance.
	Dynamic simulation of simple and more complex system with VSC-HVDC and WPP providing POD	Verification of above derivations by non-linear time domain simulation
8	Dynamic simulation of single WPP providing active power control, frequency control and POD and validation with measurements	Validate the simulation models for the rest of the chapter and boost confidence on the simulation results achieved throughout the thesis
	Dynamic simulation of a cluster of two WPPs with dedicated CC to perform coordinated frequency control and POD	Proof of concept of clustering of WPPs with very different characteristics

3.1.2 Modelling requirements

The variety of elements to be modelled, combined with the variegated nature of studies to be conducted, implies a rather diversified set of requirements on the minimum level of detail. Reported in Figure 6 is a qualitative sketch of modelling requirements for the main blocks of the models as a function of the frequencies of interest. The requirements are intended to be the minimum needed to achieve sufficiently solid results. The coloured boxes qualitatively draw the areas of interest for the different chapters, which determines the more detailed treatment in the next subsections, chapter by chapter. It should be noticed that, since those reported below are minimum requirements, when utilisation of detailed models does not excessively increase development and computational burden, models with a higher detail level than strictly required may be used. Moreover, as can be seen, the passive network elements can always be modelled by constant concentrated parameters.

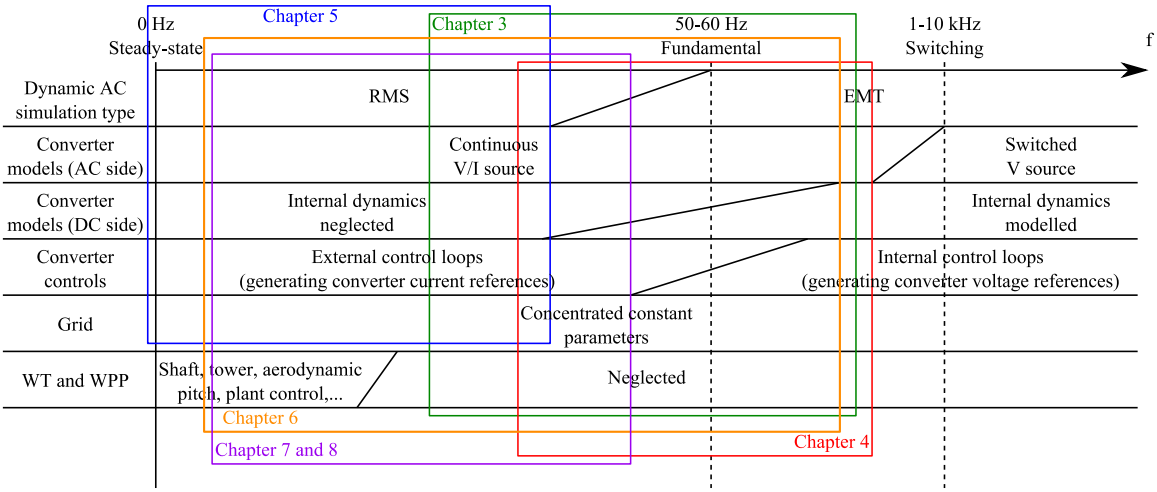

Figure 6 - Qualitative minimum modelling requirements for main blocks, chapter by chapter.

(a) Chapter 3

The simulations performed in Chapter 3 are intended to assess the accuracy of using built-in converter models of RMS type to represent VSC-HVDC converters, such as those available in DIgSILENT PowerFactory [99]. A number of publications have touched upon the topic, making use of models with different level of detail, e.g. [100]-[102]. Here, in Section 3.3, the focus is upon understanding the level of fidelity of built-in RMS models in terms of representation of the necessary dynamics to successfully conduct the studies in Chapter 6 and Chapter 7. On the other hand, some of the results derived in the literature are used to justify the modelling choices in Chapter 5.

The converter model to be used is a continuous average EMT model (as presented in [103], or Type 5 and 6 in [102]), including some internal dynamics of the converter (circulating current and its control), but lumping the converter arms' capacitors and switches into an equivalent controlled capacitor. The AC system is a stiff voltage source and the DC system should include supplementary converter capacitance, transmission line, and remote stiff DC voltage source. Only one HVDC converter station is looked at, so that the WPP model can entirely be neglected.

Besides the evaluation of RMS modes, the results of Chapter 3 also allow to justify the modelling choices in Chapter 4.

(b) Chapter 4

Chapter 4 poses the most onerous requirements in terms of BW. However, as a consequence of the scope being limited to (i) converter interaction with grid resonances and/or other converters and (ii) simulations lasting a few hundreds of ms, the number of elements to be modelled is reduced. Converter harmonic emission is out of scope, since it was treated elsewhere for WPPs [104], [105] and MMCs' harmonic generation in the relevant frequency spectrum is theoretically negligible. A modelling approach and analysis similar to what was presented in [106] can be used.

The focus is restricted to the offshore AC network, only including AC export and collection grid model and converters (HVDC and WPP). All converter models should be EMT type continuously controlled voltage sources behind reactor and transformer, their DC side being a stiff DC voltage source (independence of AC side control can be assured by decoupling means [23]). The detail level of the grid model and the number of WPP converters varies with the particular simulation.

Modal and frequency domain analysis relies upon linearized models that can be derived from the mathematical representation of the EMT model and/or be obtained numerically from the simulation model with e.g. Matlab Simulink.

Part of the results of Chapter 4, furthermore, constitute the bases for model and control selection in Chapter 6 and Chapter 7.

(c) Chapter 5

Chapter 5 requires the least level of detail because: (i) the focus is restricted to the onshore converter station and (ii) steady-state operation is concerned.

For steady-state calculations, the converter model can be a power, current or voltage source, depending on the specific assumptions. The built-in RMS PWM converter model [99] can be used to show the steady-state operating point can be reached by the dynamic model. Power control dynamics must be included, as well as the current vector limitation strategy. For a real demonstration, the dynamics of any OLTC should also be included, but are here neglected due to the focus being on the influence of the current limitation. A Thevenin equivalent can be used for the AC grid, and a stiff source for the DC side. Once again, the WPP needs not be modelled in detail.

(d) Chapter 6

The first part of Chapter 6 regards frequency control and slow DC voltage control with focus on the contribution the WPP can give to it. Converters can all be built-in RMS models as justified in Chapter 3. Their power control (P,Q,V_{DC},V_{AC}) loops should be modelled in detailed, while current control may or may not be neglected. The WPP model can be aggregated based on standard Type 4 WTG model [22]. Since the scope includes active power events spanning over several seconds, mechanical, aerodynamic, wind and pitch control model may be added to ascertain rotor speed stability. Most of the events are a concern of the WPPC, which should therefore be modelled. Due to the focus being mainly on WPP and VSC-HVDC, the power system model is generic and simple, but does of course include governor dynamics.

A discussion can be raised on the validity of built-in RMS models to represent sharp DC voltage changes, as is illustrated in Section 3.3. This is of concern in the second part of Chapter 6, where fast DC voltage control is addressed. However, the scope is limited to the contribution WPPs can give during such events, and the built-in models are deemed to provide sufficiently accurate

response for this purpose when their parameters are soundly tuned, since only overall DC grid dynamics are important and not so much their interaction with internal MMC dynamics.

(e) Chapter 7

Chapter 7 can essentially rely on the same requirements proposed for Chapter 6. However, it should be added that the power system model must include some kind of active power oscillation phenomena and ESs and AVRs must be modelled in detail on the conventional power plants. Moreover, the WTG mechanical model may include resonant modes such as shaft and tower. In these terms, a very detailed model should be used at a detailed design stage. The scope of this work, however, is to solely initially investigate the issues. Hence, only the shaft resonance is included to exemplify the problem, since it is the one with most readily available modelling and tuning information.

Frequency domain analysis can be done using the linearized model. When dealing with complex systems, reasonable approximations need to be accepted and numerical simulation may be used to extract some of the parameters. Modal analysis for very simple systems can be set up analytically, whereas in the case of large systems it is more conveniently provided by the simulation software (DIgSILENT PowerFactory in the present study).

(f) Chapter 8

The studies to be performed in Chapter 8 are essentially spanning over the same dynamic range as part of Chapter 6 (only frequency control part) and Chapter 7. As a consequence, the modelling requirements are also the same. However, a further simplification will be accepted, that is neglecting wind, aerodynamic and pitch control model for the WPP. This is allowed by the particular assumptions that will be further elucidated in Chapter 8.

3.2 Simulation models

The simulation models are briefly described in this section, from a high-level perspective. More detailed information is referred to in the literature where possible, or is included in Appendix 1 and Appendix 2. Some features of the models will be treated in the next chapters.

3.2.1 Power system

Based on the requirements introduced previously, power system models of a certain complexity are used only in Chapter 6 and Chapter 7. Power system modelling as a Thevenin equivalent (like in Chapter 3 and Chapter 5) is considered trivial and not described here. Two models are briefly illustrated in this section. As they are mainly based on state-of-art, built-in models, ample reference to literature will be given.

(a) Single machine model for active power balance and simple POD studies

Power system modelling for active power balance studies (PFC) is usually done through lumped mechanical equation and governing system blocks [76], [107]. However, since the chosen simulation software is DIgSILENT PowerFactory and the interaction of the power system with DC systems is also within the scope, a single machine model was implemented according to Figure 7. Moreover, the addition of a long line to be connected to an infinite bus allows the utilisation of the same system for simple POD studies as well. Sample data for the two cases (types of blocks and parameters) for the model are given in Appendix 1 and Appendix 2.

The dashed parts of the model need or need not be modelled based on the study. Generally:

- Active power balance studies would require modelling of load at Bus 1 and Governor and turbine. AVR and ES can be included, but the infinite bus V_B must not.
- POD studies require modelling of the infinite bus V_B and AVR and ES. The other dashed components may or may not be modelled, but will generally be neglected in order to reduce the complexity and only focus on the most fundamental mechanisms governing POD.

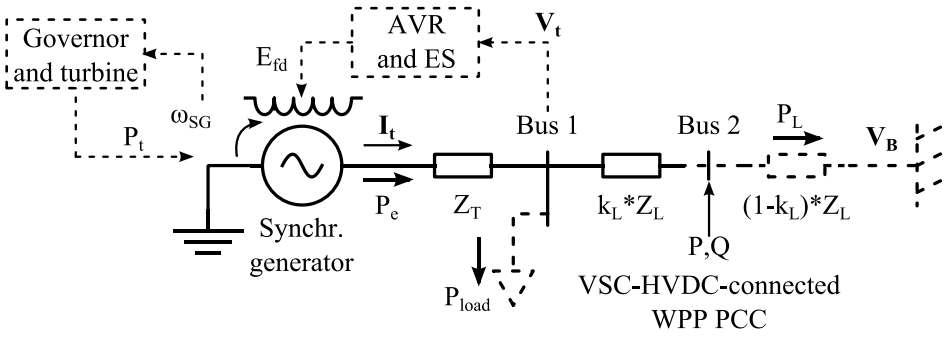

Figure 7 - Single machine model for active power balance and POD studies.

The synchronous generator model is a standard sixth order PowerFactory model [108]. Its parameters can be tuned to simplify it (e.g. 3rd order) if necessary.

(b) IEEE 12-bus system

Verification of some of the principles derived during the analysis of POD (Chapter 7) needs a slightly more detailed power system model, which is in this case the so-called modified IEEE 12-bus system model. It is described in detail in [44], [109] and their references. Here, only the system diagram is reported in Figure 8, where the connection point (Bus 1) of the VSC-HVDC connected WPP is also highlighted. Since they are very relevant in the investigations performed in Chapter 7, the AVR type and parameters are repeated in Appendix 2.

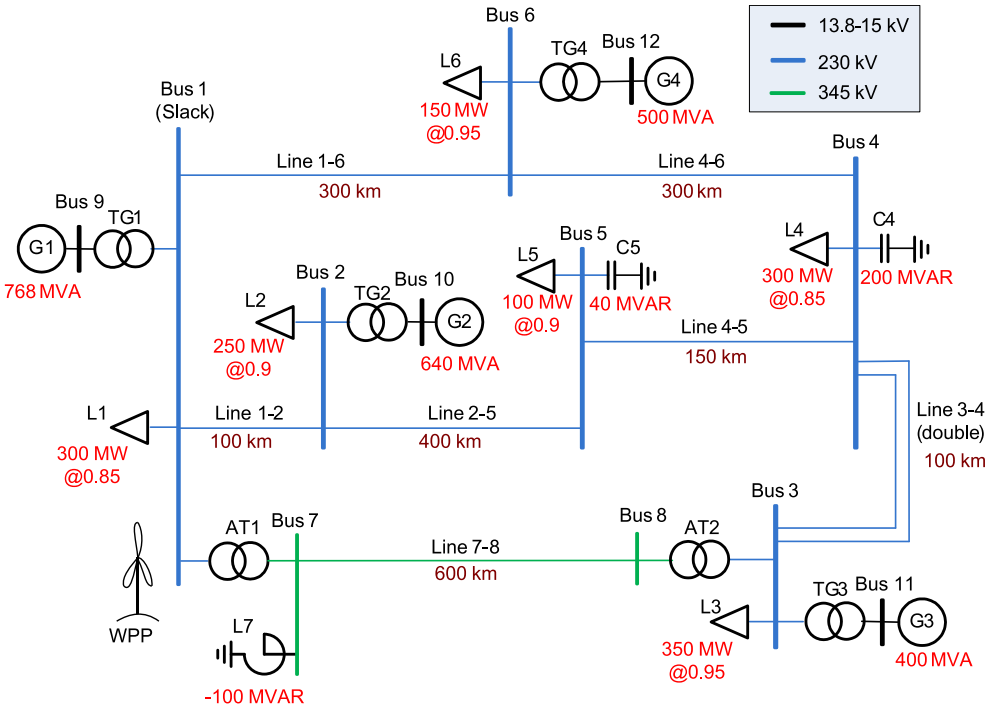

Figure 8 - Modified IEEE 12-bus system used for POD studies [109].

3.2.2 VSC-HVDC

A generic description of the model of one VSC-HVDC station is given in this section, including the high-level layout of the controllers. The functional diagram is independent of RMS or EMT implementation and can be used for both. The actual converter model is a voltage source. The section then continues by detailing three outer loop controllers, differentiating between onshore and offshore stations. More details are given in Appendix 1 and Appendix 2.

The per-unit single line model of one converter station is shown in Figure 9. The model is fully populated when it is given values for DC side capacitance (C_{DC}), phase reactor (Z_{ph}) and transformer (Z_T and Y_0) parameters. Appendix 1 describes how to obtain the model parameters from real converter circuit parameters. Besides, the magnitude and angle of the AC voltage source (V_C) are generated by the controller, while the DC current source is determined by energy conservation. Internal converter losses are disregarded. When acceptable, $Y_0 = 0$ will be assumed, and often, for brevity, the notation will be $Z_{conv} = Z_T + Z_{ph}$ or $Z_C = Z_T + Z_{ph}$. In general, AC voltages and currents will be vectors expressed in some coordinate system. Hence, the simplified notation in Figure 9 is used only for convenience.

In two- or three-level converters, a harmonic filter may be used to clean the output voltage waveform [83]. It usually behaves as a capacitance at fundamental frequency, thus also providing compensation for the reactive power consumed by phase reactor and transformer. In the majority of the simulations, it is here neglected for the following reasons:

- MMC stations do not need a harmonic filter.
- EMT simulations in this study, where modelling the filter would be important, are regarding the control of the offshore AC network (Chapter 4), where most likely there is a capacitive surplus due to the cables. As such, installing a capacitor for compensation purposes seems improbable, besides being costly for typical voltage levels at HVDC stations, especially offshore.

In some cases in Chapter 4, though, a capacitor is inserted and modelled as C_f, dashed in Figure 9.

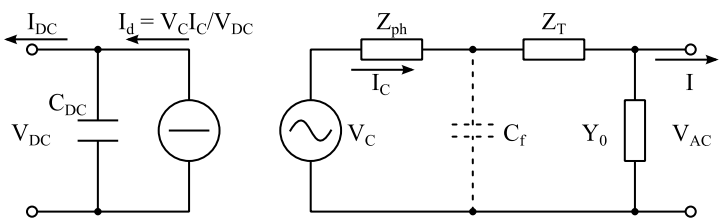

Figure 9 - Converter station electrical model, valid for EMT and RMS.

As for the control, Figure 10 depicts a generic functional diagram of it. The scheme is independent of whether the station is an onshore or offshore converter. The particular application will determine how each slot will be populated. Details on most of the blocks are given in Appendix 1 and Appendix 2, while some more information about the outer control block is reported in this section, presenting sample implementations for onshore and offshore stations. The *Angle selection* block allows to tap the desired angle reference, either measured by the PLL or internally generated in PLL-less applications (e.g. offshore). *P Droop* and *POD control* blocks will be described in more details in Chapter 4, Chapter 6 and Chapter 7 respectively. *Q Droop* is dashed as it is used only for offshore stations and is described in Chapter 4. Figure 11 shows that classical V_{AC} droop is performed in onshore HVDC stations in the block *Outer controller*.

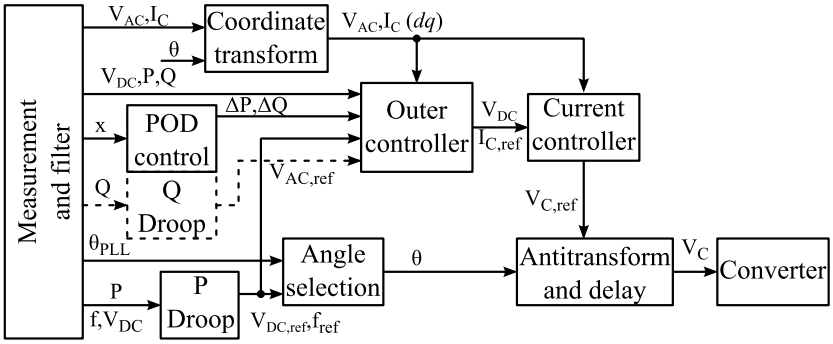

Figure 10 - Generic converter control model.

(a) *Outer controller:* Onshore station control

The *Outer controller* of an onshore HVDC station is generically that depicted in Figure 11. Implementation in SRF is considered, i.e. the controller generates current references on *dq* axes, with *d*-axis aligned with the reference voltage, as common practice in grid connected converters. Selectors (flags) allow switching between P and V_{DC} control, or a combination thereof and when running in P control, selection of closed- or open-loop control can be done. At the same time, Q or V_{AC} control or their combination can be performed, Q control being possible in closed- or open-loop fashion. Axis prioritisation in the current reference limitation block can be controlled by a flag (see Chapter 5 and Appendix 1 for further details). Considering units with PLL synchronised to the transformer's grid side terminals, the *d*-axis voltage v_d is the reference voltage (sensed by the PLL), namely V_{AC} in Figure 9.

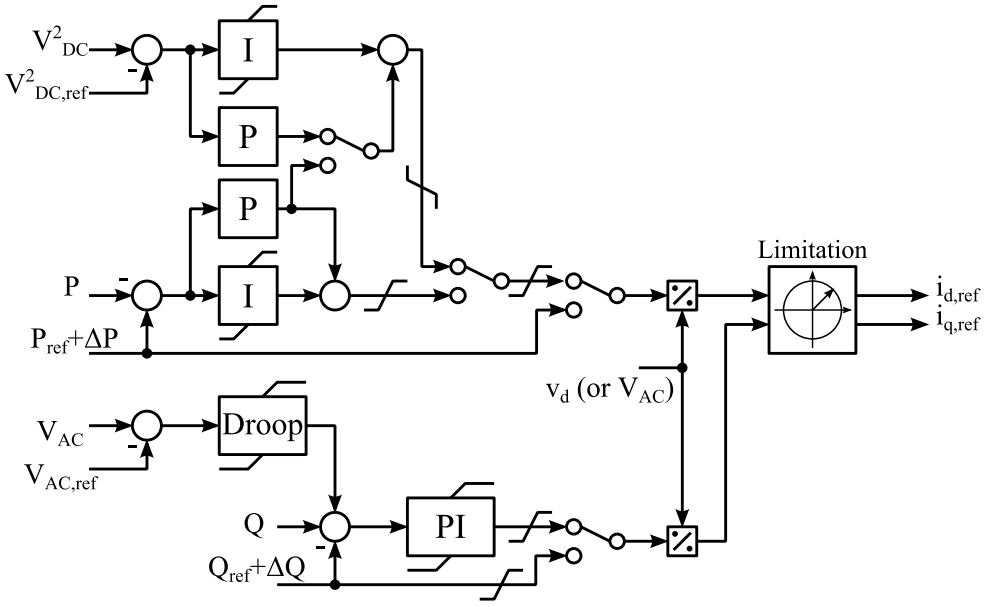

Figure 11 - Example of implementation of onshore station outer controller.

(b) *Outer controller:* Offshore station control

The *Outer controller* in an offshore station can, in this study, be selected among two different diagrams. More detailed explanation of them is given along with their design in Chapter 4. Here, only the block diagrams are reported. The nomenclature Option 1 and Option 2 is used, according to the treatment in Chapter 4, in Figure 12 and Figure 13 respectively.

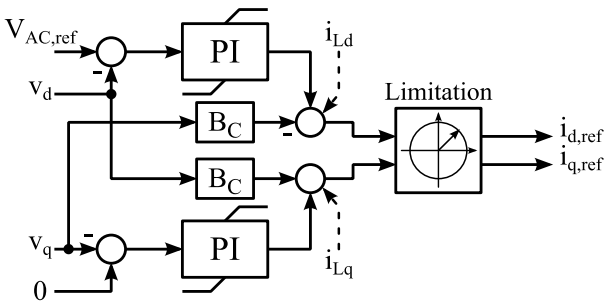

Figure 12 - Option 1 for offshore station outer controller – see Chapter 4.

Option 1 is realised according to [23]. The feed-forward of the load current $\mathbf{i}_{Ldq}$ is dashed because its utilisation depends on the actual configuration – see analysis in Chapter 4. The control is operating in SRF, usually synchronised to the PCC voltage (V_{AC} in Figure 9), but in some instances may be synchronised with the voltage over C_f (see Figure 9 and Chapter 4). Referring to the latter case, the feed-forward current would be $\mathbf{i}_{Ldq}$ = I, neglecting Y_0.

Option 2 exploits the technique exposed in [110] to bypass the current controller, which proportional gain is K_{pC} and has to be provided with a sufficiently low or nil integral gain. The scheme reported here, as exposed in [110], bypasses the current controller during normal operation but inherently offers current limitation at high currents. Reference [110] also describes a so-called power synchronisation mechanism, based on adjusting the voltage angle depending on the active power. It is not strictly needed in WPP application and is hence discarded here. It will however briefly be touched upon in Chapter 4. It should be noticed that without such power synchronisation mechanism, the scheme in Figure 13 is essentially an expanded version of that utilised in [15], with the addition of the active damping block G_{HP} and the integral voltage control action at the PCC. The reference feed-forward term with transfer function G_f may or may not be used.

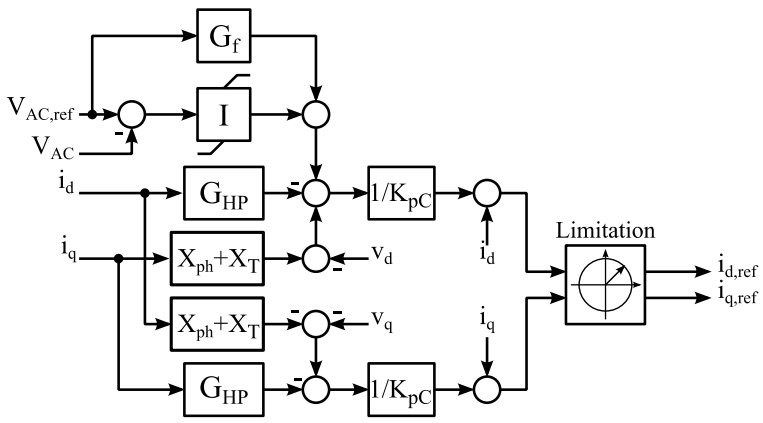

Figure 13 - Option 2 for offshore station outer controller – see Chapter 4.

3.2.3 Wind power plant

In EMT simulations, only the WTGs converter (distributed or aggregated) is modelled in detail. Electrically, it does not substantially differ from an HVDC station (Figure 9). A harmonic filter may be added in real applications [104], but is here discarded due to the fact that the focus of EMT simulations in this report is predominantly on the HVDC converters. Even the control is similar and relevant differences are discussed in Chapter 4. For this reason, the focus in this section is only on those simulations requiring an expanded WPP model and RMS solution type.

The model used in this study is built upon a kernel based on IEC standard 61400-27-1 draft [22]. Types 4A and 4B are used and scaled up to mimic an aggregated WPP. The models are expanded, when necessary (Chapter 6 and parts of Chapter 7) with pitch control, aerodynamic model and wind model, as described in Publication 9 [111].

Furthermore, some simulations in Chapter 6 and Chapter 7 need modelling of plant control (WPPC) dynamics. A WPPC was developed by expanding that found in Annex D of [22], according to the sketch in Figure 14. Sample parameters for all models are given in Appendix 2. Only the active power control loop is considered, as it is the only one being relevant throughout this report, owing to the decoupling guaranteed by the HVDC system and the fact that plant-level reactive power control in the offshore AC grid is out of scope.

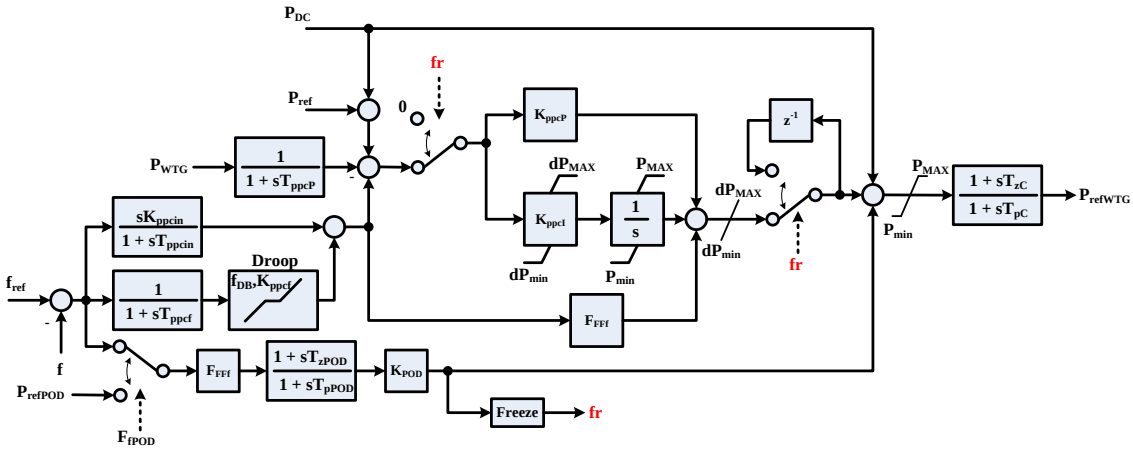

Figure 14 - WPPC: active power controller.

3.3 Model adequacy

When it is not possible to promptly evaluate model adequacy by validating it against real measurements or validated models, the target studies and subsequent requirements listed above, along with reasonable engineering judgement and published experience, are the only criteria to assess the solidity of the models in relation to the scope of work.

Based on the present scope of work and literature in the field, an assessment of the models validity could go along these lines:

- Power system modelling is well documented and sample data are readily available for essentially all typical power system components, such as SGs and their controllers, transmission lines, transformers, etc. – see e.g. [76], [107], [112], [113]. The level of detail adopted here is deemed to be solid enough for the scope.
- Modelling of VSC-HVDC systems, especially based on MMC technology, is still subject of research [97], [100]-[102], [114] and knowledge about different models' validity is being generated. Generally, events regarding abrupt disturbances on the DC side of the converters and/or blocking-deblocking of the IGBTs are the most critical to be reproduced by reduced models [100], [115]. Chapter 6 regards sudden power imbalances on the converter's DC side. Although such events are not as dramatic as DC faults, some more stress is put in this thesis on the adequacy of simplified models during such contingencies, by the analysis presented below in Section 3.3.1. The discussion also includes POD events.

- Modelling of wind power for power system studies is more mature a discipline than modelling of MMCs and standardisation bodies are releasing WTG models that can reliably be used [22]. However, power system studies of large duration (above several seconds) may need additions to such models. For example, the need to curtail active power, or boost it above the MPPT, or the presence of non-negligible wind variations may call for implementation of wind, aerodynamic and pitch model [33], [116]. References on modelling are available in the literature [21] and can be relied upon for the development of models. Features such as WPPCs may have to be modelled based on reasonable assumptions. To the author's opinion, the models used in this study are well suited for the scope. A few most relevant limitations may be stated here:
    - The mechanical model only includes the shaft resonance. As shown in [33] for IR, and considering that POD is also within the scope, a tower model would provide more fidelity. Neglecting the tower does not significantly affect the results shown here. However, it must definitely be taken into account when dialoguing with OEMs and implementing POD in real life.
    - Detailed information about WPPCs was not available, the implementation being based on reasonable assumptions, more generic available knowledge and state-of-art grid code requirements – e.g. [30], [31], [32], [42], [43],.

  It should also be noted that more confidence on a large part of the WPP models was gained by experimental verification as described in Chapter 8.

3.3.1 VSC-HVDC model evaluation

Most evaluations of MMC model adequacy in the literature [100]-[102] conclude that the converter station as seen from the AC side essentially behaves in a way that can satisfyingly be approximated by the simplified model in Figure 9. The same conclusions were reached in Publication 4 [97].

For studies where a proper representation of the DC side is needed, according to the above cited sources the fidelity of simplified models impoverishes. DC side faults and converter blocking phenomena are out of the scope here, but some interesting properties of the converters' DC side are worth highlighting, since power balance in DC grids, subject of Section 6.3, implies abrupt power imbalances on the DC side. This will help understand possible limitations of the study.

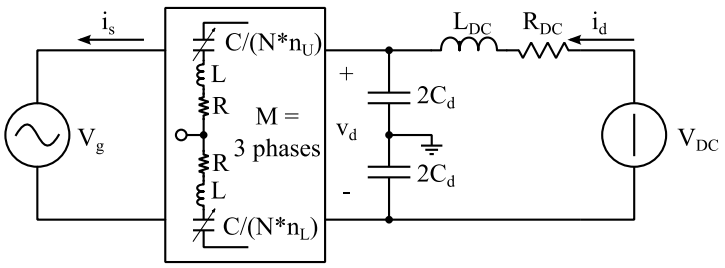

Figure 15 - Average MMC model [102] for model adequacy study.

Since the assessment does not involve faults and IGBT blocking events, but only smaller nearly-linear disturbances, the analysis will be done with an average MMC model like that presented in [103]. However, the control and dynamic analysis is updated according to the more recent publications [117] and [118]. All nomenclature in this section is the same as that used in [118]. The MMC model is connected to a stiff AC voltage source and expanded on the DC side as shown in Figure 15. The model was implemented in Matlab/Simulink. Sample parameters are

reported in Appendix 2. Grounding of the source V_{DC} is not considered here. The AC side may be assumed to be connected to a delta or groundless star transformer: hence, any zero-sequence (pole unbalanced) on the DC side, would remain within the DC network. Mid-point grounding of the DC side voltage source is here disregarded.

According to the theory developed in [118], after some manipulation, the DC voltage dynamics are governed by the following equation:

$$C_d^{'}\frac{dv_d}{dt}=\left(C_d+\frac{2MC}{N}\right)\frac{dv_d}{dt}=i_d - \frac{MP}{v_d} \tag{1}$$

Assuming P as an input, the equation can be linearized and put in state space form with states i_d and v_d. Adding the DC line dynamics governing i_d with V_{DC} as input, the following state space model is derived:

$$\begin{pmatrix}\frac{dv_d}{dt}\\ \frac{di_d}{dt}\end{pmatrix}=\begin{bmatrix}\frac{MP_0}{C_d^{'}v_{d0}^2} & \frac{1}{C_d^{'}}\\ -\frac{1}{L_{DC}} & -\frac{R_{DC}}{L_{DC}}\end{bmatrix}\begin{pmatrix}v_d\\ i_d\end{pmatrix}+\begin{bmatrix}-\frac{M}{v_{d0}} & 0\\ 0 & \frac{1}{L_{DC}}\end{bmatrix}\begin{pmatrix}P\\ V_{DC}\end{pmatrix} \tag{2}$$

Writing the characteristic equation of such second order system, one obtains the following:

$$\lambda^2+\lambda\cdot\left(\frac{R_{DC}}{L_{DC}} - \frac{MP_0}{C_d^{'}v_{d0}^2}\right)+\frac{1}{L_{DC}C_d^{'}}\left(1 - \frac{MP_0R_{DC}}{v_{d0}^2}\right) = 0 \tag{3}$$

Interesting observations can be made on such equation:

- The natural frequency ω_0 of the system varies with the initial active power P_0, but does so very slightly, due to the small value of R_{DC}.
- The system's damping factor ζ too varies with P_0 and more significantly than ω_0 does. In particular, the damping factor deteriorates as the power injection into the AC system increases. This is proven by Figure 16, where the DC side's response to 0.2 pu positive steps in i_d is shown for different initial operating point (P_0,v_{d0}).

The minimum value of C_d' to always guarantee stability independently of the control is derived by forcing the coefficient of λ to be greater than 0. For the worst case, i.e. MP_0 = 1 pu, and for reasonable values of R_{DC}, L_{DC} and v_{d0} (e.g. those reported in Appendix 2), minimum C_d' is in the order of 10-20 ms. Choosing the cell capacitance C according to the guidelines in [70] usually yields $\frac{2MC}{N}$ very near to such figure, meaning that a small C_d is sufficient to ensure stability, although performance dependence on the operating point still exists. It should be noticed, however, that a similar behaviour in terms of DC side resonance is exhibited by a two-level converter, the only difference being that MMCs provide a default amount of capacitance and decrease the requirements on C_d. Phenomena more specifically related to the interaction between the DC system and the internal dynamics of the MMC have not been noticed, and all the simplifications proposed in [118] are reasonable when using the average model. Other criteria may play a role in determining the value of C_d, but it is not possible to investigate this with an average model and more detailed modelling of the MMC is out of scope.

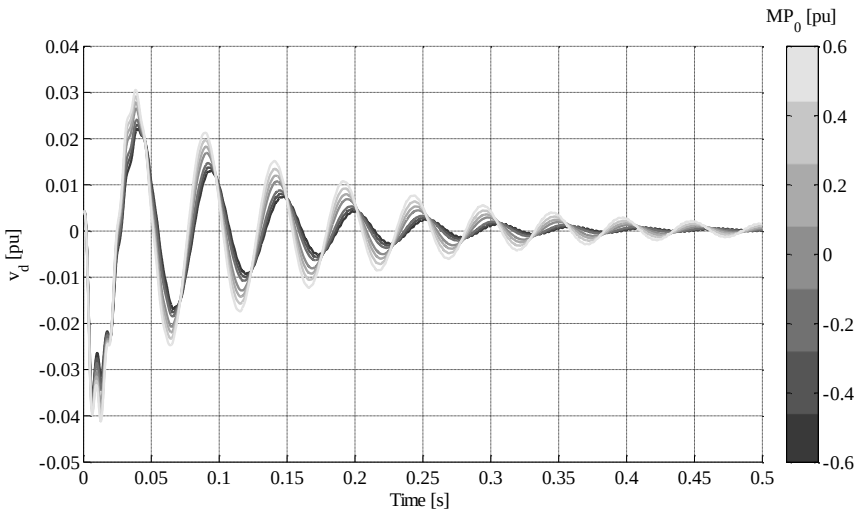

Figure 16 - DC side dynamic performance dependence on MMC active power.

A further test consists of three *d*-axis reference current ($i_{d,ref}$) steps, followed by a sinusoidal modulation of $i_{d,ref}$ with amplitude 0.1 pu and frequency 2 Hz, which can be considered as a sample POD signal to be tracked by the converter. The results are shown in Figure 17. The oscillating signal can be considered as a worst-case for POD, at least in terms of frequency [44].

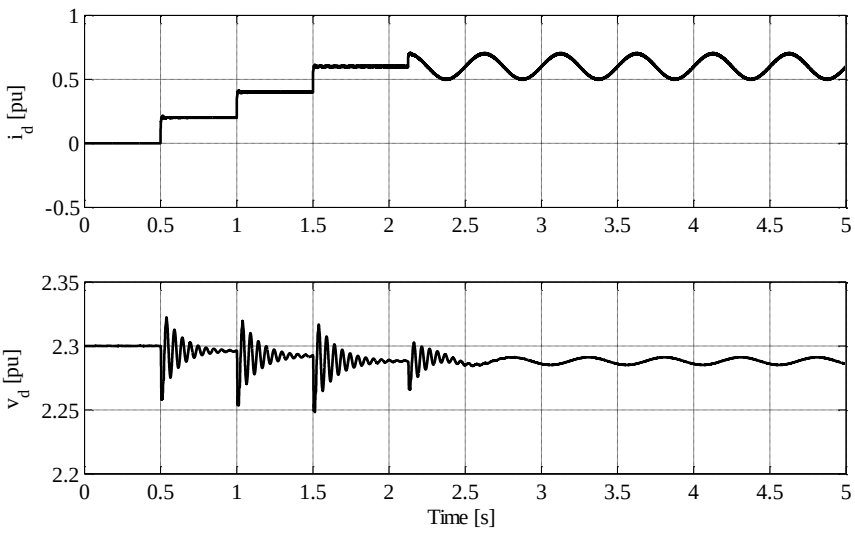

Figure 17 - Response of average MMC model to i_d current reference steps and POD signal.

The model responds well: the current steps are tracked quickly according to design and, as a consequence, the POD signal is also followed satisfyingly. The same would happen for simplified, built-in RMS models in PowerFactory.

From these brief examples, it can be concluded that, for the events within the scope of this study, the model proposed in Figure 9 can be used with sufficient confidence. To rightly represent the dynamic behaviour of the DC side, it is important to obtain, from the literature or from the manufacturer, reasonable estimations for (i) the value of cell capacitance and number of levels per arm and (ii) the additional capacitance added on the DC side. For the latter, the derivations above should be corroborated by manufacturer's data, since other design criteria than those considered here may come into play.

Besides the simulations shown here, the results presented in Publication 4 [97] are also supporting the choice of simplified models, especially concerning the AC side.

Some level of uncertainty is still present with regard to the behaviour of the DC side and in particular any possible interaction between internal converter dynamics and DC system. More detailed modelling of MMCs would be needed for a very thorough assessment and is considered out of scope.

3.4 Summary

In this chapter, an overview of the models utilised in this study was given. Models for the power system, the WPPs and the HVDC converter stations were described. The adequacy of power system models is justified by reference to the ample availability of public information on the subject. The assumptions behind modelling choices for WPPs were stated, supporting their validity for the scope and pointing out the main limitations to be addressed for better solidity of the results. More emphasis was put on the adequacy of VSC-HVDC models, as a consequence of the limited knowledge available on modern MMCs. Bearing in mind the scope of the present study, reference to relevant literature and own publications was given to support the chosen model. Moreover, sample simulations from an average MMC model implemented in Matlab/Simulink were shown to further boost confidence on the simplified model's fidelity.

Chapter 4 Offshore AC network control

This chapter regards the operation and control of the AC network placed behind the offshore VSC-HVDC converter. The reason to why it is relevant to look at this topic is initially given, outlining the open questions and main challenges and describing two state-of-art control techniques that may be employed at the offshore HVDC station. The two control options are compared firstly for operation at no-load, i.e. when only the passive elements in the network have to be maintained energised. Thereafter, the same comparison is performed when a WPP is connected in the network and producing power. As a final step, the expansion of the system to a more generic AC island with multiple WPPs and HVDC converters is analysed. The conclusions of the chapter are a recommendation of control candidates for each case, a best practice for parameter tuning and an assessment of the influence several factors have on the stability and performance. The results presented here were partially included in Publication 8 [119].

4.1 Introduction

As briefly hinted in Chapter 2, in recent studies on VSC-HVDC connection of WPPs, the control of the offshore HVDC station is often presented as a default block [15], [83] and little justification is given in terms of which control strategy is best, how the control parameters are tuned and which challenges may be encountered in the implementation. Since such offshore AC grids are dominated by PE converters and may, in case of utilisation of Type 4 WTGs, be effectively inertia-less, their control and operation is not a trivial subject.

Moreover, current and future prospects are that (i) multiple WPPs may be connected behind an offshore HVDC station (see Table 2) and (ii) offshore AC networks may eventually even host multiple HVDC converters [92], [120]. This respectively means that (i) different converter and WTG topologies and controls may be accommodated in the offshore AC grid and (ii) the master-slave approach used to date in VSC-HVDC connection of WPPs may need to be abandoned in favour of a more generic and universal control paradigm, to allow for flexible, robust and reliable control of the power flows in the offshore network and towards shore.

A number of publications have partially looked into these topics – see e.g. [85]-[87] [120], [121] – but further research is needed in the area. More generic literature on control of PE converters is helpful too in carrying out the desired analysis [23], [24], [80].

In this report, in order to restrict the scope of work and considering short-term developments, the following basic assumptions are accepted:

- The focus is limited to investigating the influence of the control of HVDC converters, while the WTGs will be assumed to have standard GSC controls, based on SRF PLL and inner fast current control operating in SRF, as for example described in [24]. Further research will be needed to drop this assumption if a distributed kind of control as that described in e.g. [87] is to be investigated. Moreover, stability investigations as seen from the WTG converter were previously performed for example in [104], [105].
- The WTGs are all Type 4 machines. In the context of this chapter, using Type 3 WTGs may lead to substantially different results, depending on the considered control events. Research has been published on the connection of Type 3 machines to HVDC [89] but more work is definitely needed and is not covered by this chapter.

This section continues by illustrating in more detail the two control candidates for the offshore HVDC converters. The main control principles are discussed and more advanced control strategies are not considered, as no information from manufacturers is readily available in such terms. Also, the relevant system configurations are briefly described. With respect to what described in Section 2.4.3, the focus is restricted to the AC offshore network and a slightly higher level of detail is used.

4.1.1 State-of-art control candidates

The state-of-art control candidates for an offshore HVDC station were briefly outlined and illustrated in Section 3.2.2(b). A distinction in two control families can roughly be made as follows and will be the base for the remainder of this chapter:

- Controller relying on internal fast current control and external voltage control. Usually, in the literature such configuration is synthesised in a vector control. The approach is described in e.g. [83], [86], [120] and the design principles can be found in [23].
- Controller directly performing voltage control. In the literature, such solution can take more or less complex forms and include supplementary control features or not, such as voltage angle control, active damping of network resonances, etc… Examples of such technique are [15], [80], [89] and one may infer that [85], [87] too make use of a similar approach, although it is not fully clear from their description.

Generally, the HVDC converter control layout is as was described in Section 3.2.2 and depicted in Figure 10. In order to distinguish between control candidates, however, the scheme in Figure 18 is more helpful. The sketch is simplified to allow for understanding of the principles and the distinction between Option 1 and 2 essentially reflects the control families above. More details about the particular implementation adopted in this chapter are given below.

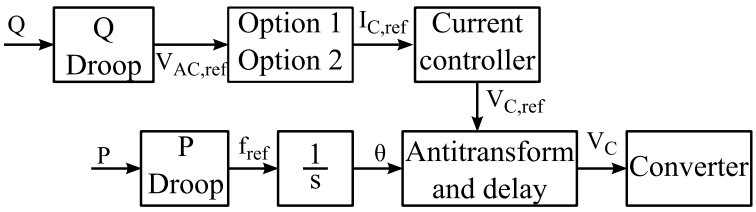

Figure 18 - Generic simplified offshore HVDC converter control layout: for description of Options 1 and 2 refer to Figure 12 and Figure 13.

Active and reactive power droop (blocks *P droop* and *Q droop*) are strictly necessary only in Section 4.4, where multiple HVDC converters need to properly share active and reactive power flows. The difference between the two controls lies in the block generating current references ($I_{C,ref}$), while all other blocks essentially have the same structure for both options. In particular, the *Current controller* block is in both cases implemented through a typical scheme – Appendix 1.

(a) Option 1

Control Option 1 makes use of a vector voltage control in *dq* coordinates aligned with the PCC voltage V_{AC} (see converter model in Figure 9). The current references are generated according to Figure 12 and are expressed by the following relations:

$$i_{Cd,ref} = K_{pV}\left(1+\frac{1}{sT_{iV}}\right)\left(v_{d,ref} - v_d\right) - B_C v_q \ (+\, i_{Ld}) \tag{4}$$

$$i_{Cq,ref} = K_{pV}\left(1+\frac{1}{sT_{iV}}\right)\left(v_{q,ref} - v_q\right) + B_C v_d \ (+\, i_{Lq}) \tag{5}$$

where B_C is the susceptance of the shunt capacitance connected at the PCC and v_d,v_q are the SRF components of V_{AC}. This could, depending on the design, mainly consist of AC cable capacitance or a shunt capacitor purposely placed at the converter terminals. The assumption is that other shunt currents (losses, transformer magnetisation) are negligible. In the specific application, without the loss of generality, the voltage references will be $v_{d,ref} = V_{AC,ref}$ and $v_{q,ref} = 0$. The PCC may also be placed between converter reactor and transformer, using a dedicated capacitor, as shown with dashed component in Figure 9 and elucidated later in this chapter.

The main advantage of this control structure is that it automatically offers current control capability, which is paramount to protecting the converter's IGBTs.

(b) Option 2

In Option 2, the current references are generated according to Figure 13, where most of the terms are added in order to cancel out the effect of the *Current controller*, which is also in this case a standard vector current control with nil integral gain. The SRF is without losing generality aligned with the converter voltage V_C, as could be noticed in Figure 13. In reality, taking into account the cancellation mentioned above, the control law will simply turn out to be:

$$v_{Cd} = \frac{K_e}{s}\left(V_{AC,ref} - V_{AC}\right) - G_{HP}(s)\cdot i_{Cd} + G_f(s)\cdot V_{AC,ref} \tag{6}$$

$$v_{Cq} = -\,G_{HP}(s)\cdot i_{Cq} \tag{7}$$

where the block $G_{HP}(s) = \frac{sk_v}{1+sT_v}$ serves as active damping for grid resonances [80] and $G_f(s)$ is a feed-forward transfer function. The block *Current controller* would therefore be superfluous, and the converter voltage V_C could be generated directly according to Eqs. (6) and (7). The approach above is used only to be able to make use of the same control structure for both options. Moreover, if current limitation is necessary, during e.g. faults, this technique can provide automatic means to guarantee proper control of the current as described in [80]. This overcomes the main disadvantage of Option 2, that is the lack of any inherent current control capability.

4.1.2 Offshore AC network configurations

The network configurations relevant along this chapter are described here, with a few more details with respect to what done in Section 2.4.3. The focus is restricted to the offshore AC part of the grid and the WPPs. The reference WPP is taken from a real study case. It is rated 996MW,

employs 166 WTGs and consists of three sections generating a rated power of 318 MW, 336 MW and 342 MW respectively. The complete PowerFactory layout of the WPP is reported in Appendix 1 (Figure 115 to Figure 119). However, lumping of the WTG converters is performed, as illustrated in Figure 19 and Figure 20.

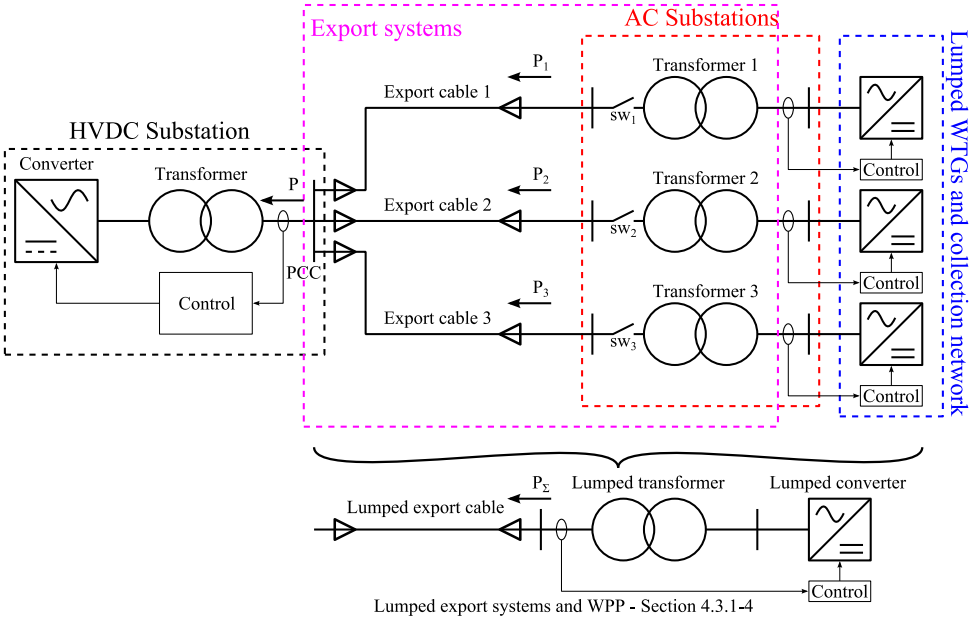

Figure 19 - Offshore AC network configuration with single HVDC converter and lumped WPP converters.

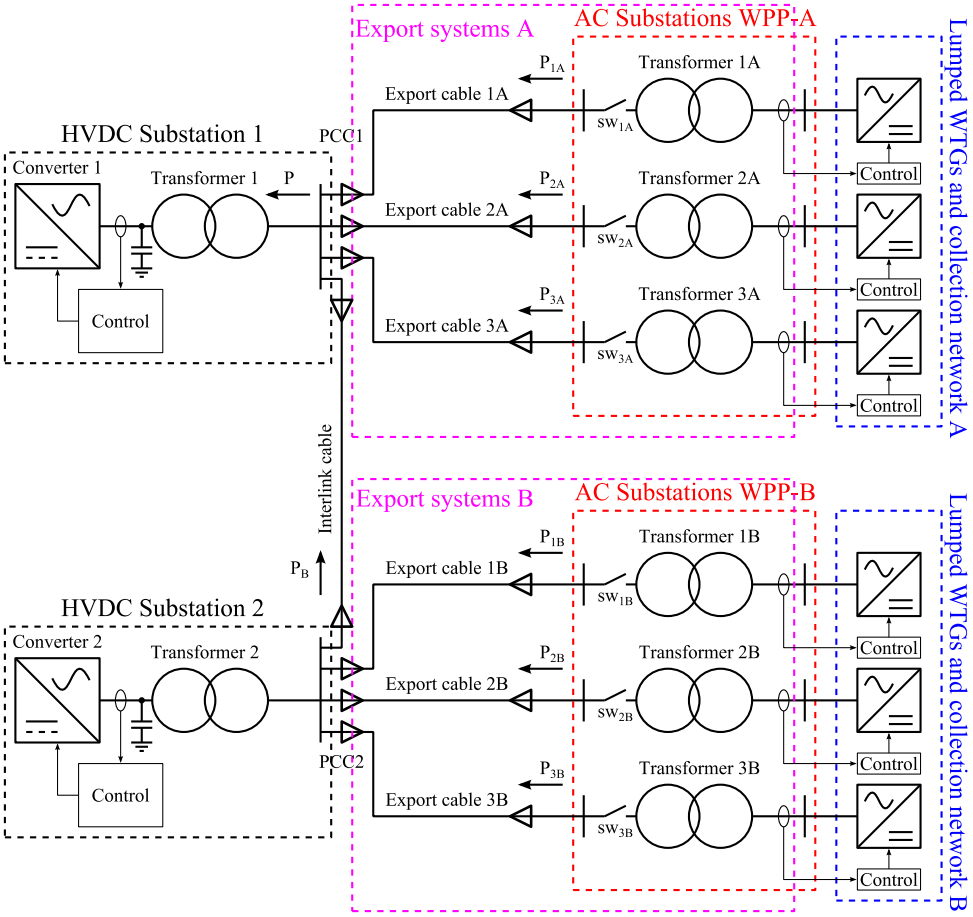

Figure 20 - Offshore AC network configuration with two HVDC converters and lumped WPP converters.

Figure 19 is valid for Sections 4.2 and 4.3. In part of the latter, aggregation of all WTG converters into one single converter is performed, as depicted at the bottom right of the figure. Figure 20 refers to the scenarios that will be simulated in Section 4.4. In this case, the WTG converters are lumped according to each WPP section.

Example mathematical modelling details for the first setup are reported in Appendix 4, while a EMT-type dynamic simulation model was created in DIgSILENT PowerFactory for each of the four cases generated by the permutation of circuit configurations and control options above.

4.1.3 Network impedance aggregation

The assumptions introduced earlier imply, besides the lumping of WTG converters, some sort of aggregation of the network impedance. In particular, all the collection network impedance is practically neglected when performing the aggregation shown in Figure 19 and Figure 20. Such aggregation was discussed analytically and empirically in [104]. Here it is briefly discussed again, but looking at it from the HVDC converter terminals.

Referring to Figure 19, the network admittance as seen from the converter internal terminals (voltage source V_C in the HVDC converter model – see Figure 9) is plotted in Figure 21 as a function of the frequency for different configurations:

- *Exp3*, *Exp2-3* and *Exp1-2-3* depict the impedance when the export systems of WPP section 3, sections 2 and 3 and sections 1, 2 and 3 are connected. The export system includes the AC export cables between HVDC station and AC substation and the substation transformer.
- *Coll* refers to the case when the three collection networks behind the AC substations are inserted, including array cables and WTG transformers. The WTGs are open circuits.
- *WTGs* is identical to the case above, but the WTGs are modelled as ideal voltage sources with a 10% series reactor.

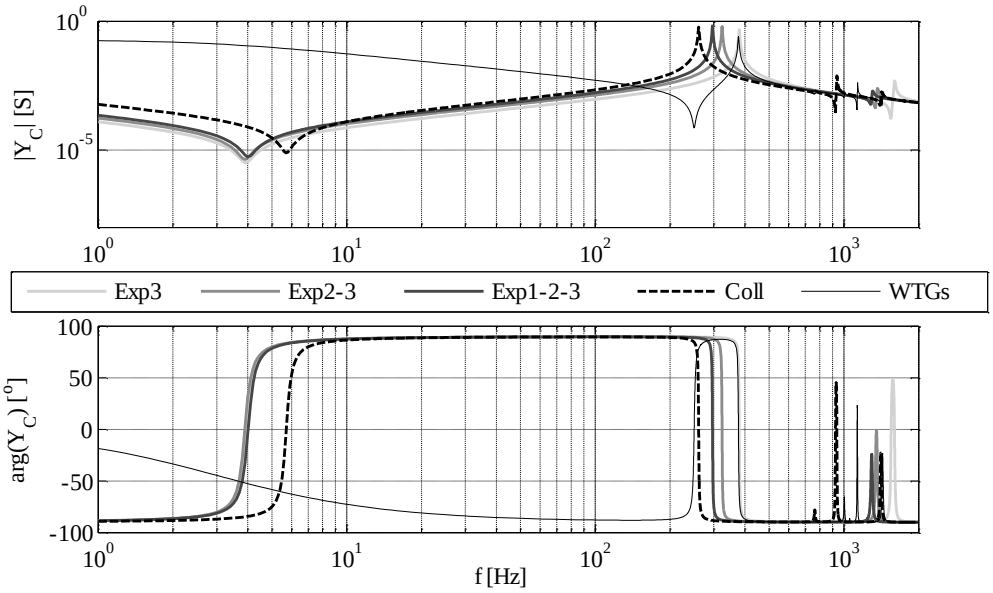

Figure 21 - Offshore network admittance as seen from the HVDC converter. Legend: see explanation above.

The following interesting remarks can be put forward by inspection of Figure 21:

- The influence of the export systems on the resonant peak around 300 Hz is very significant, due to the amount of capacitance each export system contributes with. This means that the controller will see significant differences in the impedance and it must be sufficiently robust to deal with such variations.
- The further capacitance inserted with the collection network contributes to an additional reduction of the resonant peak's frequency. A small influence is observed on the negative resonant peak around 5 Hz too (related to the magnetisation impedance of the transformer). However, this should be less critical as it is a negative peak and is both far from the target frequency (50 Hz) and well below usual current control BWs. It may however cause poorly damped voltage oscillations.
- Modelling of WTGs by ideal voltage source re-equilibrates the LC ratio in the network, bringing the positive resonant peak back to the frequency it has for case *Exp3*. Moreover, a large shift of the negative peak is observed due to the fact the parallel resonance happens with an inductance dramatically lowered by the short circuit in the WTGs. However, as widely discussed elsewhere [104], modelling of WTGs as voltage sources is not realistic at low frequency, where they behave more like a current source. Beyond the control BW they can be considered uncontrolled voltage sources, while their behaviour is intermediate at transition frequencies.
- Other minor resonant peaks at higher frequencies are influenced by the extension of the connected network. However, such peaks should be less critical than the main spike around 300 Hz.

From the above observations it is concluded that, in general, it should be enough to account for the export systems when looking at the network impedance from the HVDC converter terminals. However, one should be aware of the realistic range of variation of the resonant peak's frequency depending on the number of export and collection systems connected.

Remark 1: relevant frequency range

As observed in Figure 21, the frequency range is limited to 2 kHz. This is done since the switching frequency is assumed to be 1950 Hz (state-of-art for two-level converters) and the control BW cannot extend beyond that (in reality it theoretically cannot be more than the Nyquist frequency [104] and is usually limited to an even lower value [122]). The range may vary with MMCs, where equivalent switching frequencies can be higher, but even considering switching frequencies in the range of 10 kHz [70] and common guidelines for the inner control BW [122], the 2 kHz limit still preserves its approximate validity.

4.2 No-load operation

4.2.1 Introduction

The performance of the two control strategies outlined in Section 4.1.1 when the HVDC converter simply maintains the offshore AC network energised is evaluated in this section, by means of frequency domain analysis with Bode and Nyquist plots, corroborated by time domain EMT-type dynamic simulations. It should be noticed that such operational scenario is not relevant only for initial energisation of the offshore AC network, but also when the WTGs are offline or not producing power for any other reasons (no wind, maintenance, etc…).

Conclusions are drawn in terms of control parameter tuning, influence of network and control parameters on the performance and inherent limitations. Moreover, a recommendation of what objectives should be pursued by more specialised controls than those considered here is proposed.

It should be emphasised that all electrical components are considered linear in this study. Non-linear phenomena related to energisation such as transformers' in-rush currents and the like are neglected and the focus is purely on stability in linear conditions. Energisation with more detailed models has been the subject of Publication 18 [123] and other publications from the same main author. For this reason the term *no-load* is used here, rather than *energisation*.

4.2.2 Design of HVDC converter controller at no-load

The design of the two control candidates is illustrated here, based on frequency domain analysis.

(a) Option 1: current control design

As a common practice, with nested controllers as in Option 1, the design is performed starting from the faster internal loops and then designing the outermost loops. Within the present scope, two loops must be tuned, starting from the internal current control. The diagram depicted in Figure 22 and borrowed from [104] can be used for the design, along with classical guidelines from the literature – see e.g. [23], [24], [124]. The scheme in Figure 22 assumes a PI current controller with cross-decoupling of reactor and transformer voltages ($G_{PI}(s)$). The converter delay (modulation, dead times, etc…) is included in $G_{VSC}(s) = e^{-sTd}$, where T_d is the lumped time delay and the transfer function is expressed in the static reference frame.

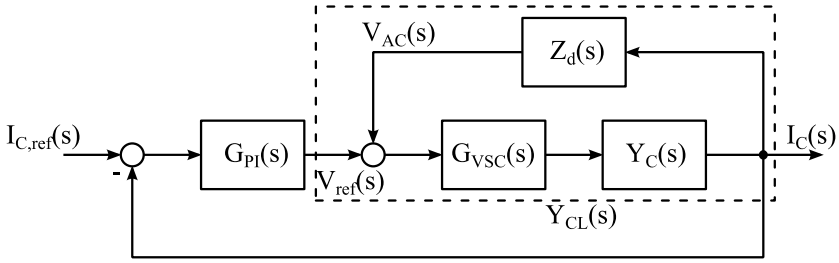

Figure 22 - Laplace domain block diagram for standard design of current controller.

Moreover, recalling the converter electrical model in Figure 9, it is:

$$Y_C = \left[(Y_0 + Y_N)^{-1} + Z_{conv}\right]^{-1} \tag{8}$$

where Y_N is the network admittance as seen from the converter terminals and $Z_{conv} = Z_{ph} + Z_T$, assuming the control is performed at the grid side of the transformer, as depicted in Figure 19. The branch with gain $Z_d = (Y_0 + Y_N)^{-1}$ represents the terminal voltage feed-forward usually employed in current controllers for disturbance rejection [104]. The usage of such loop may be questionable in this application, since the voltage is directly controlled by the converter and the occurrence of a *disturbance* in the sense typically meant in grid connected applications may not be so likely. The alternatives to using such loop are (i) avoid any kind of feed-forward and (ii) feed forward voltage references instead of actual measured voltages. Such alternatives will be briefly discussed below.

Well-known guidelines can be found in the references cited above to tune the parameters K_{pC} and T_{iC} of the current controller. Usually, after per-unitisation of all quantities, a suggested value for

the proportional gain is $K_{pC} = \omega_C L_{conv}$, where ω_C is the target BW and L_{conv} the inductance of the converter (reactor and transformer). The integral action, on the other hand, can be small, solely to make up for non-negligible losses and small parameter uncertainty. Targeting a BW ω_C = 1000 rad/s, the rules above yield the parameters listed in Table 4.

As mentioned above, due to the fact that the HVDC converter is responsible for regulating the voltage in the network, using a feed-forward of voltage V_{AC} as in Figure 22 may be substituted by feed-forward of voltage references or no feed-forward at all (both options yield the same, feedback, current control performance and design). In the block diagram, this is equivalent to assuming Z_d (s) = 0. If one does so, considering for the sake of example that only export system 3 be connected at the HVDC converter terminals, the Bode diagrams in Figure 23 are generated for open- and closed-loop transfer functions $G_{ol,CC}$ and $G_{cl,CC}$. It is important to notice that all transfer functions have been transformed into the static reference frame (αβ coordinates), using the derivations presented in [125], [126].

Table 4 - Option 1: HVDC converter current control parameters.

Parameter	Value	Unit
K_{pC}	0.88	pu
T_{iC}	0.01	s

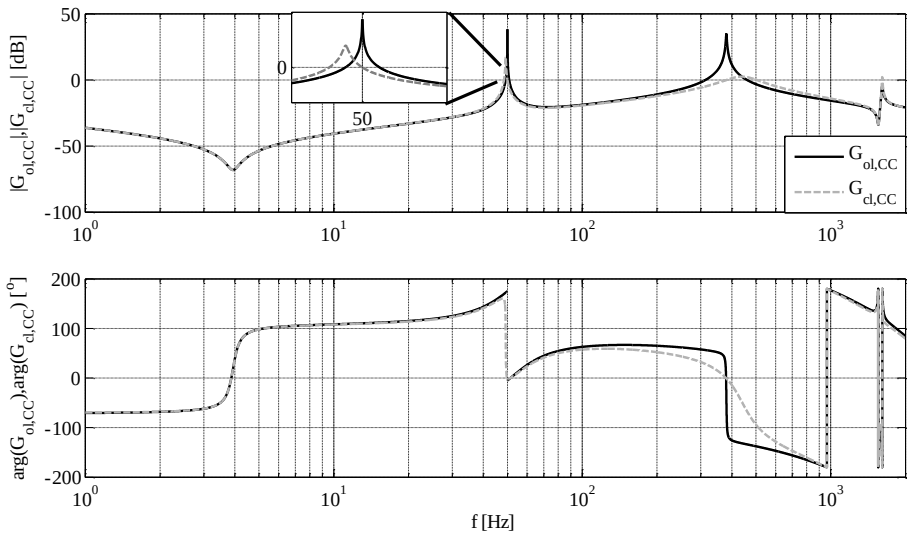

Figure 23 - Open- ($G_{ol,CC}$) and closed-loop ($G_{cl,CC}$) transfer functions for current control problem with Z_d = 0.

The following is clear by inspecting Figure 23:

- The system is stable. Due to the sufficient phase margin the resonant peak around 400 Hz is damped by the controller.
- However, the BW is far from the design specifications (which was roughly 160 Hz).
- More generally, the shape of the open-loop transfer function is quite far from a desired one [127]:
    - At frequencies below the fundamental the function is strongly negative: as a consequence, dragging it up to provide zero error at 50 Hz comes at the expense

of crossing 0 dB with a phase close to 180°, which creates a near-fundamental spike in the closed loop transfer function (see zoom-in in Figure 23).

- Moreover, at frequencies around the BW, the open-loop transfer function is increasing, instead of being decreasing with the suggested -20dB/decade.

This is owing to the particular shape of the admittance Y_C, which is completely different from that considered for usual grid-connected applications. As a result, a very poor dynamic performance is achieved, as demonstrated in the time domain simulations in Figure 24. The low frequency oscillation and very long settling time are the time domain mirror of the poorly designed frequency domain transfer functions shown in Figure 23.

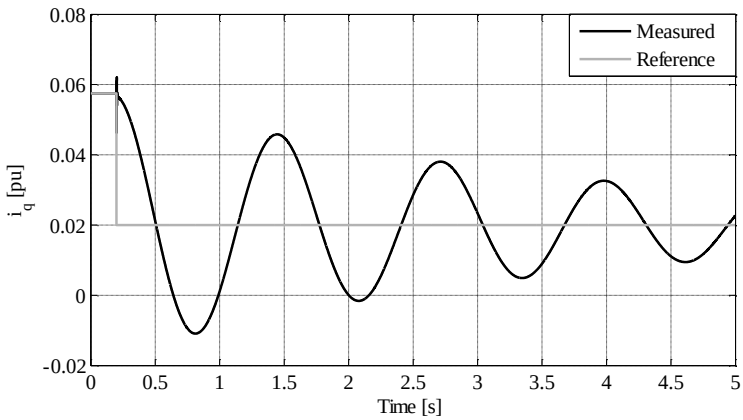

Figure 24 - Time domain response of current controller with Z_d = 0 in Figure 22.

If one adds the feed-forward of the terminal voltage assuming perfect measurement and ideal converter behaviour (G_{VSC} = 1), the closed loop form of the top-right part of Figure 22 is (Laplace variable dropped for brevity):

$$Y_{CL} = \frac{I_C}{V_{ref}} = \frac{Y_C}{1 - Y_C Z_d} = \frac{1}{Z_{conv}} \tag{9}$$

where the last equality derives from the network equation $Z_{conv} = Y_C^{-1} - Z_d$. As such, with perfect measurement and ideal VSC the design of the current controller with usual guidelines yields results as expected, as highlighted by the grey plot in Figure 25, where the BW is according to the design specification and generally the function is nicely shaped.

However, inserting a time delay in the VSC transfer function according to the utilised switching frequency [104] (i.e. T_d = 257 μs), the open-loop transfer function $G_{ol,CC}$ becomes that shown by the black plot in Figure 25. The transfer function is dramatically changed by the delay and takes a shape that is not acceptable, both in terms of BW and of behaviour around and far from the cross-over frequency.

The effect the delay has on the frequency response is somewhat unexpected, since it can clearly be noticed even at very low frequencies, despite its small value. The reason for this is to be found in the expression of the closed-loop form of the top-right part of the diagram in Figure 22. Analogously to what was done in Eq. (9), this yields:

$$Y_{CL} = \frac{I_C}{V_{ref}} = \frac{e^{-sT_d}Y_C}{1 - e^{-sT_d}Y_C Z_d} = \frac{e^{-sT_d}Y_C}{1 - e^{-sT_d}(1 - Z_{conv}Y_C)} \neq e^{-sT_d} \cdot \frac{1}{Z_{conv}} \tag{10}$$

where the third equality derives from network equations. The quantity $1 - e^{-sTd}$ is nearly nil for low frequencies but indeed very small and roughly 90° phase. The result is that at the low resonance frequency of Y_C, its magnitude may be close to or even larger than that of $Z_{conv}Y_C$, which also has phase nearly equal to 90°. The two quantities thus sum up to partly cancel out the resonance in the denominator, hence yielding the last inequality. This effect is visualised on Figure 26, where the effect of inserting the delay on numerator and denominator is shown. In grid connected applications, since Z_d contains an inductive part with rather small value, the parallel resonance happens at a larger frequency and with a less sharp notch if the resistance is the same. Consequently, the time delay effect at low frequency can be simplified to $Y_{CL} \approx e^{-sTd}Y_{conv} \approx Y_{conv}$.

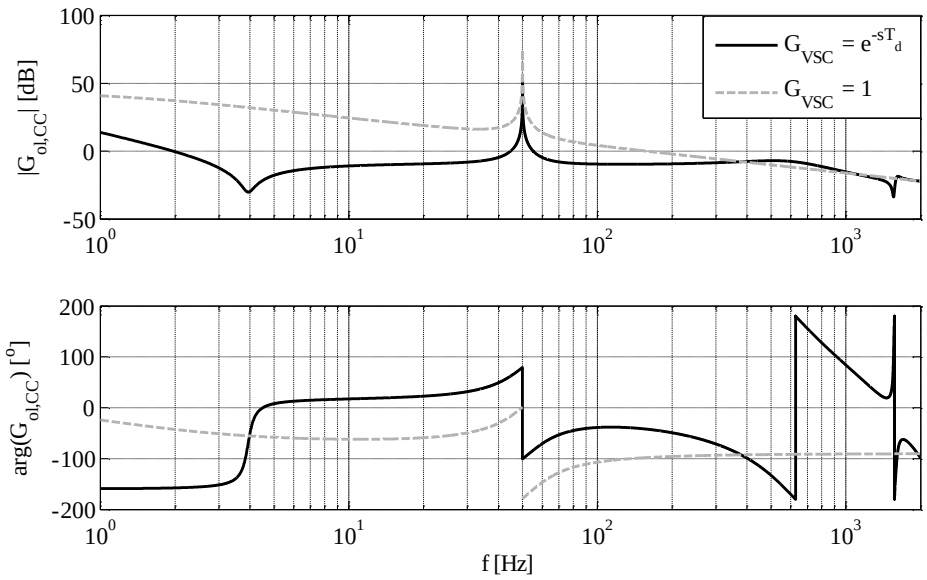

Figure 25 - Open-loop transfer function for current control problem with voltage feed-forward with perfect measurement: non-ideal and ideal VSC behaviour.

This is also proven in Figure 26, which reports two further cases to better understand:

- In dashed lines, the same case as above, but with augmented export cable length is illustrated. The cable length, and thus shunt capacitance, was multiplied by ten times. It is observed that the behaviour is similar to the reference case and only a shift in the low frequency peak is observed. The effect at 50 Hz is not as large as for the reference case, but the large impact at low frequency remains.
- In dot-dash lines, a reactor is connected at the converter terminals, which value is 1 pu, mimicking the connection to a very weak grid[4]. It can be seen that the effect at very low frequencies is as intuitively expected. Smaller gain and phase shifts happen at frequencies above 100 Hz, which are less cumbersome to tackle from a control design perspective. This demonstrates that, even for extremely weak grid connection, the phenomenon

[4] Based on several sources, e.g. [79], [81], 1 pu reactance can be considered as an extreme value for grid connectability of VSCs.

observed in the present case does not occur and the design can essentially proceed along standard guidelines.

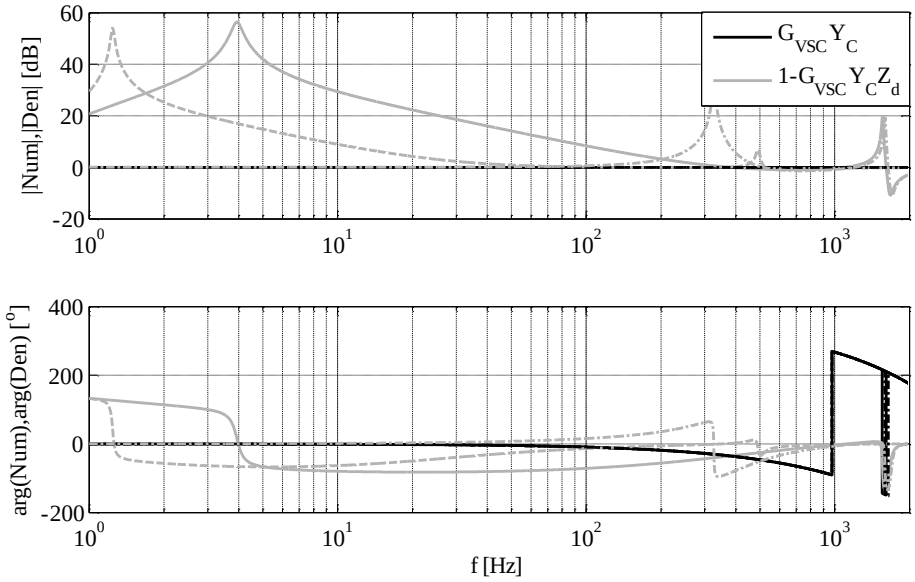

Figure 26 - Effect of time delay on numerator and denominator of Eq. (10). Solid: reference case. Dashed: export cable ten times longer. Dot-dash: grid connected with $Z_d \approx 1$ pu.

By looking at the Bode diagram in Figure 25, one may think about adapting the loop shape according to the specified BW. This could be achieved, for instance, by (i) inserting a low-pass filter in the *dq* frame, before the PI controller (cut-off frequency 100 Hz) in order to roll off the magnitude in the vicinity of the crossover frequency and (ii) increasing the proportional gain to K_{pC} = 2.29 pu so as to achieve the desired BW. This, approach, however, still has a few undesired characteristics:

- As shown by the black dashed plot in Figure 27, though the designed BW is according to specifications, the step response is performing more poorly than in the ideal scenario, most likely due to the difference at low frequency noticed in Figure 25, which is not solved by the countermeasures adopted here.
- As a confirmation of the above, unwanted gain and phase shifts at low frequencies are still present, meaning that low frequency oscillations are still induced in the response, as apparent in the step response in Figure 27. They are mirrored in the SRF at larger (near fundamental) frequency.
- Extending the previous point and considering negative frequencies too, the system results unstable even in the base design case. The supplementary filter and higher gain used in the re-design are worsening the situation at negative pulsations. This is illustrated by Figure 28, plotting the Nyquist diagram for positive and negative frequencies. According to the stability assessment tools described in [126] the system is unstable in any case at negative pulsations and the PM is even poorer for the re-designed controller. The oscillations are actually stable in the step responses in Figure 27, but this is probably due to the fact that only positive frequency oscillations institute, as the simulation is a perfectly ideal environment.
- Finally, the adjustments above may not be very robust against for example variations in the value of T_d or connected capacitance, both affecting the shape of the transfer function.

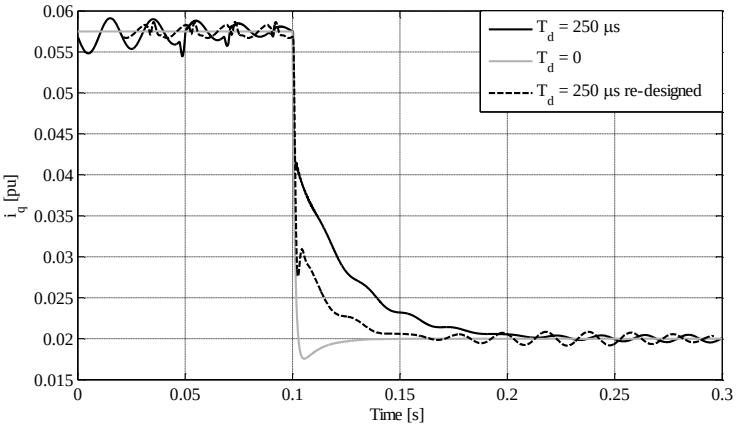

Figure 27 - Step response of current controller for the design cases described above.

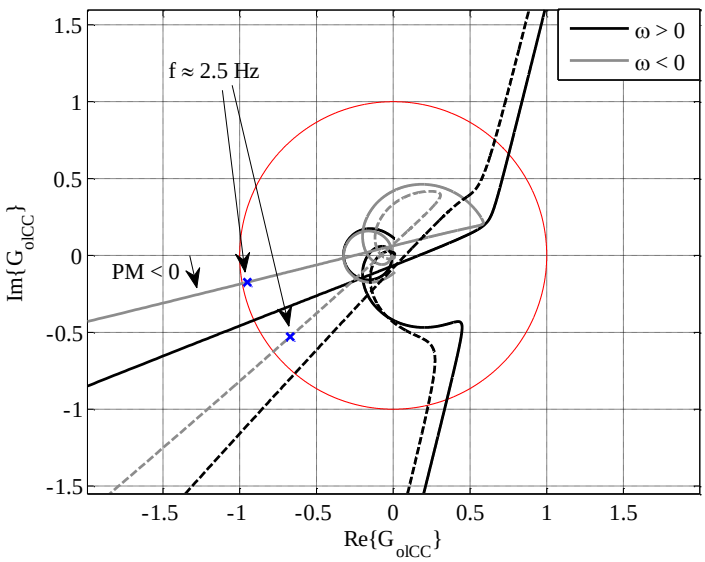

Figure 28 - Nyquist diagram for current control design at positive and negative frequencies. Solid: reference case. Dashed: re-designed current controller.

Recommendation for controller improvement

As a conclusion of the analysis done in this section, the following recommendations may be formulated in order to realise the current control design, if Option 1 is to be used:

- The delays in the VSC must be minimised, in order to avoid the phenomena described above. Indeed, the delay used here (257 µs) corresponds to half period of switching frequency equal to 1950 Hz. Such value is state-of-art for two-level converters. The delay may be reduced by more than five times in MMCs [70], which would make the design more straightforward and robust. However, to the author's experience, even 50 µs delay poses limitations. Moreover, one should bear in mind that other delays may add on top of the modulation delay. Thus, the requirement of delay minimisation is valid anyhow. Switching delay compensation techniques (moving the voltage reference vector forward) may be employed, but the evaluation of their effect was not performed here.
- Application of positive- and negative-sequence current controllers would make the frequency response symmetrical in the frequency domain, avoiding the issues highlighted

above and related to negative frequency instability. Resonant controllers, according to [24], [125] would achieve the same effect. However, the poor shape of the transfer function at low frequency would presumably not be improved by such a control structure.

Both solutions are not included in this report and especially the second is purely a theoretical speculation and would need to be supported by a more thorough analysis and demonstration. This could be material for future work.

(b) Option 1: voltage control design

In the ideal case, the voltage control design can be performed after having tuned the current controller and again following the guidelines in [23]. By assuming the reference current control design (ideal VSC), export system 3 being connected and requiring a BW $\omega_C \approx 390$ rad/s and PM $\geq 60°$, the voltage control gain and time constant were calculated and are reported in Table 5.

Table 5 - Option 1: HVDC converter voltage control parameters.

Parameter	Value	Unit
K_{pV}	0.062	pu
T_{iV}	0.1	s

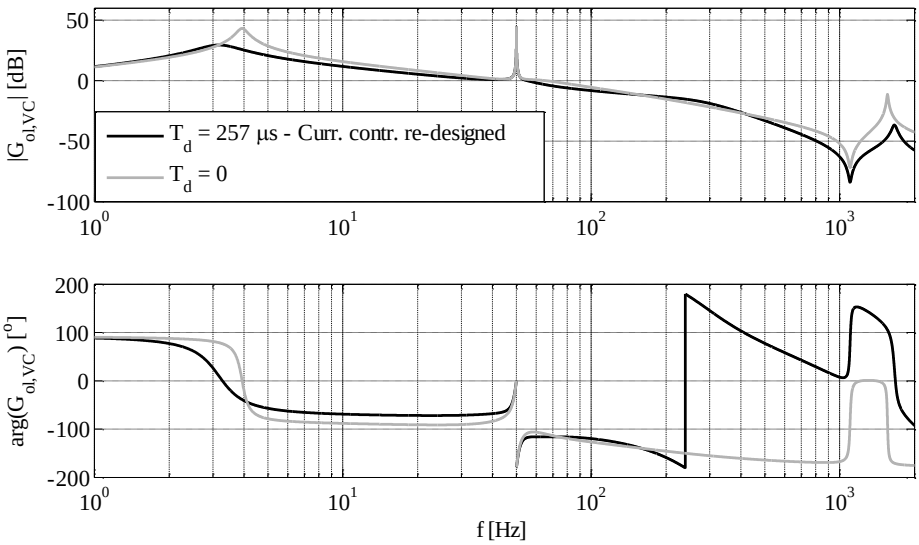

Figure 29 - Open loop transfer function for HVDC converter voltage control problem.

The open-loop control transfer function $G_{ol,VC}$ is reported as a grey curve in Figure 29. The desired BW is achieved and a sufficient PM guarantees stability.

It is important to assess what the impact of the VSC time delay is in this case. The parameters in Table 5 are used in a voltage controller feeding the current references to a current controller operating with a real VSC with T_d = 257 µs and re-designed according to what described in Section 4.2.2(a), generating the black curve in Figure 29. It can be seen that the transfer function does not dramatically differ from the ideal one. BW and phase margin are slightly reduced, but still satisfying. If the current controller is properly designed, hence, the voltage control can be tuned reasonably independently of the time delay.

Remark 1: sensitivity to connected shunt capacitance

It is important to remark, however, that the relations for designing the voltage controllers are directly dependent on the amount of capacitance connected at the converter terminals [23]. This is visualised by the step responses reported in Figure 30, where, apart from the reference case with export system 3 connected (capacitance C_3), two more cases are plotted:

- Connection of only export system 1: $C_{min} = C_1 = 0.3C_3$.
- Connection of all three export systems: $C_{MAX} = 1.7C_3$.

Evidently, a gain scheduling depending on the connected capacitance is needed to maintain satisfying performance. If a dedicated capacitor is connected at the converter terminals this problem is attenuated, but still present. If the control is performed at the terminals between converter reactor and transformer with dedicated shunt capacitance (as for example in [120] – control performed over a sufficiently large C_f in Figure 9), the control can be nearly independent of the amount of export systems connected to the converter station.

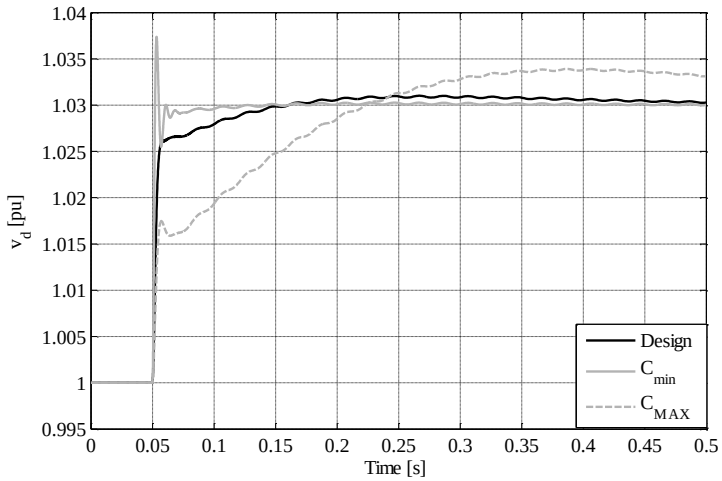

Figure 30 - Voltage reference step response and sensitivity to capacitance variation.

Remark 2: utilisation of current feed-forward terms in voltage control

A feed-forward of the current behind the capacitance is used in references [23], [120] as a disturbance rejection feature – dashed signals in Figure 12. However, in the present configuration, this would require sensing the current through the export cables' inductance, easily accessible in the π-equivalent model, but not physically. Hence, its estimation should be used instead.

Alternatively, if the voltage control is performed between converter reactor and transformer, i.e. using the capacitor C_f in Figure 9 and performing the control of the voltage across it, measuring such current is more straightforward. Adopting such a control and measurement layout, the utilisation of the feed-forward of the current helps improve the dynamics both at no-load and during loaded conditions, making the voltage control essentially independent of capacitance variations and possibly improving the dynamics in loaded scenarios.

The dramatic improvement of the performance at no-load is demonstrated in Figure 31, where the performance with varying export cable capacitance is tested when the voltage control is conducted over the intermediate capacitor C_f and the current feed-forward terms are utilised.

Current and voltage control were tuned with the procedure outlined above targeting the same BW for the current control and BW = 100 rad/s for the voltage control, using C_f with 10% reactive power (120 MVAr). A slight difference can be noticed between the three scenarios, but a comparison with Figure 30 immediately highlights the much improved robustness, the main dynamics being essentially independent of the amount of capacitance.

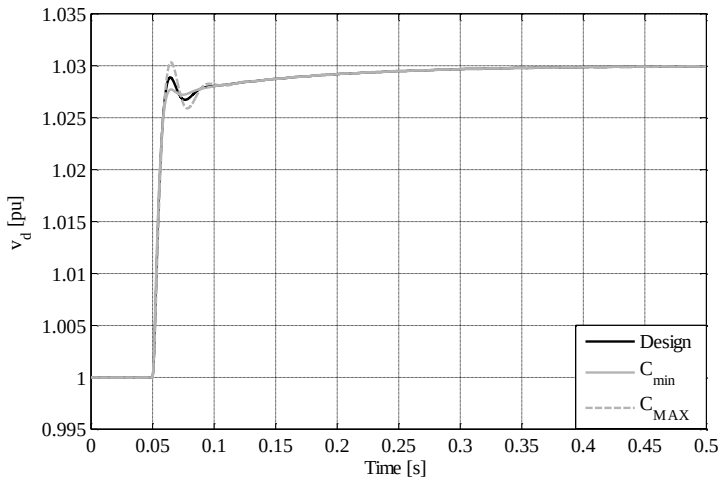

Figure 31 - Voltage reference step response and sensitivity to capacitance variation using current feed-forward.

Remark 3: different control configurations

Different control configurations may be explored too, by e.g. using the capacitor C_f, controlling the current at its transformer side and the voltage across it. To the author's experience, the current control in such configuration may give rise to resonances which are difficult to damp, but no further analysis is presented here in this respect, leaving it as an item for future work.

(c) Option 2: voltage control design

In Option 2, for convenience, all the design is performed in the SRF (*dq* coordinates), which is in this case aligned with the converter internal voltage V_C, without losing generality. In order to more easily perform the design of the controller, linearity can be assumed, by approximately considering the PCC voltage V_{AC} to be lying entirely along the *d*-axis. This is a fairly reasonable assumption for usual power angles (reactor and transformer are usually summing up to approximately 0.15-0.25 pu impedance) and is almost errorless at no-load, when currents are negligible. Under this assumption, the diagram in Figure 32 may be relied upon to derive the control design.

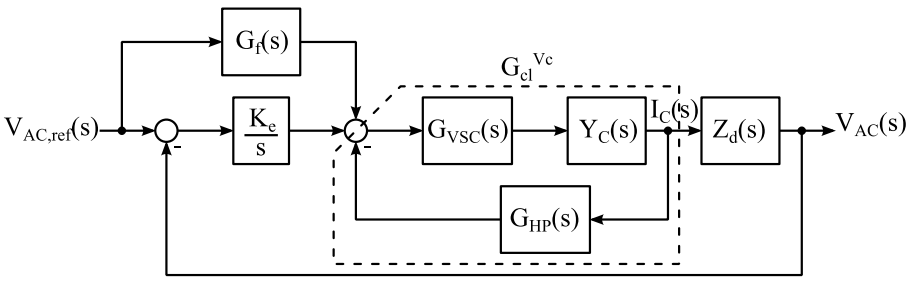

Figure 32 - Laplace domain block diagram for voltage control design in the *d*-axis.

Performing open-loop voltage control as used in [15] is possible, as the network is passive and any resonance would eventually damp. However, as highlighted in [80] and related publications, the natural damping of such resonances may not be satisfyingly large. Thus, an active damping was proposed by the same references, and particularly the use of the high-pass transfer function $G_{HP}(s) = \frac{sk_v}{1+sT_v}$. In this chapter, the gain and time constant for the active damping were set as reported in Table 6. The active damping acts as a virtual resistance and improves the damping factor of critical resonances.

Table 6 - Option 2: Parameters for active damping block.

Parameter	Value	Unit
k_v	0.024	pu
T_v	0.025	s

The closed loop expression of the internal voltage control transfer function is:

$$G_{cl}^{V_C} = \frac{G_{VSC}Y_C}{1+G_{HP}G_{VSC}Y_C} \tag{11}$$

As seen in Figure 13 and Figure 32, an integral control action and an optional reference feed-forward are added in the external voltage control loop. Its closed loop form is:

$$G_{cl}^{V_{AC}} = \frac{sG_f G_{cl}^{V_C} Z_d + K_e G_{cl}^{V_C} Z_d}{s+K_e G_{cl}^{V_C} Z_d} = \frac{1+s\frac{G_f}{K_e}}{1+\frac{s}{K_e G_{cl}^{V_C} Z_d}} \tag{12}$$

Inspection of Eq. (12) immediately yields the following considerations:

- When no feed-forward is used ($G_f = 0$) and considering that the open-loop uncontrolled transfer function $G_{cl}^{V_C} Z_d$ is very close to 0 dB for a large range of frequencies, as illustrated in Figure 33, the BW K_e rad/s can be achieved. Expectedly, increasing K_e provides increasing BW. However, the positive peak and then falling magnitude of the transfer function $G_{cl}^{V_C} Z_d$ pose control limitations (maximum BW, or a more complex controller is needed). In the real case, a further limitation on the BW is given by the phase shift introduced by grid resonance and converter delay – also seen in Figure 33. Reasonably, in the context of this study, the reachable BW naturally provided by the system should be sufficient.
- When using feed-forward, setting $G_f = \left(G_{cl}^{V_C} Z_d\right)^{-1}$ would theoretically provide infinite BW for reference tracking. More realistically, setting $G_f = 1$ in the relevant frequency range and rolling it off at higher frequencies so as to avoid excitation of resonances improves the closed loop response without excessively increasing K_e and thus preventing instability. For example, it can be $G_f = \frac{1}{1+sT_f}$.
- Interestingly, if the BW is kept sufficiently lower than the first resonance (i.e. within the spectrum where $G_{cl}^{V_C} Z_d \approx 1$), the performance is fully independent of the connected impedance, which is an advantage compared to Option 1 (see Figure 30).

The Bode diagrams in Figure 33 also report the sensitivity function [127] of the system, that is its disturbance rejection capability against disturbances directly (algebraically, with unity gain) affecting the terminal voltage V_{AC}. Such function is given by:

$$G_{cl,d} = \frac{1}{1+\frac{K_e}{s}G_{cl}^{V_C}Z_d} \tag{13}$$

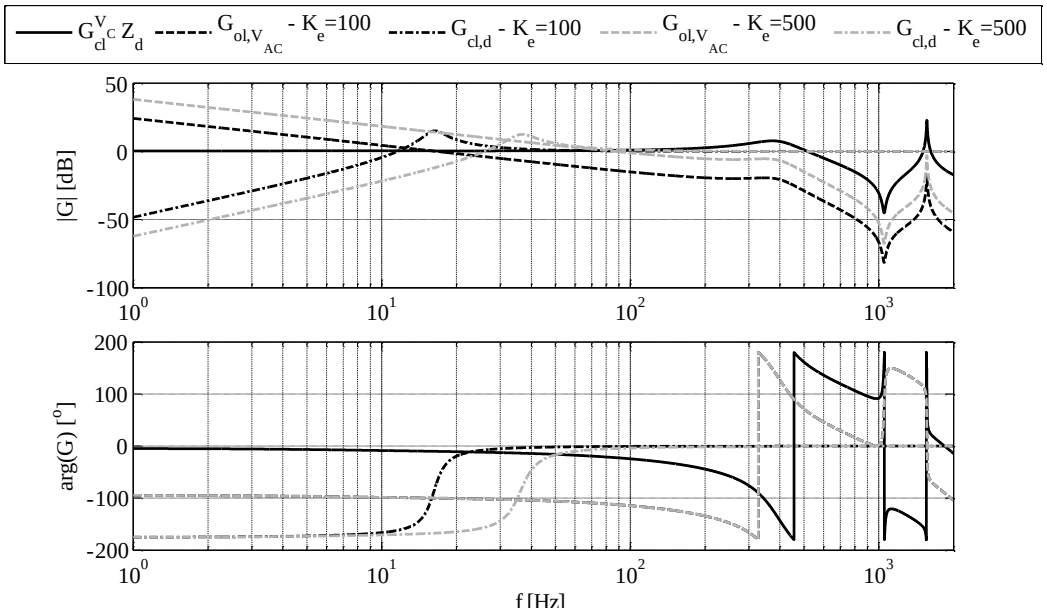

Figure 33 - Transfer functions for voltage control design in Option 2.

It can be seen that the effect of increasing the gain K_e is an augmented disturbance rejection capability. Despite being not so relevant for no-load operation, disturbance rejection capability is desirable when other elements in the network are affecting the voltage. Therefore, reference feed-forward can be used for improved reference tracking, but K_e should still be increased as much as possible to guarantee disturbance rejection[5].

The control parameters are set as in Table 7 and dynamic simulations were run in order to verify the above derivations. The results are reported in Figure 34. The effect of the feed-forward is shown and the response independency with respect to capacitance (number and/or length of export cables) is proven too – the same parameters as in the sensitivity analysis in Figure 30 have been used.

Table 7 - Option 2: Control parameters for terminal voltage control.

Parameter	Value	Unit
K_e	100	pu
T_f	0.001	s

[5] In reality, when other elements are acting in the network, the multi-variable nature of the system creates cross-couplings. However, if the HVDC station provides good disturbance rejection capability such cross-couplings should be reduced.

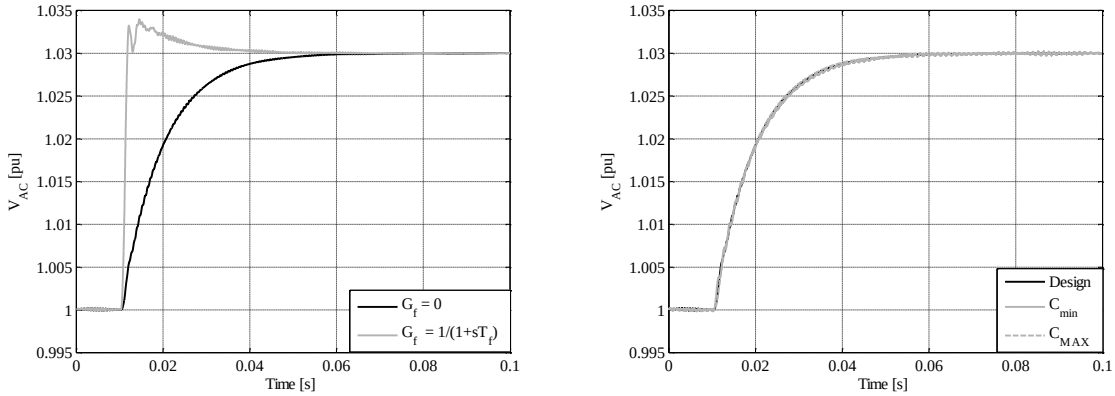

(a) Effect of feed-forward **(b) Effect of capacitance with $G_f = 0$**

Figure 34 - Response to voltage reference step for Option 2.

4.3 Operation with WPP

4.3.1 Introduction

When a WPP is operating in the network excited by the HVDC converter, the stability analysis becomes less straightforward, since the number of components and variables increases dramatically. As explained in Section 4.1.2, aggregation of WTG converters into three lumped VSCs simplifies the analysis. However, derivation of analytical results is very laborious and tedious even with three WPP converters. Hence, only one WPP converter was modelled for the analysis performed in this section. A linear model was developed in Matlab according to the derivations reported in Appendix 4 and modal analysis was applied to assess the influence of various parameters on the stability of the system and compare the performance of the two control options introduced in Section 4.1.1. In doing so, the following assumptions were accepted:

- The control of the aggregated WPP converter is *standard*, in the sense that the current control was tuned with common guidelines pertaining grid connected VSCs (i.e. proportional gain $K_{pC,WPP} = \omega_C L_{C,WPP}$, with BW $\omega_C \approx 1000$ rad/s and $L_{C,WPP}$ being the reactor and transformer inductance of the WPP converter). Also, a standard PowerFactory model for the PLL was used [128], with proportional gain $K_{pPLL} = 50$ pu and time constant $T_{iPLL} = 0.1$ s. No power control loop was implemented.
- The WPP converter is controlling the current in the export transformer and synchronised to the voltage at the HV side (export cable side – as seen in Figure 19) of the same transformer. This assumption is not realistic for a WPP, but its validity will be tested later on. Moreover, such hypothesis allows for direct extension of the results to the case where the lumped converter is another HVDC station acting as a slave.
- The aggregation of the export cable and converter to one single circuit (as reported in the bottom of Figure 19) is done as follows:
    - The export cable parameters are the default ones (see Appendix 2) and export cable 3 is taken as a reference, i.e. the default length is 24 km.
    - The converter is lumped into one unit, rated for the full WPP power, 996 MW (1200 MVA, base power).

  These assumptions may be questionable, in the sense that the export cable parameters are chosen for a power transmission level of roughly 350 MW (one third of the WPP). However, the focus in this section is to understand how the electrical parameters affect

the performance and it is thus reasonable to abstract the analysis from a very realistic design, start from default parameters and see how their variation affects the performance.

- Every analysis in this section is done by starting from a power flow where the HVDC converter fixes the voltage to 1 pu at its PCC (export cable side of the transformer) and the WPP does the same at the HV side of its transformer. The busses where the voltage is fixed for the initial power flow are essentially the measurement points in Figure 19. The power injected and absorbed by the converters depends on the specific case.
- The default settings for the HVDC converter in all calculations are the parameters tuned as was described in Section 4.2.2: Table 4 and Table 5 report the parameters for Option 1, while Table 6 and Table 7 list the parameters for Option 2. In the latter, it should be emphasised that no voltage reference feed-forward has been used, i.e. $G_f = 0$, or equivalently $T_f = \infty$ in Table 7.
- Any converter time delay is neglected in the analysis. Future work may include it.

All calculations, as mentioned, were performed in Matlab environment by setting up a linear model – see Appendix 4 – and performing modal analysis on the system matrix. The linear analysis is then corroborated by time domain EMT-type simulations in PowerFactory for selected cases. The aggregation hypothesis is verified in the time domain for one case.

4.3.2 Linear analysis of performance

A set of electrical and control parameters are varied in this section in order to assess their impact on the system performance, for both control options.

(a) Option 1: effect of WPP active power production

First of all, the initial WPP active power production is swept in the interval 0-1000 MW, providing the results reported in Figure 35, all other parameters being default. The system clearly turns unstable as the power production increases. The stability limit is reached for P ≈ 60 MW.

A different parameter tuning is attempted in order to prevent the instability, by re-setting the parameters of the voltage controller according to Table 8. The active power sweep is repeated, obtaining the results depicted in Figure 36. Clearly, the stability is much improved by the faster controller. However, it should be noticed that such a high gain may not provide the designed performance at no-load, that was achieved with the tuning in Section 4.2.2(b). Moreover, in the real case with time delays, excessively high gains may hinder stability. This means that a gain scheduling based on the power production may be needed to guarantee the desired performance.

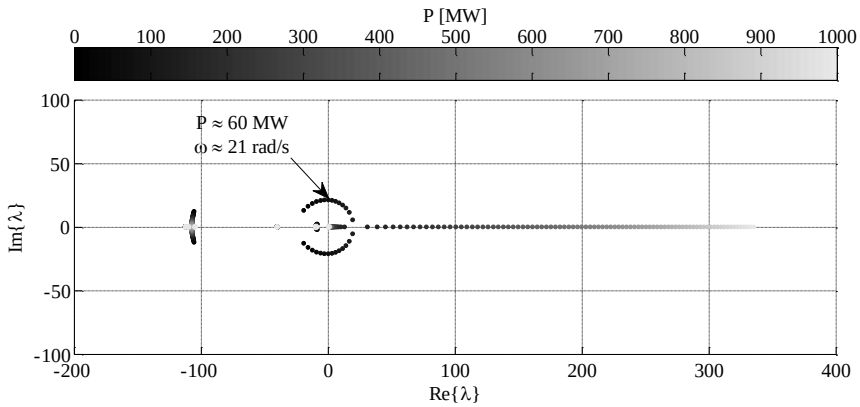

Figure 35 - Option 1: Effect of WPP active power production on eigenvalues with default control parameters.

Table 8 - Option 1: Re-tuned voltage control parameters.

Parameter	Value	Unit
K_{pV}	1.0	pu
T_{iV}	0.01	s

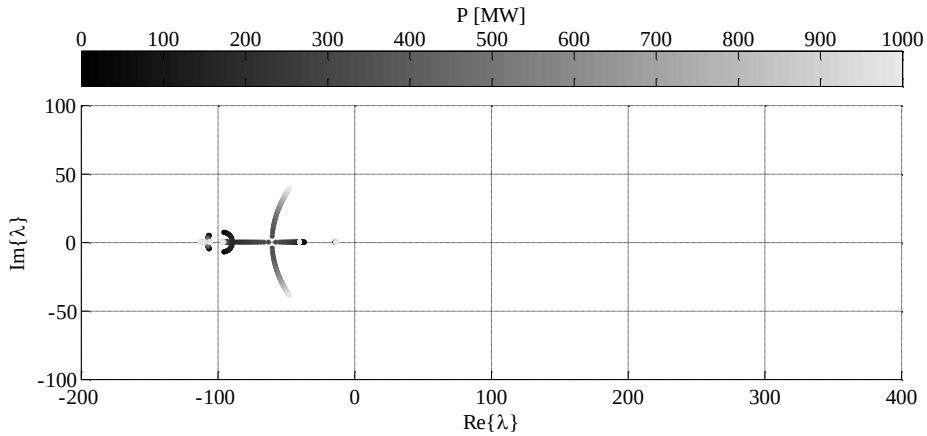

Figure 36 - Option 1: Effect of WPP active power production on eigenvalues with modified voltage control parameters according to Table 8.

(b) Option 1: effect of export cable length

The next parameter to be varied in the sensitivity analysis is the export cable length. For three values of the power production (low, medium and maximum), the export cable length is modulated within the range 0-100 km. Again, it should be noted that, although 100 km length may not be a realistic figure, the variation helps to understand what the effect of the impedances is. The figure for default parameters is demanded to Appendix 5 (Figure 127), since there always is an unstable pole in that configuration for P > 60 MW. Setting the control parameters according to Table 8, one achieves the results reported in Figure 37.

The influence of the line length is reasonably small, especially at high power levels. When the influence is largest, i.e. for P = 300 MW, the eigenvalues are anyhow very well damped.

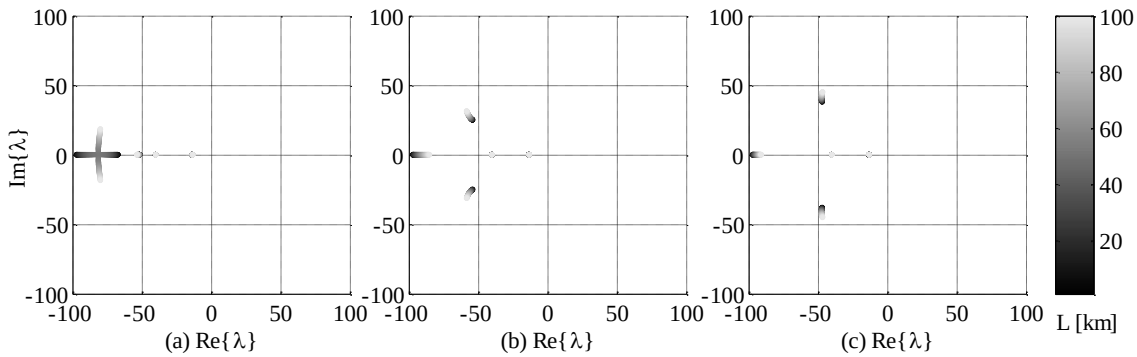

Figure 37 - Option 1: Effect of export cable length on system eigenvalues with modified voltage control parameters: (a) P = 300 MW, (b) P = 600 MW and (c) P = 1000 MW.

(c) Option 1: effect of voltage control proportional gain

The last parameter being varied is the proportional gain of the voltage controller K_{pV}, which is swept in the interval 0.062-5 pu. This is done for three power production levels, default line length and two values of controller's integral time constant T_{iV}. The results of the linear analysis

are reported in Figure 64. As the figure evinces, the reduction of integral time constant makes stability easier to achieve and the system expectedly faster, as the pole mostly affected by the gain moves towards a point further left in the LHP. Again, it is seen that as the power production increases, larger gains are desirable to maintain sufficient damping.

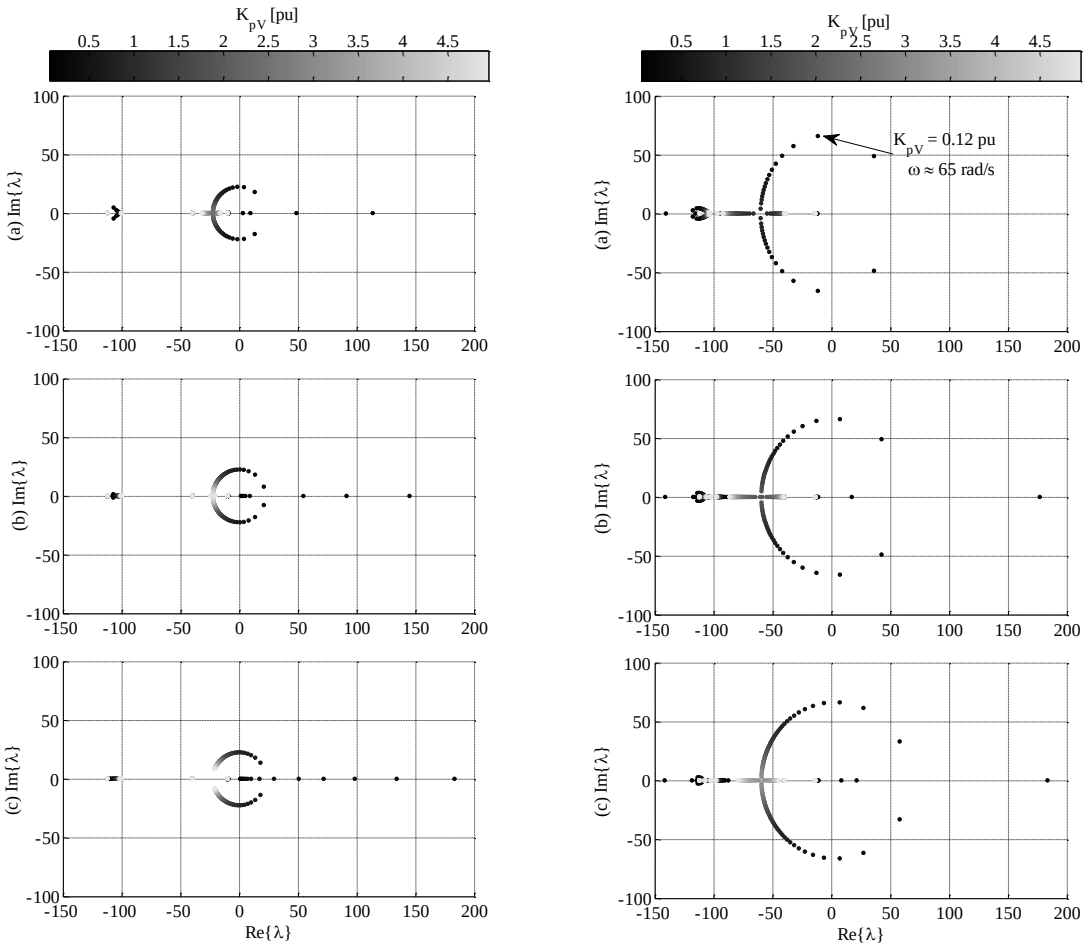

Figure 38 - Option 1: Effect of control proportional gain on system eigenvalues: (a) P = 300 MW, (b) P = 600 MW and (c) P = 1000 MW. Right: T_{iV} = 0.1 s. Left: T_{iV} = 0.01 s.

(d) Option 1: current feed-forward in voltage controller

As explained in Remark 2 in Section 4.2.2(b), the utilisation of a current feed-forward term in the voltage controller of Option 1 helps improve the dynamics. This is here illustrated by means of time domain simulations.

The default configuration in this chapter performs voltage control over the export cable capacitance, which may prevent the necessary current feed-forward terms from being readily available. Therefore, as was also done in Section 4.2.2(b), the control was moved to a dedicated capacitor C_f, placed between converter reactor and transformer and rated 10% (120 MVAr). The transformer current was used for the feed-forward (dashed signals in Figure 12). The voltage control parameters were tuned with the above procedure for proper operation at no-load. The operation was tested when the HVDC converter is connected to an aggregated WPP model and subject to a 0.01 pu step in the WPP active current (power) at t = 0.05 s and a voltage reference step from 1.0 pu to 1.03 pu at t = 0.3 s. The test was conducted at two values of the initial power production, i.e. P_0 = 300 MW and P_0 = 0 MW, the results being reported in Figure 39.

It is apparent that an essentially full independence of the power production level is achieved by employing the feed-forward, proving that, if Option 1 is to be used, the setup with dedicated capacitor and current feed-forward should better be employed. In offshore applications, installing a capacitor at such a voltage level clearly presents a disadvantage.

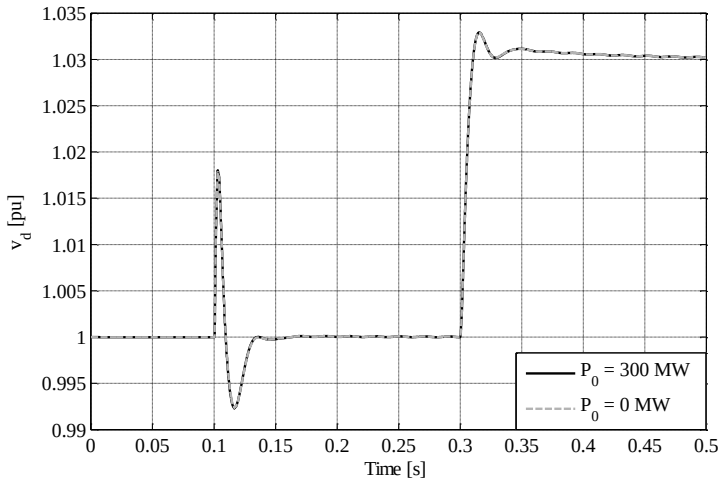

Figure 39 – Disturbance rejection and reference tracking response for Option 1 augmented with current feed-forward at two WPP power production levels.

(e) Option 2: sensitivity analysis

For Option 2, the same sensitivity analyses as for Option 1 were performed, varying power production, export cable length and control gain K_e. However, only a summary of the findings is included here, while the reader can consult Appendix 5 to visualize the results on graphics. The plots in Figure 128, Figure 129 and Figure 130 present the results for varying power, export cable length and gain K_e respectively.

The main conclusions are:

- In terms of pole sensitivity to initial power production, Option 1 and 2 perform similarly, although Option 2's main pole lies slightly more to the right in the complex plane.
- In terms of pole sensitivity to the export cable length, Option 2 presents slightly larger variations of the poles' position. However, for realistic value of power production and line length, the eigenvalues are well under control.
- In terms of pole sensitivity to the control gain K_e, only one pole moves significantly with the gain, namely the pole of the transfer function in Eq. (12), which is related to the voltage reference tracking performance and is expectedly approximately equal to $-K_e^{-1}$. Observing this, one could argue in two directions:
    - In Option 2, apart from the main pole moving with K_e, all other eigenvalues are relatively independent of the control gain. This means that the control may be tuned independently of other connected elements and requirements will be specified more easily. The interdependence between controllers seems more pronounced in Option 1, which potentially makes the tuning more challenging.
    - In Option 2 in its basic version, there is not much freedom available in terms of improving the position of some poles as for example the power production grows. Option 1, on the other hand, provides more possibilities in moving the dominant poles towards more favourable positions.

A clearer assessment and ranking of the two control options necessitates further work and the exploration of more cases, as well as possible countermeasures for the issues encountered. Furthermore, it was shown above that augmenting Option 1 with current feed-forward and performing the control over a dedicated capacitor improves Option 1's independence of the operational conditions, bringing it closer to how Option 2 behaves.

(f) Option 2: effect of active power droop

Reference [80], as previously stated, makes use of a control scheme which is a special case of Option 2 for converters connected to weak networks. It also adds a so-called power synchronisation mechanism which is essentially a power-frequency droop. It is not expected that the addition of such feature would bring about an advantage in the present case, since the HVDC converter anyway evacuates all the incoming power. However, it is interesting to briefly observe its effect, also because the mechanism is very relevant in Section 4.4.

The block *P droop* in Figure 18 is filled according to what is explained in Section 4.4.1, the proportional gain K_{PS} is set positive and negative and the same scenarios as in Section 4.3.2(d) are analysed. For brevity, all graphs are reported in Appendix 5, from Figure 131 to Figure 133. Although an immediate interpretation of the results is not straightforward, the following general observations can be put forward after inspecting the figures:

- Positive K_{PS} has a negative effect on the main complex conjugate pole, while it does improve the position of the real pole closest to the RHP, at least for realistically low values of power production.
- Negative K_{PS}, on the other hand, has the opposite effect: the complex conjugate pole's position is very slightly (almost unnoticeably) improved, while the real pole is dragged closer to the RHP.

Physically, the above may be explained as follows. The power-frequency droop with $K_{PS} > 0$ is designed for grid connected applications, where the converter adapts its voltage angle to track its power reference. When a power variation happens in the WPP, hence, the HVDC converter with $K_{PS} > 0$ actually tries to counteract such power variation, detrimentally affecting the position of the complex conjugate pole. On the other hand, the real pole close to the RHP is linked to the WPP's PLL's error cancellation (integral time constant 0.1 s). A power step in the WPP almost instantaneously changes its terminal voltage angle, which is read by the PLL. However, the HVDC converter with $K_{PS} > 0$ instantaneously changes the frequency in the same direction as the power variation, actually provoking a further WPP's terminal voltage angle deviation, momentarily increasing the PLL error and thus facilitating its angle tracking job.

4.3.3 Time domain verification

The linear analysis presented above must be corroborated by time domain simulations of the non-linear model, in order to ascertain that the derived results be correct. A time domain simulation for three selected cases with Option 1 is shown in Figure 40 (a WPP active current step is exciting the system at t = 0.1 s):

- Default parameters at the stability limit (P = 60 MW). The system, as expected is just beyond the verge of stability and starts to diverge with a frequency that is agreeing well with the theory – see Figure 35.
- Corrected (faster) PI controller and P = 300 MW, with K_{pV} = 1 pu and T_{iV} = 0.01 s. The control is very effective and the disturbance is almost unnoticeable.

- Corrected integral time constant (T_{iV} = 0.01 s), with K_{pV} = 0.12 pu and P = 300 MW, that is the operational point indicated by the arrow in the right part of Figure 38. Both the eigenvalue's frequency and its decay rate agree well with the linear analysis.

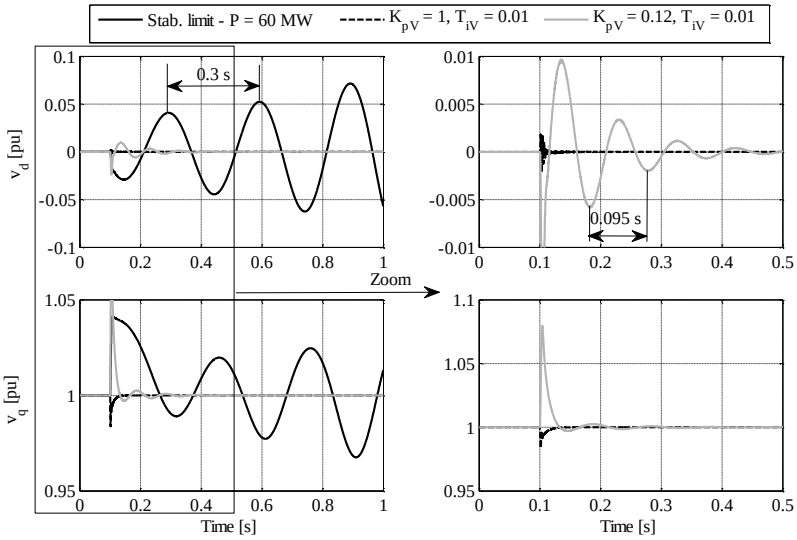

Figure 40 - Time domain verification of linear analysis for Option 1. Dashed and grey plot refer to P = 300 MW.

Results regarding Option 2 were also verified by time domain simulations. They are reported in Figure 41, for the three following cases:

- Active power P = 300 MW and default export cable length L = 24 km.
- Active power P = 1000 MW and default export cable length L = 24 km.
- Active power P = 1000 MW and default export cable length L = 100 km.

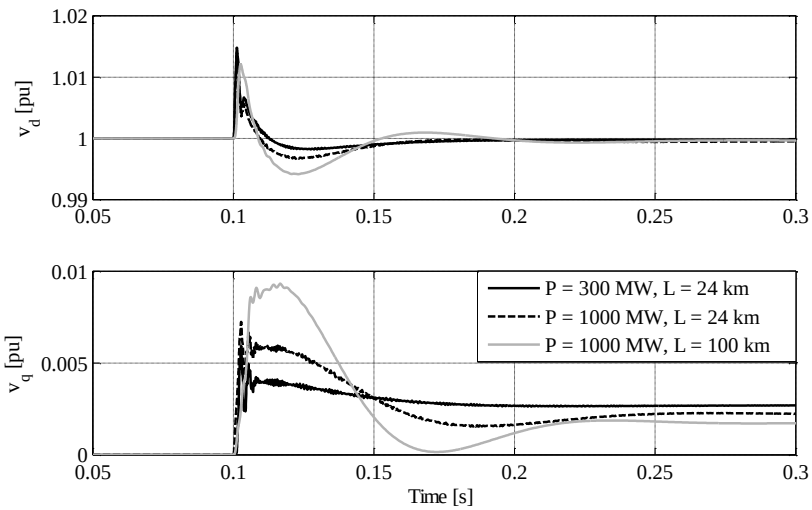

Figure 41 - Time domain verification of linear analysis for Option 2.

The results again agree well with the linear analysis. The modes are always very well damped and an immediate interpretation of the results is difficult. However, at a closer inspection, it can be noticed that the response for P = 300 MW and L = 24 km matches the linear analysis. Moreover, the increase in the power production causes an increase of the main pole's frequency and a slight

increase in its real part. Finally, a longer cable brings about a further increase in the frequency and a slight (nearly unnoticeable) decrease of the real part.

A verification for Option 2 provided with power-frequency droop is reported in Appendix 5 (Figure 134). The results, once again, satisfyingly match the linear analysis, demonstrating the poor performance expected with power-frequency droop gain $K_{PS} > 0$ and the slight impoverishment of the mode's decay rate when $K_{PS} < 0$.

4.3.4 Verification of aggregation validity

Since many of the results above were derived with aggregated model (neglecting the collection network and lumping the WTG converters), a verification of the validity of this approach must be conducted, in order to understand to what extent the results derived with the aggregated model can be extended to a real multi-converter WPP.

In order to do this, a time domain simulation was performed with two different models:

- Aggregated model based on Figure 19, where only Export system 3 and the aggregated converter 3 are operating. The converter is rated 332 MW (380 MVA), synchronised to the HV side of Transformer 3 and controls its current with BW 1000 rad/s.
- Detailed model with complete collection network behind Transformer 3 and 56 WTGs with rated power 6 MW (6.8 MVA), according to the layout reported in Appendix 1. Each WTG converter is synchronised with the MV side of its 0.69/34kV transformer and controlling its current with BW 1000 rad/s.

For both cases, the initial power flowing out of Transformer 3 towards the HVDC converter is equal to P_3 = 327.64 MW (rated power from each WTG minus losses). The voltage at the HV terminals of Transformer 3 is initially 1.0 pu in both cases. The HVDC converter is in both cases controlled with Option 2, with parameters K_e = 500 pu and G_f = 0.

At time t_1 = 0.05 s, a -0.18 pu step in the *d*-axis reference current is tested in both cases (aggregated converter in the former and each of the WTG converters in the latter). Subsequently, at time t_2 = 0.2 s, a voltage reference step is simulated in the offshore HVDC converter, by setting $V_{AC,ref}$ = 1.02 pu.

The simulation results obtained with the two models are reported for comparison in Figure 42. The bottom graph reports the *d*-axis current difference from its initial value, for WTG_1 and for the lumped converter respectively (the signals are deprived of the initial offset in order to show the controllers have exactly the same BW). v_d and v_q are sensed at the HVDC converter PCC.

It can be noticed that for the event at t_1, the lines are satisfyingly close to one another, with the exception of a certain discrepancy of the voltage v_q. The high-frequency oscillations superimposed to the detailed curves are most likely due to the further resonances introduced by the collection network and are anyhow not relevant within the scope of this study, since they are out of any control BW.

The accordance between the models during the event at t_2 is even greater, since all dynamics are almost perfectly replicated by the aggregated model. The small steady-state errors, especially in P_3, are clearly due to the additional losses introduced by the collection network.

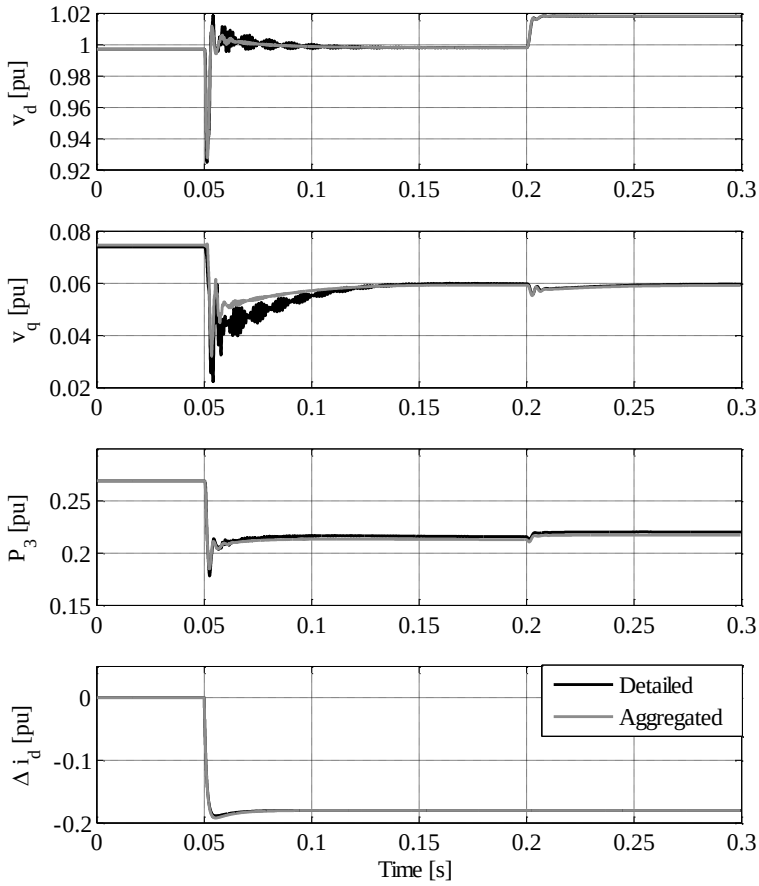

Figure 42 - Time domain validation of aggregation methodology.

4.3.5 Example study case

An example study case is run by making use of an aggregated model according to the upper part of Figure 19 in order to test the system's large-signal performance. The study case consists of the following steps:

- Initially, the HVDC converter is maintaining stable voltage with the three export cables connected at its terminals. Switches sw_1, sw_2 and sw_3 are all open.
- At time t_1 = 0.1 s the three switches are all contemporarily closed, the WPP converters connect and keep producing zero power. It should be noticed, as already mentioned in Section 4.2.1, that the transformer models are linear and no in-rush phenomena are thus taken into account by the simulation, since they are out of scope.
- At time t_2 = 0.3 s the active power production of the WPP converters is ramped up with a rate 5 pu/s until rated value (342 MW, 318 MW and 336 MW respectively).
- At time t_3 = 0.8 s the reactive power production of the WPP converters is stepped up to 0.3 pu (117 MVAr, 108 MVAr and 114 MVAr respectively).
- At time t_4 = 1.3 s the WPP converter corresponding to section 1 goes out of service, provoking a negative power step of 318 MW and 108 MVAr.
- Finally, at time t_5 = 1.8 s the active and reactive power production of the two remaining WPP converters are ramped down to zero again.

For the simulations, the settings for Option 1 are default for the current control (Table 4) and modified for the voltage control, according to Section 4.3.2(a) (Table 8), while for Option 2 K_e = 500 pu and G_f = 0 are utilised. The results are reported in Figure 43 for Option 1 and in Figure 44 for Option 2. From top to bottom, the following quantities are plotted: AC voltage at HVDC converter PCC, active power (P at the HVDC terminals, $P_1+P_2+P_3$ sum of active power sensed by WPP converters, P_{DC} active power flowing into the DC system), reactive power at the HVDC terminals and frequency sensed by the PLL installed at the WPP converter number 3.

Inspecting the figures, one can notice the following:

- Generally, the two options perform similarly and maintain stability during every event.
- The voltage control capability of Option 1 during power ramps is poorer than for Option 2 and contains a steady-state error, depending on the magnitude of the voltage control proportional gain. High gains make the error smaller. Alternatively, the controller needs be modified to achieve a type 2 kind of control or the solution illustrated in Section 4.3.2(d) should be used.
- A similar phenomenon happens with the frequency, and more pronouncedly for Option 2.
- Option 2 seems less effective against the reactive power step. Larger excursions and longer settling time are evident in essentially all traces with respect to Option 1. Further work is needed to investigate the reason for this.
- In both cases, very sharp spikes of the voltage are noticed at load rejection (step in active power absorption).

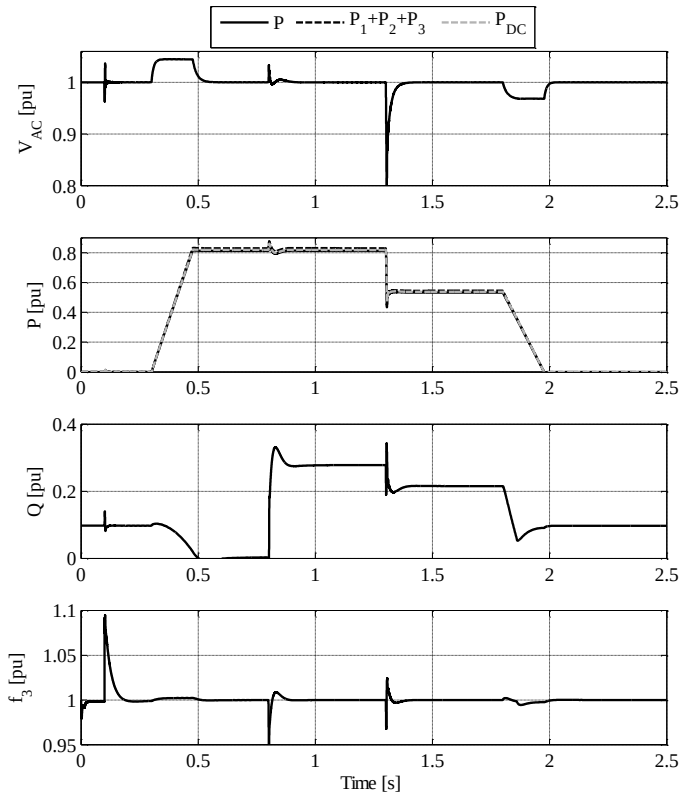

Figure 43 - Study case results for Option 1: HVDC PCC voltage, active power, HVDC reactive power, sensed frequency at Transformer 3.

Another conclusion that can be drawn from both results and particularly from the response to the converter outage at t_4 = 1.3 s, is that both controls perform extremely fast transfer of active power from the AC network to the DC side of the HVDC converter. This is relevant for the rest of this study (particularly Chapter 6 and Chapter 7), since it is clear that the control strategy does not dramatically affect the rapidity of the evacuation of active power towards the DC side. This is especially true for slower power modulations such as those happening during frequency control and POD. As a consequence, it does not matter which of the control strategies will be employed in the remainder of this study, and justifies the choice of Option 1 for all simulations performed in Chapter 6 and Chapter 7.

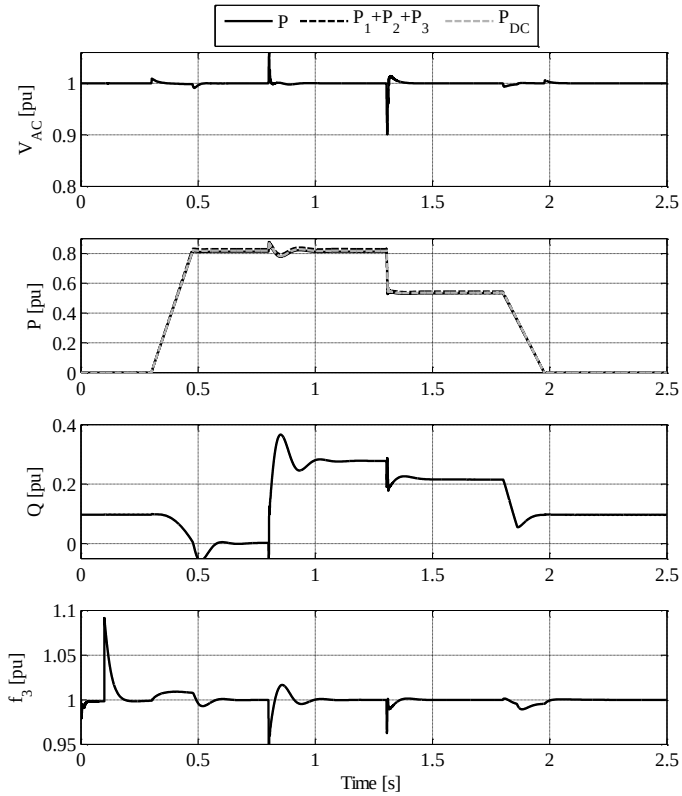

Figure 44 - Study case results for Option 2: HVDC PCC voltage, active power, HVDC reactive power, sensed frequency at Transformer 3.

4.3.6 Discussion and recommendation

The analysis carried out so far already generates a set of recommendations for the choice and design of the offshore HVDC station controller when utilised in a point-to-point connection of WPPs.

(a) Choice of control strategy

The choice of the control strategy, as discussed along this chapter, is not a trivial exercise, since both options have inherent advantages and disadvantages, which can be summarised as follows:

- Option 1 offers the great advantage of automatically performing current control and thereby protecting power electronics against over-currents. On the other hand, especially at no-load, tuning of the control parameters may not be so straightforward and various parameters influence the design (time delays, PCC connected capacitance, institution of

negative frequency oscillations). Moreover, there seems to be a larger dependence of the loaded operation on the control parameters. This, as discussed in Section 4.3.2(d), may be seen as an advantage or disadvantage. A solution to part of these problems comes with the insertion of a dedicated capacitance between converter reactor and transformer and the arrangement of the voltage control at its terminals, making use of transformer current feed-forward. However, the cost of installing a dedicated capacitor at 400 kV voltage level offshore must be evaluated.

- Option 2 is a much simpler configuration and the parameter tuning is much easier at no-load and naturally robust against variations in capacitance. No influence of the time delay can be noticed at low frequencies and instabilities at negative frequencies do not easily occur. However, Option 2 does not inherently provide current control capability, and this is a great disadvantage. Moreover, a slightly worse performance against variations in reactive power was noticed and may need to be tackled by better tuning. Finally, only dynamics related to voltage reference tracking can be finely tuned by changing the control gain, while the other modes are nearly independent on the control strategy. This, as discussed in Section 4.3.2(d), may be seen as an advantage or disadvantage.

If the improvements proposed below for Option 2 are implemented to provide current control capability, Option 2 seems to outperform Option 1, due to its simplicity, robustness and easy parameter tuning. However, since the controllers described here are the basic version of the two options and no advanced features have been inserted, Option 1 may, as far as the author knows, actually be used in real applications.

(b) Proposed improvements for better performance

The following discussion may be used as a starting point for performance improvement:

- Option 1:
  - The PCC voltage should be fed forward in the current control, to make the control transfer function more favourable.
  - The converter time delays, as shown in Section 4.2, should be minimised, to avoid unwanted influences, especially at low frequencies. Countermeasures for delay compensation should be investigated.
  - Positive- and negative- sequence current control should be performed, especially if the delays are not negligible. Making the transfer functions symmetrical with respect to zero frequency would avoid unwanted negative frequency instabilities.
  - Better robustness of the voltage control against variations of capacitance connected at the PCC and power generation level can be reached by:
    - Performing voltage control at the converter side of the transformer over a dedicated capacitor with sufficiently large value and use of transformer current feed-forward. This may not be an optimal solution in terms of reactive power balance in the offshore AC network, as a consequence of the inherent abundant cable capacitance, and certainly adds cost related to the installation of a high-voltage capacitor on an already large offshore platform.
    - Control parameter scheduling based on the operating conditions.
- Option 2:
  - Devising a scheme to quickly provide current control when the current limit is reached is paramount to Option 2's practical realisation, since the converter's

power electronics cannot withstand over-currents for more than a few milliseconds. An example of such solution is presented in [80] and related publications.

- Better parameter tuning and possible additions to the controller may be needed to improve performance, particularly in relation to fast reactive power variations. Additional damping should be provided.

All the above discussion is clearly limited to the scope of the present study. Other interesting aspects need to be investigated for real implementations, the most important probably being the behaviour of offshore HVDC converter during faults (mainly short circuits) and the development of proper control schemes for that.

Moreover, it should be emphasised once again that Type 4 WTGs were supposed to be installed in the WPPs. Relevant differences may arise when Type 3 WTGs are utilised. On one hand, the small signal control behaviour of Type 3 WTGs should be similar to Type 4's. On the other hand, events involving larger signals, such as short circuits, load rejection and islanding (loss of HVDC converter) may give rise to much more significant differences.

4.4 Operation with multiple HVDC converters

This section analyses the operation of the offshore network when multiple offshore HVDC converters are connected to it. In particular, the simplest system configuration of such a kind is taken as a reference, depicted at the beginning of this chapter in Figure 20 and consisting of two HVDC converters and two WPPs, both divided into three lumped sections. As noticed in the system's layout in Figure 20, the control of the aggregated WPP converters is synchronised to the MV terminals of the AC substation transformer. Relevant parameters are reported in Appendix 2.

It is important to notice that the described configuration could actually become reality quite soon in German waters, where some of the HVDC stations (operational, planned or under construction) are lying quite close to one another and connecting them on the offshore AC side may become attractive to possibly boost the reliability and thereby reduce the spillage of wind energy. An inspiring discussion of the main challenges and advantages of such a layout was done in [92], where some of the principles introduced in Section 4.4.1 are also discussed.

An underlying assumption along this section is that the WPPs converter controls are designed and tuned in the same way as in Section 4.3, so that the WPPs is essentially implemented as if it was connecting to a usual AC grid. Therefore, the focus in this section is mainly on assessing the performance as a function of the control strategy and parameters for the offshore HVDC converters.

4.4.1 Active and reactive power droop

When multiple HVDC converters act in the same network there may be multiple options in terms of their control. Here, some assumptions are made in order to reduce the scope of work.

First of all, as evinced by Figure 20, the control of the HVDC converters is performed at the converter side of the transformer, where a 0.084 pu (100 MVAr) shunt capacitor is also positioned. This has expectedly been noticed to be beneficial to the voltage control stability, particularly when the interlink cable is short. Inserting the transformers in between the controlled terminals reduces the interaction between the two converters. The approach was used in [120] too

and from [20] it appears that the control in real installations in the German North Sea is indeed performed at such terminal. No feed-forward of the transformers currents is performed and may be included in future work.

Furthermore, in the case when multiple converters are shouldering the control of voltage and frequency in the offshore AC network, integral control action as that provided by Option 1 and Option 2 in their default setup may not be a sensible choice [120], in the same way as it is not in conventional AC networks with multiple SGs. A proportional kind of control avoids hunting phenomena and provides programmable sharing of active and reactive power between converters. Hence, the control is accompanied by two supplementary droop blocks, namely *P droop* and *Q droop* in Figure 18. Here, a brief description of the two is given.

When both HVDC converters have to share the active power production of the WPPs, the amount of active power absorbed by each HVDC station is governed by a very simple active power-frequency droop like that depicted in Figure 45, which is allocated to the block *P droop* in the generic block diagram in Figure 18. Each converter changes its instantaneous frequency based on the error between actual and reference active power. When an active power variation happens in the WPPs, the frequency will stabilise to a level which is determined by the magnitude of K_{PS}, while the active power will be shared according to the ratio between K_{PS} for the two converters. The HVDC converters voltage angle will thus stabilise to two different levels based on K_{PS} for both converters and the network layout.

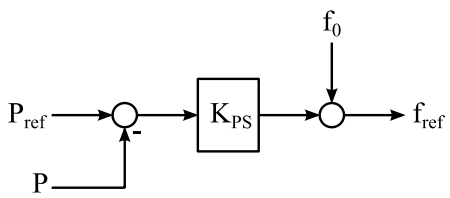

Figure 45 - Active power droop controller for HVDC converters.

A similar approach is used for sharing the reactive power and voltage magnitude control burden, through a reactive power-voltage droop control, which is depicted in Figure 46. A supplementary branch is inserted in the block, providing a derivative control action which has been noticed to help improve the response's damping in some occasions, especially when the distance between HVDC stations is not very large.

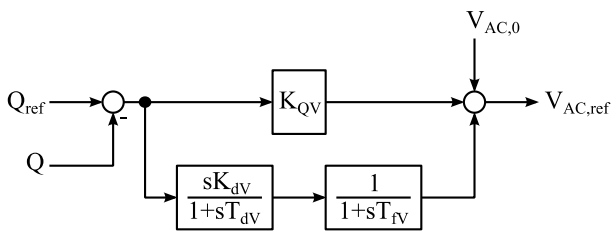

Figure 46 - Reactive power droop controller for HVDC converters.

4.4.2 Description of study cases

In order to illustrate the principles of offshore AC network control with multiple converters, three study cases are considered, in terms of control strategy utilised at the HVDC stations. They are summarised in Table 9.

Table 9 - Control of AC network with multiple HVDC converters: list of study cases.

Case	HVDC 1	HVDC 2
A – Distributed 1	Option 1 with P and Q droop	Option 1 with P and Q droop
B – Distributed 2	Option 2 with P and Q droop	Option 2 with P and Q droop
C – Master-slave	Option 1 with no droop	Power control (Figure 11)

Referring to Figure 45 and Figure 46, the parameters for the droop blocks in Case A and B are as listed in Table 10. The power controller in Case C is an open-loop kind of control, i.e. the right most switches in Figure 11 are in bottom position.

The parameters for the voltage controller Option 1 are modified with respect to those used in Section 4.3 and are set according to Table 11. The modification means a very fast response, which is justified by the analysis carried out in Section 4.3 in the absence of transformer current feed-forward. Bearing in mind the findings of Section 4.2 one should clearly make sure that either the no-load operation be stable with the new parameters or the same parameters are part of a scheduling scheme that adjusts them based on the operational condition. The current control parameters were also adapted to account for the different position of the synchronisation. For Option 2, the voltage control gain is set to K_e = 500 pu.

Table 10 - Parameter settings for droop controllers.

	HVDC 1		HVDC 2	
Case	K_{PS} [$\cdot 10^{-3}$ pu]	K_{QV} [pu]	K_{PS} [$\cdot 10^{-3}$ pu]	K_{QV} [pu]
A	3.18	0.1	3.18	0.1
B	3.18	0.1	3.18	0.1

Table 11 - Modified parameters for Option 1 voltage controller in Case A and C.

Parameter	Value	Unit
K_{pV}	2	pu
T_{iV}	0.01	s

For all study cases, the following scenario is tested:

- Initially, WPP A is producing full power (996 MW), while WPP B is synchronised but not producing any power. The voltage at each WPP converter control terminal, as well as at the HVDC converters PCC, is 1 pu in the initial power flow. For Case A and B, the HVDC converters are sharing the power equally, while in Case C the converter HVDC 2 is initially evacuating all the power produced by the WPPs.
- At time t_1 = 0.3 s WPP B ramps up its active power with a rate equal to 5 pu/s until it reaches its full power (996 MW).
- At time t_2 = 0.8 s WPP A steps up its reactive power production to 0.3 pu (360 MVAr).
- At time t_3 = 1.3 s WPP B is disconnected creating an active power step of 996 MW.
- At time t_4 = 1.8 s converter HVDC 1 goes out of service, leaving the whole control burden on the shoulders of HVDC 2.

4.4.3 Time domain simulations, discussion and recommendations

A non-linear model was implemented in PowerFactory according to the layout in Figure 20 and setting up all three cases described in the previous section. The results are reported in Figure 47, Figure 48 and Figure 49 for Case A, B and C respectively.

It is immediately and expectedly apparent that Case C does not provide robustness against the loss of one (master) HVDC converter, even when the surviving converter could in principle evacuate all the power produced by the WPPs – see last event in Figure 49. The control is totally lost when the power controlled (slave) HVDC converter is required to take over the master role. This implies that a sufficiently fast detection mechanism must be devised in order for HVDC 2 to switch to master function when HVDC 1 goes out of service. Hence, it appears much more sensible to make use of one of the other two schemes, the power reference of which can anyhow be adapted in a few hundreds of milliseconds, in case the power tracking must be very precise.

Comparison of Case A and B, on the other hand, yields a favourable judgement on Case A, since Case B, although always guaranteeing stability and somewhat acceptable performance, shows a worse response than Case A essentially for every event.

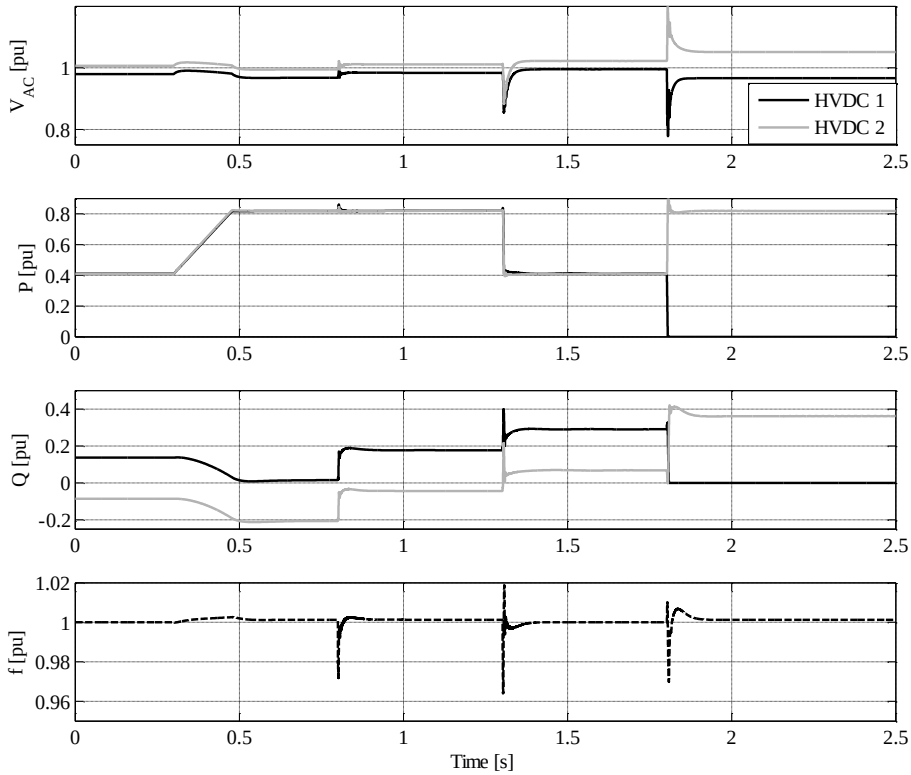

Figure 47 - Simulation results for Case A.

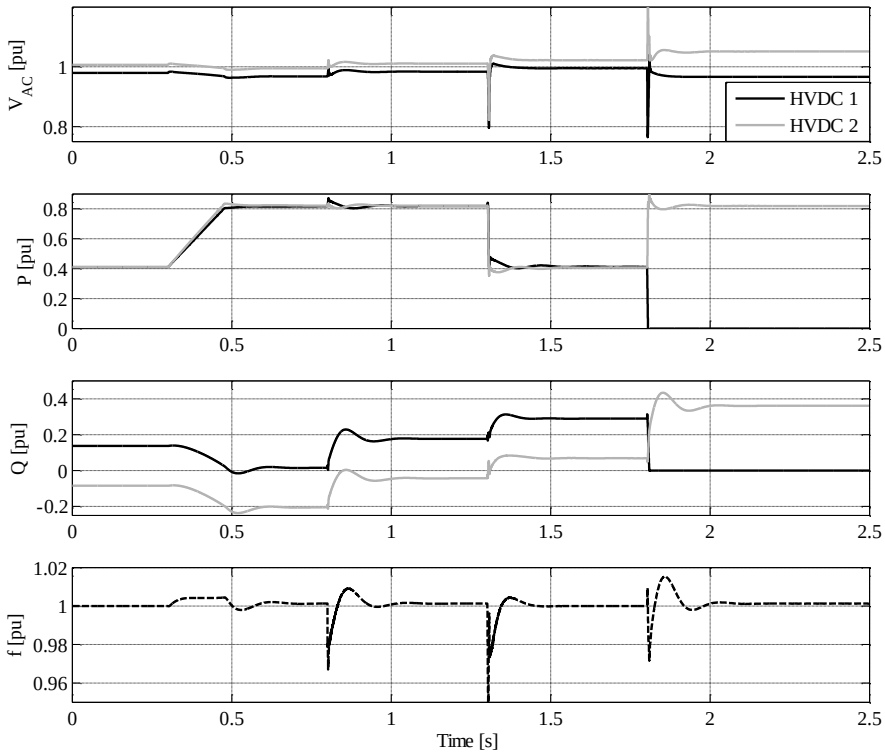

Figure 48 - Simulation results for Case B.

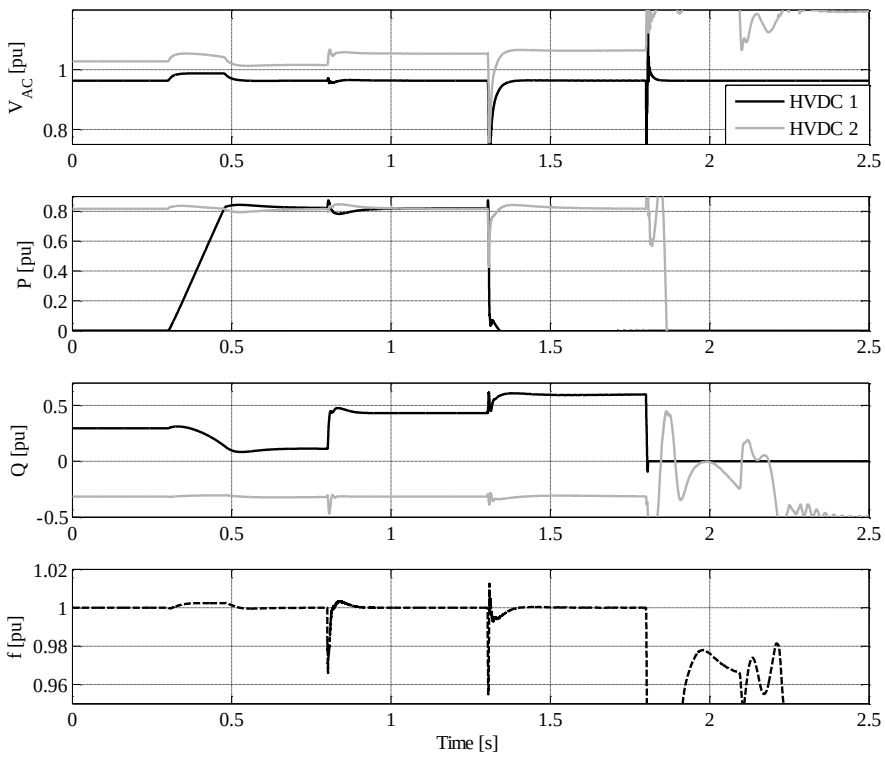

Figure 49 - Simulation results for Case C.

The steady-state behaviour is as expected for both cases and the settling values are essentially the same for both Case A and B, as one would assume, since the droop control parameters are the same for the two cases. However, Case A provides better damping and settling time of active and reactive power as well as frequency deviations. Moreover, during the active power ramp there is a larger frequency deviation in Case B. Small power oscillations between the two HVDC converters can be noticed in every event for Case B.

As a consequence, and based on the available simulation experience, Case A is the preferred one, also considering the inherent current protection it provides. However, further refinement of the control parameters for Case B and/or addition of supplementary control features may help improve the control. Furthermore, it should be borne in mind that Case A's parameters are already assuming an adaptive gain scheduling which makes its tuning slightly more complicated.

Finally, the particular scenario does not cover every possible condition and a more thorough assessment would require a larger number of simulation study cases to provide a more complete and final recommendation. A number of sensitivity analysis cases were run for Case A and B in order to better understand the influence of some parameters and verify the correct active and reactive power sharing happens when varying the droop control values. A summary of the results is reported and briefly commented in Appendix 5.

4.5 Summary

The control of offshore AC island networks behind VSC-HVDC converters was examined in this chapter. Two state-of-art control strategies were identified in the literature and described: Option 1 making use of inner vector current control and outer vector voltage control and Option 2 performing directly voltage control.

The control design for both strategies was discussed by means of transfer functions for unloaded conditions and the results were corroborated by time domain simulations. Their performance under load (connection of "standard" WPP) was then investigated with modal analysis and sensitivity studies, in order to assess the impact of circuit and control parameters on the stability and response time. Time domain simulations were used to prove the findings. Finally, the two options were compared when operating in a network hosting multiple HVDC converters that potentially share the role of master (distributed control of active and reactive power).

The main conclusions were:

- At no-load Option 2's design resulted simpler and its performance more satisfying. However, Option 1 possesses inherent current control capability, which is a great advantage. Thus, if the hurdles outlined in Section 4.2 can be overcome, Option 1 may result feasible. Recommendations as for how to proceed in this direction were formulated.
- When loaded with active power coming from the WPP, Option 2's behaviour appears less dependent on control parameters and the poles which move significantly by changing control gains do so expectedly. On one hand, this may make Option 2 slightly more robust. On the other hand, more room for optimisation and performance correction should be allowed by Option 1. As for the dependence on network parameters, Option 2 resulted slightly more sensitive, but the performance remained certainly acceptable for values within a realistic range. Modifying Option 1 by moving the controlled terminals between

converter reactor and transformer and providing it with transformer current feed-forward makes Option 1's behaviour very independent of external elements too.

- When operating in networks hosting multiple HVDC converters Option 1 provided with active and reactive power droop provided better results and therefore seemed to be preferable for real application. Further work is anyhow needed to formulate a more complete assessment.

Chapter 5 Onshore AC voltage control

Control of AC voltage from onshore VSC-HVDC stations is the subject of this chapter. Steady-state characteristics for connection to strong and weak grids and taking into account VSC-HVDC converter limitations are derived in the first part, drawing important conclusions on the extent to which a converter can contribute to a system's continuous SCP by being provided with AC voltage droop control. The second part of the chapter is dedicated to studying how the prioritisation strategy during converter current limitation affects the long-term voltage stability performance of a simple three-bus system. PV curves and steady-state calculations are used, eventually corroborated by dynamic simulations. The analysis is to a great extent independent of the WPP connected behind the HVDC link, but the findings do possibly affect its control. This is hence discussed at the end of the chapter. Most results of this chapter are among those presented in Publications 6 and 7 [90], [129].

5.1 Introduction

The potential contribution of VSCs to AC voltage control is notoriously excellent as long as they operate within their limitations. However, when limitations do occur, they are usually hard ones, meaning that a significant part of a VSC's flexibility is lost when limits are hit and limitations act instantaneously, due to the high sensitivity of PE components to excessive electrical and thermal stress. It is thus interesting for the research community to further investigate the implications such constraints have on a power system level by combining VSC's and power system's characteristics. The most interesting observations stem from analyses regarding weak networks, since in that case the interaction between AC system and VSC is much greater.

Moreover, in the specific case of HVDC, one additional factor plays an important role in assessing the above, namely the active power that a HVDC converter is supposed to exchange with the grid along with the reactive power. In case the HVDC link is an interconnector, TSOs may have sufficient control freedom to select the optimal control strategy when limits are approached. Conversely, when the HVDC is evacuating power from e.g. a WPP, control flexibility may have to be agreed upon by TSO and HVDC/WPP operator and consider the whole system and its needs.

An interesting scenario that encapsulates all the aspects above is represented by a power system approaching its long-term voltage stability limits while a large VSC-HVDC station moves

towards its current limitation. Some control freedom is still available even in current-limited mode and the selected strategy must match power system needs to enhance stability and allow for more solid countermeasures to be taken so as to bring the system sufficiently far from its stability limit again.

Section 5.2 focuses on steady-state AC voltage control and more specifically on the steady-state HVDC/AC-grid interaction through superimposition of HVDC continuous limitations and AC network characteristics. Results from dynamic simulations are used to prove some of the findings. The focus in Section 5.3 is shifted to the effect the HVDC converter's current limitation has on long-term voltage stability of a simple system. Again, the analysis is mainly in steady-state, and dynamic simulations are used to prove some of the key concepts.

Dynamic phenomena such as the influence of the control system on dynamic current and voltage control, e.g. [82], [130], are not considered here, but are also surely interesting for real applications.

All voltages and currents in this chapter are generally phasors rotating at the fundamental frequency and they should be interpreted as such in the electrical diagrams. Impedances are complex numbers. All equations, on the other hand, regard more specifically magnitudes. For convenience, and since there should not be room for confusion, unless differently specified all quantities are indicated with simple capital letters. When only real or imaginary part of the impedances will be used, it will be pointed out. When complex numbers will have to be used it will be stated explicitly and proper notation will be introduced.

5.2 Continuous AC voltage control

For the analysis carried out in this section, the system in Figure 50 can be used, where only the AC side of the HVDC converter is modelled (Figure 9). The AC network is reduced to a Thevenin equivalent (V_g,Z_g), and a separate reactive load Q_L has been inserted, initially supposed to be nil ($Q_L = 0$). Per-unit notation is most convenient, with base values given by nominal apparent power ($S_N = 1$ pu) and PCC voltage ($V_{AC,N} = 1$ pu) of the VSC.

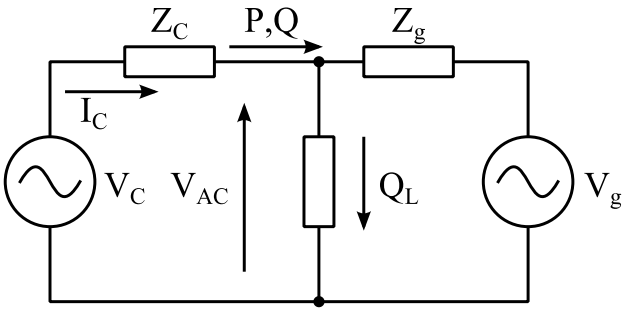

Figure 50 - Network model for derivations in Section 5.2.

Steady-state PQ characteristics of VSC-HVDC are well-known. A qualitative example is shown in Publication 7 [129] and a commercial sample is available for example in [68]. When studying the interaction with the power system, however, other kinds of curves may also be helpful, as highlighted for example in [131] for simple loads. The focus here is on Q-V_{AC} curves. Steady-state, balanced operation is assumed and any transformer's tap-changer is neglected. Additionally, the network is supposed to be lossless, which in practice means $Z_C = jX_C$ and $Z_g = jX_g$.

5.2.1 Main VSC-HVDC limitations

(a) Converter current limitation

Typically, the strictest limitation for PE devices is the converter current flowing through the transistors (I_C in Figure 50[6]). Parameterising for the active power P, the Q-V_{AC} curve for this limit can be found by plotting, in pu and considering $I_{C,MAX}$ = 1 pu:

$$|Q| \leq \sqrt{V_{AC}^2 - P^2} \tag{14}$$

The curve is a hyperbola with centre in the origin and distance between focusses varying proportionally with the active power. As expected, it degenerates into two straight lines for P = 0.

(b) DC link voltage limitation

The available DC voltage V_{DC} imposes a limit $V_{C,MAX}$ on the internal converter voltage V_C. Considering the RMS value of the fundamental in pu and assuming no third harmonic injection in the modulation index:

$$V_{C,MAX} = \frac{V_{DC}}{2} \cdot \frac{\sqrt{3}}{\sqrt{2}} \tag{15}$$

At this point, the approximation $V_C \approx V_{AC}$ (and hence $V_{AC,MAX} = V_{C,MAX}$) is helpful for plotting the locus of the DC voltage limitation in the Q-V_{AC} plane as:

$$Q \leq \left(V_{AC,MAX} - V_{AC}\right) \cdot \frac{V_{AC}}{X_C} \tag{16}$$

The relation is fully correct only when the converter voltage angle is the same as V_{AC}'s, i.e. only for P = 0. However, since X_C is typically 0.15-0.25 pu and V_{AC} does typically not drift very far from 1 pu, the above equation is approximately valid over the realistic operational range. It represents a parabola opening downwards with vertex in $\left(0, \frac{V_{AC,MAX}}{X_C}\right)$.

(c) Other limitations

Other limitations may affect the Q-V_{AC} capability of real MMCs, such as modulation index limitation and cell voltage ripple limits [70]. Here, roughly approximating what reported in [68] for a commercial MMC, the following relation is supposed to pose a further limit:

$$|Q| \leq 0.5 \text{ pu} \tag{17}$$

5.2.2 Combination with network equations

Q-V_{AC} curves for the external network with converter's P and Q injection derive from well-known formulae. They could be a particularisation of the more general PQV curves presented in [131]. Under the present assumptions, and considering for brevity only active power injection (it is the only relevant scenario in WPP application) one can derive the network constraint as:

[6] I_C is *not* the real valve current in MMCs, since the circulating current is superimposed to it. A limit value for I_C, however, does still exist.

$$Q = \frac{V_{AC}^2 - \sqrt{V_{AC}^2 V_g^2 - P^2 X_g^2}}{X_g} \tag{18}$$

The network constraint can be plotted together with the VSC limits derived above. This is done in Figure 51, for two different values of the SCR at the PCC[7], i.e. SCR = 5 and SCR = 1 respectively. Current limits and grid constraints are parameterised by active power, while the DC voltage limit is parameterised by DC voltage.

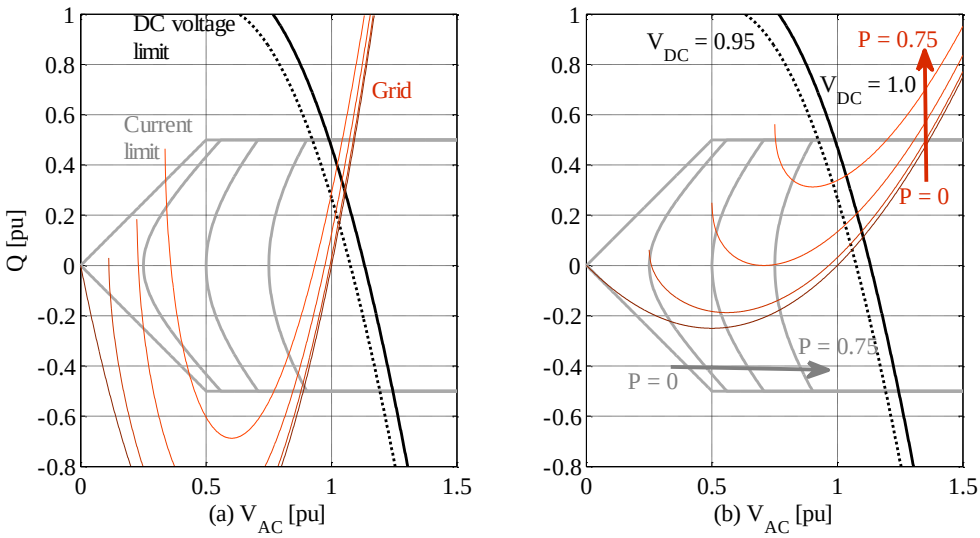

Figure 51 - Q-V_{AC} plots of network constraint and VSC-HVDC limits: (a) SCR = 5, (b) SCR = 1.

Some interesting observations can be made by looking at the figure:

- The voltage stiffness of stronger networks (SCR = 5) is apparent in Figure 51 (a), where large variations in Q are necessary to vary the PCC voltage. Conversely, the voltage in weaker AC networks (SCR = 1) is much more sensitive to Q variations.
- A 5% drop in DC voltage causes a dramatic drop in available Q. This does not only have implications in normal operation and heavily loaded conditions. One should consider this limitation also when the DC voltage falls during disturbed operation. For example, the combined frequency/DC voltage droop technique illustrated in Chapter 6 lowers the voltage during low frequency events. Since low frequency often happens due to loss of generation (i.e. active *and* reactive power supply are lost), depriving the HVDC station of Q injection capability may not be the optimal choice.

5.2.3 Droop contribution to voltage regulation

Extending the analysis above, one can add an AC voltage droop to the HVDC station and visualise it on the same Q-V_{AC} diagram. A step in Q_L can be simulated to study how the HVDC would respond to it and how this affects the voltage level in the system. This is done in Figure 52. Considering P = 0.5 pu for both SCR = 1 and SCR = 5, the thin orange curves are the grid constraint before the step in Q_L, while the thick lines are valid after the step. Two droop curves

[7]In the present context, SCR= $\frac{V_{AC,N}^2}{X_g S_N}$.

with K_{AC} = 0 pu and K_{AC} = 2 pu are plotted, where the converter controls the reactive power, in pu, according to $Q = K_{AC}(1\text{-}V_{AC})$.

A couple of interesting things can be noticed here too:

- The initial operating point being 0, after a reactive power step Q_L:
  - Without AC voltage droop (K_{AC} = 0 pu):
    - For SCR = 5 the operation moves to point A_1.
    - For SCR = 1 the operation moves to point B_1.
  - With AC voltage droop (K_{AC} = 2 pu):
    - For SCR = 5 the operation moves to point A_2.
    - For SCR = 1 the operation movers to point B_2.

  The conclusion is that, as expected, AC voltage control is more beneficial with weak networks. However, contained voltage variation comes at the expense of a large reactive power contribution from the HVDC station.
- The grid characteristic for low SCR is much less linear than for SCR = 5. This means the actual contribution of the HVDC station to voltage regulation is dependent on the operating point (initial P and Q) and the magnitude of the reactive power step Q_L. This is shown in more detail in Figure 53.
- For low SCR, operation without AC voltage droop may much more easily lead to instability for large reactive power steps Q_L, whenever the reactive demand step shifts the network curve above the horizontal droop characteristic.

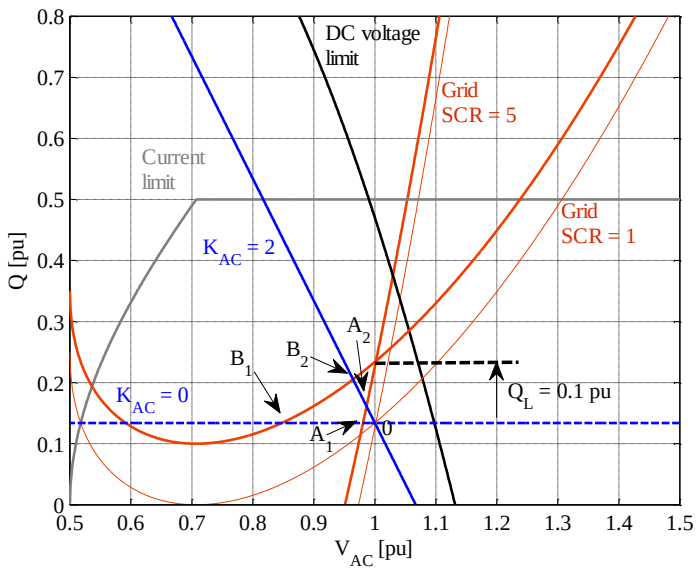

Figure 52 - Q-V_{AC} characteristics with droop control from HVDC station.

Let us know investigate a bit further what the contribution of the HVDC station to the available SCP[8] is.

[8] SCP in the context of this study is to be understood as the disturbance rejection capability of the PCC voltage against a "small" reactive power demand variation. Such definition corresponds to Eqs. (19) and (20) in typical AC networks but may be ambiguous for VSCs, where it should not be confused with the short circuit current at the PCC.

When the HVDC converter is not connected to the grid, the SCP is inversely proportional to the grid impedance Z_g. In the particular lossless case considered here, it is:

$$SCP = \frac{V_g^2}{X_g} \tag{19}$$

For grid voltage in the vicinity of 1 pu, the SCP actually becomes the inverse of X_g. It is quite easy to show (details in Appendix 4) that when the network is called to provide a certain amount of reactive power to a load Q_L, the following relation holds:

$$SCP \approx \frac{1}{X_g} \approx \left|\frac{Q_L}{\Delta V_{AC}}\right| \tag{20}$$

with ΔV_{AC} voltage variation at the PCC after insertion of Q_L. It can also be derived that, when the converter is providing AC voltage droop by a proportional gain K_{AC}, the equivalent impedance seen by a load Q_L becomes $\frac{X_g}{1+K_{AC}X_g}$ or, in other words (details in Appendix 4):

$$SCP \approx \frac{1}{X_g} + K_{AC} \tag{21}$$

which means the contribution from the converter to the equivalent system SCP is K_{AC}. This only holds under assumptions of small perturbations and linearity, as well as proximity to 1 pu voltage. Furthermore, assuming nil initial converter active power as done in Eq. (21) also affects the results, especially in weak networks, as shown in Figure 52, where the more non-linear behaviour of weak networks is depicted. The point is supported by Figure 53 too, where the equivalent SCP improvement ($\Delta SCP \approx K_{AC}$) provided by a HVDC unit with K_{AC} = 2 pu is shown for varying values of initial power P and two different values of reactive load Q_L.

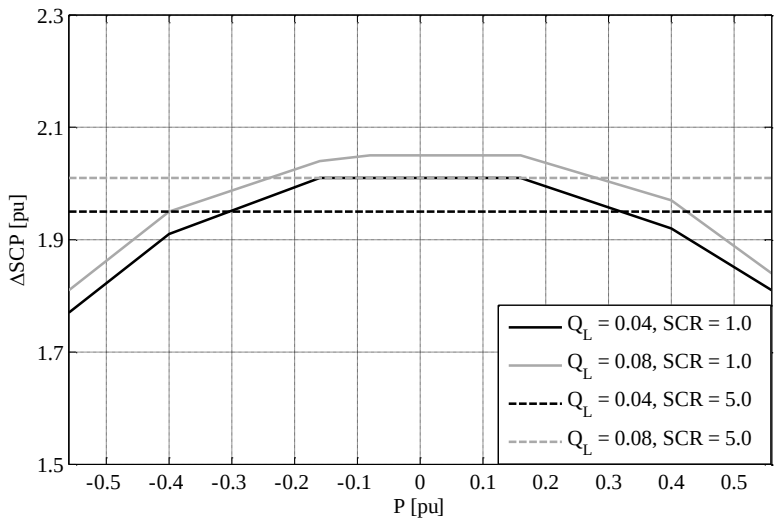

Figure 53 - SCP improvement from droop control VSC: influence of P and Q_L.

The results in Figure 53 were achieved by connecting an HVDC station modelled as outlined in Chapter 3 to an AC grid Thevenin equivalent. The HVDC station's DC side is connected to a stiff

DC voltage source, providing it with AC voltage droop control on its *q*-axis. A droop constant K_{AC} = 2 pu was used. Clearly, the initial active power has a significant impact on the real SCP improvement the HVDC station can give, while the effect of the reactive power step Q_L is less prominent.

The main reason for this is neglecting the term containing P in Eq. (18). In strong networks, X_g is so low that neglecting such term does not affect the results significantly. In weak networks, as P gains relevance thanks to a larger X_g, neglecting such term deprives the approximate results of their validity. It should be noticed, though, that a network with SCR = 1 is an *extremely* weak one, where the actual theoretical limits for connection of VSC-HVDC are approached [80]-[82] and is thus only referring to a theoretical situation. As the grid becomes stronger the approximate relations derived above gain accuracy.

5.3 Long-term voltage stability

Long-term voltage stability is one of the most classical power system problems and has emerged early [76], [132]. As LCC-HVDC found wide application, due to its non-controllable reactive power behaviour, interesting effects of such technology on this kind of stability were noticed and addressed by the research world. A large number of publications have touched upon the topic, which may by now be considered exhaustively analysed [133]-[138]. Since the application of VSC-HVDC has not spread widely yet, no investigations have studied the interaction between VSCs and power systems in terms of long-term voltage stability. In principle, due to their great controllability, VSCs should help power system stability in general and voltage stability in particular [79], or at least behave neutrally in this respect. However, when converter limitations (especially current limit) are reached, controllability is partly lost and this may have consequences on the voltage stability performance.

This section analyses the problem, illustrating its occurrence on a simple three-bus system, after having analysed how VSC-HVDC should be modelled in normal and current limited operation. A discussion of when the problem may occur in reality is done too. Conclusively, recommendations as for how to control the converters in limited current mode are derived, supplementing them with a discussion of what they mean for a WPP installed behind the HVDC link.

5.3.1 Modelling of VSC-HVDC for long-term voltage stability

This subsection proposes modelling of VSCs in current limitation as current generators. Taking the two simplest possible application examples, the behaviour of VSCs in current-limited mode is explained, highlighting its inherently voltage unstable nature.

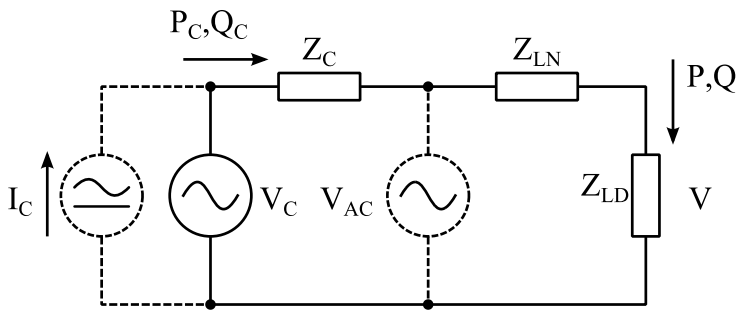

Figure 54 - Steady-state model of VSC-HVDC converter feeding isolated load.

To understand the basic phenomena governing the problem, let us first consider a VSC-HVDC station feeding an isolated load. Its steady-state operation may be modelled as in Figure 54.

Based on the operational condition, the voltage source V_C is substituted by one of the two dashed generators:

- Voltage generator V_{AC}: as long as the converter is able to maintain constant PCC voltage (assuming it is programmed to provide such control).
- Current generator I_C: when current limitation is hit (assuming the impedances in the network do not lead to steady-state 50 Hz over-voltages V_C). No control on axis prioritisation of the current is possible, the power angle being solely determined by the impedances.

Progressively decreasing the load impedance Z_{LD} with constant power factor φ_{LD} = – 0.45 rad, starting with V_{AC} = 1 pu, normalising the line impedance magnitude to Z_{LN} = 1 pu with X_{LN}/R_{LN} = 10, the PV (nose curves [76]) reported as thin dashed lines in Figure 55 are achieved on the load. Keeping the rated converter power fixed at P_N = 1 pu, the rated power factor is varied as pf_N = 1.0-0.75. The solid thick line represents the curve for no current limitation. The right plot reports the converter apparent power $S_C = \sqrt{P_C^2 + Q_C^2}$.

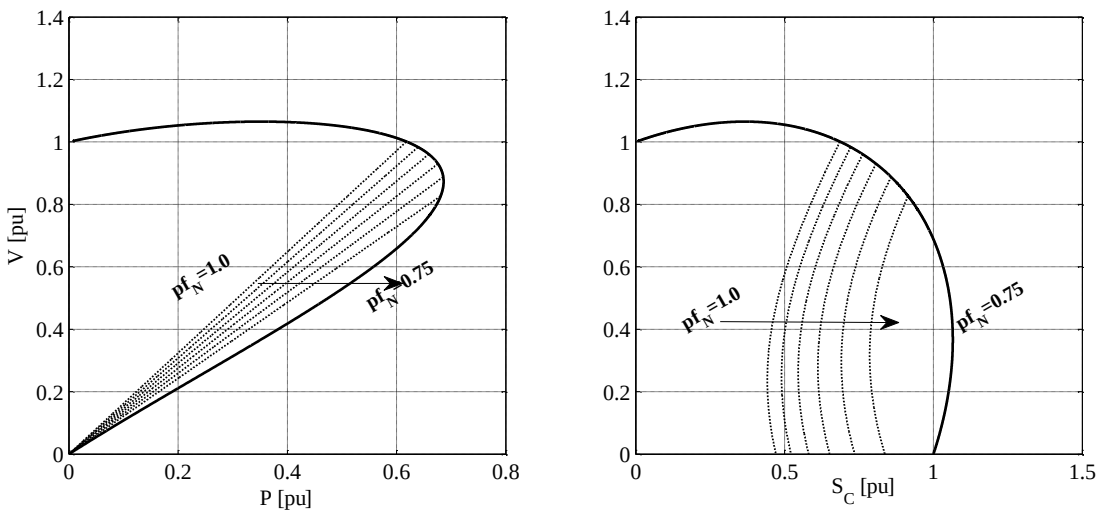

Figure 55 - PV curves on load fed by isolated VSC-HVDC: influence of rated power factor pf_N.

The figure immediately highlights the intrinsically voltage unstable behaviour of the converter during current limitation. As expected, decreasing impedance fed by constant current leads to decrease of both voltage and power. This trivial result helps understand why current-limited VSCs could potentially be dangerous when power system's voltage stability limits are approached.

Moving to a slightly more complex system, the network in Figure 56 depicts a two-bus system where the VSC-HVDC converter is exchanging complex power with an AC grid modelled by a Thevenin equivalent.

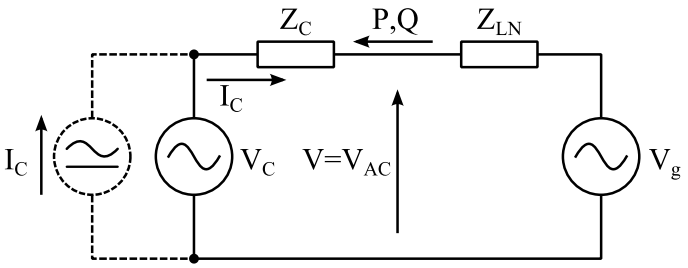

Figure 56 - Electrical model for PQ exchange between converter and AC grid.

In this case, the converter is modelled as a PQ source (load or negative load) and the equations derived in [131] can be used to understand how the system behaves in the PQV space. However, the current limitation of the VSC needs be accounted for by always limiting the converter current magnitude under its maximum value. In this case it is chosen, for the sake of example, to constrain $I_C \leq I_N$. In the PQV space, this is equivalent to drawing the cone expressed by:

$$P^2+Q^2=V \cdot I_N \tag{22}$$

and forcing the operation to not exit it. In graphical terms, this is illustrated in Figure 57. The same parameters as above have been used for Z_{LN}. V_g = 1 pu and I_N = 0.9 pu were assumed. The border between limited and unlimited operation is highlighted by a black line.

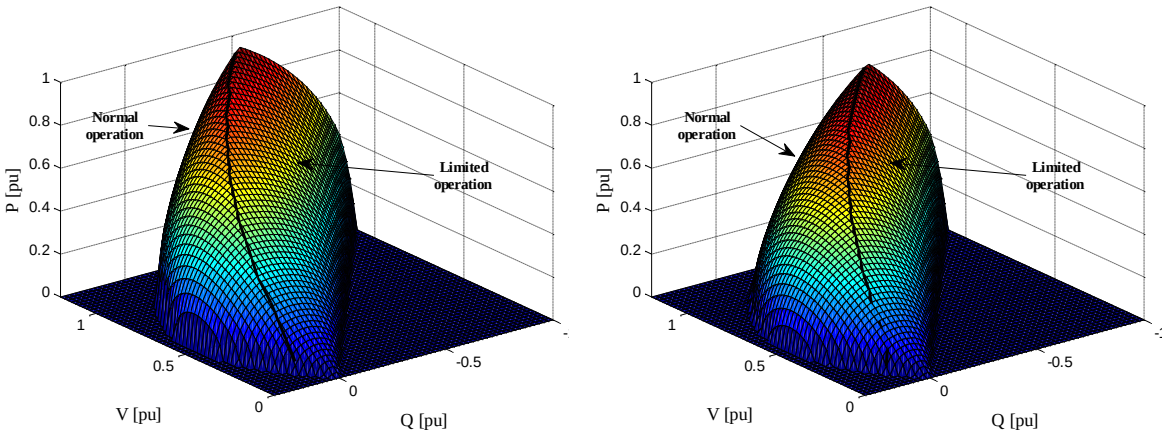

(a) P injection (inverter) **(b) P absorption (rectifier)**

Figure 57 - PQV diagrams for power exchange between VSC-HVDC and grid.

A few words are worth to be spent on the properties of Figure 57:

- On the PV plane, current limitation affects only areas with high active power injection/absorption and high reactive power injection. In most of the space, current limitation occurs beyond the voltage stability limit (tip of the nose) and therefore does not reduce the available stability margin.
- Controllability (prioritisation) of *d*- and *q*-axis currents is not completely lost in this case during current limitation. It appears from the figure that injection of reactive power increases the available active power transmission capability. On the other hand, injecting reactive power to maximise transmittable active power also implies accepting the current limitation to occur before the theoretical "unlimited" maximum active power.

- The results obtained in [139] are confirmed and summarised by Figure 57. Inverter operation allows for more active power to be flowing at the VSC terminals. This is clearly due to the fact that the transmission line Z_{LN} is not lossless and, for a given voltage V_{AC}, during inverter operation the losses are covered by the VSC, while during rectifier operation they are covered by the grid V_g.

5.3.2 Study on simple three-bus system

The intrinsic voltage-unstable nature of VSCs in current-limited mode has been elucidated above by two very simple examples. Here, the analysis is expanded to a larger system, namely that depicted in Figure 58. It comprises a grid, a VSC-HVDC converter, and a load in between. Such sketch could exemplify for example:

- A large load fed by two production areas, one being based on conventional generation (V_g) and the other being based on remote HVDC transmission (WPP or interconnector, V_{AC}).
- A large load fed by two conventional generation areas, one of them (V_{AC}) containing HVDC too and having lost its main production facilities and being left with HVDC alone.

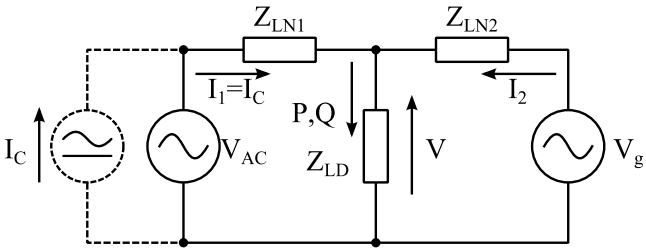

Figure 58 - Electrical model of three-bus system.

As simplifying assumptions, let us consider $Z_{LN1} = Z_{LN2}$ and $V_{AC} = V_g$ as complex numbers. In practice this means the load power is equally shared by AC grid and VSC-HVDC. These hypotheses, though quite restrictive, do not qualitatively affect the results, as will be shown later.

The generic approach that will be applied is derivation of an equivalent Thevenin circuit of the network as seen from the load terminals. Once the parameters V_{eq} and Z_{eq} of such equivalent circuit have been found, the voltage stability profile is immediately determined. Complex numbers will be used in the following.

(a) Normal operation

A further assumption for normal operation is that the VSC is able to control the voltage $\overline{V}_C$ so as to match V_g. If the load admittance is increased the equal power sharing between grid and VSC-HVDC is maintained. Under these assumptions, the converter can be modelled by a voltage source $\overline{V}_C$ and the equivalent circuit parameters will be:

$$\overline{V}_{eq} = \overline{V}_C \cdot \frac{\dot{Z}_{LN2}}{\dot{Z}_{LN1} + \dot{Z}_{LN2}} + V_g \cdot \frac{\dot{Z}_{LN1}}{\dot{Z}_{LN1} + \dot{Z}_{LN2}} = V_g \tag{23}$$

$$\dot{Z}_{eq} = \frac{\dot{Z}_{LN1}\dot{Z}_{LN2}}{\dot{Z}_{LN1} + \dot{Z}_{LN2}} = \frac{\dot{Z}_{LN2}}{2} \tag{24}$$

where complex numbers have been used. Changes in impedance distribution and/or active/reactive load sharing (differences in angle/magnitude of V_g and $\overline{V}_C$) will reflect into the value of the above parameters and influence voltage stability accordingly. The results are therefore not affected qualitatively by the added assumption and the methodology can be applied regardless of the actual impedance distribution and converter voltage angle and magnitude.

(b) Current-limited operation

If current limitation is reached, the needed control freedom for maintaining constant V_{AC} is lost by the converter. Following the approach suggested above, the VSC-HVDC station is modelled as a complex current source $\overline{I}_C$ (dashed current generator in Figure 58). The Thevenin equivalent parameters will be given, in complex numbers, by:

$$\overline{V}'_{eq} = V_g + \dot{Z}_{LN2}\overline{I}_C \tag{25}$$

$$\dot{Z}'_{eq} = \dot{Z}_{LN2} \tag{26}$$

The effect on the voltage stability of the system is evidently dramatic in terms of equivalent impedance, since it doubles under the current assumptions, drastically reducing the theoretical transmittable power. The effect on the equivalent voltage $\overline{V}'_{eq}$, on the other hand, depends on the control strategy for $\overline{I}_C$, whose magnitude is limited, but whose angle can be changed by control means. Angle and magnitude of $\dot{Z}_{LN2}$ play a role too in determining the value of $\overline{V}'_{eq}$.

To understand more clearly how the angle control strategy of $\overline{I}_C$ affects the magnitude of $\overline{V}'_{eq}$, let us expand the expression of $\overline{I}_C$ as a complex number (real axis aligned with V_g):

$$\overline{I}_C = I_{Cr} + jI_{Ci} \quad | \quad I_C = \sqrt{I_{Cr}^2 + I_{Ci}^2} = I_N \tag{27}$$

Writing the magnitude of Eq. (25) and rearranging (detailed calculation in Appendix 4):

$$\frac{V'^2_{eq}}{Z^2_{LN2}} = \left(I_{Cr} + \frac{V_g}{Z_{LN2}}\cos\theta_{LN2}\right)^2 + \left(I_{Ci} - \frac{V_g}{Z_{LN2}}\sin\theta_{LN2}\right)^2 \tag{28}$$

where $\theta_{LN2} = \operatorname{atan}\frac{X_{LN2}}{R_{LN2}}$ is the line impedance angle. The equation is that of a circle in the complex converter current plane with centre in $C = \left(-\frac{V_g}{Z_{LN2}}\cos\theta_{LN2}\,;\,\frac{V_g}{Z_{LN2}}\sin\theta_{LN2}\right)$ and radius $r = \frac{V'_{eq}}{Z_{LN2}}$. Parameterising the equation for different values of the equivalent voltage magnitude, plotting the corresponding circles and superimposing the circles with constant converter current magnitude I_C, Figure 59 is obtained, which contains interesting information in terms of how to increase the equivalent voltage and therefore the transmittable power. In Figure 59, it is supposed that I_C be limited to the nominal current I_N, which is also used as a parameter. Furthermore, the same transmission line parameters as above have been used and V_g = 1 pu still holds.

Interesting properties can be noticed in Figure 59:

- Maximisation of transmittable power happens for maximum V'_{eq}. For a given value of I_N, maximum voltage is achieved for strongly negative imaginary current. In the ideal case of lossless transmission line a pure negative imaginary current achieves maximisation of V'_{eq}. This can clearly be seen in Eq. (28) too.
- On the other hand, just imposing $I_{Cr} = 0$ in reality may not be straightforward, nor sensible, for the following reasons:
    - The relation between real and imaginary parts of the converter current with converter active and reactive power depends on the actual operational scenario (power angle). Since the VSC is supposed to fulfil other control objectives (P, V_{DC}, Q, V_{AC} control) before entering current limitation, setting $I_{Cr} = 0$ and $I_{Ci} = I_N$ in current-limited mode may be in contrast with other desired control features.
    - Raising the equivalent voltage V'_{eq} may actually lead to an excessively high converter voltage, which would not be reachable within the VSC's capabilities.
- In spite of the above, it is expected that increasing the voltage at the load bus is achieved if supplementary reactive power is provided in order to make up for the increasing consumption along the lines as the load increases. The grid voltage source V_g is uncontrolled, but the converter current $\bar{I}_C$ can be selected to be mainly reactive. Intuitively, hence, it is expected that maximisation of V'_{eq} is obtained by feeding reactive power.

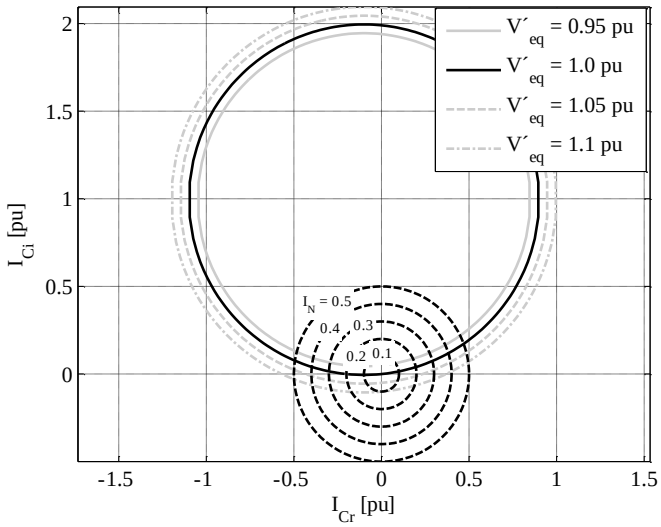

Figure 59 - Constant equivalent voltage circles and intersection with converter current locus.

To exemplify the effects of different converter current angles on the voltage stability of the system depicted in Figure 58, the PV curves are plotted for ideal case (normal operation, no current limitation, $V_{AC} = V_g$) and two values of V'_{eq} in current-limited mode in Figure 60. The complex expression of I_C for the two cases is reported too, highlighting the improvement a proper control of the current angle can bring about in the PV profile of the system: maintaining the same maximum current modulus (I_N = 0.4 pu) 8° decrease in current angle can nearly provide an additional 0.1 pu of transmittable power, improving the long-term stability. The arrows illustrate the operational point path as load increases in the worst of the two cases (V'_{eq} = 1.05 pu).

In order to more thoroughly correlate the above results with the real control philosophy of an HVDC station, the converter behaviour during current limitation is of utmost importance. More

specifically, the current prioritisation philosophy needs be taken into consideration. Current prioritisation in SRF (*dq*-frame) is a known feature and detailed description is hence demanded to Appendix 1.

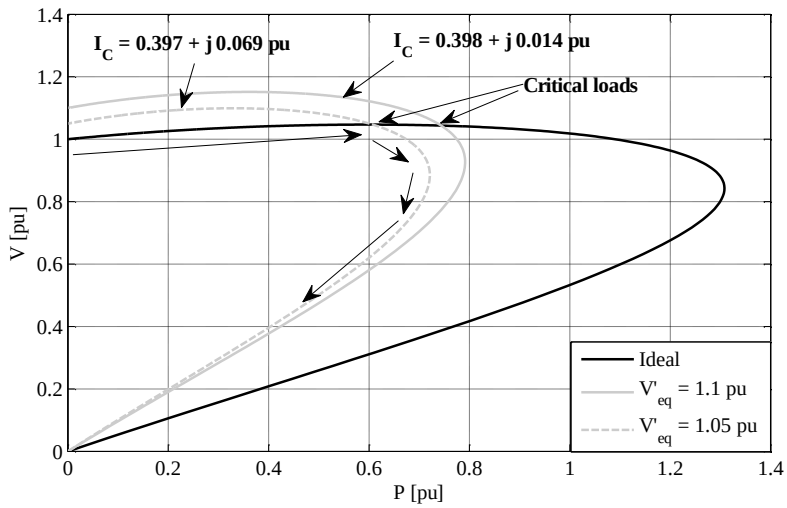

Figure 60 - PV curves for three-bus system in ideal normal operation and current-limited (I_N = 0.4 pu) mode with two different current angles.

Here, dynamic simulations are used to understand how the current prioritisation approach relates to the above analysis. The model in Figure 58 was implemented in dynamic simulation software. The VSC-HVDC station, being connected to a stiff voltage source on the DC side, is controlled in P-V_{AC} fashion according to Figure 11 (Chapter 3), but the V_{AC} droop block is substituted by a PI to guarantee zero voltage error in normal operation. The load admittance is progressively increased and the power reference of the VSC-HVDC is increased accordingly, so as to maintain equal load sharing.

The three following cases are simulated:

1. Ideal case: VSC-HVDC has sufficient current capability to maintain V_{AC} = 1.0 pu regardless of the power injection – i.e. $I_N = \infty$.
2. Limited case with I_d priority: the VSC-HVDC has current limited below I_N = 0.4 pu and the active power is given priority over the reactive power – i.e. I_{Cd} is controlled to its unlimited reference while I_{Cq} is limited according to the maximum current.
3. Limited case with vector priority: again, the converter current is limited below I_N = 0.4 pu. However, no prioritisation of I_{Cd} (P_C) or I_{Cq} (Q_C) is done – i.e. the reference current vector is only limited in its magnitude, without changing its angle.

The PV curves of the system for the three cases are plotted in Figure 61. It is apparent that, as hypothesised above, priority on P over Q is deleterious to the long-term stability (dashed line), while vector limitation, where Q can grow together with P, performs better and provides a 0.15 pu additional margin in the active power that can be delivered to the load.

The graphs in Figure 62 and Figure 63 shed further light on the operation of the system, respectively reporting the converter current in both complex plane (relative to V_g) and converter SRF and the converter active and reactive power (P_C and Q_C respectively). It can be seen that by letting Q_C grow along with P_C to support the voltage, more active power can eventually be

delivered to the load *and* produced by the VSC-HVDC. The current plot in Figure 62 is a further proof of the analytical observations derived with Eq. (28) and Figure 59.

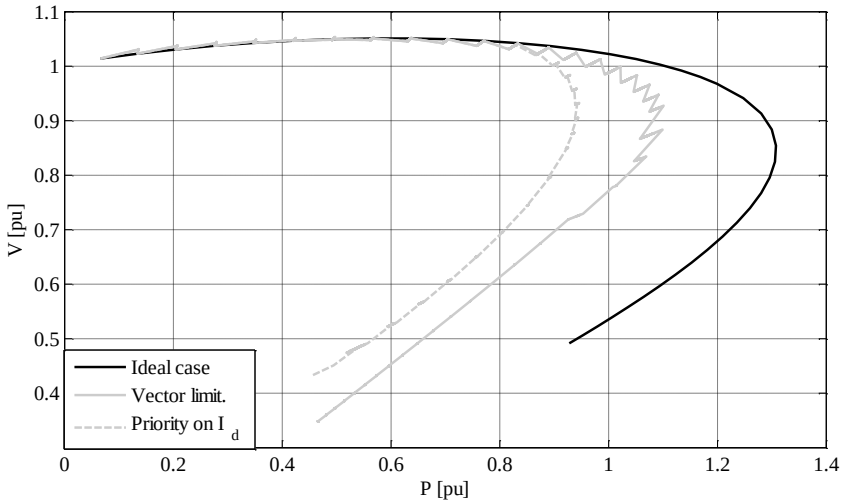

Figure 61 - Load PV curves from dynamic simulation in ideal unlimited case, I_d-priority and vector limitation. P is in pu of V_g^2/Z_{LN2}.

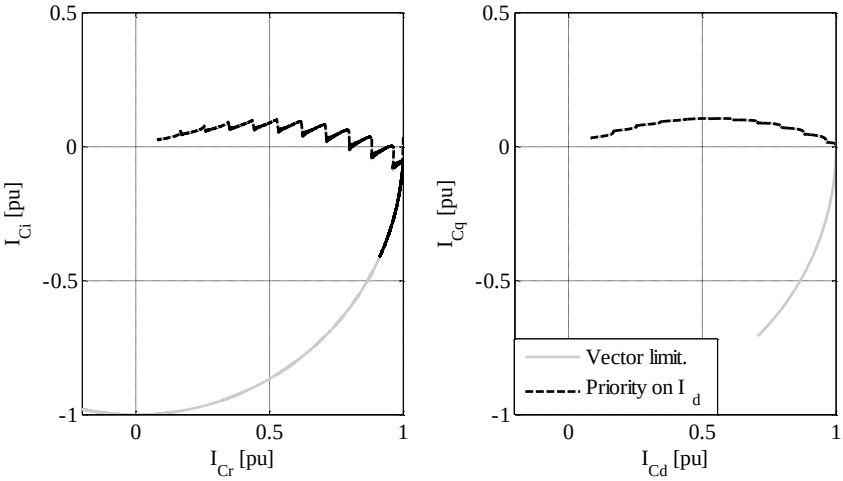

Figure 62 - Complex and SRF converter current locus for two current limited cases, in pu of converter ratings.

Several more investigations could be done on the issue, in particular pursuing the following objectives:

- Address the influence of the main assumptions behind the analysis, mainly the purely symmetrical nature of the electrical network and operational scenario.
- Investigate how the converter voltage and reactive power limits related to the available DC voltage (described above in Section 5.2) affect the operation under current limitation.
- Demonstrate a similar phenomenon can occur on larger, more realistic, heavily loaded power systems.

Nevertheless, the presented findings are deemed to be quite generic, and for example the graph in Figure 59 should be usable on a wider scale to explain the mechanisms leading to voltage collapse and determine how to improve VSC-HVDC control in current-limiting mode.

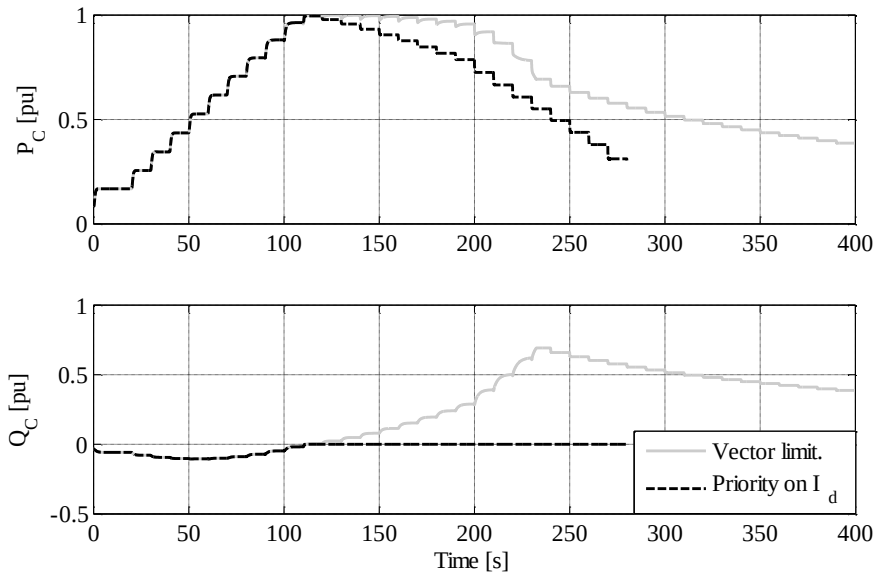

Figure 63 - Time plot of converter active and reactive power in pu of converter ratings.

5.3.3 Discussion: influence on WPP control

The findings of this section are of general nature but can be particularised for application to WPPs. Somehow, the results are particularly relevant in case of WPP connection, since the most intuitive control philosophy, from the economic perspective of the utility owning the WPP, would most certainly be prioritising P over Q, in order to deliver all wind power and maximise revenue.

However, it was proven that accompanying the injection of active power with proper support of reactive power in current limitation and approaching the tip of the nose curve actually allows for a larger amount of active power to be eventually delivered to the network and improves the voltage stability margin, giving the TSO time to take necessary countermeasures for solider long-term stability.

In other words, when the power system is heavily stressed and approaches voltage collapse, vector limitation of current or prioritisation of *q*-axis current offer multiple advantages:

- Stability margin improvement and consequent easier prevention of black-out.
- Increase of transmittable power to the loads.
- Increase of transmittable power and energy from the VSC-HVDC (and possibly WPP).

All the above points are, at the end of the day, to the advantage of TSOs, utilities as well as society as a whole.

The fact that proper reactive power support be beneficial for voltage stability is nothing new [76], but it is important to understand how the growing amount of PE converters must act to enhance the system performance as well as realise that measures that seem economically counterintuitive (prioritisation of Q or vector limitation on a VSC-HVDC link delivering wind power) may actually bring, in certain conditions, benefits to all parties involved in power system operation.

5.4 Summary

The contribution of VSC-HVDC stations to steady-state onshore AC voltage control has been the subject of the first part of the chapter. The focus was on accounting for steady-state converter limitations and their interaction with grid constraints. Thevenin representation of strong and weak networks has been used to illustrate the capability of VSC-HVDC stations to support voltage control. The special importance of voltage control for weak networks was emphasised. Interestingly, when applying AC voltage droop control, due to the non-linearity of the grid characteristics, the contribution of a VSC to the available SCP is dependent on the operating point.

The second part of the chapter was dedicated to investigating the relation between long-term voltage stability and the behaviour of VSC-HVDC in current limitation. Since the issue has not been observed to date, the occurrence of the problem was exemplified on a simple three-bus system and conclusions in relation to the desired control of the current angle to enhance voltage stability were drawn, indicating reactive power support must be guaranteed when the system is highly stressed. Items for a deeper future investigation of the phenomena were proposed. The implications the findings have for WPP control were also discussed, due to their potentially counterintuitive nature.

Chapter 6 Power balance control

The subject of this chapter is active power balance control in AC-DC grids and the contribution WPPs can give to it. Natural measures of active power balance are the frequency in AC systems and the voltage in DC systems: the chapter is arranged accordingly. In the first part concerning frequency control (IR and PFC), using a point-to-point VSC-HVDC connection of a WPP, a proposed communication-less control scheme is critically compared to one making use of communication. Moreover, other factors that affect the achievable performance are discussed. The second half of the chapter regards DC voltage control in DC grids. Since the focus is again on the WPP, a very simple three-terminal DC network is utilised to show WPP limitations and understand the implications for the rest of the network. The findings presented here were partly included in Publications 6 and 9 [90], [111], *but are here further expanded and improved.*

6.1 Introduction

Matching the power[9] balance at all times is the principal control objective in power systems, since delivery of power to customers is their reason for existing. Due to the way power systems have operated to date, i.e. in AC fashion with nearly constant frequency determined by the rotational speed (and thus torque and power balance) of SGs, historically power balance has been guaranteed by controlling frequency and ultimately the speed of SGs by means of governors regulating their mechanical power input [76], [112]. On the other hand, for various reasons, power balance control in VSC-based DC networks is implemented through DC voltage (or capacitor energy) control [1], [19], [60].

Modern WPPs are already called to contribute to frequency control – e.g. [31] – and several publications have touched upon the topic – e.g. [33], [35], [140]. The prospected installation of VSC-HVDC systems and their combination with WPPs raise new issues in relation to (i) how WPPs can contribute to frequency control being decoupled from AC systems by VSC-HVDC systems and (ii) what contribution WPPs can give to DC voltage control in DC grids. These are the topics of the next two sections. Section 6.2 is dedicated to frequency control. Section 6.3 discusses DC voltage control. Discussion of interaction between frequency and DC voltage control is out of scope here, but surely an interesting topic for future research.

[9] Along this chapter, the terms *power* and *active power* are used equivalently.

The chapter discards other ways to control the power balance, such as for example angle control in AC systems, which becomes particularly interesting in networks without any rotating mass [85] and which is partly touched upon in Chapter 4.

6.2 AC frequency control

The configuration used in this section is the default according to Section 2.4.3(c), i.e. a point-to-point VSC-HVDC connection of WPP. The attention is on both IR and PFC through frequency droop. Due to the way such a system is controlled, state-of-art WPPs may already provide the necessary support to the onshore grid frequency [33], provided that the sensed onshore frequency can be transmitted offshore with sufficient speed and reliability. All power injected by the WPP is transmitted, with small delay and losses, to the onshore PCC. However, concerns related to the need of long communication lines have pushed researchers to devise and successfully test communication-less[10] schemes to provide the same service [38], [40], [111]. Nevertheless, the advantages of eliminating long-distance communication must be weighed against real dynamic requirements of frequency control as well as realistic reliability of communication links. Hence, the communication-less scheme is here compared to a communication-based scheme as was done in Publication 9 [111]. The two solutions are summarised in Figure 64. More details are given below on the two control candidates.

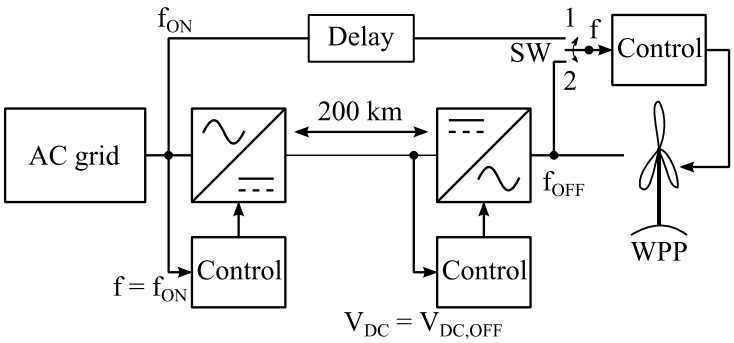

Figure 64 - Sketch of candidates for frequency control provision.

The AC grid is modelled by a lumped synchronous machine provided with generic governor model as presented in Appendix 1 and Appendix 2. The generic active power control of the WPP looks like the one shown in Figure 14 but the measurement and communication layout depends on the control candidate. The control of the VSC-HVDC stations too depends on the chosen candidate. Generally, however, the left hand side onshore station's control will be based on Figure 11, while the offshore converter (right hand side) uses a scheme such as that reported in Figure 12 (both described in more detail in Section 3.2.2). The difference will arise from which control scheme will be allocated to the block *P Droop* in Figure 10.

6.2.1 Candidate 1: communication-based scheme

The first candidate is based on standard control diagram and settings for the HVDC converters, according to the description above. The onshore frequency is directly transmitted to the WPP and its controller (Figure 14) by setting the switch SW in position 1. The communication link can be modelled by an ideal time delay, which is expressed as e^{-sT_d} in the Laplace domain. Generally,

[10] *Communication-less* means, in this context, without long-distance communication, i.e. all quantities needed by each controller can be measured "locally": for an HVDC station this means at its terminals, for a WPP it means at the PCC.

such delay is a function of the technology used and the number of elements in the communication chain, more than its distance. The block *P Droop* in Figure 10 can be left empty in both HVDC stations.

6.2.2 Candidate 2: communication-less scheme

The second candidate makes use of a coordinated control scheme of DC link energy and offshore frequency. For this purpose, besides using the default controls, the block *P Droop* in the converter control (Figure 10) needs to be filled according to Figure 65 (a) or (b) depending on whether the station is installed onshore or offshore respectively.

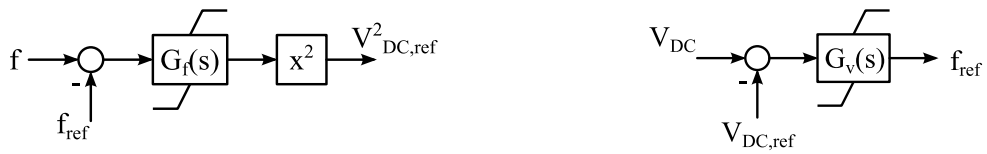

(a) Onshore converter **(b) Offshore converter**

Figure 65 - *P Droop* block for onshore and offshore converter in Candidate 2.

The transfer functions in Figure 65 (a) and (b) can for example be expressed as follows:

$$G_f(s) = \frac{K_f}{1+sT_f} \tag{29}$$

$$G_v(s) = \frac{K_v}{1+sT_v} \tag{30}$$

Proper settings of the droop gains K_f and K_v allow for perfect steady-state mirroring of the onshore frequency f_{ON} in the offshore network. Considering usual dynamics of PLL and DC voltage control, which are much faster than typical onshore frequency dynamics, if the condition $K_fK_v = 1$ is fulfilled and the filtering time constants T_f and T_v are chosen sufficiently small, onshore and offshore frequency are essentially undistinguishable, the WPP can act as though it was connected onshore and no long-distance communication is needed. The last statement is exact only by neglecting the voltage drop and power losses along the DC line, since the real steady-state offshore frequency deviation will be given by, neglecting shunt losses [40]:

$$\Delta f_{OFF} = K_fK_v\Delta f_{ON} + K_v\frac{r_{DC}}{V_{DC,OFF}} \cdot \Delta P_{OFF} = K_fK_v\Delta f_{ON} + K_v\frac{r_{DC}}{V_{DC,ON}} \cdot \Delta P_{ON} \tag{31}$$

where r_{DC} is the DC line resistance and ΔP_{OFF} (ΔP_{ON}) is the variation in active power injected into (absorbed from) the DC system by the offshore (onshore) HVDC station, approximately equal, excluding losses, to that produced by the WPP. The rightmost element in Eq. (31) can be compensated for by proper control arrangement in the onshore HVDC station and knowledge of r_{DC} [40]. Additionally, the DC line resistance must anyhow be small to reduce losses and the power variation ΔP_{OFF} (ΔP_{ON}) is small too. It is thus plausible to initially assume $\Delta f_{OFF} \approx \Delta f_{ON}$ for $K_vK_f = 1$. In the present case no compensation is initially employed, to assess its importance for a real application.

6.2.3 Comparison of control candidates

The two control candidates are compared with time domain simulations. Then, the comparison continues through a discussion, resulting in recommendation of the best control candidate for the particular application. The most relevant parameters of WPPC and HVDC system are reported in Table 12, along with the important parameters of the SG and its governor (as stated above, all synchronous generation was lumped into one SG, as in Figure 7, and modelled as detailed in Appendix 1 and Appendix 2). Moreover, the control candidates are separated according to whether or not IR is required from the WPP, according to the nomenclature reported in Table 13.

Table 12 - Relevant control parameters for frequency control simulations.

WPPC					HVDC system		SG		Governor
T_{ppcf} [s]	T_{ppci} [s]	T_d [s]	K_f [pu]	dP_{max} [pu/s]	T_f [s]	T_v [s]	H[11] [s]	D [pu]	As per Table 21 in Appendix 2
0.1	0.2	0.1	2.5	0.1	0.01	0.01	2.5	0	

Table 13 - Nomenclature of Candidates compared: all gains are in pu.

WPPC / HVDC system	$K_{ppcin} = 0$	$K_{ppcin} = 1.25$
SW = 1, $K_f = K_v = 0$	1A	1B
SW = 2, $K_f = 0.5$, $K_v = 2$	2A	2B

For all the simulations, the wind power penetration is 2.5% (WPP rated at 120 MW in a 5000 MW system). This figure is not crucial in this case, as the focus is on which control option is better in terms of frequency control provision and not on the effect the contribution from the WPP has on the power system. It should be noticed, though, that the characteristics of the power system are so as to obtain a dynamic frequency response which is quite fast. One may think of the system as an island power system, where frequency quickly settles in about 10 s after a disturbance and the poor inertia yields large frequency gradients. This is done to reproduce the worst case in terms of allowable lags, since the relative effect of any delay in the control/communication chain is magnified compared to what it would be in slower systems. Finally, the wind speed is assumed to constantly lie above rated (more specifically, it is 13 m/s) and, since PFC is required, the WPP is curtailed to produce less than the available power, providing some regulation reserves. In the particular case, the WPP is initially producing 0.9 pu (108 MW), making 0.1 pu (12 MW) available as regulation reserves. Over-production of the turbine above MPPT level is allowed in this particular case, but since the focus is on comparing alternatives for VSC-HVDC connection of WPP and not directly on the WPP performance a detailed discussion of the problem is not done here. Over-production is more carefully discussed in other publications – see e.g. [33], [141].

Candidates are compared as 1A vs 2A and 1B vs 2B. A 1000 MW (0.2 pu) load step is simulated. If one assumes this to be the size of the largest unit in the system, considering the available regulating energy K_S of the power system, maximum steady-state frequency deviation of 0.02 pu is allowed (49 Hz minimum steady-state frequency after PFC in a 50 Hz system) while the frequency nadir depends on the dynamic characteristics of the system and is in the particular case slightly above 0.96 pu (48 Hz). Assuming that the onshore HVDC station clamps the DC voltage fixed to 1 pu, the gains K_f and K_v according to Table 13 imply the following for Candidates 2:

[11] Based on 5000 MW, rated power of the lumped SG.

- The minimum DC voltage at the onshore station is approximately 0.98 pu dynamically and 0.99 pu in steady-state. These values are valid without any DC line compensation term in the controller.
- The offshore frequency will move in the same range as the onshore, meaning that the WPP can respond as if it was AC-connected directly onshore.

The choice of the parameters may be questionable. For example, depending on the real steady-state DC voltage ripple, K_v may have to be increased to make sure DC voltage variations due to frequency deviations are distinguishable from normal voltage drifts. This comes at the expense of larger disturbed DC voltage excursions and thus (i) higher power losses and (ii) reduced reactive power capability of the onshore station – see Section 5.2. Additionally, no dead-bands are adopted in any of the controllers, but would probably have to be adopted in reality, to prevent the WPP from contributing during small frequency variations.

A time domain comparison of the results for the control candidates is summarised from Figure 66 to Figure 69. The active power at the onshore PCC is reported in Figure 66 for cases 1A and 2A, while in Figure 67 the plots of onshore and offshore frequency as well as onshore and offshore DC voltage in Candidate 2A are presented. The same is done in Figure 68 and Figure 69 for Candidates 1B and 2B.

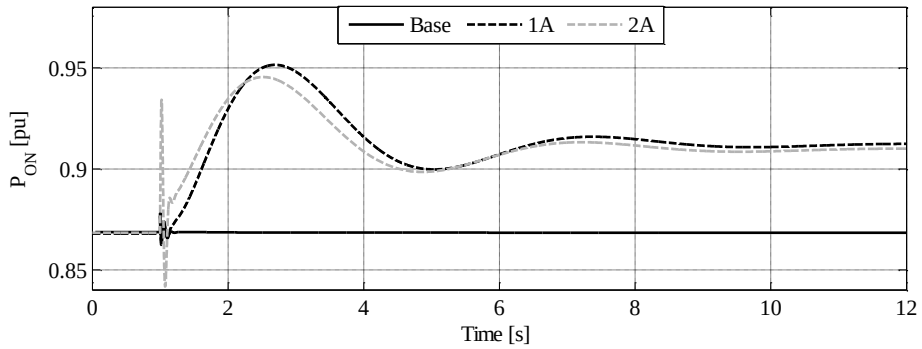

Figure 66 - Onshore power production: base case and Candidates 1A vs 2A.

The following conclusions can be drawn by exploring the figures:

- Candidate 2, thanks to the initial response of the DC voltage controlling unit (onshore HVDC station) behaves better than Candidate 1 immediately after the event, since supplementary active power is directly evacuated from the DC link in order to decrease the DC voltage and the system does not have to await the WPP response. For the same reason, though, as the frequency starts increasing again after the nadir, the frequency support at the onshore PCC is slightly diminished, since some of the incoming power is used to increase the DC voltage onshore.
- Perfect mirroring of onshore frequency in the offshore network does need compensation of the line losses. The onshore and offshore frequency curves for Candidate 2 in Figure 67 and Figure 69 are not very far apart, but using compensation improves the performance as illustrated in Figure 70 for Candidate 2B. The voltage drop on the DC line has been compensated by inserting a correction of the DC voltage reference in the onshore station given by $r_{DC} \cdot P_{ON}$, as proposed in [40]. This allows (i) essentially perfect mirroring of onshore frequency in the offshore network and as a consequence (ii) steady-

state regulating power at the onshore station practically equal to Candidate 1B, except for small additional losses.

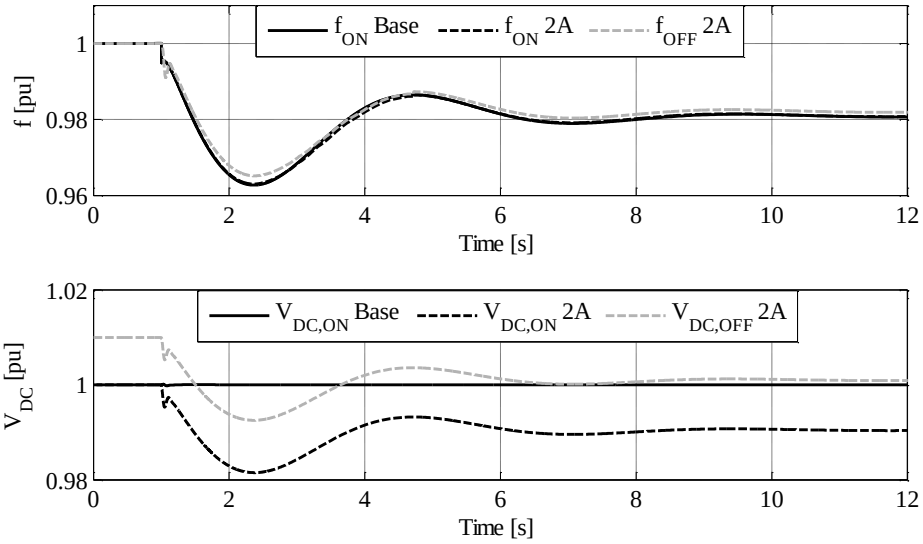

Figure 67 - Onshore and offshore frequency and DC voltage for base case and Candidate 2A.

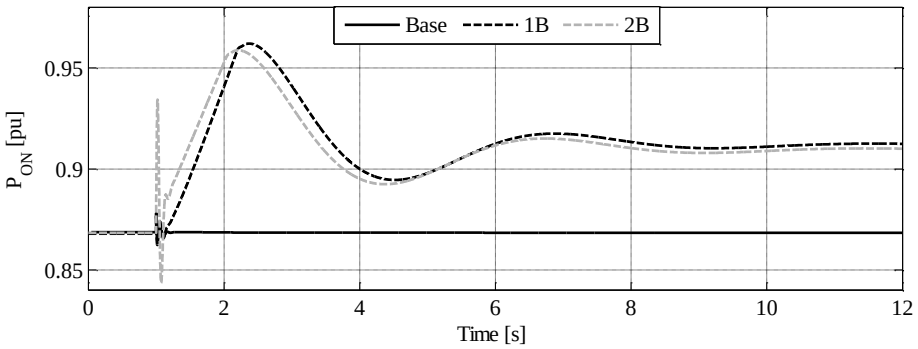

Figure 68 - Onshore power production: base case and Candidates 1B vs 2B.

Looking at the overall performance one may conclude that the two alternatives are performing very similarly from a frequency control standpoint. The following should however be considered to have a firm recommendation of which candidate is the best:

- As discussed above, modulating the DC voltage implies, besides slightly increasing the losses, reducing the reactive power production capability of the HVDC station. Low frequency events are often due to the loss of generation. If the lost generation lies sufficiently close to the VSC-HVDC station, voltage as well as frequency support may be desired from the HVDC. If this is the case, one should either (i) choose Candidate 1 or (ii) choose Candidate 2 and possibly have to oversize the DC link voltage to guarantee enough reactive power capability during disturbed operation.
- Candidate 2 results slightly better for the very initial instants after the event. As such, it should be chosen if the HVDC is connected to a system with low inertia, where reducing ROCOF is the priority during frequency drifts.

As a recommendation one may say that, considering the added control complexity, the first bullet above, the available communication technologies and the simplicity of the point-to-point configuration, Candidate 1 should be the default choice.

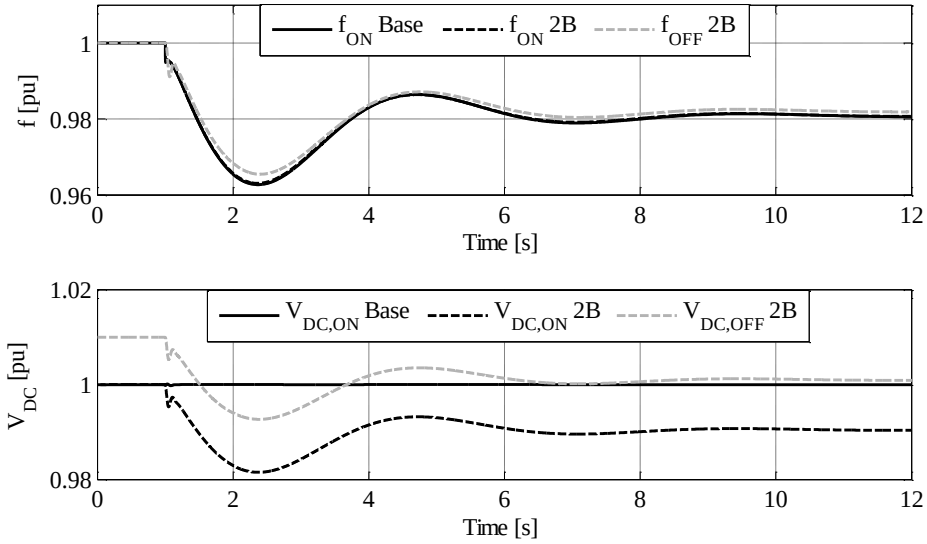

Figure 69 - Onshore and offshore frequency and DC voltage for base case and Candidate 2B.

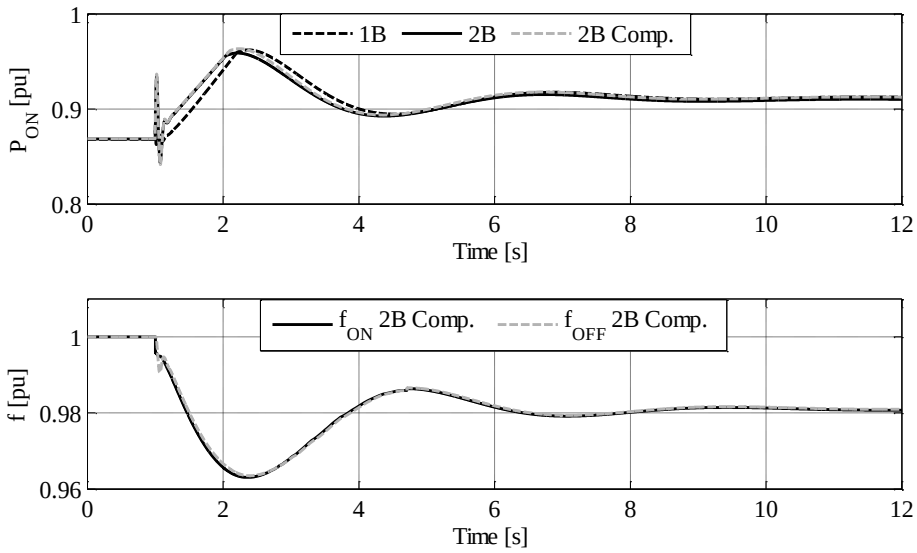

Figure 70 - Response for Candidate 2B and DC line voltage drop compensation.

(a) Candidate 1: sensitivity to communication delays

When employing Candidate 1, it is also important to understand to what extent the communication delay should be minimised, in order to choose the best alternative for the communication system. The default values for T_d in Candidate 1 is 100 ms, which may be considered a realistic approximation of what can be done in reality. As elucidated by Figure 71, increasing T_d to 300 ms expectedly worsens the response during the first instants after the disturbance. The time shift due to the delay, implies a phase lag in the power production with

respect to the frequency deviation over the whole response, but such delay is not as critical after the nadir as it is before.

It is therefore recommended to try and minimise communication delays. In doing so, one should however consider the following:

- The scenario above is, as already pointed out, extremely demanding in terms of frequency control dynamics. Looking at real systems one may consider it, if not as a worst case, certainly as a very tough one. Requirements on the maximum allowable delay are relaxed in stiffer systems.
- If ROCOF is not a crucial figure in the system, larger delays may be accepted. In very large systems, the frequency nadir may happen several seconds (instead of roughly 1 s as in the present case) after the disturbance, meaning that a few hundred ms delay would not affect the response dramatically.
- If ROCOF is a vital element, large communication delays represent one more reason to select Candidate 2.
- Contrary to what happens for POD (see Chapter 7), making the communication delay fully deterministic is not vital, although it is advisable especially if IR (or similar fast frequency response) is implemented.

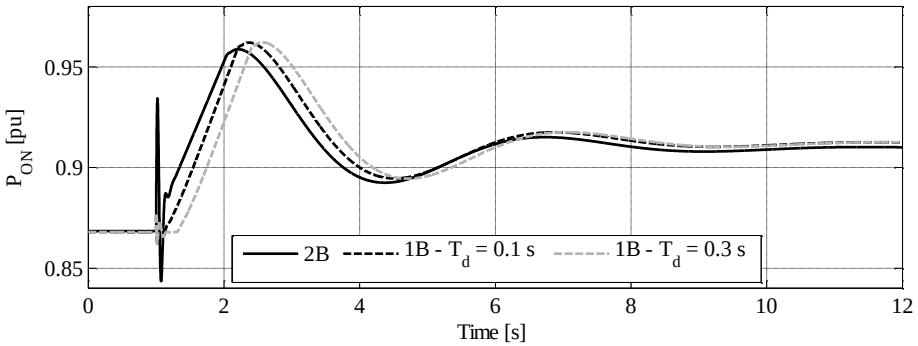

Figure 71 - Influence of communication delays on response with IR.

(b) Effect of ramp-rate limiters

Commercial WPPs, analogously to conventional units, make use of ramp rate limitations of their active power production [22] for different reasons. In opposition to what WPPs do, however, SGs are able to instantaneously and naturally deliver inertial energy when the frequency varies, simply due to their physics. This is practically impossible to do for WPPs, if based on Type 4 WTGs, mainly for the following reasons: (i) the full PE decoupling of generator and grid, (ii) the above mentioned ramp-rate limiters and (iii) the difficulty to instantaneously detect frequency variations.

The first reason does not need discussion, while the last reason is out of scope here. A few words are spent, however, to illustrate that ramp-rate limiters can have negative influence even with some kind of software-provided IR or similar fast frequency response (such as, simply, instantaneous droop regulation with sufficiently high gain). The frequency in the above simulations is measured with standard PLLs [128] and its derivative is filtered to obtain a noise-less IR power reference (according to the diagram in Figure 14 and essentially clarifying what reason (iii) above means). Such reference is summed to other power references to generate the black curve in Figure 72. The ramp-rate limiter, however, clips such reference and outputs the grey signal. A limit of 0.1 pu/s has been assumed [111]. This illustrates that, along with

communication delays, ramp-rate limiters are also relevant to derivation of requirements for implementation of fast frequency control.

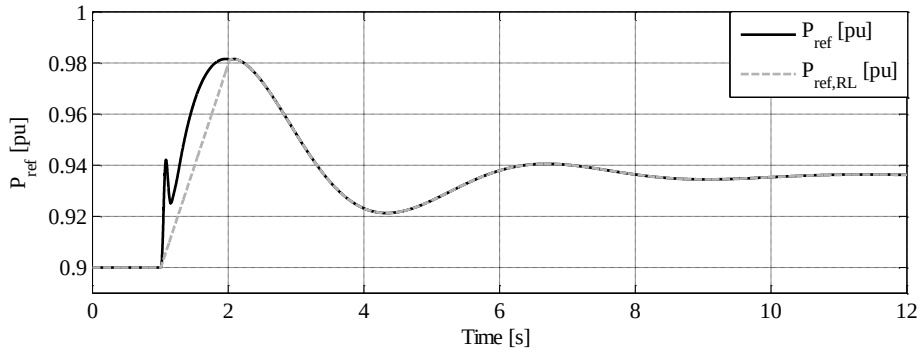

Figure 72 - Effect of ramp rate limiter on WPP active power reference for Candidate 2B.

6.3 DC voltage control

DC voltage control[12] is a somewhat more challenging task than AC frequency control. This is true from a static standpoint, as voltage is *not* a global measure of the power balance in a DC system, contrary to frequency in AC systems [60], [61]. Dynamically, the differences are possibly even more prominent, since theoretical complete depletion of stored energy in a DC system (capacitance charge) can happen in times two or three orders of magnitudes lower than for that stored in AC systems (SGs' rotating masses) [19].

Hence, if the objective is to evaluate the contribution a WPP can give to controlling the DC voltage, one cannot neglect such differences, and in particular the latter. In this section, after a brief introduction to what HVDC converters can do in terms of DC voltage control, a discussion of the realistic contribution WPPs can offer in these terms is done, terminating with an illustration of the main points by a simple study case. The focus is on the dynamic performance to regain stable operating conditions after power imbalances. Proper steady-state control (power flow, secondary control) is assumed to exist.

Firstly, however, the configuration chosen for the simulations in this section is briefly described. As briefly mentioned in Section 2.4.3(c), a three-terminal DC network is used in this context: coordinated DC voltage control makes sense only in multiterminal networks and a three-terminal layout is the simplest system to focus on the WPP contribution. The system is sketched in a simplified fashion in Figure 73, where the WPP is connected in the middle of an HVDC intertie between two AC systems. For simplicity and due to the scope of the chapter, all converters are supposed to have the same rated power – refer to e.g. [93] for discussion of other setups.

[12] DC voltage control is, in the context of this study, actually DC energy control, since the square of the voltage is used as control input. This is done to make the control linear, since the control output is the power. Controlling the voltage by modulating power is not linear and may actually lead to multiplicity of possible steady-state operating points. An alternative is to control the DC voltage by modulating the DC current. For an exhaustive discussion of these aspects, the reader is referred to [159].

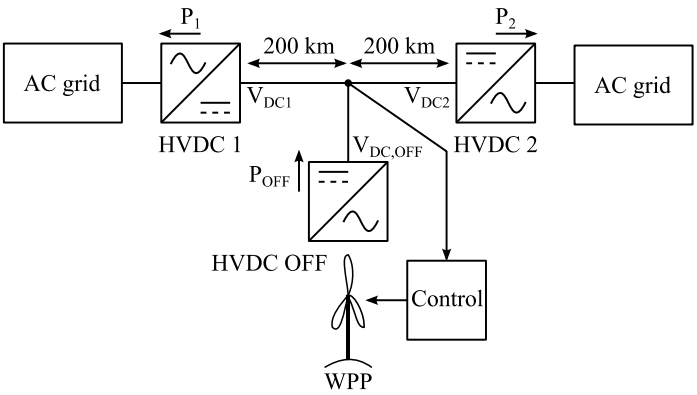

Figure 73 - Simplified DC network configuration for DC voltage control study.

6.3.1 Contribution of HVDC converters to DC voltage control

VSCs capabilities for provision of DC voltage control are excellent. In fact, their great performance is one of the factors that allow minimisation of their DC link capacitance. Their current (and thus power) can be controlled with BWs as high as 1000 rad/s or more and DC voltage control with PI compensators is usually performed with BWs up to 100 rad/s [23], [122]. DC voltage droop schemes have been proposed for power balance control in multiterminal DC grids. A HVDC converter can act nearly instantaneously in these terms and the overall dynamic response will depend on the network layout and parameters as well as on the control settings of other converters.

Although the converter's capabilities do not pose substantial limitations, other challenges may arise to limit the support they can offer:

- From a static perspective, converters do have limitations generated by current capability, DC voltage level, modulation index, cell-capacitor voltage ripple, etc… [70]. Hitting such limitations during voltage control can be avoided by properly selecting the power flow through e.g. N-1 criterion – analogously to what happens in AC systems.
- Dynamically, the rate of change of DC voltage is counteracted by the capacitance. However, it still varies with a much faster gradient than AC frequency does. For this reason, a dead-band kind of control (as the one adopted in conventional AC-connected power stations) may not be the most appropriate choice and some kind of control may have to be guaranteed even for small variations. On the other hand, too aggressively controlling the voltage may favour resonances in the DC grid. These issues have been partly discussed in some publications co-authored by the student – see e.g. [142], [143].
- Other constraints may limit the available dynamic performance of HVDC converters, particularly related to what is connected on their AC side. For instance, if only a WPP is connected at its AC terminals, its capability is surely limited, as will be discussed below. Connection to weak AC grids is another setup that could deleteriously affect the available performance – see for example [80] and related publications, or [82].

In general, it will be assumed here that onshore HVDC converters are not facing any significant limitations in the terms described above.

6.3.2 Contribution of WPPs to DC voltage control

(a) Background

As described above, the dynamic challenges imposed by DC voltage control are major and very fast control action is needed to ensure proper operation. It is clear from Section 6.2 that WPPs, depending upon control and communication setup, may pose limitations even for a service like frequency control. Obviously, such limits have an even more detrimental effect on DC voltage control. Moreover, if one excludes WTGs directly connected to the DC link, DC voltage deviations will have to reach the WPP controller by communication or coordinated control means, both options implying at least some delay.

The scope of this chapter is to investigate the contribution state-of-art WPPs may potentially give to this service. In doing so, the following assumptions will be accepted:

- The WPP is supposed to act in a multiterminal DC grid by being AC connected to one of the HVDC converters in the DC grid. Essentially, this is a state-of-art kind of assumption, reasonable due to the industrially oriented scope and surely acceptable for the first WPP installations with VSC-HVDC.
- Direct, instantaneous communication of DC voltage to the WPPC is available. In other words, the best case in terms of spurious delays is considered, only accounting for inherent WPP constraints. This allows highlighting basic limitations – further work should drop this assumption.
- Only DC voltage droop (proportional) kind of control is used. Integral action is not sensible for large grids. Derivative ("inertial") action is extremely fast in DC grids. From a WPP perspective, proportional control is fast enough to bring the WPP to the extreme of its capabilities. In other words, proportional action in DC voltage control encircles the spectrum of both droop frequency control and IR in AC grids.

(b) Implementation

Implementation of DC voltage control on the WPP is done at a plant level as depicted in the WPPC scheme in Figure 14. The following is worth being pointed out on such scheme:

- Feed-forward of the DC voltage control signal (P_{DC}) after the plant PI controller and after any plant power ramp-rate limiters is strongly recommended, for the following reasons:
    - The dynamic response strongly improves and allows delivery of most of the required active power as fast as possible.
    - Robustness against variations in PI control parameters that can occur over the WPP's lifetime is guaranteed.
- Addition of the DC voltage control signal to the PI reference is still necessary to guarantee corrections for small errors and prevent the WPP from returning to the original power set-point after the initial support to DC voltage control.
- Communication delays should obviously be made as small as possible, for the reasons highlighted above.

The signal P_{DC} in Figure 14 is generated by a dedicated controller as that depicted in Figure 74. The transfer function $G_f(s)$ models the DC voltage measurement and is in this section expressed by:

$$G_f(s) = \frac{1}{1+sT_{ppcDC}} \tag{32}$$

Squaring of the DC voltage is done in order for the controller to be coherent with the DC voltage control on the HVDC stations (Figure 11) and guarantee linearity between control output and input. A dead-band DB allows for selection of the undisturbed voltage variation range, or to prevent the WPP from being active against small imbalances.

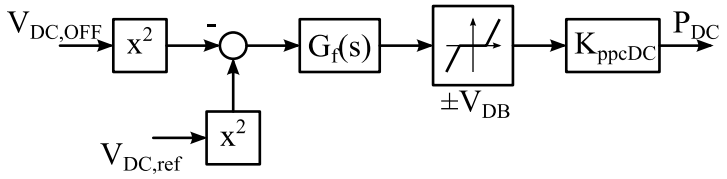

Figure 74 - DC voltage controller on WPPC.

Different ways of implementing the service may be explored such as converter-nearer approaches where DC voltage and AC frequency or voltage angle are controlled interdependently. This would be an expansion of the concepts proposed in [80], [87] to DC voltage control. The WPP converters would instantaneously respond in a distributed manner rather than commanded by a WPPC, possibly guaranteeing better dynamics. However, this is out of scope here and is left for future research.

The above bullets are better clarified by Figure 75. An open-loop kind of simulation was performed by modulating the DC voltage reference of the WPPC ($V_{DC,ref}$ in Figure 74) and observing the WPP response without feeding the voltage $V_{DC,OFF}$ back to it. The plot reports results for the three following cases:

- Case 1 – solid black line: a fully ideal situation is assumed, with all relevant measurement delays set to zero and power control of the aggregated WTG model being as fast as its current control loop allows it (open-loop P control).
- Case 2 – dashed black line: measurement delays of 10 ms for power are inserted at a WTG level and the power controller in the aggregated WTG is slightly slowed down (PI with 10 ms integral time constant).
- Case 3 – dashed grey line: same as Case 2, but the signal P_{DC} is not fed forward as in Figure 14, but only processed through PI controller and ramp-rate limiter, with the default parameters reported in Appendix 2.

Obviously, this analysis does not represent a solid assessment of how the many system parameters affect the performance, but helps highlight the importance of feeding the signal P_{DC} forward close to the output of the WPPC – Case 3 is definitely not suitable for DC voltage control events that span over a few tens of milliseconds.

Moreover, it is seen that non-ideal behaviour of WTGs and WPP (Case 2) can impoverish the dynamic performance significantly. It was noticed that when using the WPP to provide disturbance rejection, i.e. closing the DC voltage control loop in the WPP, the detriment of having non-ideal components may be even greater. Further work is needed for a thorough explanation of these phenomena and proposal of effective solutions. Here, for simplicity, the WPP response is slowed down by setting the time constant of the voltage measurement filter expressed by Eq. (32) as T_{ppcDC} = 0.1 s, leaving room for future work aimed at a more optimal design.

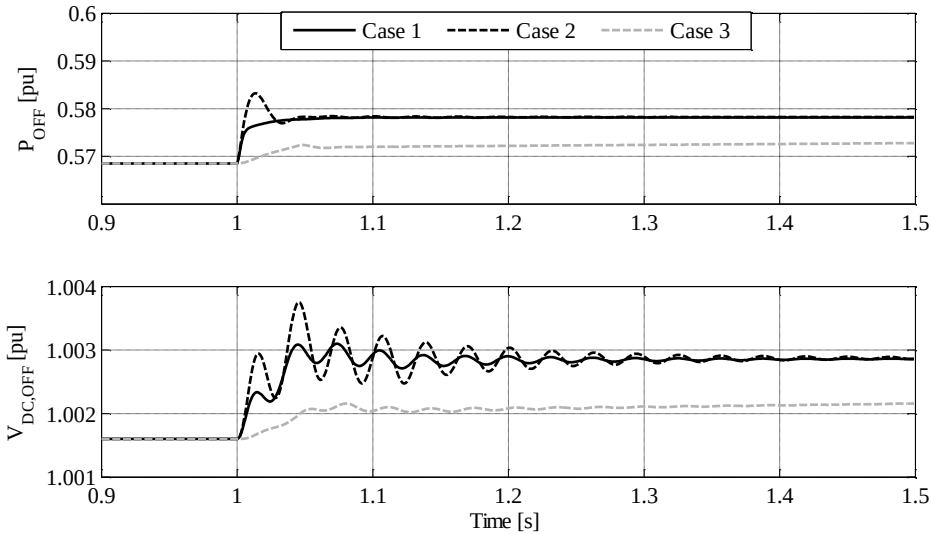

Figure 75 - Open loop simulation of DC voltage control contribution from WPP.

6.3.3 Coordinated DC voltage control

As a last step, coordinated voltage control in the layout in Figure 73 is studied. With the assumptions introduced above, the influence of the limited WPP capability on the DC voltage control scheme and in particular on the other elements sharing its burden in the network is discussed.

The relevant figures for the sample simulations shown in this section are reported in Table 14. The offshore HVDC converter (HVDC OFF) is controlled in V/f fashion based on Figure 12. Both HVDC2 and WPP are performing a droop control of V^2_{DC} according to Figure 11 (with no integral action) and Figure 74 respectively. Their gains K_p[13] and K_{ppcDC} can have two values based on the cases below:

- Case 1: K_p = 4 pu and K_{ppcDC} = 1 pu. In this case, the main DC voltage control burden is shouldered by the converter HVDC2 and ultimately the AC system connected to it. Such case may be considered as the most intuitive approach, as a consequence of the WPP limitations outlined above and the desire to maximise wind power production and hence reduce down-regulation of the WPP during undisturbed operation. Essentially it is assumed that HVDC2 takes up approximately 80% of the steady-state control effort, leaving 20% to the WPP.
- Case 2: K_p = 1 pu and K_{ppcDC} = 4 pu. The scenario is the opposite of Case 1, with the WPP taking up most of the control burden in the DC network. In this case, the WPP provides 80% of the control effort, while HVDC2 only contributes with 20%. This situation could possibly become reality if the AC grid connected to HVDC2 was a particularly weak one, in which large power variations would endanger the frequency stability.

Initially, as seen in Table 14, HVDC1 and HVDC2 are evacuating the active power from the WPP according to the scheduled power flow. The base power for all converters and WPP is 1200 MVA. Converter HVDC1 is in this case P controlled in order to easily use it to provoke active power imbalances in the DC grid. The following events are simulated:

[13] K_p is the power control proportional gain at the HVDC station – in the block *P* in Figure 11.

- At t = 1 s, a step in the power reference of converter HVDC1. The power reference is stepped up by 0.27 pu (ca. 325 MW).
- At t = 3 s, converter HVDC1 goes out of service, creating a power surplus in the DC grid of about 0.6 pu (720 MW).

Table 14 - Relevant data for coordinated DC voltage control simulations.

Initial power flow (losses neglected)			Control HVDC2	
$P_{1,0}$ [MW]	$P_{2,0}$ [MW]	$P_{OFF,0}$ [MW]	Type	K_p [pu]
395	280	675	V^2_{DC} droop	4-1
Control HVDC1			Control WPP	
Type	K_p [pu]	T_i [s]	K_{ppcDC} [pu]	V_{DB} [pu]
P control	1	0.1	1-4	0.0

The simulation results are reported in Figure 76. The left hand side shows the whole simulation, while the right hand side is a zoom-in of the most abrupt event at t = 3 s.

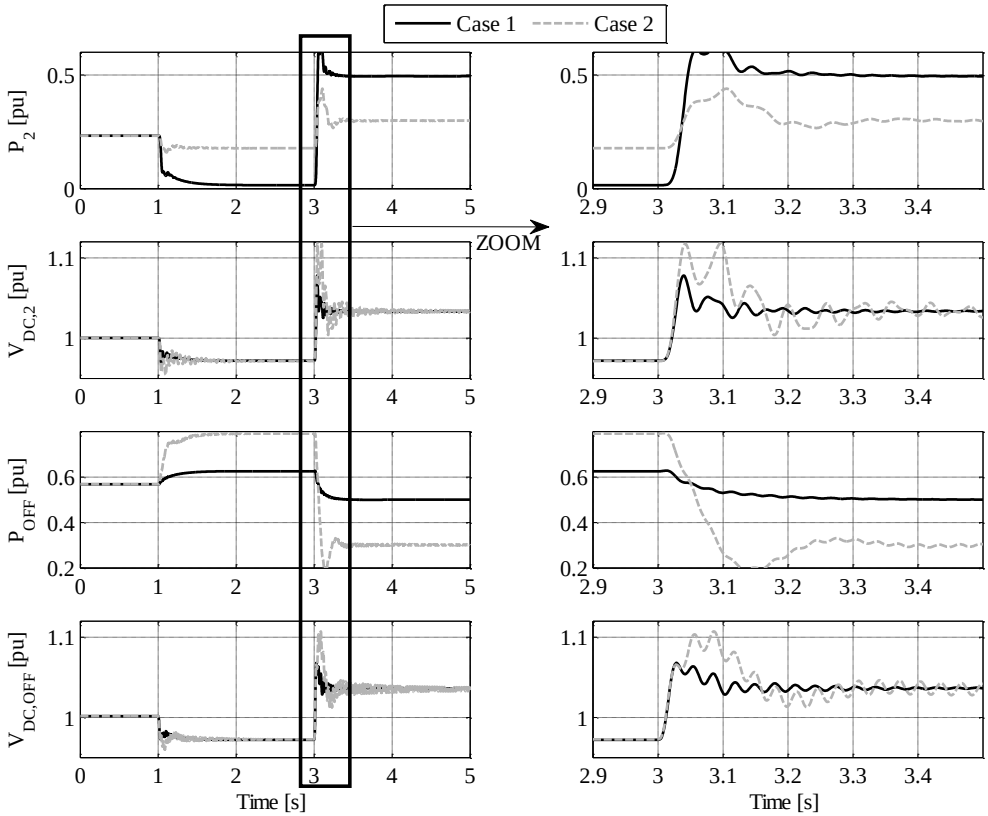

Figure 76 - Time domain simulation results for DC voltage control test. From top to bottom: HVDC2 active power and DC voltage, HVDC OFF active power and DC voltage.

In Figure 76, one can observe the following:

- Expectedly, Case 2 performs significantly worse than Case 1 in terms of limitation of transient DC voltage drifts. This is due to the limitations imposed by the WPP. In Case 2, DC voltage deviations can be twice as large as for Case 1.
- Larger voltage deviations also imply that converter HVDC2 is transiently called to partly make up for what the WPP cannot do. Until the WPP picks up the expected steady-state

share, HVDC2 is constrained to temporarily over- or under-shoot its power level to support DC voltage control though it was designed not to be the main responsible for it. The acceptability of this ultimately depends on the characteristics of the AC grid HVDC2 connects to.

- The high gain K_{ppcDC} in the WPP for Case 2, combined with its poor dynamic performance, gives rise to the resonances observed above (Figure 75). Again, a detailed description of the phenomenon is out of scope here, but it highlights that a certain design and tuning effort is needed to optimise the performance when delayed power sources (WPP) need to contribute to DC voltage control.

(a) Discussion

From the brief analysis above, one can conclude that WPPs limitations challenge proper control of DC voltage in situations where WPPs need to provide a substantial contribution to the service.

Though this scenario seems unlikely, if forecasts concerning development of large, meshed offshore DC grids with massive amount of wind power become reality, there will have to be sufficient available regulation from the onshore converters to provide DC voltage support.

Moreover, WPPs limitations for down-regulation of their power production are only dynamic. This means that other HVDC converters in the grid could provide supplementary DC voltage control support temporarily, then letting the WPPs reduce their power in steady-state. The performance of such an approach may even be enhanced by dynamically changing control gains at the HVDC stations [143]. From a practical perspective, the demand for power down-regulation in an offshore DC grid may be more common than for up-regulation, since such grid would presumably be a net producer of energy. However, this is just a speculation, and the actual scenario would also depend on who controls such a grid, as well as how.

Generally, it was shown that providing DC voltage control through the whole control chain of a WPP may be dynamically challenging even by brutally neglecting any communication delay and optimising the routing of the control signal in the WPPC. This means that other options (mentioned above) may have to be explored if WPPs are to participate quickly and reliably to the service. Such solutions would probably be based on a more distributed control philosophy, nearer to each converter and potentially eliminating elements that could worsen the performance (e.g. PLLs) [80], [87]. Nonetheless, such options are not discussed further here, and would require an EMT modelling approach for AC quantities rather than the RMS used here.

Additionally, looking at the dynamic profile of the curves in Figure 76, it can be seen that the power ramp-rates can reach a significant modulus, and this has implications for the WTGs mechanical systems. WTGs provided with FRT capability are usually designed for even larger gradients. However, such design is done considering the FRT event as a very rare one, while fast DC voltage control may have to be provided continuously. From this standpoint, it is certainly best to exclude WPPs from control during small imbalances. A dead-band should thus always be used on WPPs required to do DC voltage control.

6.4 Summary

Participation of WPPs to active power balance control in AC-DC networks was the topic of this chapter. The analysis, conducted through dynamic simulations, aimed at (i) recommendation of control candidate for frequency control provision from WPPs connected to AC grids in a point-to-

point fashion with VSC-HVDC and (ii) analysis of WPPs capabilities to contribute to DC voltage control in DC grids.

Concerning frequency control support from a point-to-point VSC-HVDC connected WPP, according to the results illustrated along the chapter and further considerations, the preferred default solution for its implementation is a scheme based on long-distance communication of the onshore frequency directly to the WPPC. A communication-less scheme was compared to such default solution and results superior in systems where limitation of initial ROCOF is the most vital figure for the frequency control.

As for DC voltage control, it was demonstrated that state-of-art WPPs and their connection to HVDC grids may pose challenges to efficient implementation of the service. WPPs can contribute satisfyingly in steady-state, in the same way as they do for frequency control, but the dynamic requirements of DC voltage control are far beyond what WPPs can do nowadays. The consequence is that either (i) WPPs should take up a very small dynamic share of DC voltage control (first hundreds of milliseconds to a few seconds) and can possibly contribute more widely on a longer term (after a few seconds) or (ii) new more advanced solutions to improve the dynamic performance should be devised, probably making use of converter-nearer controls and a more comprehensive power control scheme spanning over both DC and AC system or (iii) other ways should be evaluated to enhance the available performance from WPPs (e.g. energy storage).

Chapter 7 Power oscillation damping

This chapter regards the provision of POD from VSC-HVDC connected WPPs. It starts out by giving a brief overview of the motivations for implementing such feature in reality. The provision of POD by a VSC-HVDC station is then studied, independently of what is connected at its DC side, deriving conclusions in terms of which factors are important for practical realisation of the service. Thereafter, the implementation on a WPP in case POD is done by active power modulation is focussed on, demonstrating its effectiveness and concluding with a discussion of real limiting factors that may deteriorate the achieved performance as well as the stability of the proposed solutions. This chapter is mainly reporting results that have been inserted in Publication 10 [144], *also taking inspiration from Publication 6* [90].

7.1 Introduction

Damping of low frequency power oscillations between (groups of) SGs separated by significant electrical distance has been subject of study for power system engineers for many years [76], [132]. The fact that SGs' masses are directly coupled to the electrical grid by the equation of motion, combined with the power-angle characteristics of electrical power transmission and the desired low losses in the system can give birth, in certain circumstances, to poorly damped speed, rotor angle and thus power oscillations between SGs. This problem is usually referred to as small-signal stability [76], since it regards the capability of the system to stably return within a sufficiently small range around the initial operating point when subjected to a small disturbance. In negatively damped systems, even an infinitely small perturbation can cause the system to diverge and lose stability. Analysis of small-signal stability is usually done by linearization of system equations and applying linear mathematical tools such as modal analysis, borrowed from classical control engineering [76], [145], [146].

Typical power oscillation frequencies usually are 0.1-2 Hz, depending on their nature [44]. Frequencies as low as 0.1 Hz have actually been observed in studies regarding real systems [147] and may overlap with frequency control dynamics. Oscillations with frequency beyond 2 Hz typically originate from other physical phenomena involving shafts' torsional modes and series compensated lines [76], [148]. Here, the focus is solely on electromechanical oscillations between generators in the frequency range 0.1-2 Hz.

Besides being an indication of the system being close to small-signal instability, poorly damped oscillations are practically stressful to SGs and in particular to their prime movers and shafts, which would undergo premature wear if frequently subjected to insufficiently damped oscillations. Hence, it is desirable to find means to accelerate the oscillations' decay. In linear analysis terms, this corresponds to dragging the eigenvalue generating the oscillation deeper into the LHP. POD problem has usually been solved by installation of PSSs on conventional units to vary their excitation so as to create a supplementary damping torque on their electrical side, thereby forcing oscillations to vanish more quickly. However, as discussed in Chapter 2 (Section 2.2.2(b)), PE assets have recently been looked at for improvement of power system stability in general and small-signal stability in particular, through the provision of POD. Among these fall VSC-HVDC, WPPs and their combination. Furthermore, POD on PE installations is being inserted by TSOs in legally binding documents [42], [43]. POD from static generators becomes particularly precious when PSSs may not be effective, which usually means in inter-area oscillation modes [76], [149]. More specifically, installing POD controllers on VSC-HVDC converters and/or WPPs may be convenient as an alternative to installing new dedicated devices such as STATCOMs or SVCs.

Several studies have looked at the problem of providing POD from PE converters in general and VSC-HVDC and WPPs more specifically – see for example all references listed in Chapter 2. However, reading through the literature and bearing practical application in mind, one may spot the following gaps:

- The problem is usually tackled mathematically and firm connection to its physics is sometimes lost in the literature. Though mathematical tools are indispensable to fully understand and treat small-signal stability and related phenomena, practical implementation of the service and the necessary dialogue between TSOs, utilities and OEMs may be hindered by such an abstraction level.
- Elements that are crucial to the small-signal stability of power systems are often neglected in the literature. For example, ESs and AVRs are usually disregarded by references in the field making use of small systems – to mention a few, [53], [57] and [58].Though this may be reasonable in some cases, it is definitely not sensible when the PE converter lies close to SGs, especially when POD is provided by reactive power modulation. AVRs and ESs are usually included in studies dealing with larger systems (e.g. [44] and related publications) but their influence is usually accounted for only through the large mathematical model and not explained physically.
- Most literature regarding POD from WPPs could easily and more generally be seen as concerning POD from static power sources. To the author's knowledge, the only sources considering, at least partly, possible limitations imposed by real WPPs, are [47] and related publications, where mainly the WPP's modularity is accounted for. A discussion of several other factors that could limit the performance and/or widely impact the WPP design is still missing. If one wants to evaluate feasibility and cost of possible solutions then one cannot prescind from such factors.

This chapter attempts to fill the gaps listed above. A very simple single-machine system is used to derive approximate guidelines to tune the parameters of a proposed POD scheme installed on a generic VSC-HVDC converter fed by a stiff DC voltage source, using physical reasoning rather than mathematical derivations. The effect of AVR and ES is taken into account, to illustrate its importance. Thereafter, the HVDC system is expanded to create the default point-to-point

configuration including a WPP (Section 2.4.3(c)) and the part of POD relying on modulation of active power is implemented on the WPP. The described guidelines are used for parameter tuning on a larger power system model, proving their qualitative validity. To conclude, the analysis then moves to a discussion of several inherent WPP limitations that will influence applicability and cost of the proposed controls.

7.2 Contribution of VSC-HVDC to POD

This section presents the implementation of POD on a generic VSC-HVDC converter operating in ideal conditions: the converter is power controlled and connected to a stiff DC voltage source, in a very simple network. According to the literature gaps pointed out above, a pragmatic approach is adopted: ES and AVR are accounted for, to understand their practical importance, and physical explanation of the results is provided, demanding most of the mathematics to Appendix 1 and Appendix 4.

7.2.1 Simple case study: single-machine system

The system upon which this section is based includes one SG connected by a transmission line to an infinite bus, according to Figure 7 in Section 3.2.1(a). Here, the model is sketched again for clarity, and particularised for POD studies – see Figure 77. The load at Bus 1 is neglected. AVR and ES are modelled according to the IEEE standard type AC4A described in [113]. The model was chosen because of its simplicity and the wide application of fast kinds of AVR/ES in modern units. The influence of choosing a different model is discussed qualitatively where relevant. Governor and turbine are not modelled for the theoretical derivations, but a standard model of them is included in the time domain simulation model, according to what described in Chapter 3, Appendix 1 and Appendix 2.

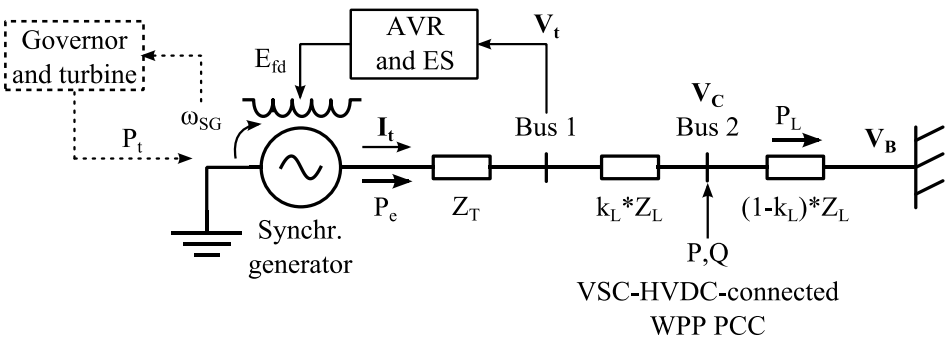

Figure 77 - Single-machine model for POD studies.

Depending on the operational point, SG and circuit parameters and AVR/ES type and settings, there can exist a poorly (or even negatively) damped oscillation mode of electromechanical nature, which is to be damped by VSC-HVDC control means, analogously to what a PSS installed on the SG would do.

A VSC-HVDC converter is connected at Bus 2 and its position along the line is controllable by varying the constant k_L. Clearly, Bus 1 and Bus 2 collapse into one bus for $k_L = 0$. In this section, the converter is supposed to be open-loop power controlled (refer to Figure 11) and connected to an ideal voltage source on its DC side. Mathematical modelling of the system considering the VSC-HVDC converter as instantaneous power source was done in [150] and some details are reported here in Appendix 4. It is furthermore assumed that the initial operating point for the

VSC-HVDC is ($P_{ref,0}$,$Q_{ref,0}$) = (0,0). A good discussion of the influence the initial operating point has on small-signal stability was done in [44].

Later in this chapter, a DC transmission system, offshore HVDC converter and WPP will be connected behind the onshore VSC-HVDC converter connected at Bus 2.

(a) Control objective

In order to more clearly formulate the control objective to be satisfied by the POD controller, let us assume that there is an eigenvalue $\lambda = \alpha + j\omega_\lambda$ with insufficient damping factor, which is defined as:

$$\zeta = -\frac{\alpha}{\sqrt{\alpha^2 + \omega_\lambda{}^2}} \tag{33}$$

Typically, insufficient damping factors for electromechanical oscillations are smaller than 0.1 [76] and the system becomes unstable when $\zeta < 0$ ($\alpha > 0$). When a static source is to help damping the oscillations the following features are desirable from a power system's perspective:

- A damping factor $\zeta \geq 0.1$ should be obtained. If that cannot be achieved, as large an increase in ζ as allowed by the converter's capabilities should happen.
- The eigenfrequency ω_λ should not be significantly affected by the action of the converter. Let us assume that its relative variation, in modulus, should not exceed 3% of the default value.
- Other eigenvalues in the system should not be significantly affected by the converter action.

7.2.2 Implementation of POD controller

Choosing control output, control input and control candidate for implementation of POD on the HVDC station is the first step to perform for the desired evaluation. In this respect, the available literature is helpful:

- Generally, a strong participation of the PE asset to the target oscillatory mode is desired, which mathematically means high controllability and observability must be guaranteed by the chosen input-output pair, but further aspects must be considered in developing the controllers.
- Natural control outputs are PCC active and reactive power reference variations (named ΔP_{POD} and ΔQ_{POD} respectively). This is done assuming that current vector control is utilised at the station [23]. Decoupled *d-q* control of the current naturally yields a decoupled P-Q control (like e.g. Figure 11). The power references are generated as $P_{ref} = P_{ref,0} + \Delta P_{POD}$ and $Q_{ref} = Q_{ref,0} + \Delta Q_{POD}$. According to literature regarding selection of input-output pairs, outputs that do not allow sufficient controllability of the target mode or impose fundamental control limitations should be discarded – see e.g. [53]. However, control of other converter terminal quantities by well-established current vector control would possibly be a combination of P and Q control. Thus, other control outputs are not considered here, but expansion of the results to other outputs should not be hard to do.
- The selection of the control input usually gives room to more discussion. Several sources have discussed the matter, an incomplete list being [44] and related publications, [53], and [58]. Even in a very simple system such as that drawn in Figure 77, the selection may

not be trivial. In general, one should pick a signal that sufficiently faithfully represents the target eigenmode and at the same time does not impose tough fundamental control limitations [53]. In this simple case, the power through the transmission line (P_e or P_L) is used, being one of the most intuitive choices from a physical standpoint. Checks on proper observability and lack of fundamental control limitations ensured the choice is a sensitive one. For some purposes, the SG's speed ω_{SG} will also be used.

- Several control candidates can be employed to implement the service. For example, [44] makes use of a scheme resembling standard PSSs, while [58], [151] somehow tackle the control problem as a whole, without de-coupling between input-output selection and control tuning. Tuning techniques are also influenced by the chosen scheme. PSS-like schemes can be tuned for instance with residue analysis or similar [46], while a scheme such as that proposed in [58] allows for a slightly more intuitive tuning approach. Here, the PSS-like scheme employed in [44] is chosen, but more intuitive a tuning technique than residual analysis is proposed. The control scheme is reported in Figure 78. The generic input u_{POD} is passed through a wash-out block to deprive it of its average value. K_{comp} compensates for the gain shift in the compensation block. K_{POD} is the actual control gain. The output can also be limited between two saturation values. The choice of the scheme in Figure 78 may be questionable also in terms of robustness against uncertain knowledge of the mode's frequency. More advanced approaches have been suggested in recent literature to selectively sense the target oscillatory mode [151], [152]. On the other hand, well-established references like [76] prefer to guarantee sub-optimal, yet robust, performance over the whole possible frequency range. Selectivity may however be more desirable for POD from PE assets than it is for PSSs. A deeper treatment of these aspects is out of scope here and the reader can refer to the above references for more insight.

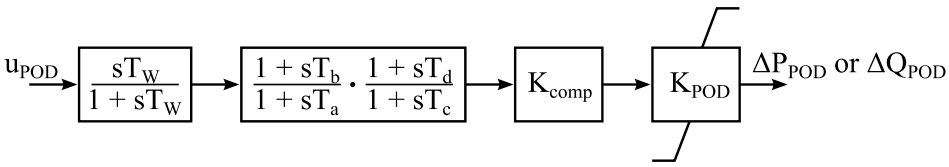

Figure 78 - PSS-like control scheme for POD implementation.

Tuning of the control parameters is described below for different input-output combinations. The principle is that by knowing the relation of the control input to the rotor angle (and thus speed) of the SG and the effect that the control output has on the SG's active power (electrical torque), the compensation block is tuned accordingly and K_{POD} regulates the magnitude of the control action.

7.2.3 Practical considerations for tuning of parameters

(a) Ideal POD controller

The ultimate objective of a POD controller is to create an electrical torque component in the SG's equation of motion that be in phase with the SG's speed deviation [76]. This will naturally increase the decay rate of the oscillation. Hence, the most natural choice of control input for a damping controller would be the SG's speed (ω_{SG}).

Furthermore, active and reactive power modulation from the HVDC converter creates such an electrical torque component by changing the SG's terminal voltage and the power angle. Which of the two quantities is influenced the most by P or Q modulation does not matter at this point,

because after linearization and neglecting sub-transient and stator electrical dynamics both influence the SG's electrical torque algebraically.

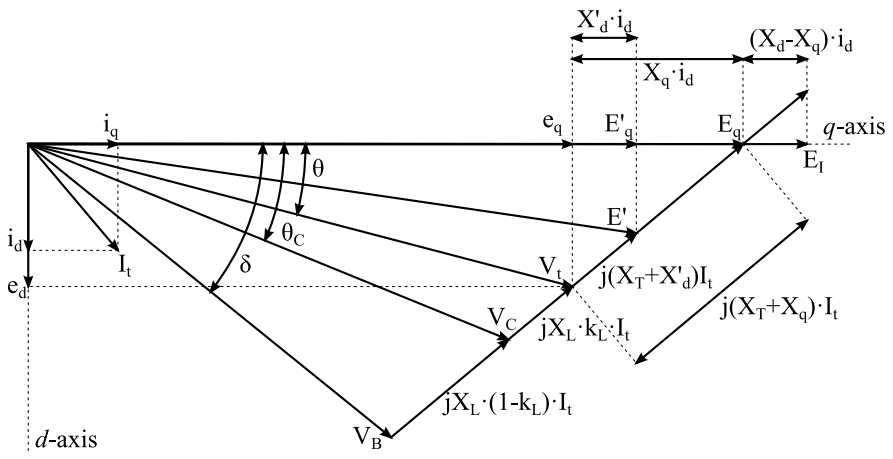

Figure 79 - Steady-state phasor diagram of single-machine system.

This can be understood by considering the steady-state phasor diagram of the network operation reported, in Figure 79 and inspired by [76] and [112] with the addition of the converter voltage V_C at Bus 2 and assuming a completely lossless configuration (all impedances are pure reactances). Both steady-state and transient vectors are reported. Generically, neglecting sub-transient dynamics, using the diagram above and performing linearization one can derive the next expression of the (small-signal) electrical torque variation at the SG:

$$\Delta T_e = \Delta P_e = k_{P_e\delta}\Delta\delta + k_{P_eE_q^{'}}\Delta E_q^{'} + k_{P_eP}\Delta P + k_{P_eQ}\Delta Q \tag{34}$$

where the first equality is true using proper per-unit notation and considering rotational speed equal to the base value, and coefficients $k_{Pe\delta}$, $k_{PeE'q}$, k_{PeP} and k_{PeQ} are the first derivatives of the SG's electrical torque expression with respect to δ, E'_q, P and Q respectively. Detailed derivation of the coefficients for this simple case is reported in Appendix 4. In a similar fashion one can derive the expression of the terminal voltage variation as:

$$\Delta V_t = k_{V_t\delta}\Delta\delta + k_{V_tE_q^{'}}\Delta E_q^{'} + k_{V_tP}\Delta P + k_{V_tQ}\Delta Q \tag{35}$$

where the meaning of the coefficients is clear. For now, let us focus on Eq. (34): the effect of the VSC-HVDC on the electrical torque is enclosed in the coefficients k_{PeP} and k_{PeQ}. Reasonably, according to the sign convention in Figure 77, one should expect $k_{PeP} < 0$ and $k_{PeQ} > 0$. As an intuitive consequence, a simple proportional control as the one summarised in Table 15 could be used when the SG speed ω_{SG} is taken as control input.

Table 15 - Control settings for ideal POD controller – see Figure 76, $u_{POD} = \omega_{SG}$.

	P POD	Q POD
K_{POD} [pu]	$K_{POD,P} < 0$	$K_{POD,Q} > 0$
$T_a = T_c$ [s]	0	0
$T_b = T_d$ [s]	0	0
K_{comp} [pu]	1	1

However, the above approach does not account for the presence of the AVR and ES. Setting $K_{POD,P}$ = -10 and $K_{POD,Q}$ = 10 and plotting the achieved damping factor improvement for the poorly damped eigenvalue ($\Delta\zeta$) as compared to the value of ζ without POD controller, for varying AVR gain K_A, the graphs in Figure 80 are obtained. Two values of the initial power production P_{e0} were chosen, i.e. 500 MW (0.417 pu) and 1000 MW (0.833 pu).

The first observation is certainly that the results are heavily affected by the presence of the AVR and ES. As hinted above, the main reason for this is that the parameters were set only considering the direct effect P and Q injection at Bus 2 have on P_e and hence the SG's electrical torque. This approach guarantees a constant damping torque. Nevertheless, it completely neglects Eq. (35) and the presence of the AVR, which takes its value as an input. The quantity $\Delta\zeta$ may not be the best to explain the phenomena involved.

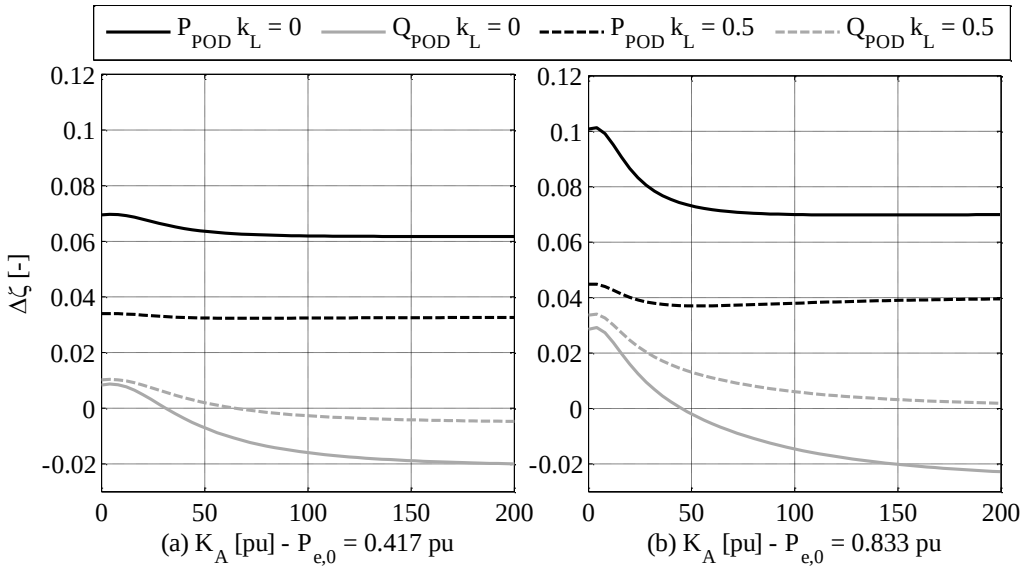

Figure 80 - Variation of target eigenvalue's damping factor at two initial power transmission values and varying AVR control gain.

Deeper analysis will be done below, but the following qualitative comments can be put forward:

- Both kinds of control lose effectiveness as the AVR action becomes stronger. The AVR processes the terminal voltage error and modifies the SG's excitation. With the utilised parameters, this creates a torque that leads voltage variations by slightly more than 90°. Voltage variations induced by the POD controller are in phase or phase-opposition with ω_{SG} according to the control settings and Eq. (35). Hence, the torque created by the AVR tends to be mainly synchronising, positive or negative.
- The SG's terminal voltage sensitivities reported in Table 16 along with the SG's active power sensitivities are also important to evaluate the results. It is noticed that, expectedly, the voltage V_t is more sensitive to Q variations than P. Moreover, the electrical distance between Bus 1 and Bus 2 also affects the sensitivities. Particularly interesting is the fact that in case of Q variations, larger distance means larger SG's active power sensitivity, but understandably smaller terminal voltage sensitivity. Consequences of these facts are the following:
    - For POD via P modulation, an initial drop in the damping contribution is noticed initially, as K_A increases. However, it appears that the plots flatten out for even larger K_A. It is not straightforward to explain this by looking at $\Delta\zeta$ only (no

information on the eigenfrequency is contained in it), but it seems as if the voltage variation caused by P modulation and processed by the AVR, eventually creating an electrical torque, exactly counteracted the natural eigenvalue's movement due to K_A variation, at least in terms of damping factor variation. It is interesting to see that, when P does not have any influence on the terminal voltage (P_{e0} = 0.417, k_L = 0.5), the curve expectedly results essentially flat, i.e. the damping contribution of the POD algorithm is independent of the AVR gain.

- For POD via Q modulation, the curve for k_L = 0.5 lies above that for k_L = 0, as expected from Table 16. Moreover, the drop of $\Delta\zeta$ with increasing K_A continues essentially over the whole range, meaning that the pole moves to more unfavourable damping factors. Considering the positive sign of k_{VtQ} (see Table 16), the AVR adds, besides its original torque components, a negative synchronising torque and a small negative damping torque. The former partly cancels out with the original AVR-related synchronising torque, while the latter adds to the original AVR-related negative damping torque [76]. The overall effect is a falling damping factor, that eventually tends to flatten out for very large K_A, as the original AVR-related synchronising torque becomes larger and larger. For k_L = 0, the drop is more pronounced and flattening happens later, as a consequence of the larger voltage sensitivity in that case.

These observations are supported also by the pole movement plot shown in Figure 79.

Table 16 - Per-unit SG's power and voltage sensitivities to P,Q injection at Bus 2.

	P_{e0} = 0.417 pu		P_{e0} = 0.833 pu	
	k_L = 0	k_L = 0.5	k_L = 0	k_L = 0.5
k_{PeP}	-0.54	-0.27	-0.71	-0.32
k_{PeQ}	0.06	0.07	0.19	0.22
k_{VtP}	-0.05	0.00	-0.07	0.02
k_{VtQ}	0.28	0.15	0.30	0.17

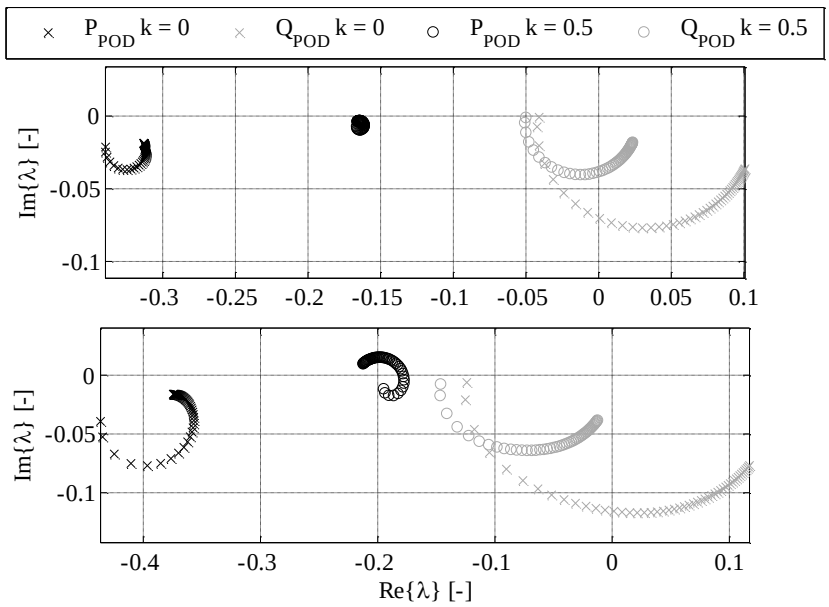

Figure 81 - Pole position variation for ideal POD controller: (a) P_{e0} = 0.417 pu, (b) P_{e0} = 0.833 pu.

The phenomena explained above closely resemble those that have been observed during tuning of classical PSSs on conventional power stations [76]. The most important conclusion that can be drawn is that AVRs should not be disregarded in the analysis of POD problem with power electronics, because erroneous results would be reached by neglecting them. This is especially true when POD controllers heavily affect the SGs' terminal voltages, since the AVR action is stronger in that case. Practically, this means that accounting for AVR is of paramount importance when looking at POD done through reactive power modulation. Though, as seen in Figure 80 (b), even when using active power there may be instances when AVRs should be accounted for to achieve correct results. To understand that, one should look at the voltage sensitivities of the target SGs to P and Q injection from the PE asset. A difference with respect to PSS tuning as described in [76] is that PSSs are installed and tuned so as *to counteract* inherent negative effects AVRs have on the damping, whereas POD tuning on PE assets must be done in order *not to trigger* negative effects of AVR. Actually, in case of high SG's voltage sensitivity the POD controller actually exploit the presence of AVRs to provide damping.

(b) Real POD controller

Sensing of the SG's speed ω_{SG} may, in many cases, not be straightforward, for several reasons, such as geographical distance or different ownership of SG and VSC-HVDC. In practice, more readily available signals may be employed for the realisation of the POD control. Such signals, as illustrated in the literature – e.g. [44], [53] –, should (i) provide a good observability of the eigenmode and (ii) not give rise to any fundamental control limitations.

In the present case, the most natural choice seems to be the active power through the transmission line (either P_e or P_L) since it is the quantity that actually one wishes to damp and well represents rotor angle and speed oscillations in the SG. Fundamental control limitations are not hit by choosing them as control inputs. Let us assume P_e is picked as input. Tuning of the control parameters may proceed along the following lines:

- Small-signal rotor angle oscillations are reflected into P_e in a proportional fashion. Small angle variations cause, keeping all other quantities constant, P_e oscillations proportional to them. The proportionality factor is, with the signs in Figure 77, positive.
- Rotor speed oscillations lead angle deviations by 90°. Hence, a controller making use of P_e as an input should provide the necessary phase shift to bring the output in phase with ω_{SG}. In other words, a 90° phase shift should be introduced in the compensation blocks.
- Taking into account the sign of the sensitivities in the first two lines of Table 16, one should set K_{POD} negative when using active power as an output and positive when using reactive power. This is correct if the phase shift in the compensation block is a lead type, while the opposite signs should be chosen in case of lag phase shift.

Once again, however, the effect of AVR and ES is neglected by the above bullets. Following them precisely and setting the parameters as per Table 17, the results plotted in Figure 82 were obtained. Only operation at $P_{e,0}$ = 0.833 pu is considered. The 90° compensation is equally split among the two zero-pole parts of the compensation block and tuning of the time constants is done according to the well-known rules based on geometric mean [23], [146] to provide flat phase compensation at the target pulsation ω_λ, which value depends on the AVR gain K_A. The negative sign for the gain in P POD is accounted for in the compensation gain K_{comp}.

Table 17 - Control settings for real POD controller – see Figure 76, $u_{POD} = P_e$.

	K_A = 1 pu		K_A = 20 pu		K_A = 40 pu	
	P POD	Q POD	P POD	Q POD	P POD	Q POD
K_{POD} [pu]	0-1	0-1	0-1	0-1	0-1	0-1
$T_a = T_c$ [s]	0.096	0.096	0.093	0.093	0.088	0.088
$T_b = T_d$ [s]	0.558	0.558	0.543	0.543	0.512	0.512
K_{comp} [pu]	-0.172	0.172	-0.172	0.172	-0.172	0.172

Observing the results in Figure 82, the following is apparent:

- For K_A = 1, the path the eigenvalue follows is approximately the desired one, since the movement is almost perfectly leftwards. This is true essentially in all cases. As a confirmation of results already reported in the literature [58], then, it can be seen that active power modulation close to the SG (k_L = 0) is very effective in improving damping, while other options need higher gains to provide the same performance. Incidentally, this could already be derived by Table 16.
- As the AVR gain increases, the locus drawn by the eigenvalue significantly differs from the desired one, particularly for reactive power modulation, and even more so when it is done close to the machine (k_L = 0). Once again, accounting for the presence of the AVR and the sensitivities presented in Table 16, the behaviour of the system can be understood. Apart from the case with active power POD and k_L = 0.5, for which the eigenvalue movement lies close to the target, in all the other cases the sensitivities and control gains are so as to create a voltage variation in phase with the speed deviation. Hence, the torque component added by the AVR when processing such voltage deviation will be mainly negative synchronising, with a small negative damping part. This drags the eigenvalue towards the real axis. In fact, for POD with Q and k_L = 0, the damping effect is completely lost (POD controller's and AVR's damping torque cancel out each other) and the pole falls almost vertically towards the real axis.

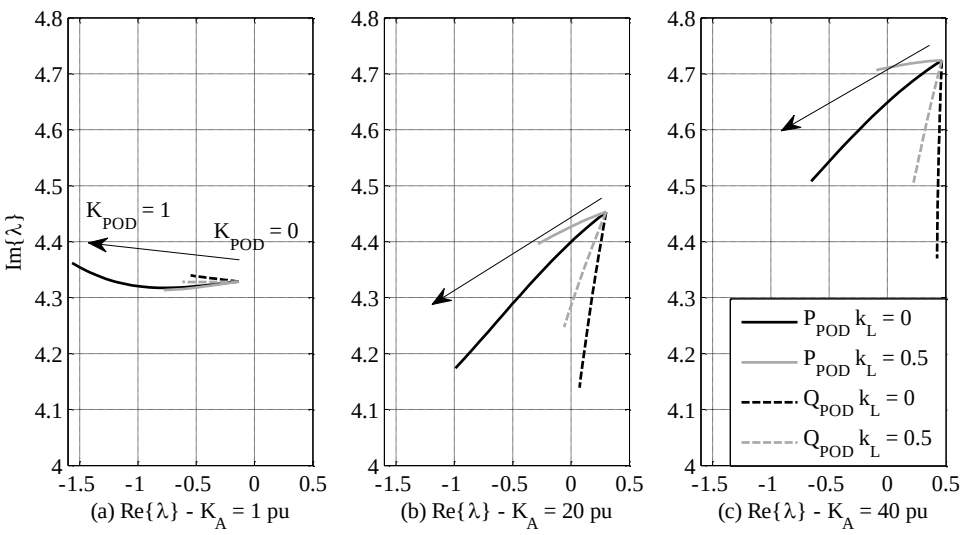

Figure 82 - Target eigenvalue movement for real POD controller and varying POD gain.

The above behaviour, once explained, can be counteracted. In order to do so, it is helpful to visualise the phenomena in graphic terms. When only one machine is concerned as in this case, phasor diagrams such as those briefly sketched in [76] can be used to better understand the

phenomena. One such diagram is drawn in Figure 83, considering the case P_{e0} = 0.833 pu. It should be noticed that, for clarity, the drawing is not on scale with any of the cases above.

The torque components added by the POD controller are named ΔT_{eP} and ΔT_{eQ} for active and reactive power modulation respectively. As mentioned above, for most of the cases the induced terminal voltage variations are in phase with such torques, their magnitude being dependent on the corresponding sensitivities. The AVR, sensing such voltage variations, provides a torque component that roughly leads them by 90°, drawn as $\Delta T_{eAVR,P}$ and $\Delta T_{eAVR,Q}$ respectively, which clearly turn out being negative synchronising ($\Delta\delta$ axis). In reality the torques will have a small negative component along the axis $\Delta\omega_{SG}$. Clearly, the overall additional electrical torque ΔT_e seen by the SG is not purely damping, but can become strongly de-synchronising. The higher the modulus of voltage sensitivities in Table 16 and the higher the AVR gain, the farther will the overall torque be from being perfectly damping. For POD via Q in the middle of the line, the small negative damping torque mentioned above can actually be as high as to cancel the damping torque given by the POD controller – see the vertical pole movement in Figure 82 (c).

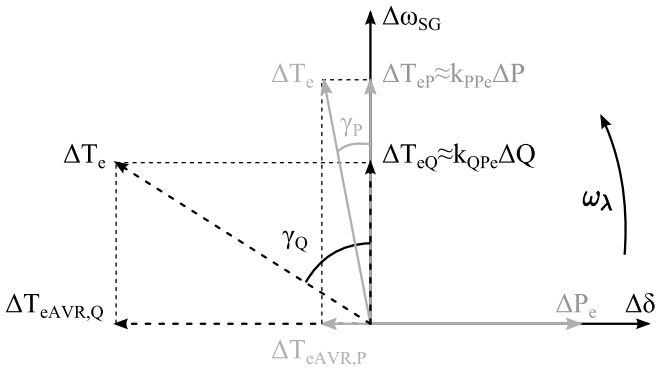

Figure 83 - Phasor-like diagram of induced electrical torques on SG. Torques induced by AVR and ES independently of the POD from VSC-HVDC are not reported.

Generally, the problem can be solved by accounting for this phenomena in the compensation performed in the POD controller. This could be done by trial and error, knowing the sign of the necessary correction from the phasor-like diagram in Figure 83 – in the case above the 90° compensation should definitely be reduced to realign the overall torque with the SG's speed. However, if one is able to quantify the torques in Figure 83, it should be quite straightforward to at least approximately compute the correction needed. Let us take as an example POD with reactive power modulation, which is the most significantly affected by the AVR. In linear conditions, the torques induced by the POD controller and subsequently by the AVR are given by the following equations:

$$\Delta T_{eQ} = k_{P_eQ} \cdot \Delta Q \tag{36}$$

$$\Delta T_{eAVR,Q} = \left.\frac{dT_e}{dE_q'}\right|_0 \cdot G_{AVR}(s)|_{s=j\omega_\lambda} \cdot k_{V_tQ}\Delta Q = k_{P_eE_q'} \cdot G_{AVR}(s)|_{s=j\omega_\lambda} \cdot k_{V_tQ}\Delta Q \tag{37}$$

where for brevity $G_{AVR}(s)$ is the modulus of the AVR transfer function and the last two factors in Eq. (37) represent the terminal voltage variation created by the POD control. Both relations above are valid in per-unit in proximity of the base speed, where P_e and T_e are equivalent. The needed corrective angle γ_Q can then be calculated by simple trigonometry:

$$\gamma_Q = \mathrm{arctg}\frac{\Delta T_{eAVR,Q}}{\Delta T_{eQ}} \tag{38}$$

The same approach can be used for POD with active power modulation, to compute γ_P. The calculated corrections must then be subtracted from the lead phase compensation utilised previously. A set of corrections was calculated for the relevant cases and modal analysis with K_{POD} = 0.5 pu was performed, obtaining the results reported in Table 18. As an example, the corresponding control parameters for k_L = 0 are reported in Table 19.

Table 18 - Calculated needed angle correction and results achieved for K_{POD} = 0.5 pu.

		P POD			Q POD		
K_A [pu]	k_L [-]	γ_P [°]	$\Delta\omega_\lambda$ [%]	$\Delta\zeta$ [%]	γ_Q [°]	$\Delta\omega_\lambda$ [%]	$\Delta\zeta$ [%]
20	0	5	-3	+30	50	<1	+10
	0.5	0	-1	+14	30	<1	+10
40	0	8	<1	+30	65	-3	+10
	0.5	-5	-1.5	+14	45	<1	+11

Table 19 - Example of phase compensation parameters for k_L = 0 and accounting for corrections from Table 18.

	K_A = 20 pu		K_A = 40 pu	
	P POD	Q POD	P POD	Q POD
K_{POD} [pu]	0.5	0.5	0.5	0.5
$T_a = T_c$ [s]	0.099	0.157	0.097	0.170
$T_b = T_d$ [s]	0.511	0.321	0.465	0.264
K_{comp} [pu]	-0.193	0.490	-0.208	0.645

It is noticed that the desired result is achieved, since in all cases a satisfying eigenvalue movement happens, with increasing damping and eigenfrequency variation below the targeted 3%. The proposed simple approach can thus be used to estimate the needed correction in this simple case. More importantly, the phasor-like diagram in Figure 83 is very useful for understanding the physics of the phenomena related to the POD provision with AVRs.

It should be noticed that the above derivations are strictly valid for the particular set of parameters utilised here, namely field time constant and AVR/ES type and parameters. The following can be said to justify the use of such settings:

- Field time constants are often large enough so as to provide a 90° lag in the response of the field circuit to signals with frequency in the POD range [76].
- It is reasonable to assume that new units are usually provided with fast, high-gain AVRs.
- When either or none of the above is a realistic assumption in a particular application, one must only calculate the expected phase shift the AVR-related torques will have compared to the POD-related torques and utilise a slightly more complex formula than Eq. (38) to derive the correction.

7.2.4 Discussion

From the analysis in this section, some important lessons were learnt that concern a real-life implementation of POD service from static power sources. The practical realisation of a feature

like POD on a PE converter will in the most general case be the result of a dialogue between the utility owning the PE asset offering the service and the relevant TSO demanding it.

Important conclusions that could drive such a dialogue were achieved during the above investigation:

- AVRs and ESs should definitely be considered in specifying requirements for development of POD controllers. This is especially vital in cases where the static power source lies close to a SG and POD via reactive power modulation is considered.
- Before making use of more or less complex mathematics proposed by the literature, one should first find out what the sensitivities of the SGs' terminal voltages and active power to P and Q injection from the static source are. Although many references look at the problem globally, measures to solve it can still be undertaken *locally*, meaning that the range of action of a power source is anyhow limited by its electrical distance to oscillating SGs as compared to its distance to the rest of the elements in the networks. Knowledge of the network impedances helps to (i) have a first idea of whether the solution can achieve the objective and (ii) narrow down the focus area to develop the controller.
- The strong dependency of POD using Q on the voltage regulation performance of the existing grid may make it somewhat less robust than its version modulating P. This means that implementation with Q modulation should rely on prompt information on the AVRs that are online at each moment, to possibly correct the control gains and phase shifts accordingly.
- It is true, on the other hand, that proper tuning of the Q POD by accounting for the AVRs can make the service almost as effective as if it was implemented with P, at least in particular cases – see Table 18.
- On the other hand, as will be highlighted below, in the case of a VSC-HVDC connected WPP, modulating P to offer POD comes at a certain cost. Such cost, being related to the whole WPP, may be higher than the cost of providing POD with Q, where a slight over-rating of the onshore HVDC station guarantees sufficient capabilities.

7.3 Combined POD from WPP and VSC-HVDC

The implementation of the POD service on a WPP is discussed in this section, always considering it as VSC-HVDC connected. Therefore, only POD through active power modulation is relevant. First, an example of possible implementation starting from the analysis carried out in the previous section is proposed. After demonstrating its effectiveness on a larger system along with reactive power POD implemented on the onshore HVDC station, some practical facets related to the practical realisation are discussed, starting with a few stability issues, continuing with the influence of control and communication delays and ramp-rate limiters and concluding with some collateral effects POD may have on WTGs.

7.3.1 Implementation of POD controller on WPP

As a conclusion of Section 7.2, it was noticed that POD through active power modulation may be the technically most suitable for implementation in real systems, owing to its better independence of the voltage regulation capabilities of the AC grid, implying a potentially easier and more robust control design. In the context of this study, if one assumes not to have any other form of large energy storage in the WPP/VSC-HVDC system, this means that the WPP must actively

participate to the service by modulating its active power production. On the other hand, POD by modulation of Q could be provided by the onshore HVDC converter seamlessly for the WPP, provided that its power rating is properly selected.

To provide the WPP with this capability, the simplest approach is chosen here, that is the communication of the signal ΔP_{POD} (derived from a controller such as that utilised in Section 7.2 and illustrated in Figure 78) to the WPPC. As depicted in Figure 14, the signal is fed-forward to bypass WPPC's PI control and ramp-rate limiters – justification for this will be given later. Moreover, the signal ΔP_{POD} is used as an input to a so called *Freeze logic*, which performs proper freezing of power reference and control error when a POD event is detected. A possible block diagram implementation of this function is sketched in Figure 84.

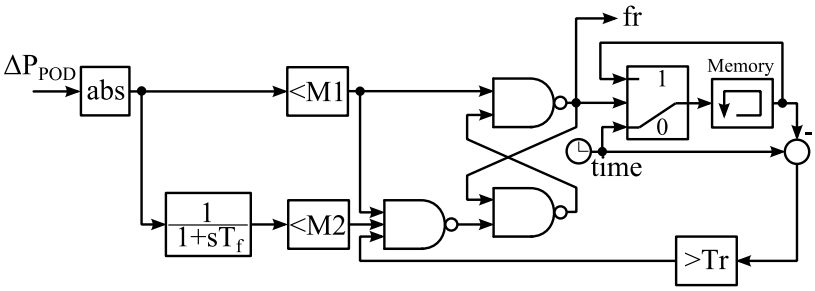

Figure 84 - Possible block diagram implementation of *Freeze logic* block in Figure 14.

The scheme is based on a set-reset latch which locks the signal "fr" to a high-state when the absolute value of the signal ΔP_{POD} rises above threshold M1. The high-state is maintained as long as (i) the absolute value of both ΔP_{POD} and its filtered versions are above thresholds M1 and M2 respectively *and* (ii) the POD event time is less than the reset time Tr. Tuning of the parameters depends on the particular application. Utilisation of the filter with time constant Tf is needed to avoid bounces in and out of the service. In a real-life application, a better solution would probably be developed as a coded algorithm, which gives more freedom and flexibility, especially if the POD must be coordinated with other services.

Some assumptions should be stated at this point, which help justify the choice for the particular implementation:

- As demonstrated in Chapter 4, the control of the offshore HVDC converter can reach large BWs compared to the frequency of POD signals. So large that the offshore converter may be assumed as instantaneously feeding the WPP power into the DC link.
- In a similar way, but this time based on literature [23], it can be assumed that the onshore station is instantaneously injecting all DC line power into the AC grid, due to the dynamics of DC voltage control usually being in the 50-100 rad/s range.
- Power controls on the WTGs may be considered very fast too, compared to POD frequencies. If they are not, then the POD controller should compensate for them before dispatching the power reference P_{WTGi}, making sure gain and phase shifts provoked by WTG's power control are cancelled out and the overall response at the onshore PCC is as desired.
- Communication delays are also affecting the performance, depending on their magnitude. Initially, no communication delay is assumed to be present in the chain going from onshore measurement point to WTG power reference. Later in this section the influence

of communication delays will be discussed, deriving requirements for implementation of POD.

It should also be added that for POD provided with reactive power modulation, the same control scheme is used to derive the signal ΔQ_{POD} (Figure 78), but the control output is used directly in the onshore HVDC station and not forwarded offshore. It is assumed, in this context, that the onshore station be properly rated to be able to provide the necessary reactive power modulation at any time, or that an agreement is reached with the TSO to limit the maximum ΔQ_{POD} when close to the operational limits.

7.3.2 Demonstration of combined POD from VSC-HVDC and WPP

The POD capability of the combined VSC-HVDC/WPP system is evaluated here by application to the power system model in Figure 8, the modified IEEE 12-bus system. The reader is referred to Section 3.2.1(b), Appendix 1, Appendix 2 and [109] for a detailed description of it. Here it suffices to say that the system has a poorly damped eigenvalue ($\omega_\lambda \approx 0.7$ Hz, $\zeta \approx 1\%$) in which SGs G1 and G2 oscillate against G3 and G4. The VSC-HVDC-connected WPP is plugged into the model at Bus 1. It is rated 500 MW (600 MVA) and initially providing $P_{WPP,0}$ = 200 MW and $Q_{WPP,0}$ = 0 MVAr at the PCC (Bus 1). The load at Bus 1 is increased accordingly to minimise the influence of the initial operating point on the small signal characteristics of the power system. Control parameter tuning, modal analysis and time domain results are described in the following. Finally, the effect of the AVRs is looked at.

(a) Control parameter tuning

Relying on the assumptions stated above, using the guidelines derived in Section 7.2.3 and observing the characteristics of the power system where POD is to be provided [44], [109], choice of the control input and tuning of the control parameters for the POD controller could be done as follows:

- A good control input according to observability analysis is the active power through the line 7-8, i.e. P_{78}. As such, it will be used as control input. The oscillatory mode is reflected into P_{78} as an effect of the angle displacement between the two generator groups. Equivalently, it will be lagging the speed deviation between generator groups by 90°.
- Although the generator with highest participation in the target eigenmode is G4, the machine that is most affected by the VSC-HVDC connected at Bus 1 is G1: 70% of active power variations from the WPP instantaneously flow into G1 (with negative sign), while G1's terminal voltage presents a 10% per-unit sensitivity to reactive power variations from the HVDC station.
- For P modulation, due to the negligible effect it has on G1's terminal voltage, one may expect to need a phase shift near 90° (with sign opposite to the overall gain $K_{POD}K_{comp}$).
- For Q modulation, the AVRs' action on G1 and G2 is very strong, according to the data in Appendix 2. Combined with the field circuits, the response has large magnitude and phase lag of approximately 90°. As such, one may expect to need a phase shift around 0° in the control chain. G1 is leading G2 in the oscillations, which are roughly in phase with G2's angle. G2's terminal voltage too is affected by the Q modulation. Hence, a slightly positive phase shift may provide even better results. It can e.g. initially be set to 10° and adjusted so to correct the pole movement: it should be decreased if the linear analysis shows a decrease in eigenfrequency and vice versa.

(b) Results: linear analysis and non-linear simulation

The practical guidelines above have been used to roughly tune the phase shift in the control chain (Figure 78). Then, the gain K_{POD} was increased and the phase shift adjusted to bring the target eigenvalue's damping factor to $\zeta \geq 5\%$ and limit the variation of its frequency to $|\Delta\omega_\lambda| \leq 1\%$. The utilised phase shifts and gains are reported in Table 20, along with the achieved damping factor and frequency variation for the critical eigenvalue, as obtained from DIgSILENT PowerFactory's modal analysis. The performance for simultaneous POD with P and Q *without* further changing the parameters is also shown in Table 20. Positive values for both K_{POD} and K_{comp} are assumed. The value of time constants (T_a, T_b, T_c, T_d) and K_{comp} is not reported, but is done with usual geometric mean technique.

Table 20 - Derived POD phase shift and gain for test on IEEE 12-bus system and achieved linear results.

POD type	Phase comp. [°]	K_{POD} [pu]	ζ [%]	$\Delta\omega_\lambda$ [%]
P	-90	12	5.1	+1
Q	+20	11.9	5.1	<1
PQ	-	-	7.2	2

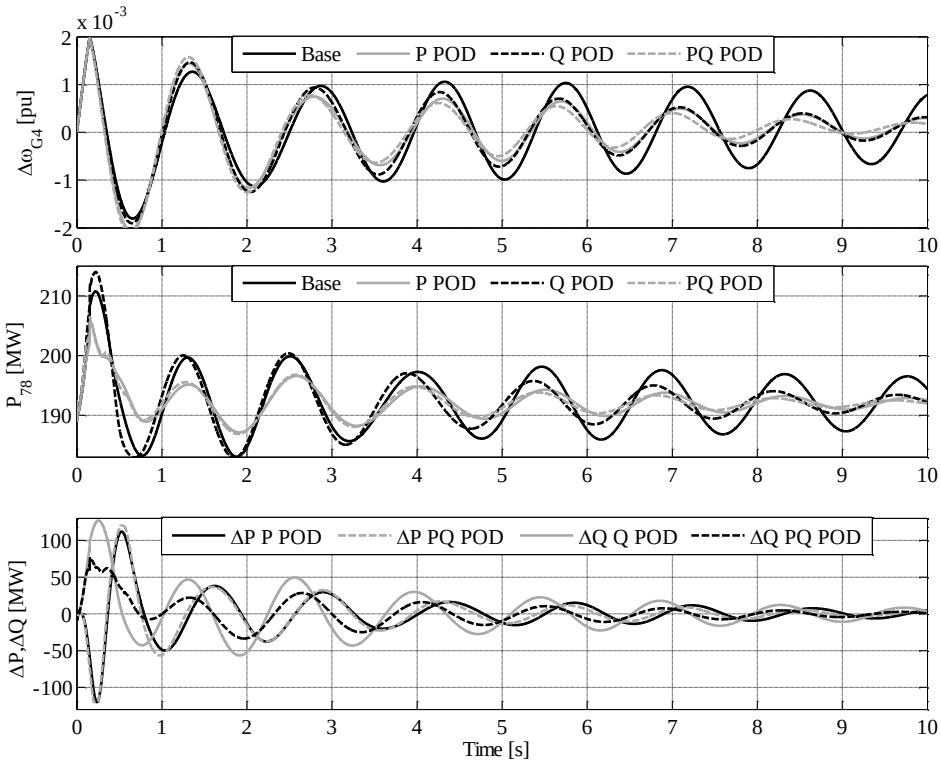

Figure 85 - Non-linear simulation results on IEEE 12-bus system for base case, P POD, Q POD and PQ POD.

It is noticed that the phase compensations well align with what stated in the guidelines above. P POD can essentially be tuned independently of the AVRs, while Q POD needs to take AVRs into account on both G1 and G2. Expectedly, the fast response of the AVRs moves the needed phase shift close to 0°. In this respect, it is worth bearing in mind that the loads in the system in Figure 8 are all constant power loads. In reference [149], it is explained that inter-area modes are damped by classical PSSs by modulating loads exploiting their voltage dependency. This phenomenon would happen even with POD with Q modulation from static sources and loads should thus be made more realistic in future studies. It is likely that the voltage dependency of loads would

reduce the phase correction due to the presence of AVRs and thus make the design slightly more independent of AVRs. A quantification of this is anyhow left for future work.

The results from modal (linear) analysis are corroborated by a non-linear simulation. A 3-phase fault is simulated and cleared at Bus 6 and the system response is recorded for base case (no POD), POD with P, Q and PQ. The results are depicted in Figure 85.

In the time domain, the results of the linear analysis are confirmed. POD with P or Q essentially provide the same damping, which is much improved compared to the base case. The oscillation frequency is slightly increased. Applying POD with PQ the damping ratio further improves and the frequency further increases slightly.

Furthermore, it can be seen that, apart from the initial spikes, the output signals of the POD controller essentially always remain in the range ± 0.1 pu (on a WPP base), which can thus be used e.g. as a saturation value for the POD controller.

(c) Effect of AVRs

To illustrate that the conclusions previously drawn regarding the effect of the AVRs are valid even in a larger system like this, it is useful to vary the parameters of the AVRs on G1 and G2. Starting from the default gain K_A reported in Appendix 2, the gain is progressively lowered for both generators to 20 pu when POD with Q modulation according to the above design is acting, observing the effect this change has on the eigenvalue's position in the complex plane. The results are summarised in Figure 86.

The black marks refer to the scenario corresponding to the second row of Table 20 and illustrate the effect of the designed POD scheme in the complex plane. As the AVR gains are progressively lowered, the eigenvalue follows the black line and loses damping due to increasing real and imaginary part. The grey marks illustrate the eigenvalue position for K_A = 20 pu for both G1 and G2. The circle refers to the base case without POD, while the cross is the eigenvalue's position for default POD with Q. Counteracting the effect of having lower AVR gains is possible by correcting the phase shift in the controller. Bringing it from +20° to +45° the grey square is obtained.

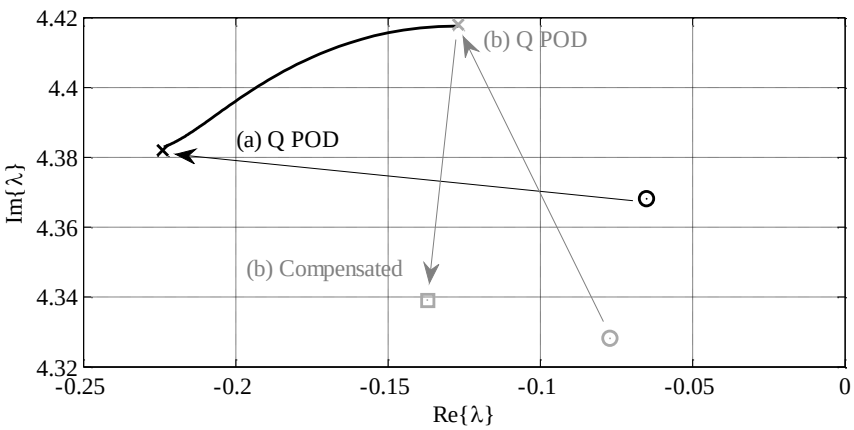

Figure 86 - AVR gains' effect on critical pole of IEEE 12-bus system: (a) high K_A on G1 and G2, (b) K_A = 20 pu.

Another conclusion that can be drawn from Figure 86 is that when strong voltage regulation is available in the grid, the achievable damping contribution of Q modulation increases due to the higher equivalent gain in the chain going from Q to the electrical torque of the SGs at the

eigenfrequency. This comes at the expense, as said, of a slightly larger complication in the calculation of the necessary control phase shift.

7.3.3 Closed loop stability and performance limitations

As explained above, it will often be the case that some electrical quantity will be used as input to the POD controller. At typical oscillation frequencies such input will be, to a good approximation, instantaneously dependent on the POD control chain output, usually P or Q at the PCC. A certain level of dependence is very likely to happen, especially if the measured signal is sensed electrically close to the PCC. This generates a closed-loop system where, roughly, only the POD control loop and the measurement feedback play a role. Besides assuring that the POD scheme interacts in the right way (providing damping) with the overall, multivariable, power system, it is also important to ensure the stability and assess the limitations of such a closed loop system. The closed loop can generically be drawn as in Figure 87.

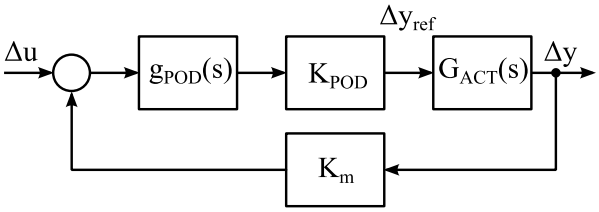

Figure 87 - Generalised diagram of POD closed loop system.

In the diagram above, $g_{POD}(s)$ is the normalised POD transfer function, which is the overall transfer function in Figure 78 divided by K_{POD}. $g_{POD}(s)$ has magnitude 1 (0 dB) at the eigenvalue's frequency. $G_{ACT}(s)$ is the "actuator" transfer function. Actuator can be considered every element interposed between the reference POD signal Δy_{ref} and the actual output at the PCC Δy (y can be, in the present case, P or Q). In the present case and taking P POD as an example, G_{ACT} contains communication delays, WPPC dynamics and delays, WTG control dynamics and delays, DC system and HVDC converters dynamics and delays. K_m represents the measurement gain and gives an idea of how much the control input is algebraically influenced by the control output. It is important to notice that such approach is strictly valid only as long as electrical transients in the network are neglected: this is usually the case for studies regarding electromechanical oscillation and using RMS network representation. Moreover, other non-proportional effects of Δy on Δu are disregarded: considering that they would most likely be integral effects related to electromechanical phenomena and the focus in this section is on relatively high frequency, this assumption is deemed to be satisfying, at least for a qualitative assessment of the phenomena.

(a) Control performance limitation

By looking at Figure 87, the closed loop transfer function is immediately derived as (Laplace operator s dropped for brevity):

$$G_{CL}(s) = \frac{g_{POD}K_{POD}G_{ACT}}{1 - K_m g_{POD}K_{POD}G_{ACT}} \tag{39}$$

When the real part of $K_m g_{POD}K_{POD}G_{ACT}$ is positive, a danger for instability exists, which will be discussed next. However, there also exists a limitation in terms of achievable gain of the control loop when the real part of $K_m g_{POD}K_{POD}G_{ACT}$ is negative and the open loop gain is increased. The maximum magnitude of the transfer function is limited to:

$$|G_{CL}| \leq \frac{1}{K_m} \tag{40}$$

Such limit clearly influences the effect that the POD controller can have on the power system, since any input oscillations cannot be amplified more than the limit. If the power system requires a larger closed loop gain in order for the critical mode to be damped efficiently, then the limitation above may compromise the implementation.

(b) Closed-loop control stability

As hinted above, the stability of the closed loop system may become a problem when the sign of the real part of $K_m g_{POD} K_{POD} G_{ACT}$ is positive. The stability of the system above can be assessed by plotting the Bode diagram of the open-loop transfer function $-K_m g_{POD} K_{POD} G_{ACT}$, where the negative sign is due to the positive feedback. At first it is useful to assume an ideal $G_{ACT}(s) = 1$. The compensation example with time constants as in the first column of Table 19 is considered and four cases are looked at, i.e. the permutation of $K_m K_{POD}$ being greater or less than zero, and the use of lead or lag compensation. The diagrams are shown in Figure 88. The magnitude of $K_m K_{POD}$ is varied between 0.01-1 pu. Only frequencies up to 300 rad/s are considered, due to the RMS representation of the network.

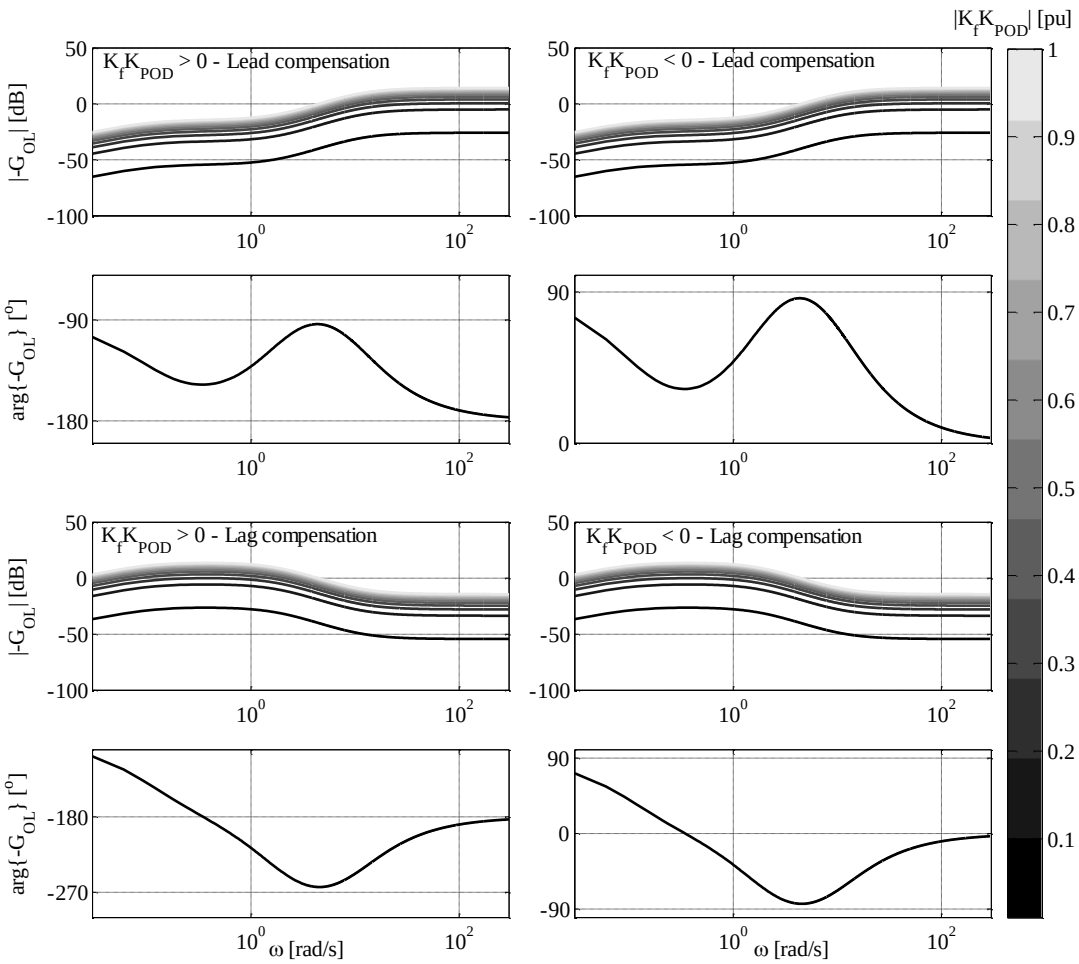

Figure 88 - Generic Bode diagrams for open loop transfer function with ideal G_{ACT}.

It is clearly seen that $K_mK_{POD} < 0$ is strongly desirable in any case to provide greater stability margin (remember the positive feedback), the best possible option in terms of phase margin expectedly being $K_mK_{POD} < 0$ and lead compensation, while the option $K_mK_{POD} > 0$ and lag compensation is potentially unstable even with ideal G_{ACT}.

It should be noticed that there may be a certain level of freedom in choosing the sign of K_mK_{POD}. For instance, in Figure 77 the eigenmode is reflected in the same way in P_L and P_e. As such, the sign of K_{POD}, given a certain sign of the compensation, will not depend on which input is used. However, K_m will have negative sign for P_e and positive for P_L. Assuming to use lead compensation as described in Section 7.2.3(b), $K_{POD} < 0$ will have to be used[14]. That means that one should choose P_L as an input to be in the best situation from a stability perspective, since in that case $K_mK_{POD} < 0$. However, the performance limitations described in Section 7.3.3(a) are encountered instead.

It is also important to remember that a non-ideal G_{ACT} most likely implies phase shifts due to control and communication delays that lessen the stability margin. For large lags, even the best option – top right – can become unstable if proper gain reduction at high frequency is not performed. Pure delays are particularly deleterious in these terms, since their response detrimentally shifts the phase to lower values without offering a corresponding gain reduction.

Let us illustrate the stability problem with a simple example, which will highlight that even without communication delays and only accounting for controllers and DC system in $G_{ACT}(s)$ instability may be approached. The case analysed along Section 7.3.2 is used as study case.

All communication delays are neglected and the WPP, based on time domain power reference step simulations of the WPP model, is modelled as two real poles at 100 rad/s and 200 rad/s, i.e.:

$$G_{WP}(s) = \frac{1}{1+0.01s} \cdot \frac{1}{1+0.005s} \tag{41}$$

The transfer function $G_{ACT}(s)$ is approximated as:

$$G_{ACT}(s) = G_{WP}(s) \cdot G_{DC}(s) \tag{42}$$

where $G_{DC}(s)$ approximates the behaviour of the DC system and HVDC converters. An example of derivation of such transfer function is reported in Appendix 4. Only POD with active power modulation is active and its design was presented in Section 7.3.2. The control input is P_{78}. The circuit parameters are so that $K_m = 0.075$ pu. The following five illustrative cases are chosen:

1. Ideal case: POD as in Section 7.3.2 (lead compensation, $K_{POD}K_{comp} < 0$) and $G_{ACT}(s) = 1$.
2. Ideal case: POD as Case 1, but lag compensation, $K_{POD}K_{comp} > 0$ and $G_{ACT}(s) = 1$.
3. Real case: POD as in Case 1 and DC system and WPP taken into account according to Eq. (42).
4. Same as Case 3, but with addition of second order filter in the POD controller, for gain reduction at high frequencies. The filter is a second order LP filter with $\omega_0 = 10$ rad/s and $\zeta = 0.5$.

[14] In Section 7.2.3(b) $K_{POD} > 0$ and $K_{comp} < 0$ were used, which is the same thing.

5. Same as Case 4, with gain and phase correction at the eigenvalue frequency ($f_\lambda \approx 0.7$ Hz) to compensate for the effect of the LP filter.

The Bode diagrams for the five cases are reported in Figure 89. The unstable nature of Case 2 is immediately observed, while Case 1 is obviously stable. However, when DC system and WPP are inserted (Case 3), the system turns unstable, due to the lack of proper gain reduction at high frequencies. Insertion of the second order LP filter guarantees stability again, although with rather poor phase margin. The phase margin is further reduced when gain and phase compensation is adopted to retune the POD to the initial magnitude and phase shift at the target frequency – Case 5. An improvement in the design is clearly necessary to give more phase margin, but the point to be stressed here is that high-frequency stability problems are possible even with the best combination of lead compensation and $K_m K_{POD} < 0$.

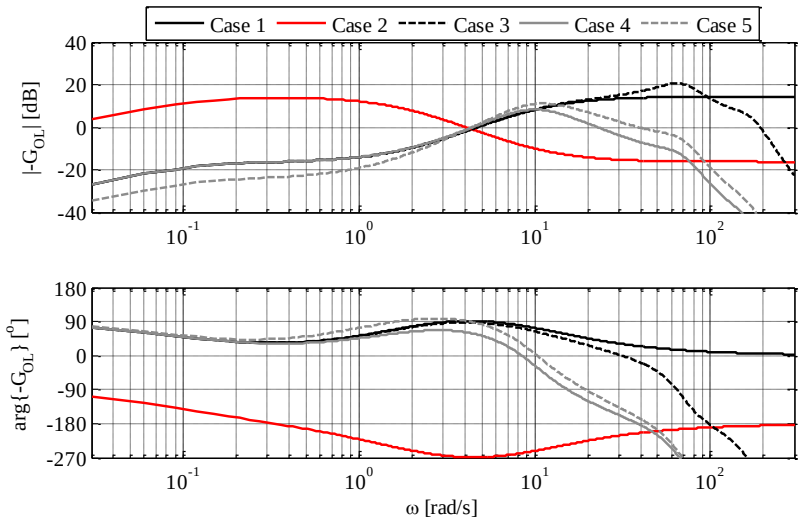

Figure 89 - Example of Bode plot for open loop POD transfer function: description of cases above.

Some of the cases above are reported in the time domain simulation shown in Figure 90, to demonstrate the expected instability of Case 2 and 3 and the almost equivalency of Case 1 and 5 (the small difference is due to the fact that $G_{DC}(s)$ is not accounted for in the additional compensation in Case 5). The instability of Case 3 does not diverge owing to the fact that the POD controller is provided with saturation limits. Its frequency is around 125 rad/s which, considering the numerous approximations, is satisfyingly close to what can be evinced from the Bode diagram in Figure 89.

In order to avoid the design challenges encountered due to the stability problems, it may be more sensible to employ lag compensation, to exploit its inherent gain reduction at higher frequencies. However, if doing so, either (i) another measurement should be used that allows the gain $K_m K_{POD}$ to be negative or (ii) the value of K_m should be so small that the open-loop transfer function never be above 0 dB – see the four bottom graphs in Figure 88. Furthermore, the possible problems described here are another indication that frequency-selective techniques as that mentioned above and described in [152] may actually be very attractive for this kind of application.

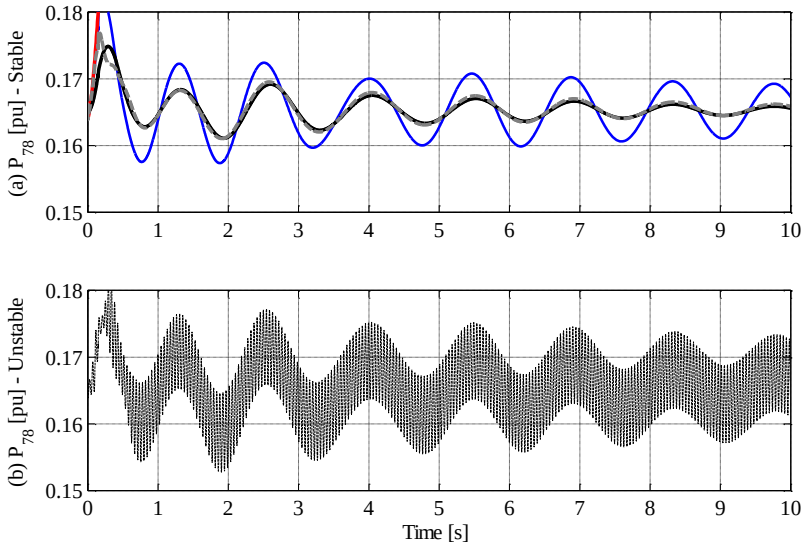

Figure 90 - Time domain simulation of selected cases. Top plot: (blue) base case with no POD, (red) Case 2, (black) Case 1, (gray) Case 5. Bottom plot: high-frequency unstable case (Case 3).

(c) Requirements for better performance and stability

As a conclusion of the brief analysis above, the following qualitative requirements may be formulated to enhance performance and stability:

- The possibility of implementing frequency-selective schemes to extract the relevant oscillatory mode should be seriously evaluated, to avoid stability issues.
- On the other hand, if a well-known PSS-like scheme like that employed here is to be used, the following mitigating measures should be taken to remain far from instability:
    - The measurement feedback K_m should be minimised, to the extent possible. This gives more freedom, since the closed-loop magnitude is not strictly limited. Moreover, this lowers the value of the open-loop transfer function, making it easier to obtain solid stability.
    - As already known from the literature, an input Δu providing good mode observability and an output Δy ensuring good mode controllability should be chosen. This minimises the required closed-loop gain to achieve the desired damping.
    - Placement of the measurements should consider the issues illustrated along this subsection. The most desirable properties are that K_m be minimised and $K_m K_{POD} < 0$.

7.3.4 Sensitivity to communication and control delays

As evinced by all the analysis above, precise phase shift of signals related to POD is vital to the successful provision of the service. Not only may wrongly phase-shifted signals reduce the effectiveness of the damping action provided by the WPP and VSC-HVDC, but they may even have a negative effect on the eigenvalues as compared to the base case. Generally, undesired phase shifts can stem from control or communication systems. In the case of controllers, the magnitude of the signals may be affected too, along with their phase. Sources of delays may typically be the following:

- WTG controls, WPPC and HVDC converters control are all affecting the provision of POD through the system considered here. As stated above, the control of HVDC converters and WTGs is expected to have a negligible influence, but should definitely be accounted for in control design if it is relevant. As for the WPPC, if POD signals are going through the whole power control chain – let us assume it is based on a PI, for simplicity – this may have a great effect on the POD, introducing both gain and phase shifts.
- WPPCs are typically used to guarantee plant-level services such as POD. Delays in a WPPC may derive from (i) its sampled nature, with sampling intervals as large as several tens of milliseconds in modern controllers and (ii) its complex hierarchical and modular structure that implies additional communication delays in the chain going from operator order to WTG.
- Possible remote sensing of the control inputs can add further delays in the communication chain. If the signal is measured by another operator and/or through a GPS-based system delays can become very significant [44].

Concerning the sampled nature of WPPCs, according to the sampling theorem [153], a maximum sample rate of 250 ms is allowed to theoretically guarantee correct performance at the maximum POD frequency (2 Hz), if all controllers are properly synchronised. To the author's knowledge, such figure is outperformed by modern WPPCs and should not impose strong limitations.

As for delays created by other devices in the control chain, let us go back to the simple system in Figure 77. Assuming linearity, a lumped communication delay T_d = 0-500 ms is inserted in the control block diagram (Figure 78). It is modelled as an ideal delay e^{-sT_d} for time domain simulations and as its second order Padé approximation for linear analysis [154]. The inertia constant of the SG (initially H = 1 s, giving an eigenfrequency $f_\lambda \approx 0.71$ Hz) is changed to H_m = 1s and H_M = 16 s, giving eigenfrequencies $f_{\lambda m} \approx 1.36$ Hz and $f_{\lambda M} \approx 0.36$ Hz respectively. Active power POD is considered, as it is the one where more delays may arise in VSC-HVDC-connected WPPs. Varying T_d in the specified range, the plots in Figure 91 are obtained for the three cases and POD parameters designed to achieve $\zeta \approx 10\%$ in all cases. The AVR gain is K_A = 40 pu.

It can be immediately noticed that an increasing time delay understandably has a synchronising effect, as the eigenvalues move upwards for small delays. Larger delays provoke increasing eigenvalue's real part, further deteriorating the damping. Expectedly, the degree of resilience to communication delays depends on the eigenfrequency. At lower frequency (H_M, right top graph and dashed black line in bottom graph) a higher communication delay can be tolerated than at higher frequencies, especially if the damping ratio is used as performance indicator. The system becomes unstable for T_d = 82 ms for H_m, T_d = 120 ms for H, and T_d = 205 ms for H_M.

Delays can be compensated for quite easily, as is exemplified by the centre top graph, where a 100 ms delay has been counteracted by a lead compensation block. However, compensation of very large delays may not be practically easy with rational functions. Moreover, it should be noticed that the needed angle phase shift to compensate for the delay T_d at the frequency ω_λ is given by $\varphi_d = \omega_\lambda T_d$. The eigenfrequency ω_λ may be uncertain to some extent, but one still wants to minimise the uncertainty on the compensation angle φ_d. As a consequence, the following requirements should be fulfilled by a practical realisation of POD:

- Communication delays should be minimised to the extent this is possible.

- Communication delays should be made deterministic, i.e. their value should be fixed and well-known, independent of operational point and control parameters, so that they can be compensated for very robustly.

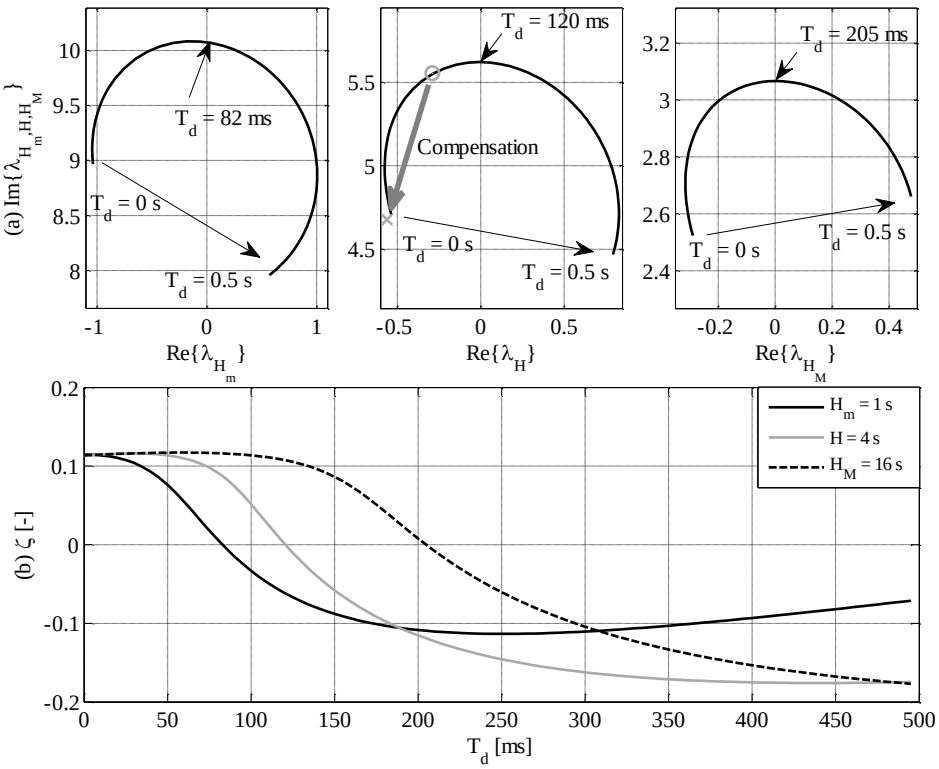

Figure 91 - Influence of communication delay on POD performance for varying eigenfrequency.

The first bullet above must clearly be pursued bearing its cost in mind, while the second item should possibly be fulfilled anyhow. It should be noticed that the feed-forward solution in the WPPC – see Figure 14 – goes in the direction of achieving both objectives above: (i) delays related to the control chain are avoided, minimising the total delay and (ii) the total delay will eventually be independent of variations of the PI parameters and only depend on the sample time and controllers synchronisation, which can more easily be made deterministic.

7.3.5 Ramp-rate limiters

Another factor that could deleteriously affect the performance during POD provision is the presence of active power ramp-rate limiters which are usually installed on WTG controllers and WPPCs. The drawbacks of non-negligible ramp-rate limiters are mainly (i) reduced validity of design approach assuming linearity and (ii) distortion of the signals. Not only can the latter problem lessen the POD effectiveness by attenuating the signals' amplitude, but also create phase distortions that deteriorate the performance even further. In order to derive a requirement in terms of necessary ramp-rate, let us hypothesise that:

- The POD controller is working unsaturated, i.e. in linear conditions, at the very limit of saturation.
- The saturation levels of the POD controller are $\pm\Delta P_{MAX}$.
- The eigenvalue to be damped has frequency ω_λ and real part α.
- All other power references in the WPP are constant.

Under the assumptions above and assuming, without losing generality, the POD event takes place at t = 0 with nil phase, the signal ΔP_{POD} may be expressed as:

$$\Delta P_{POD} = \Delta P_{MAX} \cdot \sin(\omega_\lambda t) \cdot e^{\alpha t} \tag{43}$$

Taking the derivative of such signal, its maximum value is $\omega_\lambda \Delta P_{MAX}$. Assuming for instance ΔP_{MAX} = 0.1 pu and considering the realistic range of POD frequencies mentioned here, the requirement for minimum allowable ramp-rate limitation will be:

$$0.063\ \frac{pu}{s} \leq \left.\frac{dP}{dt}\right|_{min} \leq 1.26\ \frac{pu}{s} \tag{44}$$

Figures such as those mentioned in Chapter 6 are much lower than the upper limit above, meaning that a relaxation of the parameter would be necessary in most cases. It should be noticed that the solution shown in Figure 14 bypasses WPCC's ramp-rate limiters. As such, if the most stringent limits are imposed at a plant level, the proposed scheme may solve the problem. However, it must still be ensured that WTGs' ramp-rate limiters are sufficiently large and the overall design of WTGs takes into account the possible additional stress related to the POD.

7.3.6 Collateral effects on WTGs

(a) Available energy and recovery period

Since POD is a dynamic, oscillatory service which does not require the delivery of net energy to the grid, it is technically sound to superimpose it to the power reference of the WPP even when such reference is determined by the MPPT table. In other words, and contrary to a service like PFC, POD does not necessarily need the WPP to curtail its power production to reserve some power for the service. This has significant implications in terms of energy production and related earnings.

However, similarly to what has been done for IR [33], [141], the rotor speed stability must be ensured when WTGs are called to extract more energy than they would do according to their MPPT scheme. Reference [33] is inspiring in these terms, where a derivation of the available energy for overproduction ΔE_{av} as a function of wind speed and design parameters is proposed. Once ΔE_{av} is calculated, the requirement for the maximum power modulation during POD can be written.

Let us assume to be in the worst case, i.e. when the first swing of the POD signal ΔP_{POD} is perfectly rectangular with amplitude ΔP_{MAX} and the oscillation frequency is f_λ. The following constraint must be satisfied:

$$\Delta P_{MAX} \cdot \frac{2}{f_\lambda} \leq \Delta E_{av} \tag{45}$$

Among the parameters above, ΔP_{MAX} is the result of a compromise between TSO requirements and WPP capability and cost, while f_λ is provided by the TSO. Finally, ΔE_{av} is an OEM's design parameter which depends on a number of other parameters and has an influence on the cost too.

Taking sample figures for ΔE_{av} from [33][15] and assuming ΔP_{MAX} to be in the range of 0.1 pu, only extremely low values of f_λ may result in the above constraint being violated. Moreover, it should be borne in mind that in the case of POD the negative semi-period of the POD waveform naturally helps the rotor speed's recovery immediately after the positive swing. As was proven in [150], only the combination of very low frequency and high damping of the signal ΔP_{POD} can be critical to the WTG's rotor speed stability. However, if ΔP_{POD} is a well-damped signal, it is not sensible to demand POD from the WPP and the problem may thus not exist.

(b) WTG's shaft oscillations and other resonances

The extremely frequency-selective nature of POD requires the WPP to deliver active power modulation at a very specific frequency. Active power oscillations, unless proper control means are devised, can find their way all the way to the WTG rotor. If the GSC is programmed to maintain constant DC-link voltage, the POD power reference will be given to the RSC and the modulated power will be evacuated by the GSC, and this will happen instantaneously, in a time scale related to POD frequencies. When exciting the WTG's mechanical side with active power oscillations, any mechanical resonance should definitely be avoided, to avoid premature wearing of the mechanical system. Examples of elements that can create resonances are the generator shaft [21], the tower [33] and the blades. Here, the shaft is taken as an example, to illustrate the problem.

Referring to the two-mass mechanical part of the standard WTG model [22], four parameters are characterising the power transmission through the shaft, namely generator's and rotor's inertia constants (H_{GEN} and H_{ROT} respectively), the shaft stiffness K_{SH} and the shaft damping factor C_{SH}. The characteristic equation of the model yields the following natural frequency and damping ratio:

$$\omega_{SH} = \sqrt{\frac{K_{SH}}{2}} \cdot \sqrt{\frac{H_{ROT} + H_{GEN}}{H_{ROT} H_{GEN}}} \tag{46}$$

$$\zeta_{SH} = \frac{C_{SH}}{4} \cdot \sqrt{\frac{2}{K_{SH}}} \cdot \sqrt{\frac{H_{ROT} + H_{GEN}}{H_{ROT} H_{GEN}}} \tag{47}$$

Taking as a base case the default parameters listed in Appendix 2, each of them is varied by 25% and natural frequency and damping ratio are plotted against each other, generating the grey-shaded area in Figure 92[16].

It is evident that even for a rather large span of variation of the parameters, the resonance always lies in a relevant range for POD events. Without proper countermeasures there is a risk to excite shaft oscillations that would endanger the integrity of the WTG. Moreover, this kind of check should be performed for all resonances in the mechanical system.

An open list of solutions to this problem is proposed, qualitatively discussing each of them:

[15] The figures reported in the cited reference are valid for a Type 3 WTG. However, since ΔE_{av} is a parameter that mainly depends upon mechanical and generator properties, Type 4 wind turbines may provide similar values.

[16] The graph in Figure 92 was plotted using C_{SH} = 0.44, which is a plausible figure for the shaft standing alone, while the higher value reported in Appendix 2 refers to a case when the natural damping is increased by control means. The parameter does not influence the frequency anyhow, which is the important figure in this context.

- Reach an agreement with the TSO that POD cannot be provided by the WPP at certain frequencies.
- Do not let oscillatory terms at dangerous frequencies reach the mechanical side, by e.g. installation of notch filters in the control. Proper DC-link ratings are needed to absorb power fluctuations at the critical frequencies and limit voltage fluctuations. A larger DC capacitance and/or voltage over-rating may be needed.
- Maintain constant torque on the mechanical side and, when providing POD, decrease the average power level and superimpose the POD component, burning the excess energy in a resistor. This comes at the expense of installing a resistor. Such a device is anyhow used in some WTGs for FRT purposes, but the one for POD would presumably be larger. This approach requires the TSO to accept a lower average power delivery during POD events.
- Similar approach to the above, but installing the POD control and resistor at the onshore HVDC station. This would again require the resistor (presumably a more expensive one, but only one instead of several), but the advantage would be that it would be placed onshore and not in the WTGs' nacelles. Moreover, the overall control and communication system would be simplified.
- Utilise a separated energy storage device, more conveniently installed onshore.

Clearly, all the above means that early dialogue between TSO, WPP developer and OEM needs to take place to make sure the right kind of information is exchanged and the POD controller is developed in the proper way. As for the proposed solutions, the final choice would be determined by the overall cost of each of them.

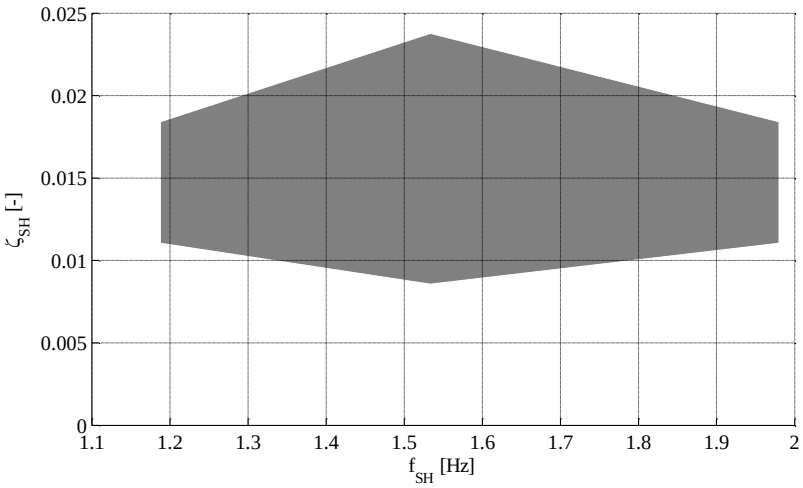

Figure 92 - Shaft's system resonance frequency and damping ratio for varying mechanical model parameters.

7.4 Summary

The provision of POD from a VSC-HVDC connected WPP was the subject of this chapter. Firstly, POD from a generic power source in a very simple network was used to assess which factors are important to fuel the discussion between TSOs and owner of a PE asset on which POD is to be installed. As a conclusion, it turned out that AVRs, though often neglected in the literature, are crucial for the assessment of POD performance and the tuning of the control parameters. Moreover, the usefulness of SGs' active power and terminal voltage sensitivities to active and reactive power modulation of the converter with POD was highlighted. Practical

guidelines to reach an approximate parameter tuning from purely physical considerations were devised, which are useful to avoid complex mathematics at least at an initial stage.

After demonstrating the successful implementation of the service on a VSC-HVDC-connected WPP in a larger power system model, some potentially limiting factors for real applications were treated, deriving requirements in terms of:

- Closed-loop performance stability: a best-practice for optimal placement of measurements and choice of compensation sign was derived based on limitations on the closed loop performance and stability of the POD controller when its input is algebraically influenced by its output.
- Sensitivity to delays: minimisation of communication delays is strongly suggested, along with an effort to make them as deterministic as possible. A few possible solutions that help pursue these objectives were discussed.
- Ramp-rate limiters: a simple constraint to avoid distortion of the POD signals was proposed.
- Collateral effects:
    - Based on state-of-art, WTG rotor speed stability did not appear to constitute a serious problem.
    - Mechanical resonances need be addressed in advance with the OEMs to avoid unwanted damages to the WTG's mechanical system.

Chapter 8 Experimental verification of clustering of WPPs

This chapter illustrates the simulation and experimental verification of clustering of WPPs to co-ordinately provide active power control and system services related to it, namely frequency control and POD. A dynamic model including two aggregated WPPs, two WPPCs and one open-loop CC (dispatcher) is described, building upon previous chapters. The results derived employing only one WPP are validated with measurements obtained during an experimental verification, the setup of which is also described along this chapter. Simulations of a cluster of two WPPs are then presented, utilising the validated models. Conclusions are drawn by highlighting main challenges and providing a recommendation for future implementation of such a configuration in real life.

8.1 Introduction – Clustering of wind power plants

8.1.1 Why clustering WPPs?

Nowadays, offshore WPPs are operated as single units with a dedicated WPPC that performs the required control actions at their PCC. In these terms, the state-of-art was discussed in Chapter 2. WPPs usually are part of clusters of generation facilities within a single operator's fleet and are thus dispatched set-points by a central, slower, controller. However, in future applications, clustering of just WPPs may become attractive for example because of the following reasons:

- Control actions requiring intermediate dynamic performance may not be delivered by an operator's central dispatcher, particularly if such features are of local nature. An example of it could be POD, but even frequency control may be too fast to be handled instantaneously by central controllers.
- For several reasons, the possibility to choose multiple WTG suppliers may be a way to drive cost of energy down. For large WPPs with multiple export circuits, this may even happen within the same WPP project. Moreover, one could evaluate whether to bundle, from a control standpoint, existing WPPs which PCCs are close to one another. The options to lay out the control of such a configuration have been briefly discussed in Chapter 2 – Section 2.4.3(b).

- Looking at the WPP connection through VSC-HVDC, the large WPP's size combined with the fact that grid compliance may need to be fulfilled onshore make clustering even more attractive. The latter point is not relevant in current HVDC installations (Germany), but may be so elsewhere (e.g. the UK).

In reality, a certain level of "clustering" of WPPs is already performed in e.g. WPPs with multiple control points, but is always limited to power/voltage reference control and, to the author's knowledge, to WPPs consisting of WTGs supplied by the same manufacturer and with identical dynamic characteristics.

8.1.2 Challenges in clustering of WPPs

An exhaustive discussion of all challenges related to the clustering of WPPs is out of the scope of this study and would require a much more extensive treatment, but a few of the challenges are mentioned here, in accordance with the scope of work:

- Usually, WPPs are provided with their own WPPC, as described in previous chapters. Assuming that one wants to maintain the two WPPCs, operation of the two separate controllers must be stable, robust and not show conflicts of any kind in all operational conditions. The fact that such WPPCs may be developed by different manufacturers implies that dynamic performance and control philosophy may differ. Moreover, each controller may be driving, besides the WPP, supplementary equipment such as reactive compensation, increasing the potential risk of conflict.
- When bundling two or more WPPCs to provide services which require coordinated and properly synchronised response, the above mentioned different dynamic behaviour must be accounted for in dispatching the control signals. For instance, a service like POD (Chapter 7) fully relies on the capability to deliver an appropriately synchronised modulation of active and/or reactive power, with precisely the desired phase shift.

8.1.3 Assumptions and limitations

The subject of clustering of WPPs is vast and cannot be fully covered by one chapter. The focus of this chapter is hence restricted by accepting the following assumptions and limitations:

- In the available experimental facility, only single WTGs are available. Each WTG will hence be treated as an aggregated WPP. This is also a usually accepted assumption for system studies involving WPPs. In real life, however, this imposes limitations in terms of power variability, due to the fact that the wind speed at one turbine is more variable than the average aggregated wind speed over a WPP.
- The WTGs utilised at the test facility are either driven by a dynamometer (no limitations due to the incoming wind) or do not allow for power "over-production" (above available). Therefore, it is assumed that both frequency control and POD are provided by starting from a curtailed operation and sufficient margin has been reserved for the additional control action.
- The limits on available sample rate and the presence of mechanical resonances on one of the WTGs restrict the relevant frequency spectrum to be less than or equal to 0.1 Hz.
- The focus is restricted to active power control. This is due to the fact that the services relevant for this study involve only active power modulation – frequency control, see Chapter 6, and POD through HVDC connection, see Chapter 7. Reactive power control is also a very interesting topic in clustering of WPPs, since it can usually be done much

faster than active power control and involves other compensating equipment. It is however out of the scope of this work and may be analysed in future work.

- Among the different possible layouts for CC and measurements, the focus is here restricted to a configuration where there is an additional CC that dispatches references to two separated WPPCs, each of them controlling one WPP. The CC does so in open-loop, i.e. it assumes a satisfyingly correct knowledge of the dynamic performance of the WPPCs, which can thus be compensated for before signal dispatch. This assumption also implies that the WPPs are located sufficiently near one another. A brief discussion of some options was done in Section 2.4.3(b). The reader can refer to Figure 93 as well as Figure 94 for a high-level visualisation of the system and control layout.
- An-open loop test is performed, which means the original control inputs are not sensed directly in the network. This implies that the findings of this chapter will help shed light on the performance of the cluster of WPPs, but no information will be gained on its interaction with the rest of the power system. This is simply due to the fact that the vast majority of the experiments were conducted grid-connected and disturbing the grid with a real contingency is not possible.

As can be noticed, some of the limitations are due to the need for a restricted scope of work, while some of them are owing to the current test facility setup. Some of the hypotheses may be relaxed in future work in the field.

8.2 Experimental setup

The experimental setup used for the tests is depicted in Figure 93 and is a subset of the available test devices installed at NREL [155].

The following devices were utilised for the tests:

- General Electric Type 4 WTG (WTG 1), rated at 2.75 MW and consists of a PMSG and FSC. The WTG under test is driven by a 5 MW dynamometer that can operate in torque and speed control mode. The WTG has its own power/torque controller. For the purpose of this study, the turbine must follow the given active power reference.
- Siemens Type 4 WTG (WTG 2), rated at 2.3 MW and operating with an IG. The machine is installed in the field and provided with a dedicated WPPC (WPPC 2). WPPC 2 is not a commercial version of it, due to the fact that the WTG is used for research purposes and does not have to comply with strict connection requirements. Therefore, some of its characteristics are not optimal for the purpose of this study, as will be explained below. For the purpose of this study the turbine is required to follow the given active power reference. However, in opposition to WTG 1, the power order is given to WPPC 2 rather than to the WTG control. WPPC 2 can, in the current setup, only provide active power reference tracking (subject to wind constraints). Other more advanced functions such as frequency control are available but deactivated.
- ABB CGI, rated 7 MVA (short term 39 MVA) [156]. The device is provided with dedicated voltage controller that can set amplitude, phase angle and frequency of simulated 13.2 kV voltage. For the purpose of this study, the CGI must maintain voltage and frequency at its terminals equal to the given references.
- User-built CC and WPPC 1 running on dedicated National Instruments PXI. For the purpose of this study, the CC needs to dispatch active power references to WPPC 1 and WPPC 2. WPPC 1 must receive orders from the CC and dispatch them to WTG 1. In

WPPC 1, for power reference tracking and frequency control the controller runs in closed loop, processing the measurements at the WTG's terminals. WPPC 1 can perform frequency control only when not commanded by the CC and running stand-alone.

As also highlighted by Figure 93, communication between the controllers of WTG 1 and the processors executing CC and WPPC 1 happens through shared memory using SCRAMNet real-time protocol. The controllers' clocks are synchronised within 1 ms but can run e.g. at 100 Hz update rate. The communication to WPPC 2, however, is implemented with Modbus protocol via the LAN and operates with 1 Hz clock. Since the communication loop in CC and WPPC 1 is not synchronised with the communication loop in WPPC 2, delays between 1 s and 2 s can be expected over the Modbus channel. More details about the characteristics of the Modbus communication are reported in Appendix 6.

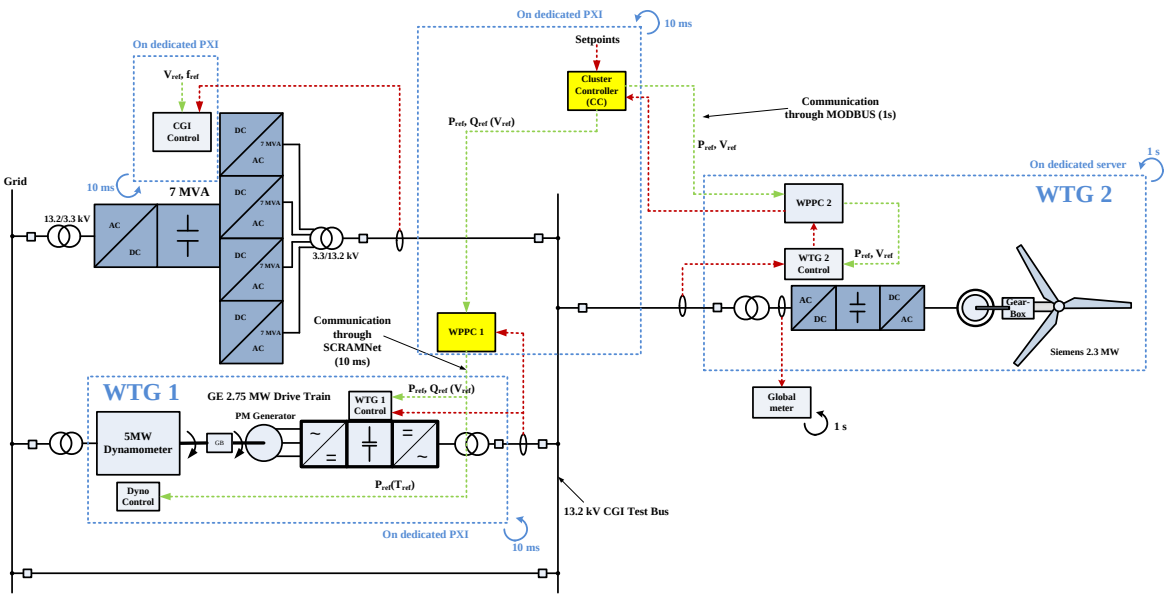

Figure 93 - Experimental setup – courtesy of NREL.

The CGI Test Bus, as shown, can be connected to the CGI or directly to the external 13.2 kV network. The latter is actually the case for all tests involving WTG 2, since its connection to the CGI is planned for future work at the facility.

8.3 Modelling and implementation

Modelling and implementation of the various components and controllers are discussed in this section. All modelling was performed in DIgSILENT PowerFactory after testing of controllers' functionalities in Matlab/Simulink. The implementation of CC and WPPC was performed in National Instruments' LabView language on a real-time controller (PXI).

8.3.1 Overview

The overall, high-level block diagram of the model that was set up in PowerFactory is depicted in Figure 94. Standard static generator models are used to represent the WTG converters and are the interface between the controllers and the grid model. A VSC model is used to model the CGI, the control of which only clamps voltage and frequency to their reference value. For most of the tests performed here, a stiff voltage source would be sufficient to model the grid. However, one test

with frequency variation was carried out, which necessitates a voltage source with controlled frequency. The uncontrolled VSC model is anyhow equivalent to a stiff voltage source for the purpose of this study [99]. The frequency signal f, when measured, is sensed by a SRF PLL like that described in [128] and used for all simulations in this study. The frequency signal provided to the CC is measured by the PLL implemented in the WTG converter controller.

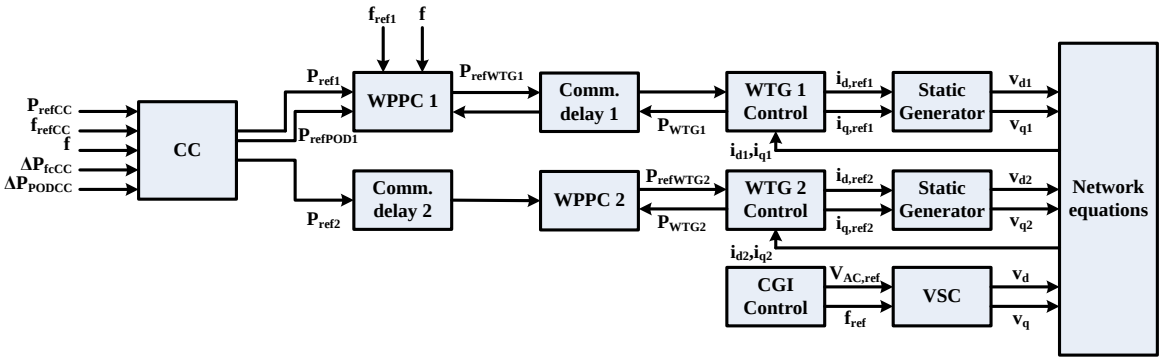

Figure 94 - Overall model diagram.

8.3.2 Cluster controller

As emphasised above and in Figure 93, the CC is performing a simple open-loop dispatch of the power reference signals. The output power references must be sent to either the user-built WPPC 1 or the commercial WPPC 2. As will be further discussed below, there are a few significant differences between the two controllers:

- The dynamic performance, depending on the control parameters.
- The position of the POD control signal – see Section 8.3.3.
- The availability of frequency control capability – see Sections 8.3.3 and Appendix 6.

As a consequence, the CC should provide the possibility to make up for such differences in order to achieve the desired coordinated response. This is done by selectors and compensation blocks. Moreover, the possibility to derive the POD control signals from a frequency variation is also provided by the CC and could be applied e.g. in VSC-HVDC connected WPPs. The generic block diagram of the proposed CC is reported in Figure 95. The model in PowerFactory was coded in DSL for convenience.

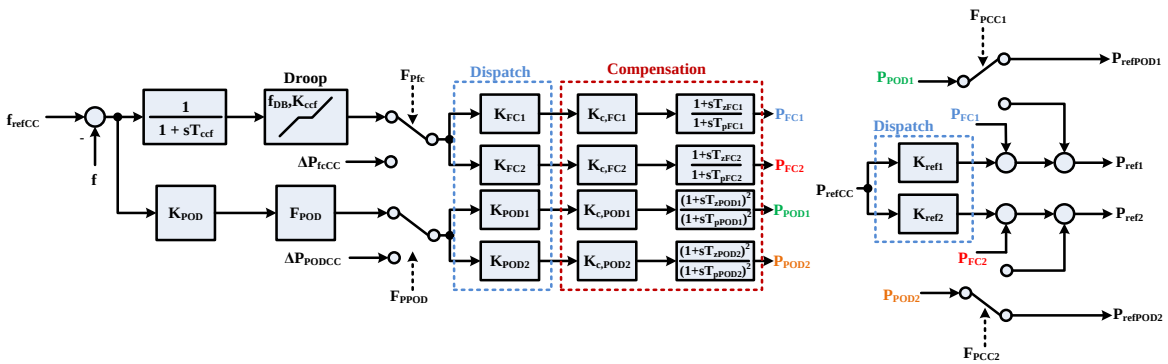

Figure 95 - Cluster controller block diagram – only active power path.

The output signals P_{ref1}, P_{ref2}, $P_{refPOD1}$ and $P_{refPOD2}$ are sent to WPPC 1 and WPPC 2 respectively. Actually, WPPC 2 can only receive the signal P_{ref2}, since it does not feed-forward the POD signal $P_{refPOD2}$. Gains, flags and time constants settings depend on the particular test and whether the output signals are directed to WPPC 1 or WPPC 2. The dispatch is performed with simple gain blocks, but more sensible strategies may be used in real applications, such as for example based on the actual available power of each WPP.

8.3.3 Wind power plant controllers

(a) WPPC 1

The WPPC 1 model was described in Chapter 3 (Figure 14) and is not repeated here. Its implementation is an augmented version of that outlined in the draft IEC standard 61400-27-1 [22] Annex D. The only significant difference with such IEC standard is the possibility to feed-forward the input POD signal, so as to bypass the PI controller and obtain a faster and more robust response. Together with the feed-forward, a freezing algorithm was developed according to Figure 84. It serves to freeze power reference and PI controller output when a POD event is detected.

For convenience, the model has been coded with DSL in PowerFactory. Default parameters for the model are reported in Appendix 6 in Table 37.

(b) WPPC 2

The WPPC 2 model was directly derived from the draft IEC standard 61400-27-1 [22] Annex D and is shown in Figure 96. As can be seen, the main difference from WPPC 1 developed in this study lies in the absence of feed-forward of the POD signal. According to the standard, apart from being provided with frequency and PI controllers, ramp rate limitations are imposed on reference input and reference output and integrator state. The output and integrator state are also limited in modulus between minimum and maximum value. A zero-pole block is placed before the output: by properly setting its parameters (first order Padé approximation), it can be used to emulate the delays related to the plant controller (e.g. output dispatcher function).

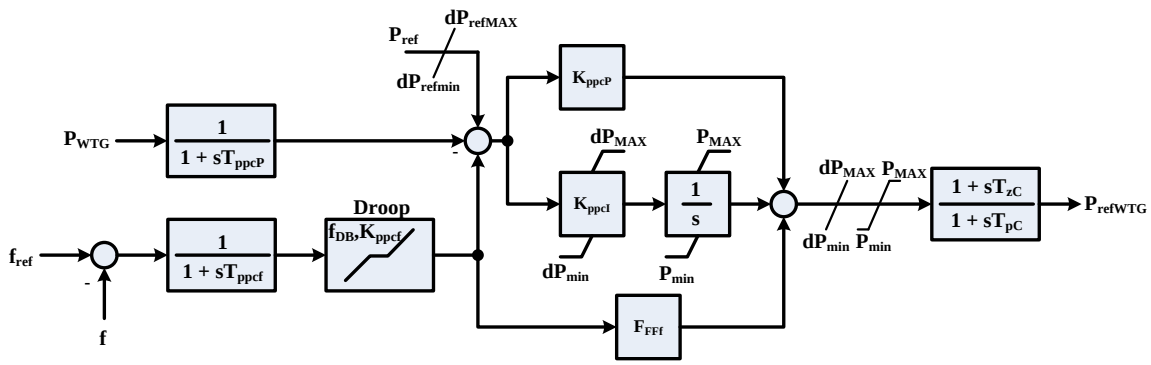

Figure 96 - WPPC 2 active power control block diagram.

The model was coded in DSL with PowerFactory. The parameters for the model and experiments are reported in Appendix 6. It should be mentioned once again that WPPC 2's frequency control functionality is deactivated at the test facility, since the unit does not have to comply with strict connection regulation and has never been used for this kind of tests before.

8.3.4 Wind turbine generators

The WTG models are purely based on the draft IEC standard 61400-27-1 models [22], as follows:

- WTG 1 is modelled by a Type 4A model, owing to the fact that no shaft resonances were noticed during previous measurement campaigns on the grid side active power production, since there is no large rotor inertia in the machine driven by the dynamometer.
- WTG 2 is modelled by a Type 4B kind of model, since this kind of machine usually presents shaft resonances. However, it should be noticed that the available sample rate of the power production – see Section 8.2 – may not allow for clear visualisation of the shaft torsional mode. Furthermore, no measurement with WTG 2 operating alone and able to clearly excite the shaft mode was performed and the dominant dynamics in the available measurements are certainly related to WPPC 2. As a consequence, a Type 4A model may be suitable too for the scope of this study. Type 4B is anyhow chosen to have a more realistic platform for possible future usage of the models.

The block diagrams of the models are not reported here, but the reader can refer to [22] for more details. The models' active power control parameters are reported in Appendix 6. It should be noticed that the main parameters for WTG 1 are very reliable, as they stem from the validation in Section 8.4.2. However, the parameters for WTG 2 are plausible parameters but cannot be considered fully accurate, since the WTG model was not validated in stand-alone. Since the main dynamics that can be observed in the tests conducted in this chapter are certainly related to WPPC 2, small variations in WTG 2's parameters do not affect the test results significantly.

8.3.5 Communication delays

Communication delays are simply modelled as perfect lumped delays, which in the Laplace domain are expressed by $e^{-sT_{di}}$, with T_{di} being the time delay of communication block *i*. The great difference between the communication channels is in the position of the communication channel and in the value of T_{di}, as stated previously and evidenced by Figure 93. In the case of communication between WPPC 1 and WTG 1, the sample rate of both loops is 10 ms, and they are synchronised through SCRAMNet clock within 1 ms. Totally different is the situation for the communication between CC and WPPC 2, which happens asynchronously every 1 s, meaning that the actual delay can fall in the interval 1-2 s.

8.3.6 Implementation

The only blocks actually implemented for conducting the present tests were CC and WPPC 1. A simplified functional sketch of the implementation is shown in Figure 97. The controllers were coded with LabView graphic language operating with continuous time (Laplace domain) blocks.

The main loop and communication loops are running in parallel and communicating between them through shared variables. The Modbus communication loop also performs the necessary discretisation to comply with the input format in WPPC 2 – see Table 34 in Appendix 6. Initialisation and termination loops are executed once at the beginning and end of the test respectively, in order to properly take initial control and most safely hand the control back to the default controllers once the test is finished.

The Modbus communication loop was also used in stand-alone for some of the tests, in order to manually change the power reference of WPPC 2.

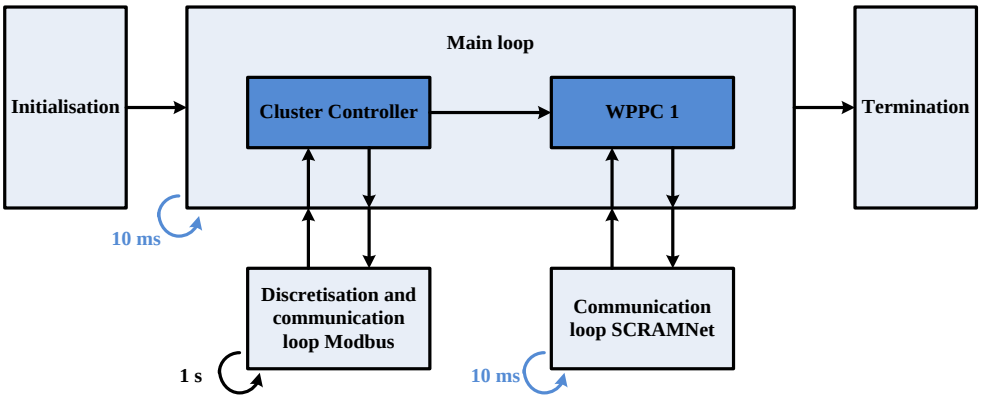

Figure 97 - Functional sketch of implementation on PXI.

8.4 Model validation

In this section, the models described above are validated one by one by comparing simulation results to measurement data obtained at the test facility.

WTG 2 and WPPC 2 are treated as one single black box, since only measurements from WPPC 2 were available. The validation of WTG 2 as a stand-alone block would require access to measurements directly on the WTG. The validation of this control channel is presented in Section 8.4.1, together with the validation of the compensation in the CC.

WTG 1 and WPPC 1 are validated in Section 8.4.2. The WTG model can be validated in stand-alone. WPPC 1 model is also validated for power reference steps, frequency control and POD. The latter can either be input as a dedicated signal or derived from a frequency oscillation, as can be seen in Figure 14.

8.4.1 WTG 2 and Cluster controller

In this section, the models of WTG 2 and WPPC 2 are validated as a single block. The phase compensation functionality of the CC is also verified.

While reading this section, one should bear in mind once again the limitations that were previously mentioned and reported in Table 34 in Appendix 6, i.e.:

- Modbus communication and measurement sample rate equal to 1 s.
- WPPC 2 resolution equal to roughly 4.35% of rated power (i.e. the power reference to WPPC 2 can be given with 100 kW resolution).
- Asynchronous operation of Modbus communication loops on PXI and WPPC 2.

(a) Power reference step

Two power reference steps were tested by sending a command to WPPC 2. The turbine was at that moment producing full power. The exact wind speed was not recorded, but was stably above rated wind, this being true for all tests in this section. The power reference was stepped down to 0.8 pu (≈ 1840 kW) at time t_1 = 8.44 s and then to 0.61 pu (≈ 1400 kW) at time t_2 = 42 s. The results are reported in Figure 98. The resulting parameters of WTG 2, WPPC 2 and communication can be found in Appendix 6 (Table 36, Table 38 and Table 39).

As can be seen, the model response appears satisfyingly accurate as compared to the measurements. The delay, ramp rate limitation and settling time constant are all agreeing very well. In the first step, there exists a larger discrepancy between model and measurement. This is explained by noticing that the solid black plot in Figure 98 is the reference sent to WPPC 2 *in the model*, while *in reality* such signal is quantised with 100 kW steps, which means the real WTG actually receives 1800 kW reference during the first event.

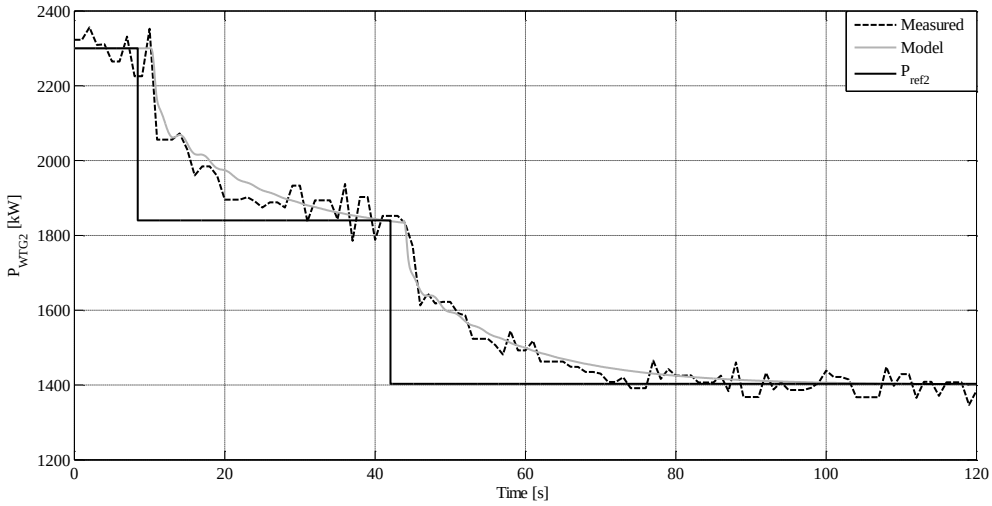

Figure 98 - Validation of reference step for WPPC 2.

The conclusion is that the main dynamics of WPPC 2 (driving WTG 2) are validated and the model can be used for power reference tracking with good confidence that it represents the real implementation. A small simple improvement to the model would be the quantisation of the power reference. However, a new and dedicated commercial version of WPPC 2 would offer a much better resolution. As already mentioned, the machine installed at the test facility does not have to comply with strict requirements and had never been used for this kind of test before. It is also important to stress once again that the communication delay used in the model is subject to a large degree of uncertainty, due to the asynchronous nature of the communication. Such parameter may hence have to be refined when comparing the model to other measurements.

(b) Frequency control event

The second test that was performed at the facility included CC, WPPC 2 and WTG 2. The test consisted in modulating the frequency input of the CC (signal f in Figure 95) according to what illustrated by Figure 145 in Appendix 5. The signal is the recording of a real frequency event in the Western Interconnection in the US. The realistic frequency data are input starting from $t_1 \approx 185$ s and continue for several tens of seconds. At around $t_2 \approx 330$ s the actual frequency event takes place.

The results for this test are reported in Figure 99 and Figure 100. As stated in the assumptions in Section 8.1.3, the WTG needs be curtailed in order to provide power up-regulation. Therefore, the reference power is initially stepped down to 1600 kW. Actually, the frequency variation starts already before the WTG settles to the new reference point. The data stemming from the previously described power reference step validation were used in this test and the CC parameters were set according to Appendix 6 (Table 40), while WPPC 2, WTG 2 and communication parameters were left as tuned in the previous section (Table 36, Table 38 and Table 39).

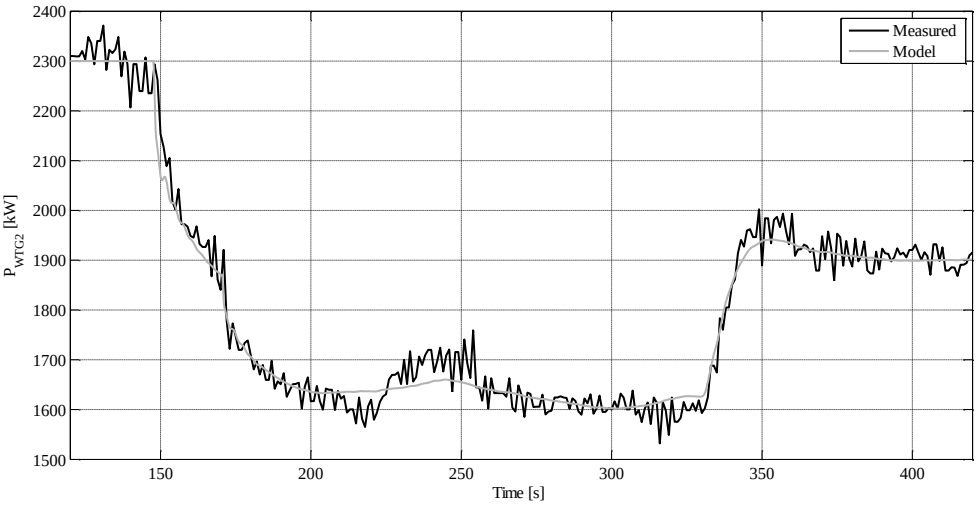

Figure 99 - Validation of frequency control event for WPPC 2 and CC: produced power.

An inspection of the figure reveals a model response that is matching the measurements quite well, also considering the limitations mentioned several times above. Particularly, the power regulation during the frequency event is nicely represented by the model, with correct timing, ramp rate and slight overshoot. Moreover, one should take into account again the non-deterministic nature of the communication delay, which may lead to small differences in the timing of the response.

Small discrepancies are present before t = 250 s and during the overshoot. Once again, they are explained quite easily by bearing in mind that the power reference sent to WPPC 2 is quantised in 100 kW steps. This is more clearly illustrated by Figure 100, where WPPC 2's power reference P_{ref2} is shown for both the model and the real devices.

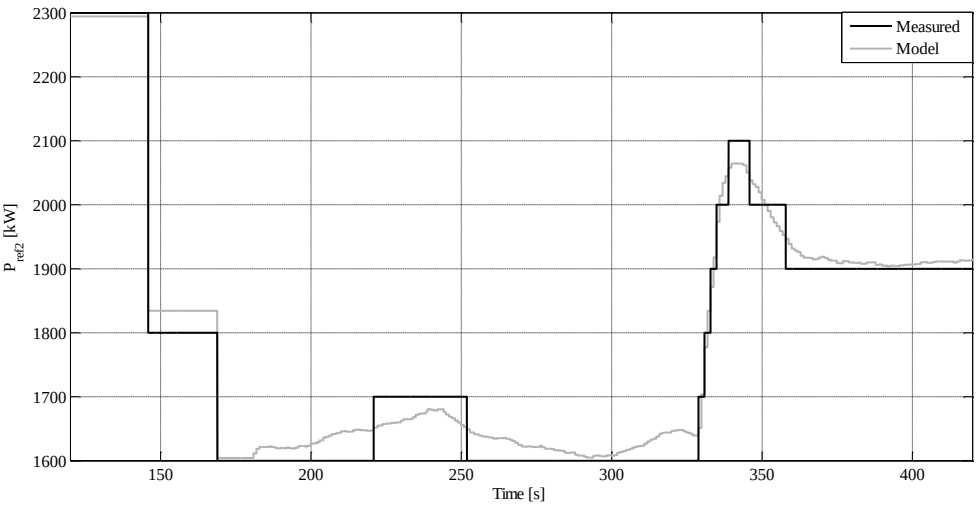

Figure 100 - Validation of frequency control event for WPPC 2 and CC: reference power to WPPC 2.

It is hence concluded that the validation is successful and the models of CC and WPPC 2 can be used quite confidently for studies involving frequency control. Once again, quantisation of the

power reference would improve the response, but real commercial units would anyway offer a much finer resolution.

(c) Power oscillation damping

The last test to validate CC, WPPC 2 and WTG 2 models was the emulation of a POD event. A ±300 kW oscillation with frequency 100 mHz was input to the CC model's signal ΔP_{PODCC}. Such oscillation damps out after several periods, so as to emulate, at its tail, a real electromechanical power oscillation. The initial power reference P_{refCC} is lowered to 1400 kW, to make sure there is sufficient head for superimposing the oscillations. The CC performs a phase and gain shift of the oscillation according to the data summarised in Appendix 6 (Table 40), so as to counteract the effect of WPPC 2's PI controller, measurement and communication delays. It should be noticed that, once again, the PI parameters and communication delays according to Table 38 and Table 39 are not necessarily figures that would be used in a commercial implementation, but are determined by the purpose the specific WTG at the test facility is used for. Moreover, the asynchronous communication imposes an uncertainty of up to 1 second on the communication delay. Hence, only a rough estimation of the needed compensation was done, based on the Bode diagram in Figure 101.

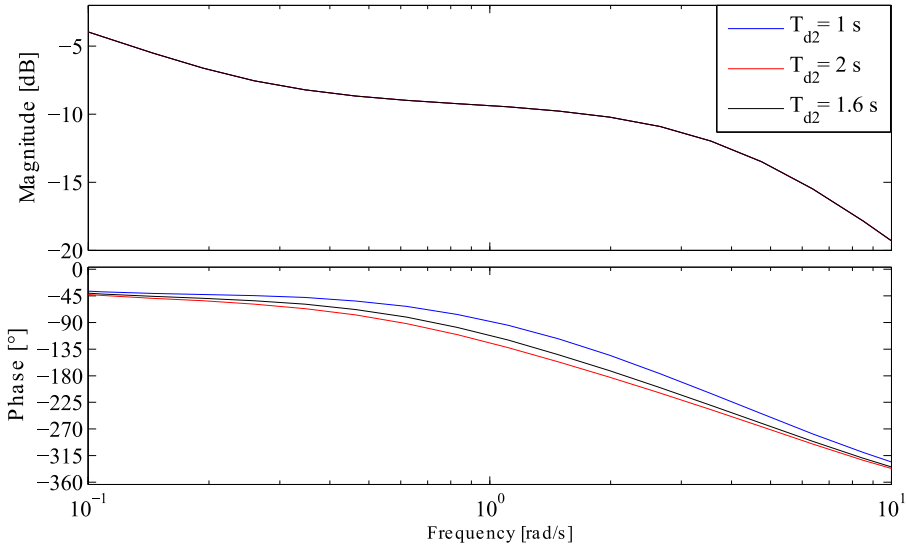

Figure 101 - Bode diagram of G_{WPP2} for estimation of compensation for three values of communication delay.

The diagram reports the transfer function $G_{WPP2} = G_{Td2}G_{CL,WPPC2}$, where G_{Td2} is the communication delay transfer function and $G_{CL,WPPC2}$ is the closed loop of the plant controller transfer function, based on the parameters reported in Table 38 and the scheme in Figure 96 and assuming, due to its fast dynamics compared to the range which is relevant here, WTG 2 to be an ideal plant (unity gain). At the target frequency of 0.1 Hz (0.628 rad/s) the needed gain compensation is roughly 9 dB (2.82 pu) and the phase compensation can vary between 65° and 90° depending on the time delay T_{d2}. The parameters tuned as in Table 40 give a phase compensation of 90° and a gain compensation of 3 pu (i.e. the worst case, T_{d2} = 2 s, with even a slight gain overcompensation)[17]. Due to the uncertainty on the communication delay, this rough estimation of the compensation is considered sufficient here, but definitely leaves room for improvement.

[17] It should be noted that the compensation tuning was done offline based on measurments previously taken, which might not necessarily have had a communication delay T_{d2} = 1.6 s as in the displayed test session.

The results of the test and its comparison with the model are presented in Figure 102. Measured and modelled WTG power are shown. For a better assessment, the actual desired power reference is reported too, as solid black plot.

It can be seen that, despite expectedly chopping the first power swing due to delays and compensation, and also considering all limitations mentioned above, the achieved experimental results are quite closely matching the model's response. The phase shift of the sinusoidal wave is essentially correct, while variations in the magnitude are most likely again due to the presence of coarse quantisation in the measurement. Moreover, the uncertainty in the compensation to apply also affects the results negatively, since the measurement might be gain overcompensated. A comparison between reference and modelled response (solid curves in Figure 102) in fact shows slightly higher gain and phase compensation than needed. The error in gain compensation is expected, while the one in phase compensation stems from having taken a worst case value for T_d, while in the model it is actually T_{d2} = 1.6 s. It seems that the phase compensation in the measurement is correct, perhaps due to additional delays that are not accounted for in the model. However, with the available sample time and resolution such conclusion cannot be certain.

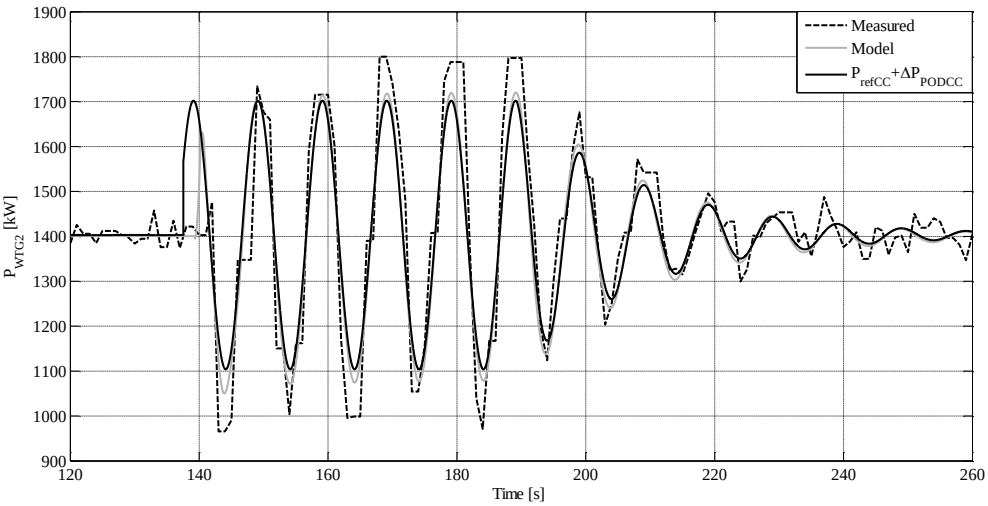

Figure 102 - Validation of 100 mHz POD event for CC and WPPC 2.

From this particular test, besides confirming the conclusions of previous subsection, one can also realise that the requirements put forward in Chapter 7 in terms of determinism and minimisation of communication delays are surely sensitive. With small delays, the uncertainty on the real phase shift is reduced. Hence delays must be minimised. On the other hand, synchronisation of the Modbus communication loops running on PXI and WPPC 2 is desirable, since it dramatically reduces the phase shift uncertainty. Implementation of synchronous communication channels is thus recommended, but was not possible in this case due to the particular test facility setup and no accessibility to WPPC 2. One should also bear in mind that the oscillation frequency considered here is at the very low end of possible POD frequencies. Larger, yet realistic, frequencies would pose even stricter requirements in these terms.

8.4.2 WTG 1 and WPPC 1

Validation of WTG 1 and WPPC 1 is conducted in this section. The actual setup varies with the kind of test to be performed and may involve WTG 1, WPCC 1 and CGI.

(a) Power reference steps

First of all, WTG 1's active power step response is validated in stand-alone, when WTG 1 is operated connected to the grid. A 0.06 pu (165 MW) step is tested and the parameters of WTG 1 model are set as per Table 35 in Appendix 6. The results are plotted in Figure 103. Only the power production deviation from initial value is shown.

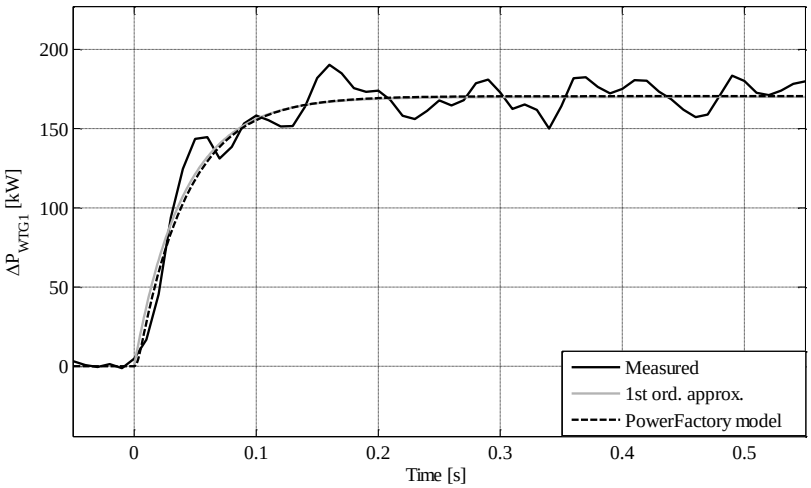

Figure 103 - Validation of power reference step to WTG 1.

It can be noticed that the agreement between the measurement, the model and a first order low-pass approximation with time constant equal to 40 ms is very precise. Only the measurement noise introduces differences between simulated and measured response.

The second test is, once again, a power reference step test. However, this time both WPPC 1 and WTG 1 are online. The WTG is connected to the external grid and its parameters in the model are as determined by the previous validation. Three steps in P_{ref1} are tested, setting the parameters of WPPC 1 as in Table 37 in Appendix 6 both in the model and in the PXI. The results in Figure 104 were achieved.

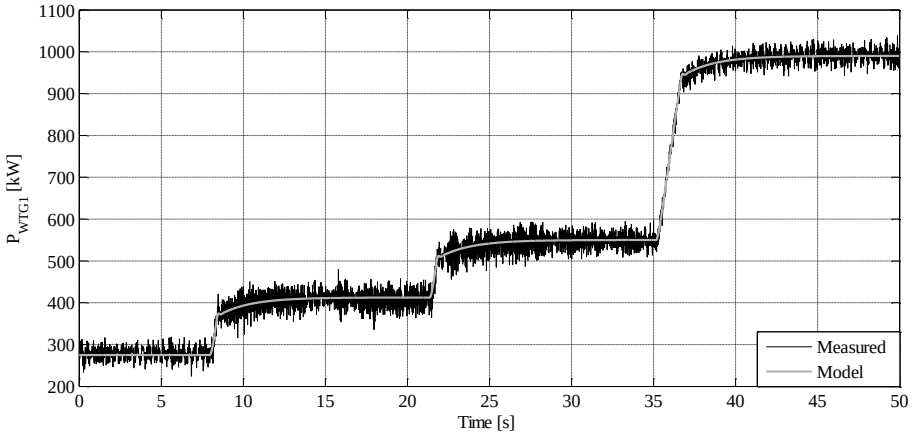

Figure 104 - Validation of power reference step for WPPC 1.

Once again, the agreement between measurement and simulation is very clear. Apart from the measurement noise, the model is a very good representation of the real device.

(b) Frequency control event

The next test is a frequency control event, analogous to that performed in Section 8.4.1(b) with WPPC 2 and WTG 2. In this case, however, the CGI was used to impose a real frequency deviation at the WTG terminals. The frequency was read by WPPC 1 and processed according to the parameters reported in Table 37 in Appendix 6. The results are shown in Figure 105.

Clearly, the model shows a response which is very close to the measurement. Again, some measurement noise is superimposed to the average value, but the latter is following the simulated response essentially exactly. The model can therefore be used with great confidence to represent the system WPPC 1 + WTG 1 for frequency control studies.

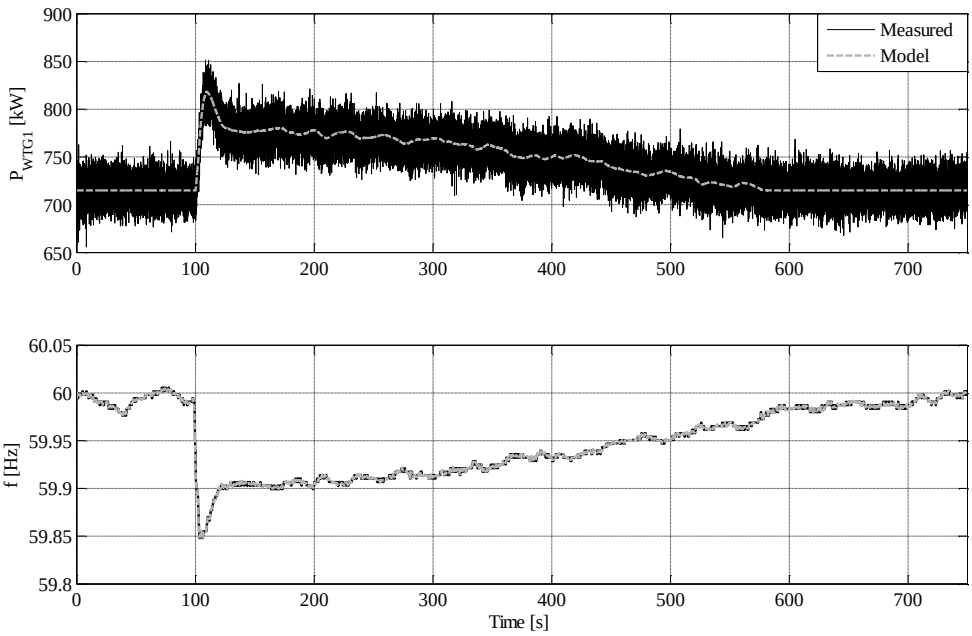

Figure 105 - Validation of frequency control event for WPPC 1.

(c) Power oscillation damping

Power oscillation damping is the last test that was performed to validate the models. A signal $P_{refPOD1}$ with peak to peak magnitude 0.1 pu (275 kW) and frequency 200 mHz was input to WPPC 1 and superimposed to the steady-state power reference, according to the WPCC scheme in Figure 14. After a few cycles, the signal is damped out so as to emulate a real POD event. The modelled and measured responses are shown in Figure 106.

Once again, the model matches the measurement fairly well, apart from the measurement noise. Before the oscillation starts, the reference power in the model is slightly higher than the average power produced in the measurement. This is due to the fact that the freeze algorithm freezes control error and output based on their last value, which might not be exactly equal to the average value, due to imperfect filtering of the power production. However, taking into account this small adjustment, the responses during the oscillation are fairly well aligned with each other.

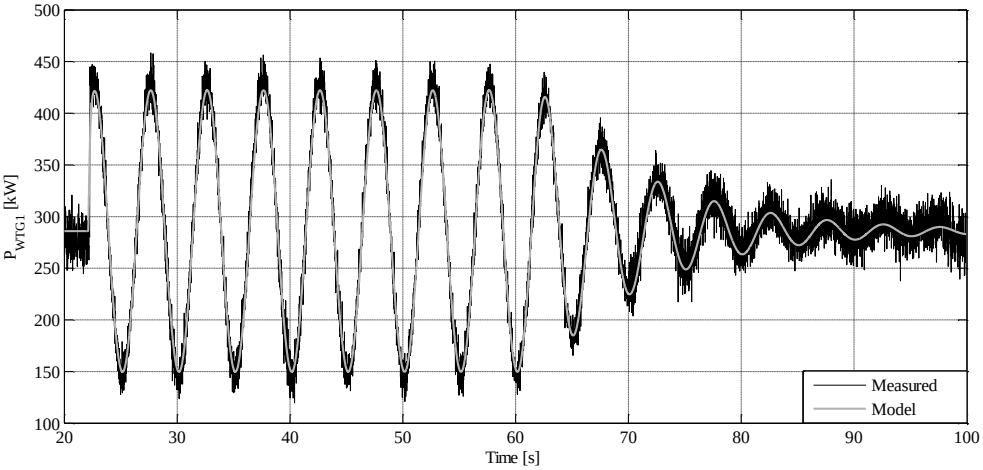

Figure 106 - Validation of 200 mHz POD emulation for WPPC 1.

Two more validations of POD events are shown in Appendix 5, Figure 143 and Figure 144. They are referring to:

- A case where the oscillation frequency is 500 mHz. The time constants of the POD compensation in WPPC 1 have been re-tuned to T_{zPOD} = 0.36 s and T_{pPOD} = 0.281 s and K_{POD} = 0.884 pu, in order to make up for the small communication and WTG 1 control delay. The results are shown in Figure 143.
- A case where the oscillation frequency is again 500 mHz, but the power modulation signal is derived from a frequency oscillation with the same frequency and amplitude ±0.1 Hz (±0.00167 pu) provoked by the CGI and setting the parameters F_{fPOD} = 1, K_{POD} = 60 pu, K_{ppcf} = 0. Also, the initial steady-state power is larger than in previous tests. The results are depicted in Figure 144.

8.4.3 Discussion

The validation of WPPC 1 and WTG 1 is obviously of a much better quality than that obtained with CC, WPCC 2 and WTG 2, especially in the case of POD. This is due to the absence of any big limitation in terms of sample rate, communication delay and resolution. Once again, hence, this demonstrates how advantageous it is to have small and deterministic delays in the control and communication chain, especially for events like POD, and even more considering that POD frequency can reach 2 Hz and only fractions of Hz were tested in this chapter. Even an almost optimal configuration like that used in WTG 1 and WPPC 1 would need compensation for POD events with frequency at the high end of the possible spectrum.

Moreover, it is also proven that feeding the POD forward after the PI controller like in WPPC 1 is very convenient, since no compensation for the PI controller needs be used and only a small correction for the phase shift introduced by communication and WTG 1 controller is necessary. Additionally, avoiding the WPPC closed-loop also eliminates one level of uncertainty in the position of spurious delays in the control chain, since one element is skipped: when a signal needs to be processed by two cascaded control loops, besides the magnitude of the delays, their position in the control chain also has a significant impact on the overall phase shift. Furthermore, if one considers that the values of the PI parameters may vary during the lifetime of the WPP, robustness against these variations is automatically guaranteed by the proposed signal layout. Proper synchronisation of the POD signal with respect to its reference is already challenging at

0.1 Hz, while the high end of the POD frequency spectrum is most likely not achievable in practice with the inherent present limitations at the test facility on WPPC 2 and WTG 2.

It should be emphasised again, however, that the limitations stem from the particular test setup and are not intrinsic in any of the devices used at the facility. Re-arranging and coordinating existing hardware and software in a limited period of time allowed achieving the results presented here, which are affected by the limitations mentioned several times, but the track for future work is clearly drawn observing the limitations emerged.

8.5 Simulation of cluster of WPPs

A couple of simulations exemplifying the clustering of WPPs are illustrated in this section, making use of the models validated in the previous section. Validation of the whole setup with field measurements was not possible before the submission of this report. The value of the simulation results should anyhow be sufficient, since the two control channels are essentially independent, based on the open-loop structure of the CC.

Two examples are shown for illustrative purposes, that is frequency control case and POD case.

8.5.1 Frequency control

A frequency control event analogous to those considered in previous sections has been simulated by using CC, two WPPCs and two aggregated WTGs (WPPs). It is assumed that both WPPs have sufficient power to perform the control actions. All parameters are set according to Appendix 6, with the exception of those reported in Table 41. Quantities are per-unitised, since the results should hold for generic clusters of WPPs. The results in terms of power production from the two WPPs are reported in Figure 107. The frequency signal utilised in the simulation is the same as previously, i.e. that plotted in Figure 145.

Inspecting Figure 107 it can be observed that the system responds as expected. The slightly faster response of WPP 1 is owing to the control parameters. WPP 2's response can be corrected, if necessary, with the dedicated compensation blocks in the CC and/or update of the PI parameters.

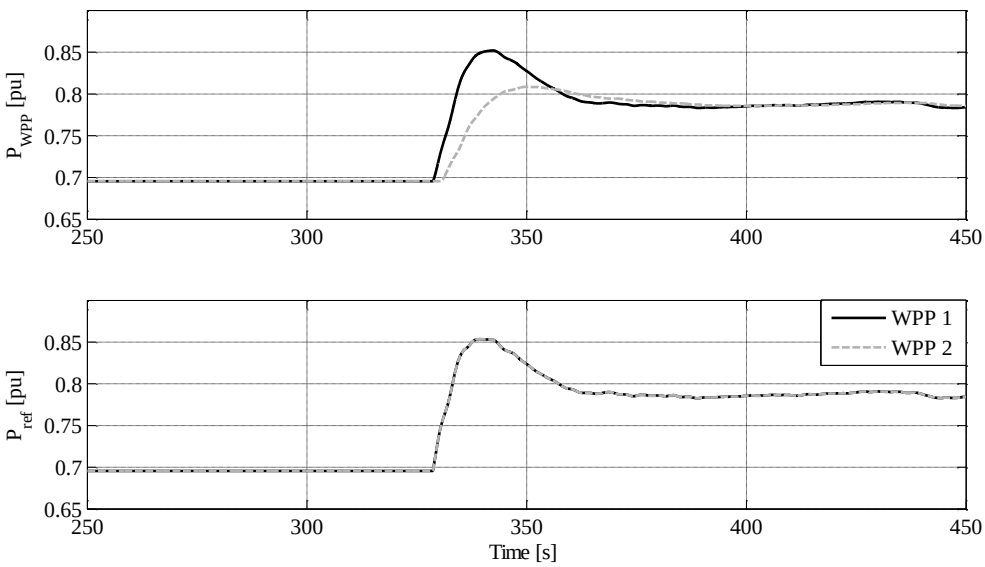

Figure 107 - Response of cluster of WPPs to frequency control event.

8.5.2 Power oscillation damping

A POD event with oscillation frequency 100 mHz was simulated as exemplifying case, using the same setup as in the frequency control case above and default parameters for every model, except for those reported in Table 42. An extract of the results is reported in Figure 108.

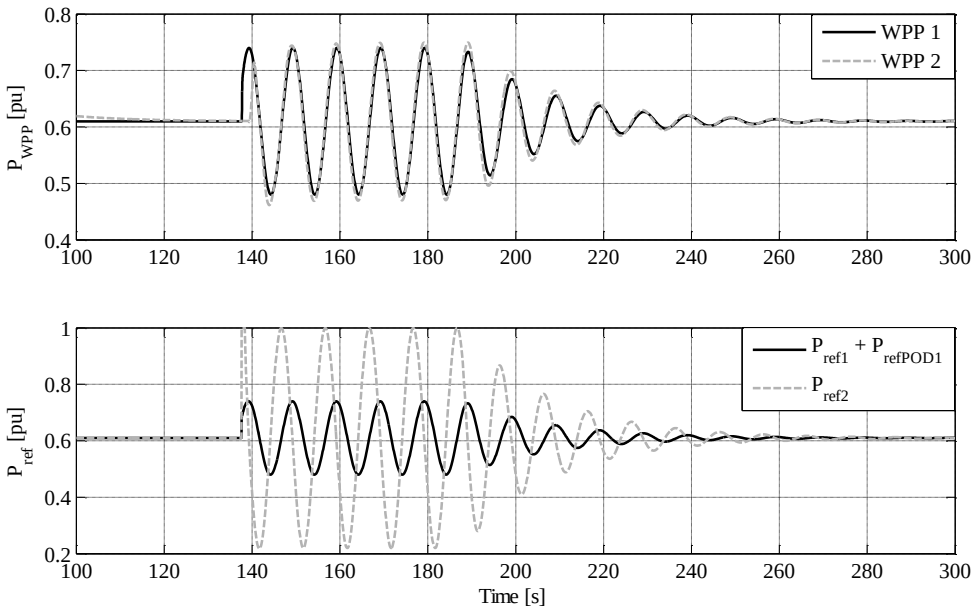

Figure 108 - Response of cluster of WPPs to POD event.

The results, once again, confirm the expectations. The desired coordinated response is achieved. WPP 2 is slightly over-compensated. Indeed, it can be observed in the bottom plot that the needed compensation is significant. The improvements suggested along the chapter and summarised in the next section would help reduce the needed compensation and make it more deterministic, so as to more easily obtain the desired aggregated response. The first step in future work, however, will be to validate even these simulations with field experiments.

8.6 Summary and recommendation

The clustering of WPPs with very different characteristics has been the subject of this chapter. Coordinated active power control and system services related to it (frequency control and POD) have been considered by developing a CC, which dispatches power orders to two WPPCs and related WTGs.

Dynamic models were implemented in PowerFactory and validated with field measurements obtained during tests performed at NREL. Considering the limitations imposed by the current test setup, the validation yielded good results and the available models can be used with confidence for system studies. However, based on the limitations, recommendations for future improvements are proposed:

- Updating WTG 2 and its plant controller WPPC 2 would allow for a more realistic comparison with the user-built WPPC 1. It should be borne in mind that WTG 2 and WPPC 2 were never used for this kind of studies before and they do not need to comply with strict grid codes at the test facility. Thus, their performance is by choice far from

commercial installations and an update of their functionality would provide new possibilities. Possible items for future updates may be:
    - Reduction of sample rate in the communication to WPPC 2.
    - Increase the resolution of the communication to WPPC 2.
    - Implement synchronous communication between all devices.
- In general, the recommendations put forward in Chapter 7 in terms of control and communication delays for implementation of POD have been confirmed – see Section 7.3.4.

The chapter concluded with the simulation of an actual emulated cluster of WPPs, employing the validated models and proving the cluster control concept for active power control and related services. The fact that very different WPPCs can in principle be accommodated in the same cluster is a quite valuable conclusion from this study. As future work in the field one could mention:

- Experiments and measurements should be performed with the clustered configuration simulated in Section 8.5. Such tests were planned but could not be included in this report.
- Other layouts and features could be tested, such as for example a closed-loop CC or different dispatch functions making use of information related to available power at the different WPPs.
- Reactive power control and related services have not been considered in this chapter, though they may be extremely interesting too when dealing with clusters of WPPs, due to their potentially faster dynamics and coordination with other compensation devices. Further work can hence be proposed in this regard. However, if the analysis is to be supported by measurements at the same facility, the limitations mentioned above should definitely be overcome first, due to the higher dynamic requirements of reactive power control.

As a general result, finally, the experimental experience gained in this chapter allowed to build confidence on some of the models that were used throughout this study.

Chapter 9 Conclusion and outlook

This final chapter summarises the findings of the Ph.D. study. For each topic, the main conclusions are listed and directions for future work in the field are suggested. The findings are divided by chapter.

9.1 Summary

9.1.1 Chapter 3

Modelling requirements were discussed for the variegated set of calculations and simulations that were performed in the investigations. A categorisation of modelling requirements based on the study cases was proposed and it was concluded that the simulation models described in Chapter 3 were appropriate for all of them.

Some doubts may be related to the utilisation of default built-in dynamic models of VSCs for events that abruptly affect DC bus dynamics in most modern VSC-HVDC converters (MMCs). Simulation of an average MMC model demonstrated that, for the purpose of this study, for MMCs with large number of cells and for symmetrical disturbances, the built-in models representation should be sufficiently accurate.

9.1.2 Chapter 4

In Chapter 4 the control of the offshore AC network lying behind the offshore HVDC converter was discussed. Two state-of-art control strategies for the offshore HVDC converter were compared, the former (Option 1) making use of standard vector control with inner current loop and outer voltage loop and the latter being a direct voltage control (Option 2). Their performance was assessed in different operational scenarios, drawing the following conclusions:

- Control at no-load results more challenging with Option 1, especially current control when HVDC converter delays are not negligible. Recommendations for improved design were put forward.
- When connected to a WPP, Option 2 showed slightly less sensitiveness to control gains. This could be judged in different ways. On one hand, independence on control gains may make design of single components more straightforward. On the other hand, less room for correction of performance is left to the HVDC converter.

- When operating with multiple HVDC converters, it was expectedly clear that sharing the master role enhances the resiliency against several contingencies. Moreover, Option 1 with active and reactive power droops performed better than Option 2 in the base study case. However, Option 2 appeared slightly more robust against variations of the operational scenario.

9.1.3 Chapter 5

Onshore AC voltage control from VSC-HVDC was looked at from two perspectives. For the analysis, in both of them a steady-state representation of the VSC-HVDC converter was utilised, while simulations including dynamic models were used to corroborate the theory.

(a) Continuous AC voltage control

Static characteristics of the main limitations of a VSC-HVDC converter were drawn in the Q-V_{AC} plane, namely current limitation, DC voltage limitation and others from literature. Lines corresponding to converter AC voltage droop control were plotted too. Such plots were overlapped with an equivalent grid's constraints in the same plane, observing the interaction between converter and grid. The main conclusions were:

- Drops in DC voltage heavily affect the reactive power production capability. This has implications, besides for AC voltage control, for example for the study in Chapter 6 – see Section 9.1.4(a).
- AC voltage droop control is vital for connection to weak networks, to avoid instabilities. Provision of droop control, however, comes at the expense of large reactive power excursions.
- Weak networks' characteristics may be non-linear in the Q-V_{AC} plane. This means that the contribution of an AC voltage droop controlled VSC-HVDC station to continuous voltage control and available SCP is dependent on the operating point, predominantly on the active power production/absorption.

(b) Long-term voltage stability

The effect of VSC-HVDC converters on the long-term voltage stability profile of heavily stressed power systems was investigated, paying particular attention to the converter behaviour during current limitation. The main findings were the following:

- VSC-HVDC converters in current-limited mode are intrinsically voltage unstable and may therefore negatively affect voltage stability if their share and position in the power system are critical.
- It is possible, by proper control of the current angle during limitation, to maximise the voltage stability margin. The exact strategy to perform such control cannot but rely on the knowledge of the rest of the network, which may not be readily available. Intuitively, however, reactive power should be prioritised. On the other hand, purely injecting reactive power may not be a realistic solution in terms of converter voltage level.
- Dynamic simulations showed that limiting the current vector magnitude without changing its angle (or prioritising reactive power) is superior to prioritising active power. This has practical implications for the control of a VSC-HVDC station connecting a WPP. Though prioritisation of active power may seem the most intuitive solution from the WPP operator's standpoint, vector limitation or priority on reactive power is the most optimal solution for both TSO and WPP operator.

9.1.4 Chapter 6

Power balance control in AC-DC networks was focussed on, in particular looking at the contribution WPPs can provide to it. Naturally, frequency control is the means to reach power balance control in AC grids, while DC voltage control is the equivalent means in DC networks.

(a) Frequency control

The simplest possible configuration was considered, i.e. a point-to-point VSC-HVDC connection of a WPP. Both PFC and IR were included in the scope. The following results were achieved:

- Two solutions for frequency control provision with and without long-distance communication were developed and compared, concluding that:
    - Frequency control dynamics are usually so slow that communication speed requirements are very much relaxed and both schemes perform satisfyingly. As a consequence, the price paid by added control complexity may outweigh the advantage of reduced communication.
    - Utilisation of communication-less schemes brings about a sub-optimal DC voltage level, and thus (i) additional losses and (ii) reduced converter reactive power capability during events that may actually require voltage support besides frequency control – see Section 9.1.3(a).
    - The communication-less approach, thanks to the inherent behaviour of the onshore HVDC station, is more suitable for applications where inertia and ROCOF are the crucial figures in frequency control.
- As a consequence of the above, the scheme making use of communication seems the best solution for a point-to-point connection. The evaluation may change when the system is connected to an AC grid with poor inertia and critically high values of ROCOF.
- Other factors such as active power ramp-rate limiters in WPPs are limiting the available performance where the required power gradient is higher, such as during IR. In systems with low inertia, along with applying the communication-less scheme, it is recommended to relax such ramp-rate limits as much as needed.

(b) DC voltage control

DC voltage control in a simple three-terminal DC grid was analysed by time domain dynamic simulations. Particularly, the performance of WPPs for such service was observed, leading to the main findings below:

- Due to much faster dynamics compared to frequency control, the WPP performance is poor and having a solid estimate of control/communication delays is crucial to understanding the extent to which WPPs can contribute to DC voltage control.
- During the first instants of a DC voltage disturbance, other (onshore) converters connected to the DC network besides the WPP are called to compensate for power unbalances. As such:
    - Heavily wind-penetrated systems may encounter difficulties in providing robust DC voltage control during abrupt disturbances.
    - Tuning of control parameters on onshore converters must take into account what the added initial DC voltage control burden means for the AC system they connect to.

9.1.5 Chapter 7

POD was successfully implemented on a VSC-HVDC connected WPP based on a state-of-art POD control scheme and providing the WPPC model with dedicated POD signal. The controller was tested successfully on a simple test network and on a larger power system model. In terms of real-life implementation of the service, the following conclusions were reached:

- Besides those that are usually treated in the literature, other aspects that are crucial to design and effectiveness of POD on a generic static power source are the following:
    - Direct influence of active and reactive power modulation from the VSC-HVDC station on the nearby SGs' terminal voltage and electrical power.
    - Voltage regulation capability of the AC network, despite being often disregarded in the literature. Fast, high-gain, voltage regulation, especially in the vicinity of the PCC, may heavily affect the POD control parameter tuning, especially when it is done by modulating reactive power.
    - Direct influence of the control output on the control input. Possible high-frequency instabilities can take place based on the immediate effect the control output (active or reactive power) has on the control input. To mitigate the risk of instabilities, requirements have been proposed.
- Practical guidelines for initial parameter tuning were defined, which rely on basic physical phenomena rather than a more complex mathematical analysis of the system. Parameters can then be refined around such values.
- Commercial WPP limitations are often neglected in the literature and were more closely looked at here concluding that:
    - Control and communication delays must be minimised and made deterministic to the extent possible, so that their value is small and precisely known.
    - Early dialogue must be instituted between developers, TSOs and OEMs to ensure target POD frequencies and WTG mechanical resonances do not overlap. If they do, solutions have been qualitatively proposed.
    - WTG rotor speed stability should not represent a problem in case POD is implemented by over-production of the WPP above available power for a short period.
    - Ramp-rate limitations may have to be relaxed or by-passed with respect to state-of-art figures, depending on the design requirements for POD.

9.1.6 Chapter 8

The proof of concept for clustering of WPPs was performed in Chapter 8, focussing on active power control, frequency control and POD. It was shown that potentially even WPPs with significantly different characteristics can be accommodated and co-ordinately controlled in clusters of WPPs.

Furthermore, experimental verification of the models utilised throughout the report was performed, building confidence on most of the results presented throughout the report.

Moreover, the experiments helped highlight that the recommendations proposed in Chapter 7 in terms of control and communication delays for implementation of POD are perfectly sound and should be followed in real implementations.

9.2 Future work

9.2.1 Chapter 4

The room for future work in Chapter 4 is certainly vast. Some main points to be looked at could be the following:

- Realise the suggested improvements for control Option 1 and verify their soundness.
- Assess the benefits and drawbacks of employing a more distributed control, i.e. upgrading the control of the WTG converters to automatically participate in the control of the network.
- Analyse the possible behaviour of HVDC converters during short circuits. This is of crucial importance for several design stages and very few sources are available in the literature on the topic.
- Inclusion of Type 3 WTGs along with Type 4, so as to assess potential differences in the performance, especially during faults.

9.2.2 Chapter 5

More work could be done with regard to the influence of VSC-HVDC and WPPs on the long-term voltage stability of power systems. It would be interesting to understand how the ratings of the converter station affect the available performance in terms of power that could be delivered by the station *and* to the load. For now, apparent and active power ratings of the converter are supposed to be equal to one another.

Also, a better characterisation of the influence the findings of this study have on the control of what lies behind the VSC-HVDC station (WPP, DC grid, interconnector) is desired.

Finally, demonstration of the findings on a large power system would enhance the confidence that the simple theoretical derivations performed here can be extrapolated to more realistic power systems.

9.2.3 Chapter 6

In terms of generic power balance control, future work may regard the coordination of power balance control between multiple AC and DC networks. Equations to easily derive the grids' steady-state frequency and DC voltages are still missing and would be useful to understand the AC/DC system interaction and derive requirements in terms of e.g. droop control gains and reserves for the various power system components.

As for the implementation of power balance control on WPPs, a more realistic representation of WPPs with real sampled controllers and including further details would increase the level of confidence in the results as well as help to point out further relevant limitations. If some limitations had to be relaxed, an estimation of the cost of doing so would have to be estimated.

9.2.4 Chapter 7

The work on POD may also gain value by an even more faithful representation of WPPs and VSC-HVDC controllers. Furthermore, the practical guidelines presented in this work may possibly be refined and supported by deeper mathematical insight. Also in the case of POD, much

work should be done to quantify the costs of a real implementation based on the qualitative requirements derived in this study and compare such cost with the alternatives'.

Looking further ahead, the provision of POD to AC grids through multiterminal DC networks is also an interesting subject for possible future research.

9.2.5 Chapter 8

Several points were left out of scope in Chapter 8. Clustering of WPPs is a wide subject and only a first proof of concept was performed. In particular, the next items may be addressed:

- Experimental validation of the clustering of WPPs providing frequency control and POD. This was planned but could not be included in this report.
- Extension of the studies to other control layouts: for example single master controller with no WPPCs, closed-loop CC with WPPCs, etc…
- Extension to reactive power control and related services, also including supplementary compensation equipment.

Bibliography

[1] Cigré WG B4.52, “HVDC Grid Feasibility Study,” Cigré, Paris, 2013.

[2] J. De Decker and P. Kreutzkamp et al., “Offshore Electricity Grid Infrastructure in Europe,” OffshoreGrid, Brussels, 2011.

[3] European Union, “The 2020 climate and energy package,” 2014. [Online]. Available: http://ec.europa.eu/clima/policies/package/index_en.htm. [Accessed 23 October 2014].

[4] North Seas Countries Offshore Grid Initiative - WG1, “Initial Findings - Final Report,” NSCOGI, 2012.

[5] ENTSO-E, “10-Year Network Development Plan,” European Network of Transmission System Operators for Electricity, Brussels, 2014.

[6] L. Zeni, T. Haileselassie, G. Stamatiou, A. G. Eriksen, J. Holbøll, O. Carlsson, K. Uhlen, P. Sørensen and N. A. Cutululis, “DC grids for integration of large scale wind power,” in *EWEA Offshore*, Amsterdam, 2011.

[7] J. Glasdam, L. Zeni, M. Gryning, J. Hjerrild, L. Kocewiak, B. Hesselbæk, K. Andersen, T. Sørensen, M. Blanke, P. E. Sørensen, C. L. Bak and P. C. Kjær, “HVDC Connected Offshore Wind Power Plants: Review and Outlook of Current Research,” in *12th Wind Integration Workshop*, London, 2013.

[8] N. A. Cutululis, L. Zeni, W. Z. El-Khatib, J. Holbøll, P. Sørensen, G. Stamatiou, O. Carlson, V. C. Tai, K. Uhlen, J. Kiviluoma and T. Lund, “Challenges Towards the Deployment of Offshore Grids: the OffshoreDC Project,” in *13th Wind Integration Workshop*, Berlin, 2014.

[9] United Nations, “Kyoto protocol to the United Nations framework convention on climate change,” 1998. [Online]. Available: http://unfccc.int/resource/docs/convkp/kpeng.pdf. [Accessed 23 October 2014].

[10] T. J. Price, “James Blyth - Britain's first modern wind power pioneer,” *Wind Engineering*, vol. 29, no. 3, pp. 191-200, 2005.

[11] Global Wind Energy Council, »Global Wind Statistics 2012,« GWEC, Brussels, 2012.

[12] European Wind Energy Association, “The European offshore wind industry - key trends and statistics 2014,” EWEA, Brussles, 2015.

[13] "4C Offshore Website," 4C Offshore Ltd, [Online]. Available: www.4coffshore.com. [Accessed 24 October 2014].

[14] "LORC Website," LORC, [Online]. Available: www.lorc.dk. [Accessed 24 October 2014].

[15] R. Sharma, "Electrical Structure of Future Off-shore Wind Power Plant with a High Voltage Direct Current Power Transmission," Technical University of Denmark, Lyngby, 2011.

[16] S. Lauria, M. Schembari and F. Palone, "EHV AV interconnection for a GW-size offshore winf-farm cluster: Preliminary sizing," in *IEEE International Energy Conference (ENERGYCON)*, Dubrovnik, 2014.

[17] W. Fischer, R. Braun and I. Erlich, "Low Frequency High Voltage Offshore Grid for Transmission of Renewable Power," in *IEEE PES Innovative Smart Grid Technologies Europe*, Berlin, 2012.

[18] R. Blasco-Gimenez, S. Añó-Villalba, J. Rodríguez-D'Derlée, F. Morant and S. Bernal-Perez, "Distributed Voltage and Frequency Control of Offshore Wind Farms Connected with a Diode-Based HVdc Link," *IEEE Transactions on Power Electronics*, vol. 25, no. 12, pp. 3095-4005, 2010.

[19] T. K. Vrana, "System Design and Balancing Control of the North Sea Super Grid," Norwegian University of Science and Technology, Trondheim, 2013.

[20] Cigré B4-55, "HVDC Connection of Offshore Wind Power Plants," Cigré, Paris, May 2015.

[21] V. Akhmatov, Induction generators for wind power, Brentwood: Multi-Science, 2005.

[22] IEC Standard 61400-27-1, *Electrical simulation models - wind turbines (FINAL DRAFT)*, IEC, 31 October 2014.

[23] A. Yazdani and R. Iravani, Voltage-Sourced Converters in Power Systems: Modeling, Control and Applications, John Wiley & Sons, 2010.

[24] R. Teodorescu, M. Liserre and P. Rodriguez, Grid Converters for Photovoltaic and Wind Power Systems, 1st ed., Chichester: Wiley & Sons, 2011.

[25] O. Gomis-Bellmunt, A. Junyent-Ferré, A. Sumper and J. Bergas-Jané, "Control of a Wind Farm Based on Synchronous Generators With a Central HVDC-VSC Converter," *IEEE Transactions on Power Systems*, vol. 26, no. 3, pp. 1632-1640, 2011.

[26] D. Jovcic and N. Strachan, "Offshore wind farm with centralised power conversion and DC interconnection," *IET Generation, Transmission and Distribution*, vol. 3, no. 6, pp. 586-595, 2009.

[27] L. Trilla, O. Gomis-Bellmunt, A. Junyent-Ferre and A. Sudria-Andreu, "Analysis of total power extracted with common converter wind farm topology," in *19th International*

Conference on Electrical Machines (ICEM), 2010.

[28] M. de Prada Gil, O. Gomis-Bellmunt, A. Sumper and J. Bergas-Jané, "Analysis of a multi turbine offshore wind farm connected to a single large power converter operated with variable frequency," *Energy*, vol. 36, no. 5, pp. 3273-3281, 2011.

[29] T. Ackermann, Wind Power in Power Systems, Wiley, 2012.

[30] EirGrid, "EirGrid Grid Code - Version 4.0," EirGrid, 2011.

[31] Energinet.dk, "Technical regulation 3.2.5 for wind power plants with a power output greater than 11 kW," Energinet.dk, Fredericia, 2010.

[32] National Grid Electricity Transmission, "The Grid Code - Issue 5, Revision 7," NGET, Great Britain, 2014.

[33] G. C. Tarnowski, "Coordinated Frequency Control of Wind Turbines in Power Systems with High Wind Power Penetration," Technical University of Denmark, Lyngby, PhD thesis, 2011.

[34] O. Goksu, R. Teodorescu, C. L. Bak, F. Iov and P. C. Kjær, "Instability of Wind Turbine Converters During Current Injection to Low Voltage Grid Faults and PLL Frequency Based Stability Solution," *IEEE Transactions on Power Systems*, vol. 29, no. 4, pp. 1683-1691, 2014.

[35] M. Altin, "Dynamic Frequency Response of Wind Power Plants," Aalborg University, Aalborg, PhD thesis, 2012.

[36] I. Margaris, S. Papathanassiou, N. Hatziargyriou, A. Hansen and P. Sørensen, "Frequency Control in Autonomous Power Systems with High Wind Power Penetration," *IEEE Transactions on Sustainable Energy*, vol. 3, no. 2, pp. 189-199, 2012.

[37] G. Giebel, T. Gocmen Bozkurt, P. Sørensen, M. Mirzaei, N. K. Poulsen, M. R. Skjelmose and J. R. Kristoffersen, "Estimation and Experimental Validation of the Available Power of a Downregulated Offshore Wind Power Plant," in *13th Wind Integration Workshop*, Berlin, 2014.

[38] Y. Pipelzadeh, B. Chaudhuri and T. C. Green, "Inertial Response from Remote Offshore Wind Farms Connected Through VSC-HVDC Links: A Communication-Less Scheme," in *IEEE PES General Meeting*, 2012.

[39] T. M. Haileselassie and K. Uhlen, "Primary Frequency Control of Remote Grids Connected by Multi-terminal HVDC," in *IEEE PES General Meeting*, 2010.

[40] Y. Phulpin, "Communication-Free Inertia and Frequency Control for Wind Generators Connected by an HVDC-Link," *IEEE Transactions on Power Systems*, vol. 27, no. 2, pp. 1136-1137, 2012.

[41] B. Silva, C. Moreira, L. Seca, Y. Phulpin and J. Pecas Lopes, "Provision of Inertial and Primary Frequency Control Services Using Offshore Multiterminal HVDC Networks," *IEEE Transactions on Sustainable Energy,* vol. 3, no. 4, pp. 800-808, 2012.

[42] ENTSO-E, "Network Code for Requirements for Grid Connection Applicable to all Generators," ENTSO-E, Brussels, 2013.

[43] ENTSO-E, "Draft Network Code on High Voltage Direct Current Connections and DC-connected Power Park Modules," ENTSO-E, Brussels, 2014.

[44] A. Adamczyk, "Damping of Low Frequency Power System Oscillations with Wind Power Plants," Aalborg University, Aalborg, PhD thesis, 2012.

[45] A. Adamczyk, R. Teodorescu and P. Rodriguez, "Control of Full-Scale Converter Based Wind Power Plants for Damping of Lower Frequency System Oscillations," in *IEEE PowerTech,* Trondheim, 2011.

[46] A. Adamczyk, R. Teodorescu, F. Iov and P. Kjær, "Evaluation of Residue Based Power Oscillation Damping Control of Inter-Area Oscillations for Static Power Sources," in *IEEE PES General Meeting,* San Diego, 2012.

[47] T. Knuppel, "Impact of Wind Power Plants with Full Converter Wind Turbines on Power System Small-Signal Stability," Technical University of Denmark, Lyngby, PhD thesis, 2012.

[48] T. Knuppel, J. N. Nielsen, K. H. Jensen, A. Dixon and J. Østergaard, "Power oscillation damping capabilities of wind power plant with full converter wind turbines considering its distributed and modular characteristics," *IET Renewable Power Generation,* vol. 7, no. 5, pp. 431-442, 2012.

[49] T. Knuppel, J. Nielsen, K. Jensen, A. Dixon and J. Østergaard, "Small-signal stability of wind power system with full-load converter interfaced wind turbines," *IET Renewable Power Generation,* vol. 6, no. 2, pp. 79-91, 2011.

[50] T. Knuppel, J. N. Nielsen, K. H. Jensen, A. Dixon and J. Østergaard, "Power Oscillation Damping Controller for Wind Power Plant Utilizing Wind Turbine Inertia as Energy Storage," in *IEEE PES General Meeting,* 2011.

[51] G. Tsourakis, B. M. Nomikos and C. D. Vournas, "Contribution of Doubly Fed Wind Generators to Oscillation Damping," *IEEE Transactions on Energy Conversion,* vol. 24, no. 3, pp. 783-791, 2009.

[52] J. L. Domínguez-García, F. D. Bianchi and O. Gomis-Bellmunt, "Analysis of the damping contribution of power system stabilizers driving wind power plants," *Wind Energy,* vol. 17, no. 2, pp. 267-278, 2012.

[53] J. L. Domínguez-García, C. E. Ugalde-Loo, F. Bianchi and O. Gomis-Bellmunt, "Input-output signal selection for damping of power system oscillations using wind power plants,"

Electric Power & Energy systems, vol. 58, pp. 75-84, 2014.

[54] K. Elkington, “The Dynamic Impact of Large Wind Farms on Power System Stability,” KTH, Stockholm, PhD thesis, 2012.

[55] M. Ndreko, A. A. van der Meer, B. G. Rawn, M. Gibescu and M. A. van der Meijden, “Damping Power System Oscillations by VSC-Based HVDC Networks: A North Sea Grid Case Study,” in *12th Wind Integration Workshop,* London, 2013.

[56] Y. Pipelzadeh, B. Chaudhuri and T. C. Green, “Wide-area Power Oscillation Damping Control through HVDC: A Case Study on Australian Equivalent System,” in *IEEE PES General Meeting,* 2010.

[57] L. Harnefors, N. Johansson, L. Zhang and B. Berggren, “Interarea Oscillation Damping Using Active-Power Modulation of Multiterminal HVDC Transmissions,” *IEEE Transactions on Power Systems,* vol. 29, no. 5, pp. 2529-2538, 2014.

[58] M. Bongiorno, “Use of Power Electronic Converters for Power Systems Stability Improvements,” Chalmers University of Technology, Gothenburg, 2010.

[59] T. K. Vrana, Y. Yang, D. Jovic, S. Dennetière, J. Jardini og H. Saad, »The Cigre B4 DC Grid Test System,« *Electra 270,* pp. 10-19, October 2013.

[60] J. Beerten and R. Belmans, “Analysis of Power Sharing and Voltage Deviations in Droop-Controlled DC Grids,” *IEEE Transactions on Power Systems,* vol. 28, no. 4, pp. 4588-4597, 2013.

[61] B. Berggren and others, “Method and control device for controlling power flow within a DC power transmission network”. Switzerland Patent WO2012/000549A1, 5 January 2012.

[62] E. Prieto-Araujo, F. D. Bianchi, A. Junyent-Ferré and O. Gomis-Bellmunt, “Methodology for Droop Control Dynamic Analysis of Multiterminal VSC-HVDC Grids for Offshore Wind Farms,” *IEEE Transactions on Power Delivery,* vol. 26, no. 4, pp. 2476-2485, 2011.

[63] J. Liang, T. Jing, O. Gomis-Bellmunt, J. Ekanayake and N. Jenkins, “Operation and Control of Multiterminal HVDC Transmission for Offshore Wind Farms,” *IEEE Transactions on Power Delivery,* vol. 26, no. 4, pp. 2596-2604, 2011.

[64] G. O. Kalcon, G. P. Adam, O. Anaya-Lara, S. Lo and K. Uhlen, “Small-Signal Stability Analysis of Multi-Terminal VSC-Based DC Transmission Systems,” *IEEE Transactions on Power Systems,* vol. 27, no. 4, pp. 1818-1830, 2012.

[65] T. M. Haileselassie, “Contro, Dynamics and Operation of Multi-terminal VSC-HVDC Transmission Systems,” NTNU, Trondheim, PhD thesis, 2012.

[66] N. Ahmed, A. Haider, L. Angquist and H.-P. Nee, “M2C-based MTDC System for Handling of Power Fluctuations from Offshore Wind Farms,” in *IET Conference on*

Renewable Power Generation, 2011.

[67] ABB, "Gotland HVDC Light," [Online]. Available: http://new.abb.com/systems/hvdc/references/gotland-hvdc-light. [Accessed 19 November 2014].

[68] ABB, "HVDC Light - It's time to connect," ABB AB Grid Systems - HVDC, Ludvika, 2013.

[69] A. Lesnicar and R. Marquardt, "An Innovative Modular Multilevel Converter Topology Suitable for a Wide Power Range," in *IEEE PowerTech Conference*, Bologna, 2003.

[70] B. Jacobson, P. Karlsson, G. Asplund, L. Harnefors and T. Jonsson, "VSC-HVDC Transmission with Cascaded Two-Level Converters," in *Cigré Session*, Paris, 2010.

[71] A. Cross, D. Trainer and R. Crookes, "Chain-Link based HVDC Voltage Source Converter Using Current Injection," in *9th IET International Conference on AC and DC Power Transmission*, London, 2010.

[72] C. Davidson and D. Trainer, "Innovative Concepts for Hybrid Multi-Level Converters for HVDC Power Transmission," in *9th IET International Conference on AC and DC Power Transmission*, London, 2010.

[73] Cigré WG B4-37, "VSC Transmission," CIGRÉ, Paris, 2005.

[74] A. Gustafsson, M. Saltzer, A. Frakas, H. Ghorbani, T. Quist and M. Jeroense, "The new 525 kV extruded HVDC cable system," [Online]. Available: http://www05.abb.com/global/scot/scot221.nsf/veritydisplay/7caadd110d270de5c1257d3b002ff3ee/$file/the%20new%20525%20kv%20extruded%20hvdc%20cable%20system%20white%20paperfinal.pdf. [Accessed 19 November 2014].

[75] K. R. Padiyar, HVDC Power Transmission Systems, Tunbridge Wells: New Academic Science, 2011.

[76] P. Kundur, Power System Stability and Control, New York: McGraw-Hill, 1994.

[77] C. M. Franck, "HVDC Circuit Breakers: A Review Identifying Future Research Needs," *IEEE Transactions on Power Delivery*, vol. 26, no. 2, pp. 998-1007, 2011.

[78] J. Hafner and B. Jacobson, "Proactive Hybrid HVDC Breakers - A key innovation for reliable HVDC grids," in *Cigré International Symposium - The electric power system of the future - Integrating supergrids and microgrids*, Bologna, 2011.

[79] S. Johansson, G. Asplund, E. Jansson and R. Rudervall, "Power system stability benefits with VSC DC-transmission systems," in *Cigré session*, Paris, 2004.

[80] L. Zhang, "Modelling and Control of VSC-HVDC Links Connected to Weak AC Systems," KTH, Stockholm, PhD Thesis, 2010.

[81] A. Egea-Àlvarez, “Multiterminal HVDC transmission systems for offshore wind,” Universitat Politecnica de Catalunya, PhD Thesis, 2014.

[82] J. Z. Zhou, H. Ding, S. Fan, Y. Zhang and A. M. Gole, “Impact of Short-Circuit Ratio and Phase-Locked-Loop Parameters on the Small-Signal Behavior of a VSC-HVDC Converter,” *IEEE Transactions on Power Delivery,* vol. 29, no. 5, pp. 2287-2296, 2014.

[83] S. K. Chaudary, “Control and Protection of Wind Power Plants with VSC-HVDC Connection,” Aalborg University, Aalborg, 2011.

[84] L. Zhang, L. Harnefors and H.-P. Nee, “Modeling and Control of VSC-HVDC Links Connected to Island Systems,” *IEEE Transactions on Power Systems,* vol. 26, no. 2, pp. 783-793, 2011.

[85] C. Heising, D. Meyer, R. Bartelt, M. Koochack Zadeh, T. Lebioda and J. Jung, *Power-electronic asset characteristics for arbitrary multi-terminal grid configurations,* TenneT and Avasition, 2012.

[86] T. C. Young Ho, L. Ran, A. García-Cerrad, J. L. Zamora-Macho and P. Brogan, “Voltage Source Converter AC Voltage Controller Design and Dynamic Response for a Large Offshore Wind Farm Network,” in *2nd International Conference on Renewable Energy Research and Applications*, Madrid, 2013.

[87] R. Bartelt, C. Heising, D. Meyer and V. Staudt, “Comparison of converter-near controls for HVDC-connected offshore wind-power plants focussing on the dynamic performance,” in *13th Wind Integration Workshop*, Berlin, 2014.

[88] S. K. Chaudary, R. Teodorescu, P. Rodriguez and P. C. Kjær, “Control and Operation of Wind Turbine Converters during Faults in an Offshore Wind Power Plant Grid with VSC-HVDC Connection,” in *IEEE Power and Engineering Society General Meeting*, Detroit, 2011.

[89] L. J. Cai, U. Karaagac and J. Mahseredjian, “Doubly-Fed Induction Generator Wind Turbine with VSC-HVDC Grid Connection - Interaction Analyses,” in *13th Wind Integration Workshop*, Berlin, 2014.

[90] L. Zeni, T. Lund, A. Hansen, P. Sørensen, P. Kjær, B. Hesselbæk and J. Glasdam, “Coordinated system services from offshore wind power plants connected through HVDC networks,” in *Cigré session*, Paris, 2014.

[91] Z. Wang, H. Lin, B. Jiang, J. Wu and G. Wang, “Study on Key Technologies of VSC-HVDC and Application in Offshore Wind Power Plant in China,” in *13th Wind Integration Workshop*, Berlin, 2014.

[92] V. Lescale, P. Holmberg, R. Ottersen and Y. Hafner, “Paralleling offshore wind farm HVDC ties on offshore side,” in *Cigré Session*, Paris, 2012.

[93] North Seas Countries' Offshore Grid Initiative, “Discussion Paper: Possible Market

Arrangements for Integrated Offshore Networks," Deliverable 5, 2013.

[94] A. G. Laukhamar, L. Zeni and P. E. Sørensen, "Alternatives for Primary Frequency Control Contribution from Wind Power Plants Connected to VSC-HVDC Intertie," in *European Wind Energy Conference*, Barcelona, 2014.

[95] O. Despouys and e. al., "Advanced results of control and protection of DC networks: behaviour, optimisation and grid extension," TWENTIES project deliverable 5.3, 2013.

[96] O. Gomis-Bellmunt, J. Liang, J. Ekanayake, R. King and N. Jenkins, "Topologies of multiterminal HVDC-VSC transmission for large offshore wind farms," *Electric Power Systems Research,* vol. 81, pp. 271-281, 2011.

[97] J. Glasdam, L. Zeni, J. Hjerrild, L. Kocewiak, B. Hesselbæk, P. E. Sørensen, A. D. Hansen, C. L. Bak and P. C. Kjær, "An Assessment of Converter Modelling Needs for Offshore Wind Power Plants Connected via VSC-HVDC Networks," in *12th Wind Integration Workshop*, London, 2013.

[98] M. Sztykiel, R. da Silva, R. Teodorescu, L. Zeni, L. Helle and P. C. Kjær, "Modular Multilevel Converter Modelling, Control and Analysis under Grid Frequency Deviations," in *EPE Joint T&D and Wind Chapters*, Aalborg, 2012.

[99] PowerFactory 15.1, *Technical reference documentation - PWM Converter,* Gomaringen: DIgSILENT, 2011.

[100] J. Peralta, H. D. S. Saad, J. Mahseredjian and S. Nguefeu, "Detailed and Averaged Models for a 401-Level MMC-HVDC System," *IEEE Transactions on Power Delivery,* vol. 27, no. 3, pp. 1501-1508, 2012.

[101] H. Saad, J. Peralta, S. Dennetière, J. Mahseredjian, J. Jatskevich, J. Martinez, A. Davoudi, M. Saeedifard, V. Sood, X. Wang, J. Cano and A. Mahrizi-Sani, "Dynamic Averaged and Simplified Models for MMC-Based HVDC Transmission Systems," *IEEE Transactions on Power Delivery,* vol. 28, no. 3, pp. 1723-1730, 2013.

[102] Cigré B4-57, "Technical Brochure 604 - Guide for the development of models for HVDC converters in a HVDC grid," Cigré, Paris, December 2014.

[103] A. Antonopoulos, L. Angquist and H.-P. Nee, "On Dynamics and Voltage Control of the Modular Multilevel Converter," in *13th European Conference on Power Electronics and Applications.*, IEEE, 2009.

[104] Ł. H. Kocewiak, "Harmonics in Large Offshore Wind Farms," Aalborg University, Aalborg, PhD thesis, 2012.

[105] J. Glasdam, "Harmonics in Offshore Wind Power Plants Employing Power Electronic Devices in the Transmission System," Department of Energy Technology, Aalborg University, PhD thesis, 2015.

[106] Ł. H. Kocewiak, J. Hjerrild and C. L. Bak, “Wind turbine converter control interaction with complex wind farm systems,” *IET Renewable Power Generation Special Issue,* pp. 1-10, 2012.

[107] A. J. Wood and B. F. Wollenberg, Power generation, operation and control, 2nd ed., Wiley & Sons, 1996.

[108] PowerFactory 15.1, *Technical reference documentation - Synchronous Machine,* Gomaringen: DIgSILENT, 2011.

[109] A. Adamczyk, M. Altin, Ö. Göksu, R. Teodorescu og F. Iov, »Generic 12-Bus Test System for Wind Power Integration Studies,« i *EPE Joint Wind Energy and T&D Chapters Seminar,* Aalborg, 2012.

[110] L. Zhang, L. Harnefors and H.-P. Nee, “Power-Synchronization Control of Grid-Connected Voltage-Source Converters,” *IEEE Transactions on Power Systems,* vol. 25, no. 2, pp. 809-821, 2010.

[111] L. Zeni, I. Margaris, A. Hansen, S. P. and P. Kjær, “Generic Models of Wind Turbine Generators for Advanced Applications in a VSC-based Offshore HVDC Network,” in *The 10th IET Conference on AC/DC Transmission,* Birmingham, 2012.

[112] A. Paolucci, Lezioni di Trasmissione dell'Energia Elettrica, Padova: CLEUP, 1998.

[113] D. Lee and others, “IEEE Recommended Practice for Excitation System Models for Power System Stability Studies,” IEEE, 1992.

[114] U. Gnanarathna, A. Gole and R. Jayasinghe, “Efficient Modelling of Modular Multilevel HVDC Converters (MMC) on Electromagnetic Transient Simulation Programs,” *IEEE Transactions on Power Delivery,* vol. 26, no. 1, pp. 316-324, 2011.

[115] N. Ahmed, L. Ängquist, S. Norrga and H.-P. Nee, “Validation of the continuous model of the modular multileveel converter with blocking/deblocking capability,” in *The 10th IET Conference on AC and DC Power Transmission,* Birmingham, 2012.

[116] A. D. Hansen, M. Altin and N. A. Cutululis, “Modelling of wind power plant controller, wind speed time series, aggregation and sample results,” DTU Wind Energy, Roskilde, 2015.

[117] L. Angquist, A. Antonopoulos, D. Siemaszko, K. Ilves, M. Vasiladiotis and H.-P. Nee, “Open-Loop Control of Modular Multilevel Converters Using Estimation of Stored Energy,” *IEEE Transactions on Industry Applications,* vol. 47, no. 6, pp. 2516-2524, 2011.

[118] L. Harnefors, A. Antonopoulos, S. Norrga, L. Angquist and H.-P. Nee, “Dynamic Analysis of Modular Multilevel Converter,” *IEEE Transactions on Industrial Electronics,* vol. 60, no. 7, pp. 2526-2537, 2013.

[119] L. Zeni, B. Hesselbæk, P. E. Sørensen, A. D. Hansen and P. C. Kjær, “Control of VSC-HVDC in offshore AC islands with wind power plants: comparison of two alternatives,” in

accepted for publication in PowerTech 2015, Eindhoven, 2015.

[120] M. Raza and O. Gomis-Bellmunt, "Multi-Infeed Control of VSC-HVDC Transmission System for Offshore Wind Power Plant Integration," in *13th Wind Integration Workshop*, Berlin, 2014.

[121] C. Heising et al., "System dynamic and power-quality study," TenneT, Hamburg, 2011.

[122] L. Harnefors, L. Zhang and M. Bongiorno, "Frequency-domain passivity-based current controller design," *IET Power Electronics*, vol. 1, no. 4, pp. 455-465, 2007.

[123] W. Z. El-Khatib, D. Schwartzberg, I. Arana Aristi, J. Holbøl and L. Zeni, "Transients in VSC-HVDC connected offshore wind power plants," in *The 11th IET Conference on AC/DC Power Transmission*, Birmingham, 2015.

[124] L. Harnefors, "Control of VSC-HVDC Transmissions," PESC Tutorial, ABB Power Systems, Ludvika, Sweden, 2008.

[125] D. Zmood, D. Homes and G. Bode, "Frequency Domain Analysis of Three Phase Linear Current Regulators," *IEEE Transactions on Industry Applications*, vol. 37, no. 2, pp. 601-610, 2001.

[126] L. Harnefors, "Modeling of Three-Phase Dynamic Systems Using Complex Transfer Functions and Transfer Matrices," *IEEE Transactions on Industrial Electronics*, vol. 54, no. 4, pp. 2239-2248, 2007.

[127] S. Skogestad and I. Postlethwaite, Multivariable Feedback Control - Analysis and Design, Wiley, 2007.

[128] PowerFactory 15.1, *Technical reference documentation - Phase Measurement Device*, Gomaringen: DIgSILENT, 2013.

[129] L. Zeni, H. Jóhannsson, A. D. Hansen, P. E. Sørensen, B. Hesselbæk and P. C. Kjær, "Influence of Current Limitation on Voltage Stability with Voltage Sourced Converter HVDC," in *ISGT Conference Europe*, Copenhagen, 2013.

[130] L. Zhang, H.-P. Nee and L. Harnefors, "Analysis of Stability Limitations of a VSC-HVDC Link Using Power-Synchronization Control," *IEEE Transactions on Power Systems*, vol. 26, no. 3, pp. 1326-1337, 2011.

[131] H. Jóhansson, "Development of early warning methods for electric power systems," PhD thesis, Technical University of Denmark, Lyngby, 2010.

[132] P. Kundur, J. Paserba, V. Ajjarapu, G. Andersson, A. Bose, C. Canizares, N. Hatziargyriou, D. Hill, A. Stankovic, C. Taylor, T. Van Custem and V. Vittal, "Definition and Classification of Power System Stability," *IEEE Transactions on Power Systems*, vol. 19, no. 2, pp. 1387-1401, 2004.

[133] Cigré WG 14.05, “On voltage and power stability in AC/DC systems,” Technical Brochure, Cigré, Paris, 2003.

[134] D. L. H. Aik and G. Andersson, “Influence of load characteristics on the power/voltage stability of HVDC systems,” *IEEE Transactions on Power Delivery,* vol. 13, no. 4, pp. 1437-1444, 1998.

[135] D. L. H. Aik and G. Andersson, “Voltage and Power Stability of HVDC Systems - Emerging Issues and New Analytical Methodologies,” in *VII SEPOPE,* Curitiba, 2000.

[136] D. L. H. Aik and G. Andersson, “Voltage stability analysis of multi-infeed HVDC systems,” *IEEE Transactions on Power Delivery,* vol. 12, no. 3, pp. 1309-1318, 1997.

[137] B. Franken and G. Andersson, “Analysis of HVDC converters connected to weak AC systems,” *IEEE Transactions on Power Systems,* vol. 5, no. 1, pp. 235-242, 1990.

[138] O. B. G. A. M. Nayak, D. G. Chapman and J. B. Davies, “Control Sensitivity Indices for Stability Analysis of HVdc Systems,” *IEEE Transactions on Power Delivery,* vol. 10, no. 4, pp. 2054-2060, 1995.

[139] J. Z. Zhou and A. M. Gole, “VSC transmission limitations imposed by AC system strength and AC impedance characteristics,” in *10th IET Conference on AC and DC Power Transmission,* Birmingham, 2012.

[140] G. C. Tarnowski, P. C. Kjær, P. E. Sørensen and J. Østergaard, “Study on Variable Speed Wind Turbines Capability for Frequency Response,” in *European Wind Energy Conference,* Warsaw, 2009.

[141] L. Zeni, A. Rudolph, J. Munster-Swendsen, I. Margaris, A. D. Hansen and P. Sørensen, “Virtual inertia for variable speed wind turbines,” *Wind Energy,* vol. DOI:10.1002/we, 2012.

[142] T. K. Vrana, L. Zeni and O. B. Fosso, “Active Power Control with Undead-Band Voltage And Frequency Droop Applied to a Meshed DC Grid Test System,” in *Energycon,* Firenze, 2012.

[143] T. K. Vrana, L. Zeni and F. O. B, “Dynamic Active Power Control with Improved Undead-Band Droop for HVDC Grids,” in *The 10th IET Conference on AC/DC Power Transmission,* Birmingham, 2012.

[144] L. Zeni, S. Goumalatsos, R. Eriksson, M. Altin, P. Sørensen, A. Hansen, P. Kjær and B. Hesselbæk, “Power Oscillation Damping from VSC-HVDC connected Offshore Wind Power Plants,” *IEEE Transactions on Power Delivery,* submitted, under review.

[145] E. Hendricks, O. Jannerup and P. H. Sørensen, Linear Systems Control: determinitstic and stochastic methods, Springer, 2008.

[146] K. Ogata, Modern Control Engineering, Prentice Hall, 2010.

[147] MED-EMIP, “Medring Update vol.II - Analysis and Proposal of Solutions for the Closure of the Ring and North-South Electrical Corridors,” Euro-Mediterranean Energy Market Integration Project, 2010.

[148] L. Harnefors, “Analysis of Subsynchronous Torsional Interaction With Power Electronic Converters,” *IEEE Transactions on Power Systems,* vol. 22, no. 1, pp. 305-313, 2007.

[149] M. Klein, G. Rogers, S. Moorty and P. Kundur, “Analytical investigation of factors influencing power system stabilizers performance,” *IEEE Transactions on Energy Conversion,* vol. 7, no. 3, pp. 382-390, 1992.

[150] S. Goumalatsos, “Investigation of Power Oscillation Damping service by offshore wind power plants connected via Voltage Source Converter High Voltage Direct Current link,” Master thesis, Technical University of Denmark, Lyngby, 2014.

[151] M. Beza and M. Bongiorno, “An Adaptive Power Oscillation Damping Controller by STATCOM With Energy Storage,” *IEEE Transactions on Power Systems,* vol. 30, no. 1, pp. 484-493, 2015.

[152] M. Beza and M. Bongiorno, “A fast estimation algorithm for low-frequency oscillations in power systems,” in *14th European Conference in Power Electronic Applications*, 2011.

[153] C. E. Shannon, “Communication in the presence of noise,” *Proceedings of the IRE,* vol. 37, no. 1, pp. 10-21, 1949.

[154] V. Hanta and A. Procházka, *Rational Approximation of Time Delay.*

[155] NREL National Wind Technology Center, *Controllable Grid Interface Test System,* National Renewable Energy Labo, Accessed 06/03/2015 at http://www.nrel.gov/water/pdfs/53800.pdf.

[156] P. Koralewicz, P. Joerg and E. Guidi, *Presentation: Power Electronic Grid Simulator - Platform of drives and power quality products for power electronics testing,* ABB, Accessed on 06/03/2015 at http://www.nrel.gov/electricity/transmission/grid-simulator-workshop-2.html.

[157] PowerFactory 15.1, *Technical reference documentation - General Load,* Gomaringen: DIgSILENT, 2013.

[158] PowerFactory 15.1, *Technical reference documentation - Static Generator,* Gomaringen: DIgSILENT, 2011.

[159] T. K. Vrana, J. Beerten, R. Belmans and O. B. Fosso, “A classification of DC node voltage control methods for HVDC grids,” *Electric power systems research,* vol. 103, pp. 137-144, 2013.

Appendix 1 Simulation models: description

Simulation models: governing system

The governing system is modelled with a generic governor model. Its PowerFactory block diagram is shown in Figure 109. The model can flexibly adapt depending on the parameters. In this study, the actual configuration is quite simple, as evinced by the standard parameters reported in Table 21 (Appendix 2). This model is used when operating with the model in Figure 7, while the description of the corresponding governing system models for the system in Figure 8 is entirely demanded to [44] and its references, since it is not so important for POD studies.

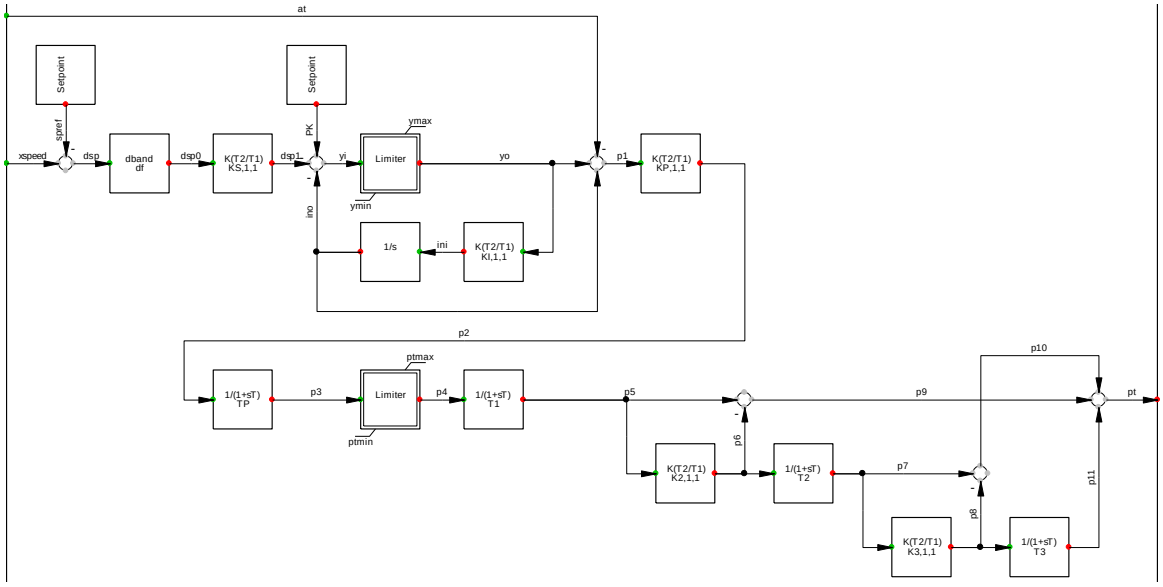

Figure 109 - Generic governing system model: PowerFactory block diagram.

Simulation models: ES and AVR

In the simulations, the ES and AVR model illustrated in Figure 110 has been used, which is a simplified version of Type AC4A [113], without transient gain reduction and (because of ideal measurement) and no under- over-excitation limits, since only the linear operational range is concerned in the report. Sample parameters are reported in Table 22 (Appendix 2). The model is used on the simple system shown in Figure 7.

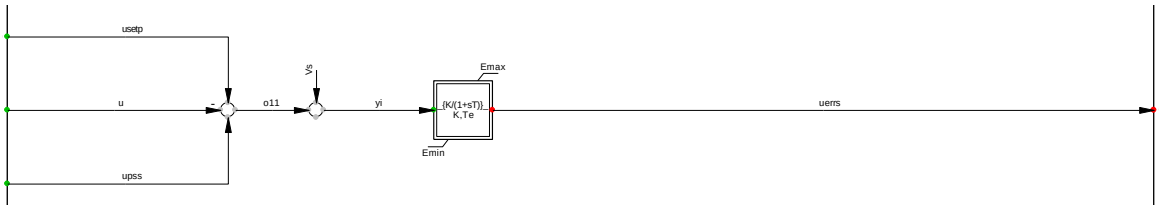

Figure 110 - ES and AVR model: PowerFactory block diagram.

As described in the dedicated reference [44], the system in Figure 8 makes use of ES and AVR models of Type ST1A [113], the block diagram of which is reported in Figure 111. Sample parameters are reported in Table 23 (Appendix 2).

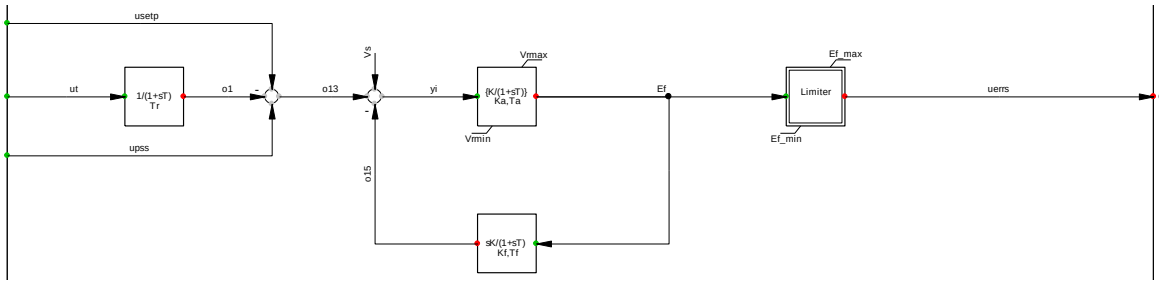

Figure 111 - ES and AVR models used in IEEE 12-bus system: PowerFactory block diagram.

Simulation models: loads

Standard PowerFactory models are used in all studies – see [157]. Default parameters are used for the voltage dependency of active and reactive power consumption when using the simple model in Figure 7. The loads in Figure 8, however, are constant active power loads so as to demonstrate the effectiveness of POD independently of the loads' voltage dependence [149].

Simulation models: VSC-HVDC systems

The simulation model for each converter station is reported in the main body in Figure 9 and is based on the standard PWM converter model in PowerFactory [99]. The way to populate the model with electrical parameters is as follows:

- The DC side capacitor is calculated, according to the model and nomenclature in Section 3.3.1 and [118], as:

$$C_{DC} = C_d + \frac{2MC}{N} \tag{48}$$

  which is therefore the parallel of the capacitance between DC poles and the capacitance which is connected at every instant in each converter leg.
- The phase reactor resistance and inductance are computed, again according to [118] and what shown in Section 3.3.1, as:

$$R_{ph} = \frac{R}{2} \tag{49}$$

$$L_{ph} = \frac{L}{2} \tag{50}$$

- The parameters Z_T and Y_0 are derived from the transformer short circuit and no-load parameters. Inclusion of a possible filter capacitance can be lumped into Y_0 (which can be moved to the converter side of the transformer), or inserted as dedicated shunt impedance.

More about these calculations is reported in Publication 4 [97]. The DC lines are represented as concentrated π-equivalents with capacitance C_L and series parameters R_{DC} and L_{DC}.

As for the control models, most of them have been described throughout the report, but the remaining blocks are described here.

Coordinate transformation

The coordinate transformation from static to synchronous reference frame (αβ to *dq*) is performed with well-known formulae. Neglecting the *0*-axis component:

$$\begin{bmatrix} x_d \\ x_q \end{bmatrix} = \begin{bmatrix} \cos\theta & \sin\theta \\ -\sin\theta & \cos\theta \end{bmatrix} \cdot \begin{bmatrix} x_\alpha \\ x_\beta \end{bmatrix} \tag{51}$$

where x is a generic physical quantity and θ is the PCC voltage angle read by the PLL or generated by the internal frequency integrator.

Antitransform and delay

The anti-transform is performed by inverting Eq. (51), while the VSC delay is an ideal delay expressed in Laplace domain by e^{-sT_d}. The VSC delay happens in αβ frame [104].

Angle selection

The angle selection block is simply a selector which allows to tap either the angle coming from the PLL or the angle generated by the internal frequency integrator. Detailed block diagram of this model is superfluous.

Measurement and filter

Standard measurement blocks from PowerFactory are used, possibly filtered, in some cases, with first order blocks. For voltage and current the filter is neglected, since its time constant should be lower than the targeted frequency range. Active and reactive power are usually filtered with time constant T_m = 10 ms.

The PLL block is a standard PowerFactory PLL [128]. The block diagram is repeated here for clarity, only in its EMT version – for the purpose of this study the RMS model is identical.

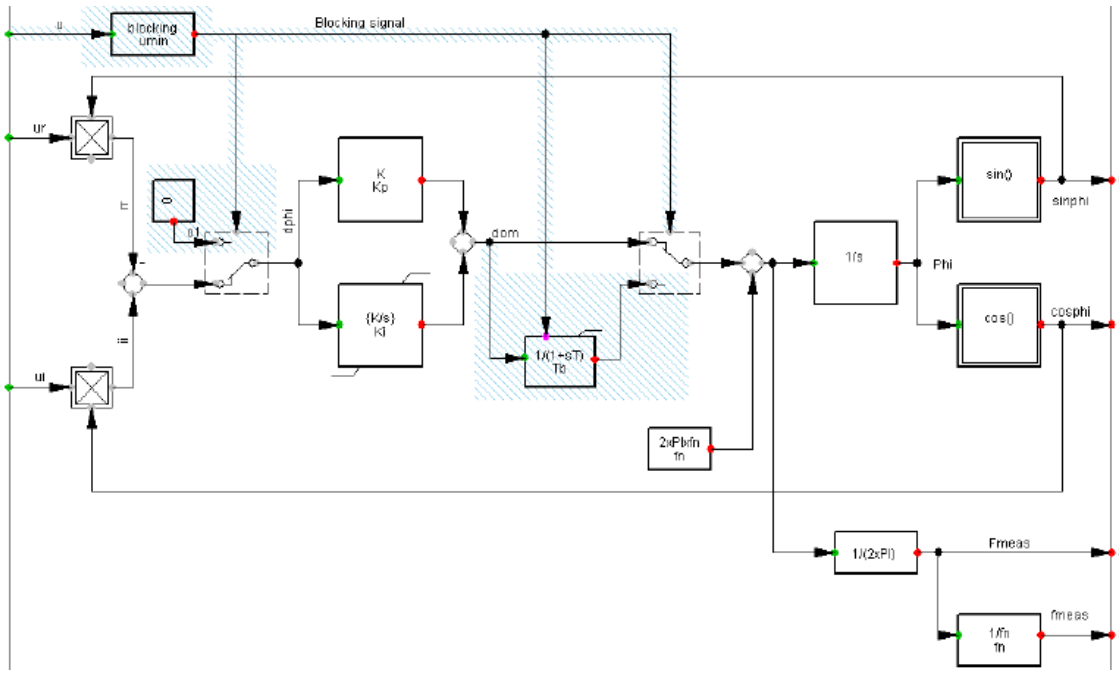

Figure 112 - Standard PLL - EMT simulations [125]: PowerFactory block diagram.

Current controller

The PowerFactory diagram of the current controller is sketched in Figure 113. As can be seen, besides the standard controller, additional filters and selectors are present. The selector allows for feeding forward of measured or reference voltages. The active damping block parameterised by k_v and T_v is inserted only to make the controller general and is usually not employed throughout the report. The gain Knorm depends on the type of modulation used in the PWM converter model [99].

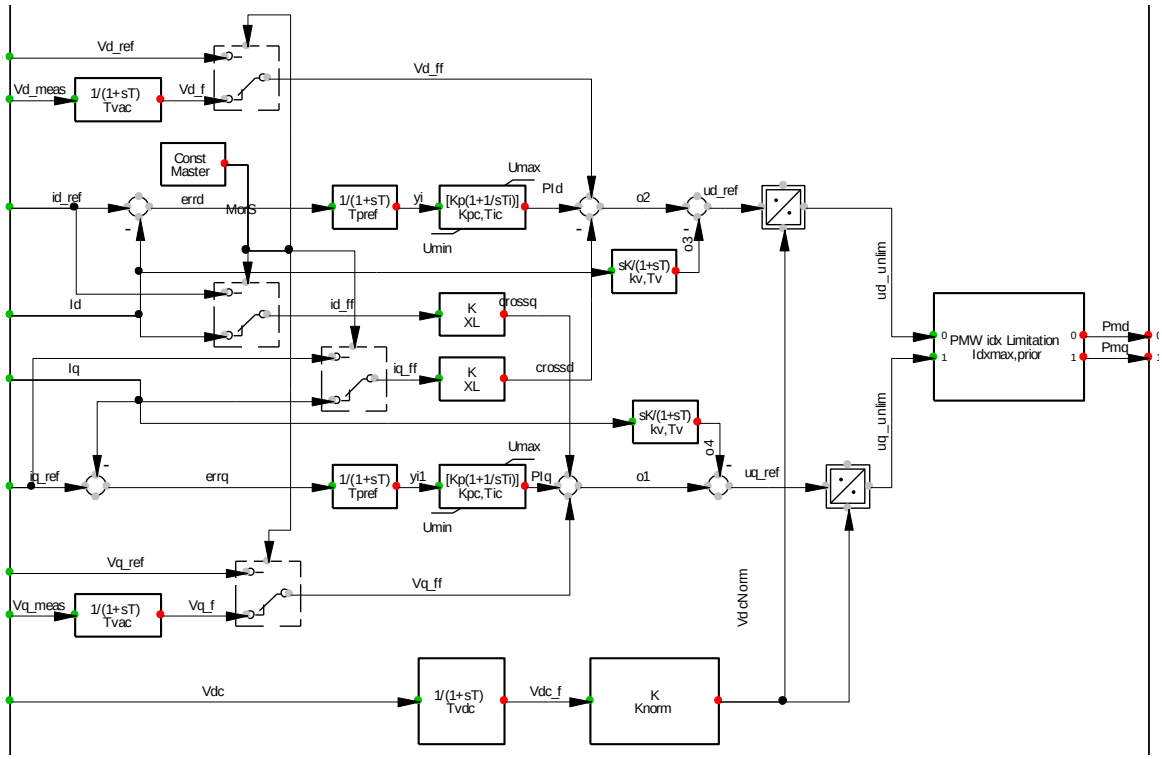

Figure 113 - Current controller: PowerFactory block diagram.

Simulation models: current prioritisation for *Outer controller* block

As emphasised in Chapter 5, the current prioritisation strategy has strong impacts on the performance when and HVDC converter is acting within a system approaching its long-term stability limits.

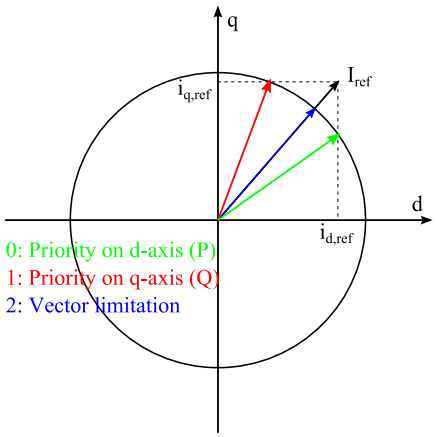

Figure 114 - Current prioritisation.

For this reason, despite current prioritisation is a well-known feature, it is briefly reported here, explaining the three possibilities. The vector diagram illustrating what happens in the current prioritisation block is depicted in Figure 114. This is what the rightmost block in Figure 11 to Figure 13 does through depending on the setting of a parameter.

Simulation models: PowerFactory layout of full WPP model in Chapter 4

The PowerFactory grids for the reference WPP utilised in Chapter 4 are shown in Figure 115 to Figure 119 and contain the HVDC system, the export system and the three WPP sections, consisting of array cables, WTGs and WTG transformers. Relevant sample parameters are reported in Appendix 2.

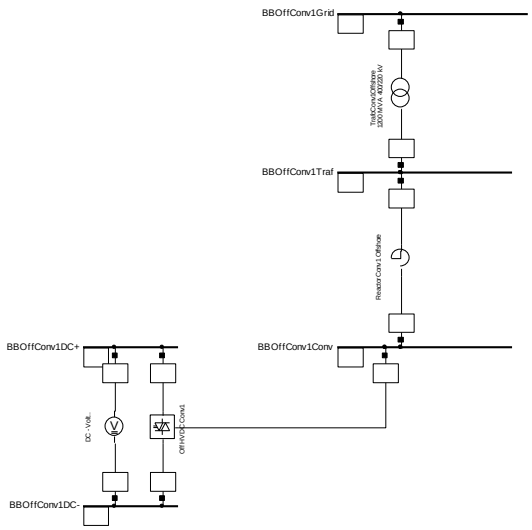

Figure 115 - Reference WPP: HVDC system model in PowerFactory.

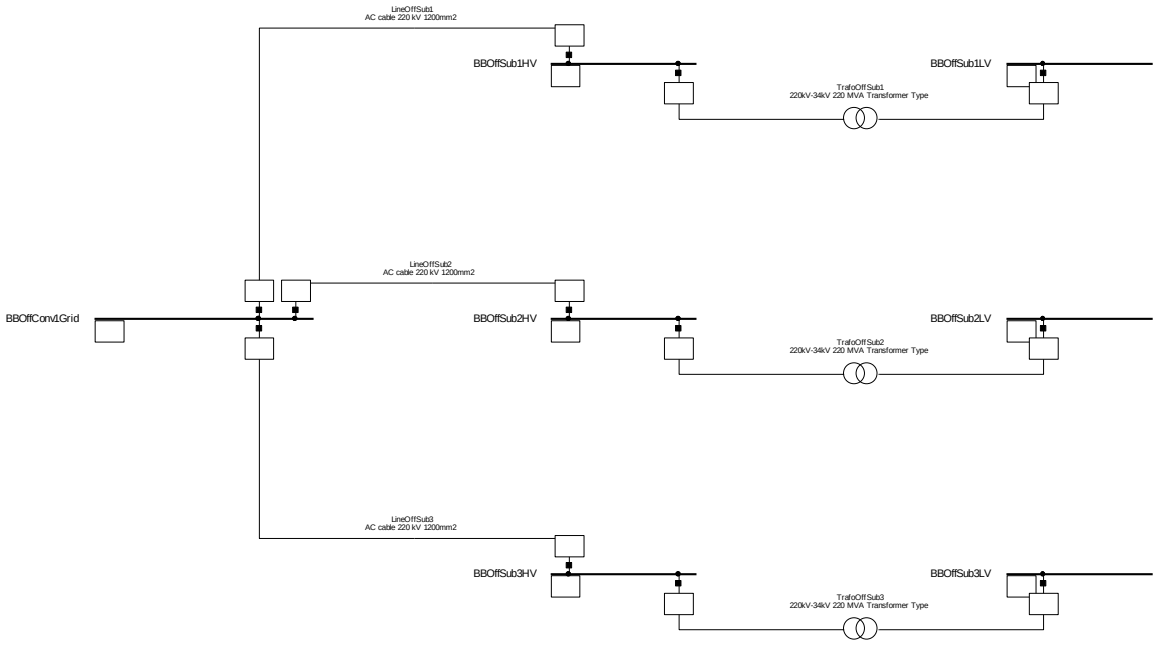

Figure 116 - Reference WPP: export system model in PowerFactory.

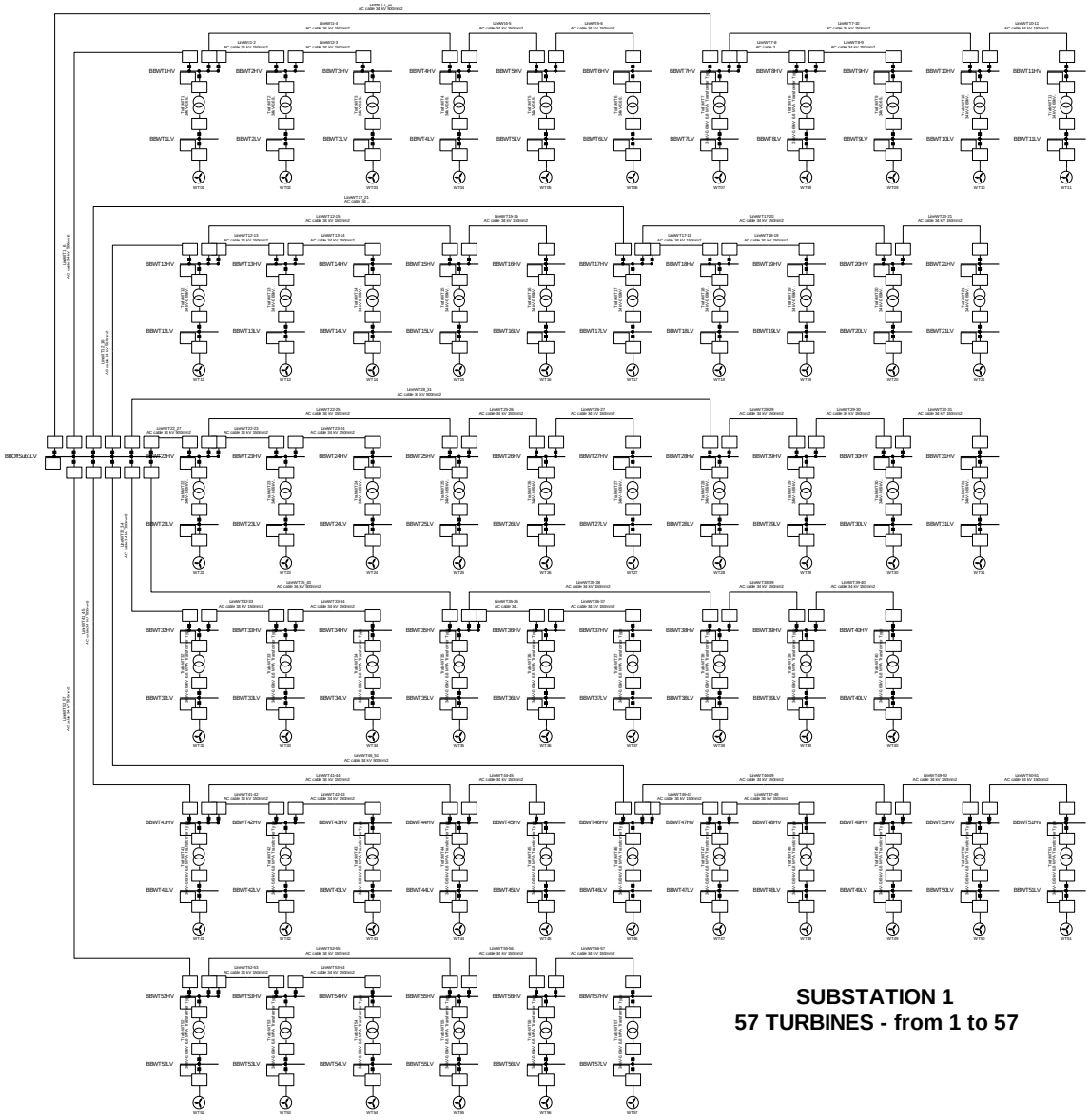

Figure 117 - Reference WPP: section WPP1 model in PowerFactory.

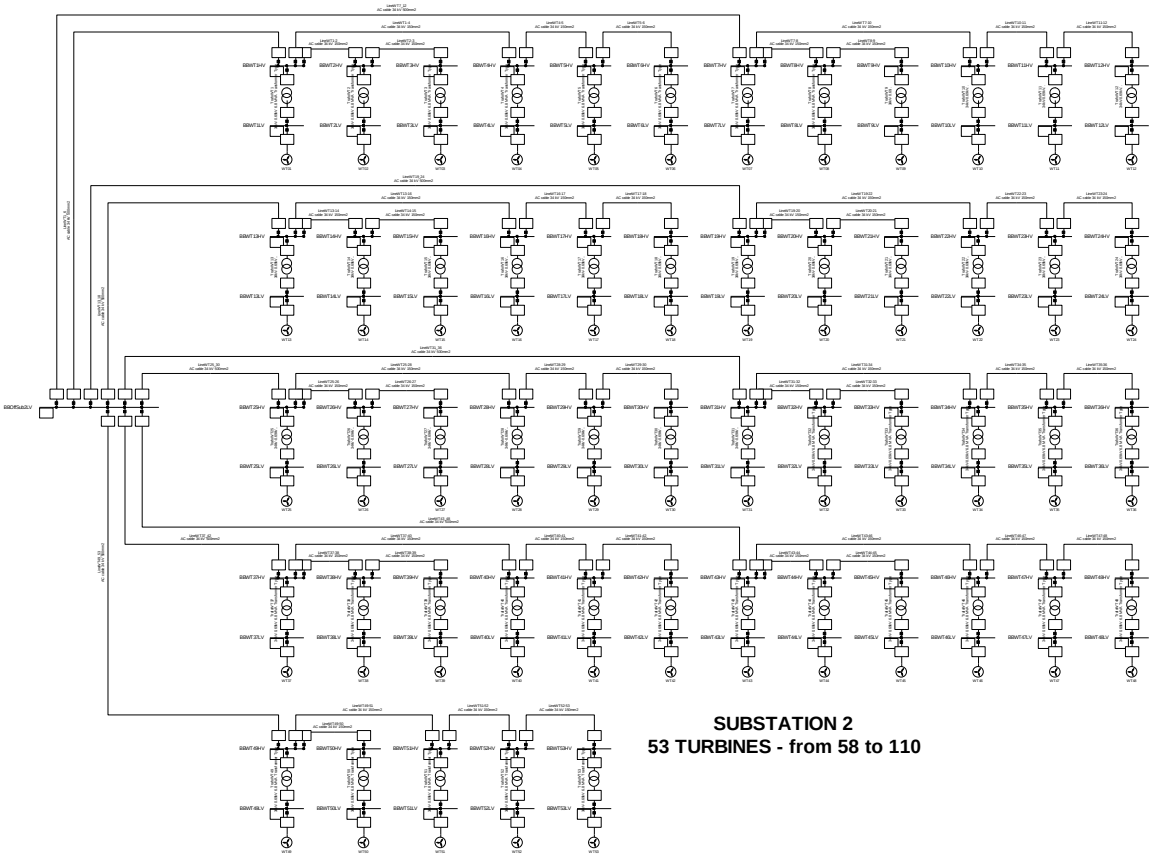

Figure 118 - Reference WPP: section WPP2 model in PowerFactory.

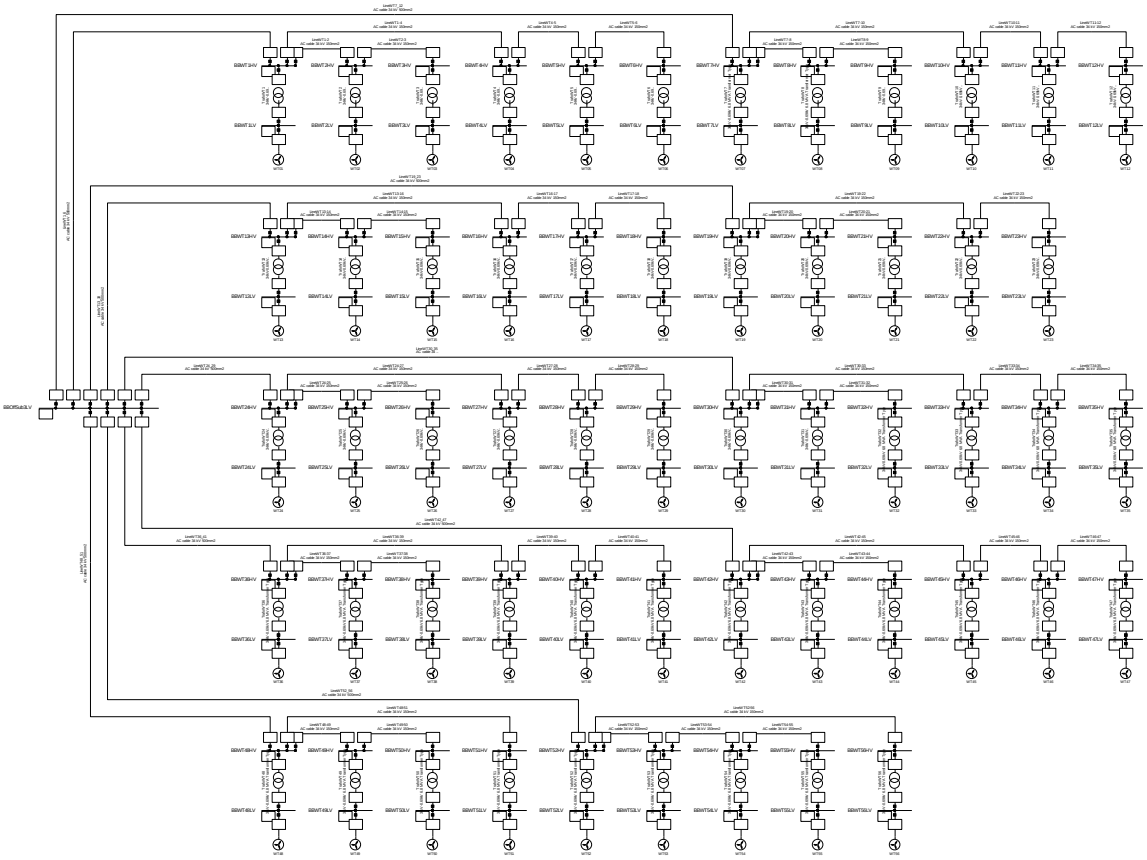

SUBSTATION 3
56 TURBINES - from 111 to 166

Figure 119 - Reference WPP: section WPP3 model in PowerFactory.

Appendix 2 Simulation models: data

Sample parameters: governing system model

The model in Figure 109 (Appendix 1) is populated with the following parameters.

Table 21 - Sample parameters for governing system model.

Parameter	Value	Unit	Parameter	Value	Unit
df	0.003	pu	T_2	0.1	s
K_S	10	pu	T_3	0.1	s
K_I	0	pu/s	K_3	0	pu
K_P	1	pu	y_{min}	0	pu
T_P	0.1	s	pt_{min}	0.1	pu
T_1	1	s	y_{max}	1.001	pu
K_2	0	pu	pt_{max}	1.25	pu

Sample parameters: ES and AVR model

Sample parameters for the model in Figure 110 (Appendix 1) are reported below. It is worth to note that gain K_A is varied in Chapter 7.

Table 22 - Sample parameters for ES and AVR model.

Parameter	Value	Unit
K_A	200	pu
T_A	0.04	s
E_{min}	-4.53	pu
E_{max}	5	pu

In Chapter 7, when operating with the model reported in Figure 8, sample parameters for the ES and AVR models (Figure 111 in Appendix 1) are reported in Table 23.

Table 23 - Sample parameters for ES and AVR models in IEEE 12-bus system.

Parameter	G1	G2	G3	G4	Unit
T_r	0	0	0	0	s
K_A	200	272	272	200	pu
T_A	0.015	0.02	0.02	0.015	s
K_f	0	0.0043	0.0043	0	pu
T_f	1	0.06	0.06	1	s
V_{rmin}	-100	-2.73	-2.73	-100	pu
E_{fmin}	0	0	0	0	pu
V_{rmax}	100	2.73	2.73	100	pu
E_{fmax}	5	2.73	2.73	5	pu

Sample parameters: VSC-HVDC systems

Sample parameters for the HVDC converter station electrical model are reported in Table 24. More parameters, also including DC line, etc… can be found in [102].

Table 24 - Sample parameters for HVDC converter electrical model.

Parameter	Value	Unit
C_{DC}	30	ms
Z_{ph}	$(1+ j\omega\cdot 0.51)\cdot 10^{-3}$	pu
Z_T	$(6+ j\omega\cdot 0.38)\cdot 10^{-3}$	pu
I_0	0.03	%
P_0	$0.21\cdot 10^{-3}$	pu
C_L	20	μs/km
L_{DC}	$10\cdot 10^{-6}$	pu/km
R_{DC}	$0.086\cdot 10^{-3}$	pu/km

Sample parameters for the PLL reported in Figure 112 (Appendix 1) are listed in Table 25.

Table 25 - Sample parameters for standard PLL.

Parameter	Value	Unit
K_P	50	pu
K_I	500	pu/s

Sample parameters for the standard current controller (Figure 113 in Appendix 1) and for electrical parameters as those reported in Table 24 are listed in Table 26. In simulations making use of Option 2 in Chapter 4, the integral time constant is set to $T_{iC} = \infty$.

Table 26 - Sample parameters for current controller.

Parameter	Value	Unit	Parameter	Value	Unit
k_v	0	pu	Master	0	-
T_v	0.025	s	K_{norm}	1.25	pu
K_{pC}	0.88	pu	T_{Vdc}	0.05	s
T_{iC}	0.01	s	T_{Vac}	0	s
X_L	0.28	pu	T_{pref}	0	s
Idx_{max}	1	pu	U_{min}	-1.25	pu
prior	2	-	U_{max}	1.25	pu

Sample parameters: WPP

Relevant sample parameters for the WPP are presented here, in Table 27 for the WTG active power control model and in Table 28 for the WPPC.

Table 27 - Sample parameters for active power control of WTG model Type 4B.

Parameter	Value	Unit
T_{ufilt}	0.01	s
dp_{maxp}	0.5	pu/s
T_{pordp}	0.04	s
T_{paero}	5	s
i_{pmax}	1	pu

Table 28 - Sample parameters for WPPC model.

Parameter	Value	Unit	Parameter	Value	Unit	Parameter	Value	Unit
dP_{MAX}	0.1	pu/s	f_{DB}	±0.0005	pu	F_{FFf}	0	-
dP_{min}	-0.1	pu/s	K_{ppcf}	20	pu	T_{zPOD}	0	s
K_{ppcP}	0.5	pu	T_{ppcf}	2	s	T_{pPOD}	0	s
K_{ppcI}	0.5	pu/s	T_{zC}	-0.025	s	F_{fPOD}	0	-
T_{ppcP}	0.01	s	T_{pC}	0.025	s	K_{POD}	1	pu
P_{MAX}	1	pu	T_{ppcin}	0.2	s	K_{ppcin}	0	pu
P_{min}	0	pu						

The parameters reported here are indicative. Other relevant parameters are those related to the mechanical two-mass model, listed in Table 29.

Table 29 - Sample parameters for mechanical two-mass model.

Parameter	Value	Unit
H_{GEN}	0.93	s
H_{ROT}	5.81	s
K_{SH}	150	pu/s
C_{SH}	4	pu

Other blocks are used for some of the simulations, i.e. those included in the WPP model description in Publication 9 [111] and a model with a similar structure is described for instance in [116]. However, the parameters utilised in other blocks are not dramatically influential for the purpose of this report. Therefore, the reader is referred to the cited sources for more information on models' structure and sample data.

Sample parameters: simulations in Chapter 4

Sample parameters for the export cables going from HVDC station to the three AC substations are listed in Table 30. Parameters L_i are the length of the *i*-th export cable.

Table 30 - Sample parameters for export cables.

Parameter	Value	Unit	Parameter	Value	Unit
V_{nom}	220	kV	G	0.1	μS/km
I_{nom}	1	kA	L_1	7	km
R (AC @ 20°C)	0.045	Ω/km	L_2	10	km
L	0.4	mH/km	L_3	24	km
C	0.2	μF/km			

In the simulations of the full detailed model (Section 4.3.4), each WTG converter is provided with its own current controller, parameterised according to Table 31. All parameters that are not reported are nil. The WTG converters are modelled with static generators [158]. The value of X_L is essentially the WTG transformer reactance.

Table 31 - Sample parameters for WTG converter current controller for simulations of detailed model.

Parameter	Value	Unit	Parameter	Value	Unit
K_{pC}	0.32	pu	Master	0	-
T_{iC}	0.01	s	K_{norm}	1	pu
X_L	0.1	pu	T_{Vac}	0	s
Idx_{max}	1.3	pu	U_{min}	-1	pu
prior	2	-	U_{max}	1	pu

When the simulations were performed with the aggregated model synchronised at the HV (220 kV) side of the AC substations transformers (Sections 4.3.1 to 4.3.4), sample parameters for the aggregated converter model are reported in Table 32. The parameter X_L represents, in this case, the sum of converter phase reactor and export transformer reactance.

Table 32 - Sample parameters for aggregated WTG converter current controller when synchronised at HV side of AC substation transformer.

Parameter	Value	Unit	Parameter	Value	Unit
K_{pC}	1.02	pu	Master	0	-
T_{iC}	0.01	s	K_{norm}	0.79	pu
X_L	0.32	pu	T_{Vac}	0	s
Idx_{max}	1	pu	U_{min}	-1	pu
prior	2	-	U_{max}	1	pu

For all other cases, i.e. when the aggregated converters are synchronised at the LV (34 kV) side of the AC substation transformers (Figure 19) in Section 4.3.5 and subsequent, sample parameters of the current controller may be those listed in Table 33.

Table 33 - Sample parameters for aggregated WTG converter current controller when synchronised at LV side of AC substation transformer.

Parameter	Value	Unit	Parameter	Value	Unit
K_{pC}	0.64	pu	Master	0	-
T_{iC}	0.01	s	K_{norm}	0.79	pu
X_L	0.2	pu	T_{Vac}	0	s
Idx_{max}	1	pu	U_{min}	-1	pu
prior	2	-	U_{max}	1	pu

Appendix 3 Control parameter tuning

The tuning of control parameters for the special cases of offshore HVDC converter and POD controllers was discussed in detail in the dedicated chapters (Chapter 4 and Chapter 7). It is hence not repeated here. In this Appendix, only brief informative notes and references to the tuning of generic current controllers and DC voltage controllers for the onshore HVDC station is treated.

Current control tuning

Guidelines for basic current control tuning are found e.g. in [23], [122], [124] and can directly be derived from the vector expression of the current through the converter reactor. The generic expression of the equation governing the current through a reactor is given by (assuming connection to a stiff voltage source):

$$L\frac{d\mathbf{i}}{dt} = \mathbf{u} - \mathbf{v} - (r+j\omega L)\mathbf{i} \tag{52}$$

where L is the inductance of the reactor, r its resistance, ω the pulsation of the voltage and current, **i** the current, **u** the converter voltage and **v** the stiff grid voltage. By executing the well-known decoupling and setting the converter voltage references as $\mathbf{u} = \mathbf{u}_{ref} = \mathbf{u}'_{ref} - j\omega L\mathbf{i}$. Furthermore, the voltage reference $\mathbf{u}'_{ref}$ can be built by adding the current control signal coming from a PI compensator and the filtered PCC voltage vector, so as to improve the disturbance rejection [23]:

$$\mathbf{u}'_{ref} = \alpha L\cdot(\mathbf{i}_{ref} - \mathbf{i}) + k_i\cdot\int(\mathbf{i}_{ref} - \mathbf{i})dt + \frac{\alpha_f}{\alpha_f+s}\cdot\mathbf{v} \tag{53}$$

Plugging (53) into (52) by neglecting the integral term for a moment, considering r very small, solving for the current and moving to the Laplace domain:

$$\mathbf{i} \approx \frac{\alpha}{s+\alpha}\cdot\mathbf{i}_{ref} - \frac{s}{(s+\alpha)(s+\alpha_f)L}\cdot\mathbf{v} \tag{54}$$

It is noticed that the current can be controlled with BW α by selecting $K_{pC} = \alpha L$ and no steady-state control error is present. A small integral action is anyhow desired to make up for uncertainties in the knowledge of L and the non-negligible value of r. Considering usual values for the BW (as high as some thousands of rad/s), an integral time constant T_{iC} = 10 ms may be appropriate, to cancel any small errors within a couple of fundamental cycles. Guidelines as for how to tune α_f are reported e.g. in [122].

It should be noticed that what reported here neglects, limitations given by the switching frequency and sampling time, as well as any delays. Moreover, the current measurement is considered ideal. Another underlying assumption is the fact that voltage references and converter voltage are the same per-unit quantities, i.e. a division of the voltage references by the available DC voltage is

performed before the modulation process, which decouples AC and DC dynamics [23]. Thus, the design performed with the guidelines above must always be corroborated by time simulations. However, the procedure is considered common practice in PE applications.

To particularise the design to the notation used in this report, one should consider only the AC part of Figure 9, neglecting Y_0 and considering $\mathbf{u} = V_C$, $\mathbf{v} = V_{AC}$, $L = L_{PH}+L_T$ as well as $r = r_{PH}+r_T$.

DC voltage control design

The design of the DC voltage controller for onshore HVDC stations can be done based on [23], [124] or any other similar reference. The design can be based on the block diagram shown in Figure 120.

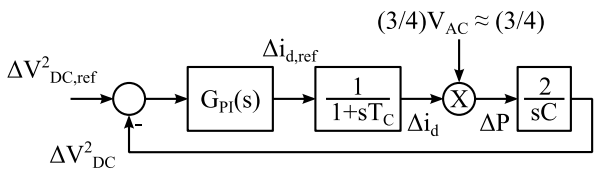

Figure 120 - Simplified block diagram for design of DC voltage controller.

Each block represents:

- $G_{PI}(s) = \frac{K_{pDC}s + K_{iDC}}{s}$ is the transfer function of the PI voltage controller.
- $\frac{1}{1 + sT_C}$ is the converter transfer function. Under reasonable assumptions, $T_C = \alpha^{-1}$, where α is the current controller BW as designed above.
- $\frac{2}{sC}$ is the transfer function of the DC system, where C is the pole-to-ground capacitance. The output is the pole-to-ground DC voltage squared. This means that, referring to Figure 9, $C = 2C_{DC}$ and controlled quantity is the square of half of V_{DC} in Figure 9.
- The multiplication by $(3/4)V_{AC}$ is to take into account the fact that amplitude invariant transformation of voltage and current is used, as well as the fact that only half the total converter power P is varying the pole-to-ground DC voltage and energy. Moreover, the assumption $V_{AC} \approx 1.0$ pu is accepted.

The open loop transfer function becomes:

$$G_{OL} = \frac{3}{2} \cdot \frac{1}{sC} \cdot \frac{1}{1+sT_C} \cdot \frac{K_{pDC}s+K_{iDC}}{s} \tag{55}$$

Realistically neglecting the current control dynamics by setting $T_C = 0$, the closed loop dynamics are described by:

$$G_{CL} = \frac{3}{2} \cdot \frac{K_{iDC}}{C} \cdot \frac{1+sT_{iDC}}{s^2+\frac{3}{2} \cdot \frac{K_{pDC}}{C} \cdot s+\frac{3}{2} \cdot \frac{K_{iDC}}{C}} \tag{56}$$

The equation above shows that the response is a second order with an added zero, which can be used to increase the phase margin around the cut off frequency to avoid instability and improve

the damping, also considering the simplifying assumptions that have been accepted compared to a real case [23].

Using the guidelines reported in [124], one can set $K_{pDC} = \frac{2}{3}\alpha_{DC}C$ and $K_{iDC} = \frac{2}{3}\alpha_{DC}^2 C$. Substitution in Eq. (55) shows that the BW becomes slightly lower than α_{DC}, while plugging the above into Eq. (56) yields a closed loop response governed by:

$$G_{CL} = \frac{\alpha_{DC}(s+\alpha_{DC})}{s^2+\alpha_{DC}s+\alpha_{DC}^2} \tag{57}$$

which characteristic equation has natural frequency $\omega_0 = \alpha_{DC}$ and damping ratio $\zeta = 0.5$. Examples of step response and Bode diagrams for BW = 100 rad/s and C = 50 ms are shown, for illustrative purposes in Figure 121 and Figure 122.

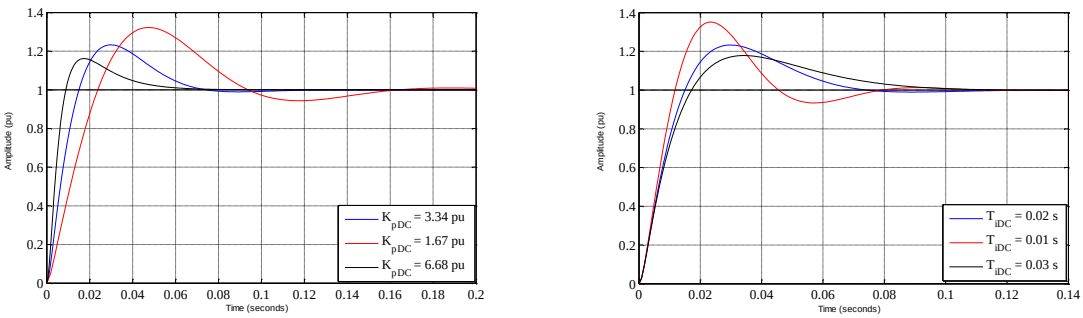

(a) Sensitivity to K_{pDC}. (b) Sensitivity to T_{iDC}.

Figure 121 - Example of step response for DC voltage controller.

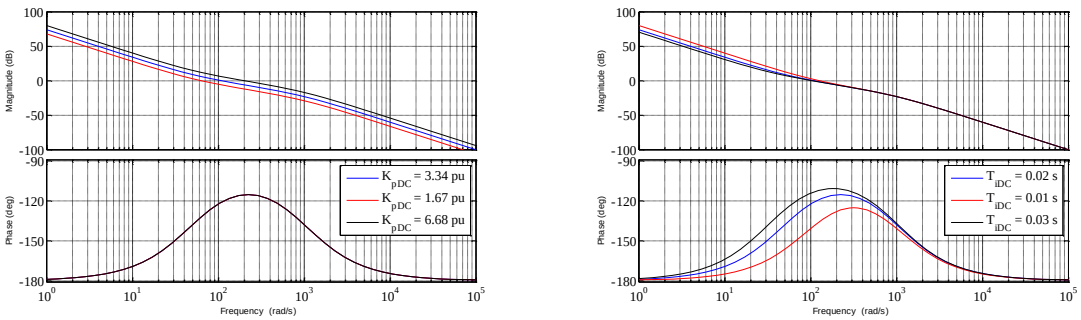

(a) Sensitivity to K_{pDC}. (b) Sensitivity to T_{iDC}.

Figure 122 - Example of open loop Bode diagram for DC voltage controller.

Appendix 4 Mathematical derivations

Example of small-signal model derivation for Chapter 4

An example of small-signal model derivations for the studies in Chapter 4 can be illustrated by using the electrical diagram sketched in Figure 123, which is the single line representation of the three-phase system. Balanced operation is considered. Bold letters indicate vectors. The impedances are complex numbers. As can be evinced by the figure, the active power droop is included – it will be exemplified for Option 2 only. The generic scheme with both voltage and current controller for the HVDC converter allows accommodating both Option 1 and Option 2. The power measurement may or may not be filtered by a first order block. The WPP converter only performs current control – power control can be added straightforwardly. The left capacitor C_L may, in reality, contain also a possible filter capacitance. However, for the reasons outlined in Chapter 4, it is assumed that only the cable contributes to the capacitance. The same simplification is clearly done on the WPP converter too. The configuration in Figure 123 essentially is, neglecting transformer shunt impedance and cable isolation losses, the one depicted in the bottom part of Figure 19.

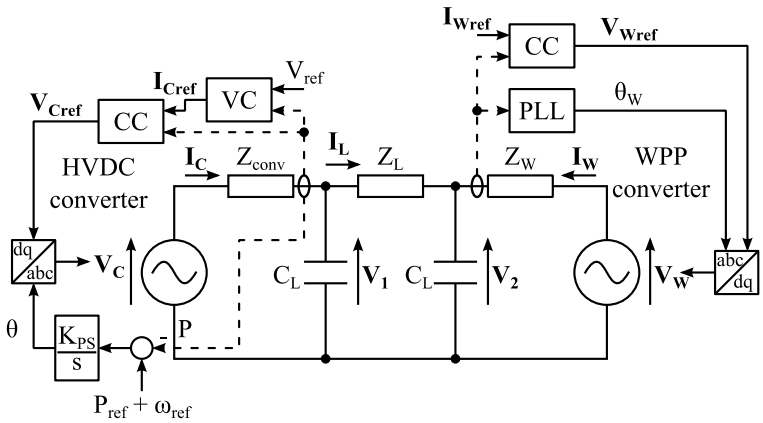

Figure 123 - Electrical and control diagram for small-signal derivations.

The series impedances are assumed to be resistive-inductive, i.e. $Z_{conv} = r_C + j\omega L_C$, $Z_L = r_L + j\omega L_L$ and $Z_W = r_W + j\omega L_W$. In the following, the derivation of the small signal model is exemplified for Option 1 and Option 2 with this simple system. Deriving the same kind of analysis on a larger system with several can be done along the same lines but results more tedious and laborious. It can be more conveniently done by building a model in e.g. Matlab/Simulink and linearising it with dedicated commands. PowerFactory, although featuring modal analysis, does so only for RMS models and does not allow performing linear analysis on EMT. Moreover, analytically deriving a mathematical model for a simple system provides better insight on some characteristics of the system and immediate feeling of the effect some of the parameters may have on the performance.

Network equations

Any of the busses can be chosen as reference for writing the network equations. Once they are expressed in the reference frame synchronous with such bus (SRF), their expression will be

independent of the chosen bus. Writing the equations in a vector form and dividing them along the two axes yields the following system:

$$C_L \frac{dv_{1d}}{dt} = i_{Cd} + i_{Ld} + \omega C_L v_{1q} \tag{58}$$

$$C_L \frac{dv_{1q}}{dt} = i_{Cq} + i_{Lq} - \omega C_L v_{1d} \tag{59}$$

$$L_L \frac{di_{Ld}}{dt} = v_{2d} - v_{1d} - r_L i_{Ld} + \omega L_L i_{Lq} \tag{60}$$

$$L_L \frac{di_{Lq}}{dt} = v_{2q} - v_{1q} - r_L i_{Lq} - \omega L_L i_{Ld} \tag{61}$$

$$C_L \frac{dv_{2d}}{dt} = i_{Wd} - i_{Ld} + \omega C_L v_{2q} \tag{62}$$

$$C_L \frac{dv_{2q}}{dt} = i_{Wq} - i_{Lq} - \omega C_L v_{2d} \tag{63}$$

$$L_W \frac{di_{Wd}}{dt} = v_{Wd} - v_{2d} - r_W i_{Wd} + \omega L_W i_{Wq} \tag{64}$$

$$L_W \frac{di_{Wq}}{dt} = v_{Wq} - v_{2q} - r_W i_{Wq} - \omega L_W i_{Wd} \tag{65}$$

Taking the HVDC converter control reference frame as overall reference, the *d*-axis will lie along $\mathbf{V_1}$ in case of control with Option 1, i.e. $\mathbf{V_1} = v_{1d} \cdot e^{j\theta}$, while it will be aligned with the vector $\mathbf{V_C}$ in case of control with Option 2, i.e. $\mathbf{V_C} = v_{Cd} \cdot e^{j\theta}$. The chosen reference system does clearly not have an impact on the eigen-properties of the system, but it does affect the mathematical handling of controllers operating on a different reference frame. The reference frame for the WPP converter controller is aligned with the voltage vector $\mathbf{V_2} = v_{2d} \cdot e^{j\theta_W}$. Calling *PQ* the reference frame where the WPP converter operates, a rotational transformation must be applied to bring the quantities expressed in *PQ* frame into the *dq* frame:

$$\mathbf{V_W} = T_{\theta w-\theta} \cdot \mathbf{V_{W,PQ}} \tag{66}$$

$$\mathbf{I_W} = T_{\theta w-\theta} \cdot \mathbf{I_{W,PQ}} \tag{67}$$

where the rotational matrix $T_{\theta w-\theta}$ is given by:

$$T_{\theta w-\theta} = \begin{bmatrix} \cos(\theta_W - \theta) & -\sin(\theta_W - \theta) \\ \sin(\theta_W - \theta) & \cos(\theta_W - \theta) \end{bmatrix} \tag{68}$$

Inversion of the relationships is immediate since the matrix is 2x2 and orthogonal.

HVDC converter control

Some assumptions are added here, in order to simplify the expressions:

- Perfect measurement for voltages and currents.
- Perfect modulation process, i.e. algebraic multiplication of DC voltage and modulation index, without additional delays.
- Division of the voltage references by the available DC voltage, providing decoupling between AC and DC system dynamics. In this way, the voltage references can directly be used, as a consequence of the previous assumption, as converter voltages.

Option 1

The lowest level of control (current control), generates converter voltages as follows:

$$v_{Cd} = u_{Cd} + v_{1d} - \omega L_C i_{Cq} \tag{69}$$
$$v_{Cq} = u_{Cq} + v_{1q} + \omega L_C i_{Cd} \tag{70}$$

The assumption is clearly to have decoupling of reactor voltage and feed-forward of the terminal voltage, as this is considered the basic structure from the analysis and Chapter 4. The current controller operates according to the following equations:

$$u_{Cd} = K_{pC} \cdot (i_{Cdref} - i_{Cd}) + x_{Cd} \tag{71}$$
$$\frac{dx_{Cd}}{dt} = \frac{K_{pC}}{T_{iC}} \cdot (i_{Cdref} - i_{Cd}) \tag{72}$$
$$u_{Cq} = K_{pC} \cdot \left(i_{Cqref} - i_{Cq}\right) + x_{Cq} \tag{73}$$
$$\frac{dx_{Cq}}{dt} = \frac{K_{pC}}{T_{iC}} \cdot \left(i_{Cqref} - i_{Cq}\right) \tag{74}$$

The voltage controller will operated similarly, but on the PCC voltage $\mathbf{V_1}$.

$$i_{Cdref} = i^*_{Cd} - \omega C_L v_{1q} \tag{75}$$
$$i_{Cqref} = i^*_{Cq} + \omega C_L v_{1d} \tag{76}$$
$$i^*_{Cd} = K_{pV} \cdot (v_{1dref} - v_{1d}) + x_{Vd} \tag{77}$$
$$\frac{dx_{Vd}}{dt} = \frac{K_{pV}}{T_{iV}} \cdot (v_{1dref} - v_{1d}) \tag{78}$$
$$i^*_{Cq} = K_{pV} \cdot \left(v_{1qref} - v_{1q}\right) + x_{Vq} \tag{79}$$
$$\frac{dx_{Vq}}{dt} = \frac{K_{pV}}{T_{iV}} \cdot \left(v_{1qref} - v_{1q}\right) \tag{80}$$

As can be seen, according to the strategy used in Chapter 4, the current feed-forward in Eqs. (75)-(76) is not utilised here. This concludes the representation of the HVDC converter control with Option 1.

Option 2

During normal operation, the control of the HVDC converter with Option 2 results in an even less elaborated model. Considering Eqs. (6)-(7), which describe the control law in normal operation, the following equations can be written:

$$v_{Cd} = v_{ref} - \frac{k_v}{T_v} i_{Cd} + \frac{k_v}{T_v} x_{vd} \tag{81}$$
$$v_{Cq} = - \frac{k_v}{T_v} i_{Cq} + \frac{k_v}{T_v} x_{vq} \tag{82}$$
$$\frac{dx_{vd}}{dt} = \frac{1}{T_v} \cdot (i_{Cd} - x_{vd}) \tag{83}$$
$$\frac{dx_{vq}}{dt} = \frac{1}{T_v} \cdot \left(i_{Cq} - x_{vq}\right) \tag{84}$$

The active power and voltage control are expressed by:

$$\frac{dv_{ref}}{dt} = K_e \cdot (V_{ACref} - |\mathbf{V_1}|) = K_e \cdot \left(V_{ACref} - \sqrt{v_{1d}^2 + v_{1q}^2}\right) \tag{85}$$

$$\frac{d\theta}{dt} = K_{PS} \cdot (P_{ref} - P) + \omega_{ref} = K_{PS} \cdot \left(P_{ref} - v_{1d} i_{Cd} - v_{1q} i_{Cq}\right) + \omega_{ref} \ (=\omega) \tag{86}$$

Of course, both equations above need to be linearized based on the initial operating point. The second equation results full decoupled from the rest of the system when $K_{PS} = 0$ and can thus be discarded in that case. As a consequence, the network equations (58)-(65) and control relations (69)-(84) become all linear. This concludes the description of Option 2's controller model.

WPP converter control

As mentioned above, the derivation of the equations of the WPP controller is slightly more complicated than for the HVDC, at least formally, due to the different coordinate system. However, it can proceed along the same lines.

The converter voltages in *dq* coordinates are given by Eq. (66), where the *PQ* coordinates converter voltage vector is generated by:

$$v_{WP} = u_{WP} + v_{2P} - \omega_W L_W i_{WQ} \tag{87}$$

$$v_{WP} = u_{WQ} + v_{2Q} + \omega_W L_W i_{WP} \tag{88}$$

while the current controller works according to the following relations:

$$u_{WP} = K_{pCW} \cdot (i_{WPref} - i_{WP}) + x_{WP} \tag{89}$$

$$\frac{dx_{WP}}{dt} = \frac{K_{pCW}}{T_{iCW}} \cdot (i_{WPref} - i_{WP}) \tag{90}$$

$$u_{WQ} = K_{pCW} \cdot \left(i_{WQref} - i_{WQ}\right) + x_{WQ} \tag{91}$$

$$\frac{dx_{WQ}}{dt} = \frac{K_{pCW}}{T_{iCW}} \cdot \left(i_{WQref} - i_{WQ}\right) \tag{92}$$

where K_{pCW} and T_{iCW} have been used to distinguish them from the HVDC converter's gain and time constant. In Eqs. (87)-(88) the factor ω_W (which consists of several states – see PLL equations below) can be substituted by a constant value depending on how the controller works. By using Eq. (66) and combining Eqs. (87)-(92) the vector $\mathbf{V_W}$ is created by:

$$\begin{aligned} v_{Wd} = {} & K_{pCW} \cos(\theta_W - \theta)\, i_{WPref} - K_{pCW} \sin(\theta_W - \theta)\, i_{WQref} - K_{pCW} i_{Wd} - \omega_W L_W i_{Wq} + \\ & + \cos(\theta_W - \theta)\, x_{WP} - \sin(\theta_W - \theta)\, x_{WQ} + v_{2d} \end{aligned} \tag{93}$$

$$\begin{aligned} v_{Wq} = {} & K_{pCW} \sin(\theta_W - \theta)\, i_{WPref} + K_{pCW} \cos(\theta_W - \theta)\, i_{WQref} - K_{pCW} i_{Wq} + \omega_W L_W i_{Wd} + \\ & + \sin(\theta_W - \theta)\, x_{WP} + \cos(\theta_W - \theta)\, x_{WQ} + v_{2q} \end{aligned} \tag{94}$$

The last equations that need be derived to complete the model are those describing the dynamics of the PLL. Since a standard PLL is used in PowerFactory [128], it operates according to:

$$\frac{dx_{PLL}}{dt} = K_{iPLL} v_{2Q} = K_{iPLL} \cdot \left[-v_{2d} \sin(\theta_W - \theta) + v_{2q} \cos(\theta_W - \theta) \right] \tag{95}$$

$$\frac{d\theta_W}{dt} = K_{pPLL} v_{2Q} + x_{PLL} = K_{iPLL} \cdot \left[-v_{2d} \sin(\theta_W - \theta) + v_{2q} \cos(\theta_W - \theta) \right] + x_{PLL} \ (=\omega_W) \tag{96}$$

It is apparent that even with constant frequency (Option 1 or Option 2 with $K_{PS} = 0$) and assuming the usage of a constant frequency for the decoupling in Eqs. (87)-(88), the system is non-linear and hence needs linearization for construction of the small-signal model, which is performed based on initial steady-state power flow conditions.

The small-signal dynamics will be described by the usual relation:

$$\dot{\mathbf{x}} = \mathbf{A}\cdot\mathbf{x} + \mathbf{B}\cdot\mathbf{u} \tag{97}$$

The state vector will be:

- For Option 1:
  $\mathbf{x}=[i_{Cd}\ \ i_{Cq}\ \ v_{1d}\ \ v_{1q}\ \ i_{Ld}\ \ i_{Lq}\ \ v_{2d}\ \ v_{2q}\ \ i_{Wd}\ \ i_{Wq}\ \ x_{Cd}\ \ x_{Cq}\ \ x_{Vd}\ \ x_{Vq}\ \ x_{WP}\ \ x_{WQ}\ \ x_{PLL}\ \ \theta_W]^T$
- For Option 2:
  $\mathbf{x}=[i_{Cd}\ \ i_{Cq}\ \ v_{1d}\ \ v_{1q}\ \ i_{Ld}\ \ i_{Lq}\ \ v_{2d}\ \ v_{2q}\ \ i_{Wd}\ \ i_{Wq}\ \ x_{vd}\ \ x_{vq}\ \ v_{ref}\ \ \theta\ \ x_{WP}\ \ x_{WQ}\ \ x_{PLL}\ \ \theta_W]^T$

The input vector will be:

- For Option 1:
  $\mathbf{u}=[v_{1dref}\ \ v_{1qref}\ \ i_{WPref}\ \ i_{WQref}]^T$
- For Option 2:
  $\mathbf{u}=[V_{ACref}\ \ P_{ref}\ \ i_{WPref}\ \ i_{WQref}]^T$

The system matrices **A** and **B** can be derived by all equations in this section, making sure the states (angles) generated by Eq. (86) and (96), as well as their derivative specified by the same equations (frequencies) are correctly used in the linearized version of all equations. Moreover, the initial power flow solution can be determined analytically or by dedicated software. Once the model is set up, it can be used for linear analysis.

Derivations for Section 5.2.3 (continuous AC voltage control).

The simple calculations in this section were obtained by particularising the more general formulae found e.g. in [131] for the particular case of P = 0 and lossless impedances.

When reactive load Q_L is connected to the grid Thevenin equivalent in the right part of Figure 50 the steady-state operation is governed by the equation:

$$V_{AC}^2 - V_g V_{AC} + Q_L X_g = 0 \tag{98}$$

Solving such equation for V_{AC} yields:

$$V_{AC} = V_g \cdot \frac{1 + \sqrt{1 - 4\frac{Q_L X_g}{V_g^2}}}{2} \approx V_g \cdot \left(1 - \frac{Q_L X_g}{V_g^2}\right) = V_g \cdot (1 + \Delta V_{AC}) \tag{99}$$

where the approximation is obtained by Taylor expansion considering small perturbations around $Q_L = 0$. Realistically assuming $V_g = 1$ pu, Eq. (20) follows immediately.

If, on top of the reactive power Q_L, the contribution of the converter through droop control is also included, Eq. (98) takes the form:

$$V_{AC}^2 - V_{AC} V_g + Q_L X_g + K_{AC} X_g \cdot (V_{AC} - V_g) = 0 \tag{100}$$

Notice that in the above equation it is assumed that the converter P is equal to zero. As demonstrated in Chapter 4 this assumption is a sound one only in relatively strong networks.

By considering small variations of the PCC voltage about 1 pu, i.e. $K_{AC} \approx K_{AC} V_{AC}$, and rearranging the terms, the equation becomes:

$$V_{AC}^2 - V_{AC} V_g + \frac{Q X_g}{1 + K_{AC} X_g} = 0 \tag{101}$$

Comparing this with Eq. (98), the approximate formula in Eq. (21) is obtained directly, yielding the SCP contribution from an AC voltage droop controlled VSC.

Derivation of circles in Figure 59 **(long-term voltage stability).**

Writing the complete complex form of Eq. (25), keeping in mind V_g is real:

$$V'_{eqr} + jV'_{eqi} = V_g + Z_{LN2}(I_{Cr}\cos\theta_{LN2} - I_{Ci}\sin\theta_{LN2}) + jZ_{LN2}(I_{Ci}\cos\theta_{LN2} + I_{Cr}\sin\theta_{LN2}) \tag{102}$$

Calculating the square of the magnitude of both sides yields:

$$V_{eq}'^2 = \left(V_g + Z_{LN2}(I_{Cr}\cos\theta_{LN2} - I_{Ci}\sin\theta_{LN2})\right)^2 + \left(Z_{LN2}(I_{Ci}\cos\theta_{LN2} + I_{Cr}\sin\theta_{LN2})\right)^2 \tag{103}$$

Computing the squares gives:

$$V_{eq}^{'2} = V_g^2 + Z_{LN2}^2\left(I_{Cr}^2 + I_{Ci}^2\right) + 2V_g Z_{LN2}(I_{Cr}\cos\theta_{LN2} - I_{Ci}\sin\theta_{LN2}) \tag{104}$$

Dividing by Z^2_{LN2}, posing $V_g^2 = V_g^2\left(\cos^2\theta_{LN2} + \sin^2\theta_{LN2}\right)$ and lumping the squares, Eq. (28) is finally obtained.

Derivations of coefficients k_{xy} in Section 7.2 (linearized model for POD).

To derive the four coefficients in Eq. (34), the expression of the SG's electrical torque (power) has to be written in non-linear form. Reference is made to the system in Figure 77. Depending on whether the expression is written using the terminal voltage, the VSC voltage or the infinite bus voltage, the electrical torque is determined by the following:

$$T_e = P_e = \frac{E_q^{'} V_C}{kx_L + x_T + x_d^{'}} \cdot \sin\theta_C + \frac{V_C^2}{2} \cdot \frac{x_d^{'} - x_q}{(kx_L + x_T + x_d^{'})(kx_L + x_T + x_q)} \cdot \sin 2\theta_C \quad (105)$$

$$T_e = P_e = \frac{E_q^{'} V_t}{x_T + x_d^{'}} \cdot \sin\theta + \frac{V_t^2}{2} \cdot \frac{x_d^{'} - x_q}{(x_T + x_d^{'})(x_T + x_q)} \cdot \sin 2\theta \quad (106)$$

$$T_e = P_e = \frac{E_q^{'} V_{th}}{x_E + x_d^{'}} \cdot \sin\delta + \frac{V_{th}^2}{2} \cdot \frac{x_d^{'} - x_q}{(x_E + x_d^{'})(x_E + x_q)} \cdot \sin 2\delta \quad (107)$$

where $x_E = x_T + x_L$. Obviously, when k = 0, the Eqs. (105) and (106) are perfectly equivalent, besides yielding the same value of the torque. In Eq. (107) the infinite bus voltage V_B is substituted for by a Thevenin equivalent voltage V_{th}, which takes into account the initial power injection from the VSC.

The small-signal expression of the magnitude of SG terminal voltage and VSC voltage as a function of their *dq* components is given by:

$$V_t = \left.\frac{v_d}{V_t}\right|_0 \cdot v_d + \left.\frac{v_q}{V_t}\right|_0 \cdot v_q \quad (108)$$

$$V_C = \left.\frac{v_{Cd}}{V_C}\right|_0 \cdot v_{Cd} + \left.\frac{v_{Cq}}{V_{Ct}}\right|_0 \cdot v_{Cq} \quad (109)$$

where the subscript 0 denotes the initial operating point. For simplicity, in this Appendix, no distinction is made in the nomenclature between the variables and the small perturbations, as the text should be self-explaining. Eq. (108) will be useful later to determine the four coefficients in Eq. (35).

The coefficients $k_{Pe\delta}$ and $k_{PeE'q}$ of Eq. (34) immediately derive from linearization of Eq. (107), analogously to the same coefficients derived in [76]:

$$k_{Pe\delta} = \left.\frac{E_q^{'} V_{th}}{x_E + x_d^{'}} \cdot \cos\delta + \frac{V_{th}^2 (x_d^{'} - x_q)}{(x_E + x_d^{'})(x_E + x_q)} \cdot \cos 2\delta\right|_0 \quad (110)$$

$$k_{PeE'q} = \left.\frac{V_{th}}{x_E + x_d^{'}} \cdot \sin\delta\right|_0 \quad (111)$$

The other coefficients involve the P and Q injection of the VSC. To derive the necessary relations accounting for them, the equivalent, small-signal, circuit in Figure 124 can be used. The VSC is modelled as an ideal current source, since its control dynamics are much faster than electromechanical phenomena related to POD. All voltages are phasors and the impedances are assumed to be lossless. As V_{th} includes the initial power flow of the VSC, I_C only represents the

small variations of VSC current. The effect of the initial power on the small-signal behaviour is neglected here and will be qualitatively described below.

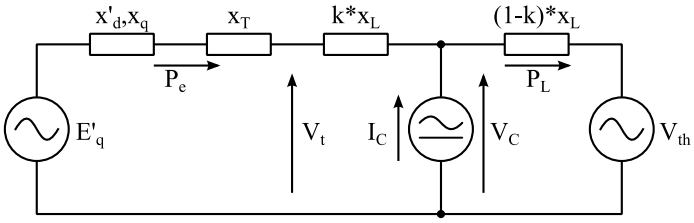

Figure 124 - Equivalent small-signal electrical diagram of simple system.

Disregarding saturation and other non-linear phenomena one can decouple the analysis according to the SG's axes and apply the superposition principle. The d- and q-axis equivalent diagrams are shown in Figure 125. The magnitude of the voltage sources is derived by observation of Figure 79.

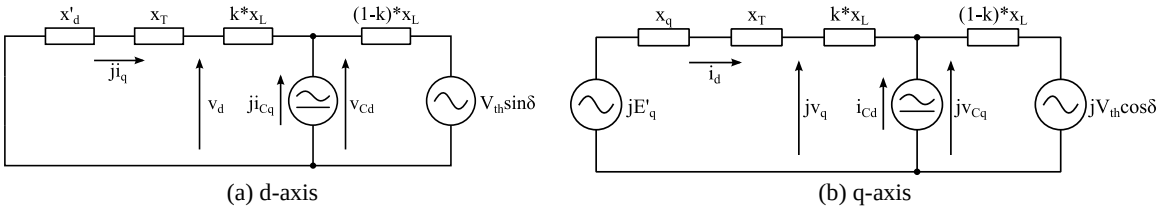

(a) d-axis (b) q-axis

Figure 125 - Decoupled equivalent circuit.

Firstly, it is necessary to express the VSC currents along the two coordinates as a function of the control variables directly utilised for POD control, i.e. P and Q. Since the VSC control axes are clamped to the voltage V_C by the PLL, the following holds:

$$i_{Cd} = \frac{P}{V_C} \cdot \sin\theta_C + \frac{Q}{V_C} \cdot \cos\theta_C \tag{112}$$

$$i_{Cq} = \frac{P}{V_C} \cdot \cos\theta_C - \frac{Q}{V_C} \cdot \sin\theta_C \tag{113}$$

Under the assumption of neglecting the initial VSC power injection, the small-signal VSC currents along the SG's field coordinates will be:

$$i_{Cd} = \left.\frac{\sin\theta_C}{V_C}\right|_0 \cdot P + \left.\frac{\cos\theta_C}{V_C}\right|_0 \cdot Q \tag{114}$$

$$i_{Cq} = \left.\frac{\cos\theta_C}{V_C}\right|_0 \cdot P - \left.\frac{\sin\theta_C}{V_C}\right|_0 \cdot Q \tag{115}$$

Considering Figure 125 and applying the superposition principle, the SG terminal voltage can be expressed, along the two axes, as:

$$v_d = V_{th}\sin\delta \cdot \left(1 - \frac{x_L}{x_E + x_q}\right) - i_{Cq} \cdot \frac{x_L(1-k)(x_T + x_q)}{x_E + x_q} \tag{116}$$

$$v_q = V_{th}\cos\delta \cdot \left(1 - \frac{x_L}{x_E + x_d'}\right) + E_q' \cdot \frac{x_L}{x_L + x_d'} + i_{Cd} \cdot \frac{x_L(1-k)(x_T + x_d')}{x_E + x_d'} \tag{117}$$

The same can be done for the VSC voltage, yielding the following:

$$v_{Cd} = V_{th} \sin\delta \cdot \left[1 - \frac{x_L(1\text{-}k)}{x_E+x_q}\right] - i_{Cq} \cdot \frac{x_L(1\text{-}k)\left(x_T+x_q+kx_L\right)}{x_E+x_q} \tag{118}$$

$$v_{Cq} = V_{th} \cos\delta \cdot \left[1 - \frac{x_L(1\text{-}k)}{x_E+x_d^{'}}\right] + E_q^{'} \cdot \frac{x_L(1\text{-}k)}{x_L+x_d^{'}} + i_{Cd} \cdot \frac{x_L(1\text{-}k)\left(x_T+x_d^{'}+kx_L\right)}{x_E+x_d^{'}} \tag{119}$$

Applying the chain rule to Eq. (105):

$$k_{PeP} = \left.\frac{dT_e}{dV_C}\right|_0 \cdot \left.\frac{dV_C}{dP}\right|_0 + \left.\frac{dT_e}{d\theta_C}\right|_0 \cdot \left.\frac{d\theta_C}{dP}\right|_0 \tag{120}$$

$$k_{PeQ} = \left.\frac{dT_e}{dV_C}\right|_0 \cdot \left.\frac{dV_C}{dQ}\right|_0 + \left.\frac{dT_e}{d\theta_C}\right|_0 \cdot \left.\frac{d\theta_C}{dQ}\right|_0 \tag{121}$$

The first terms on the right hand side of the above equations directly stem from the linearization of Eq. (105) and inserting Eqs. (114) and (115) into Eqs. (118) and (119). The rightmost terms also need the expression of the angle θ_C. By trigonometry, from Figure 79:

$$\theta_C = \tan^{-1}\frac{v_{Cd}}{v_{Cq}} \tag{122}$$

Proceeding as stated, one obtains:

$$\left.\frac{dT_e}{dV_C}\right|_0 = \frac{E_q^{'}}{x_T+x_d^{'}+kx_L}\sin\theta_C + V_C\left.\frac{x_d^{'}\text{-}x_q}{\left(x_T+x_d^{'}+kx_L\right)\left(x_T+x_q+kx_L\right)}\sin 2\theta_C\right|_0 \tag{123}$$

$$\left.\frac{dT_e}{d\theta_C}\right|_0 = \frac{V_C E_q^{'}}{x_T+x_d^{'}+kx_L}\cos\theta_C + V_C^2\left.\frac{x_d^{'}\text{-}x_q}{\left(x_T+x_d^{'}+kx_L\right)\left(x_T+x_q+kx_L\right)}\cos 2\theta_C\right|_0 \tag{124}$$

$$\left.\frac{dV_C}{dP}\right|_0 = \frac{1}{V_C^2}\left.\left[-v_{Cd}\cdot\frac{x_L(1\text{-}k)\left(x_T+x_q+kx_L\right)}{x_E+x_q}\cdot\cos\theta_C + v_{Cq}\cdot\frac{x_L(1\text{-}k)\left(x_T+x_d^{'}+kx_L\right)}{x_E+x_d^{'}}\cdot\sin\theta_C\right]\right|_0 \tag{125}$$

$$\left.\frac{dV_C}{dQ}\right|_0 = \frac{1}{V_C^2}\left.\left[v_{Cd}\cdot\frac{x_L(1\text{-}k)\left(x_T+x_q+kx_L\right)}{x_E+x_q}\cdot\sin\theta_C + v_{Cq}\cdot\frac{x_L(1\text{-}k)\left(x_T+x_d^{'}+kx_L\right)}{x_E+x_d^{'}}\cdot\cos\theta_C\right]\right|_0 \tag{126}$$

$$\left.\frac{d\theta_C}{dP}\right|_0 = \frac{1}{V_C^3}\left.\left[-v_{Cq}\cdot\frac{x_L(1\text{-}k)\left(x_T+x_q+kx_L\right)}{x_E+x_q}\cdot\cos\theta_C - v_{Cd}\cdot\frac{x_L(1\text{-}k)\left(x_T+x_d^{'}+kx_L\right)}{x_E+x_d^{'}}\cdot\sin\theta_C\right]\right|_0 \tag{127}$$

$$\left.\frac{d\theta_C}{dQ}\right|_0 = \frac{1}{V_C^3}\left.\left[v_{Cq}\cdot\frac{x_L(1\text{-}k)\left(x_T+x_q+kx_L\right)}{x_E+x_q}\cdot\sin\theta_C - v_{Cd}\cdot\frac{x_L(1\text{-}k)\left(x_T+x_d^{'}+kx_L\right)}{x_E+x_d^{'}}\cdot\cos\theta_C\right]\right|_0 \tag{128}$$

The last relationships are obtained by applying the chain derivation rule to Eq. (122). Combining Eqs. (123)-(128) into Eqs. (120)-(121) yields the last two coefficients of Eq. (34).

As for the coefficients of Eq. (35), using Eq. (108) and (116)-(117) the following relations are derived:

$$k_{Vt\delta} = \left.\frac{dV_t}{d\delta}\right|_0 = \left.\frac{v_d}{V_t}\cdot V_{th}\cdot\left(1-\frac{x_L}{x_E+x_q}\right)\cdot\cos\delta - \frac{v_q}{V_t}\cdot V_{th}\cdot\left(1-\frac{x_L}{x_E+x_d^{'}}\right)\cdot\sin\delta\right|_0 \quad (129)$$

$$k_{VtE'q} = \left.\frac{dV_t}{dE_q^{'}}\right|_0 = \left.\frac{v_q}{V_t}\cdot\frac{x_L}{x_E+x_d^{'}}\right|_0 \quad (130)$$

$$k_{VtP} = \left.\frac{dV_t}{dP}\right|_0 = \left.\frac{1}{V_t^2}\left[-v_{Cd}\cdot\frac{x_L(1-k)(x_T+x_q)}{x_E+x_q}\cdot\cos\theta_C + v_{Cq}\cdot\frac{x_L(1-k)(x_T+x_d^{'})}{x_E+x_d^{'}}\cdot\sin\theta_C\right]\right|_0 \quad (131)$$

$$k_{VtQ} = \left.\frac{dV_C}{dQ}\right|_0 = \left.\frac{1}{V_t^2}\left[v_{Cd}\cdot\frac{x_L(1-k)(x_T+x_q)}{x_E+x_q}\cdot\sin\theta_C + v_{Cq}\cdot\frac{x_L(1-k)(x_T+x_d^{'})}{x_E+x_d^{'}}\cdot\cos\theta_C\right]\right|_0 \quad (132)$$

In more complex systems, the coefficients derived analytically in this Appendix are more conveniently computed numerically or by simulations.

One underlying assumption is neglecting the initial power of the VSC in the small-signal derivations. To the author's experience, such assumption usually guarantees reasonably accurate results, at least in terms of assessment of the effect the P and Q modulation have on the critical eigenvalue of the system. More attention must be paid when either of the following happens: (i) the AVR has low gains, (ii) the POD gains are high, (iii) the POD is implemented by modulation of Q.

Derivation of transfer function $G_{DC}(s)$ in Section 7.3.3.

The overall DC system transfer function to be plugged into the right hand side of Eq. (42) can be derived quite easily by accepting a few assumptions:

- The whole offshore HVDC converter has infinite BW, i.e. the power is instantaneously evacuated from its AC side to its DC side. This is justified by the findings in Chapter 4.
- The current controller of the onshore HVDC converter is ideal too, and only the DC voltage control dynamics are relevant. This is justified by usual current control BWs (≥ 1000 rad/s) as compared to POD frequencies.
- The operation is with V_{DC} = 1 pu. This, though being quite a rough approximation, allows for some formal simplifications, since DC current and power are equivalent. This assumption should definitely be borne in mind when analysing the results.
- Shunt losses are neglected in the DC cable.

With the above hypotheses, the diagram in Figure 126 can be used to derive the transfer function between the power entering the AC terminals of the offshore HVDC converter and the power reaching the AC terminals of the onshore HVDC converter.

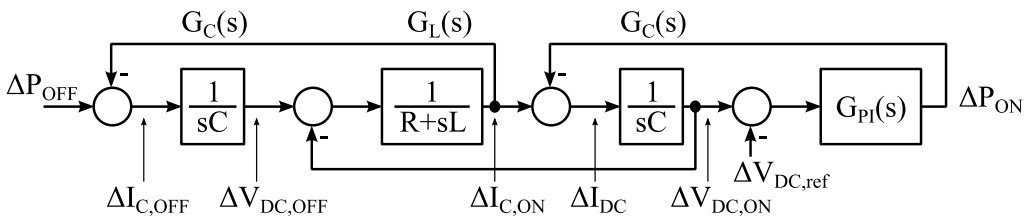

Figure 126 - Block diagram for calculation of DC system approximated transfer function.

The meaning of blocks and parameters is clear: C is the total capacitance at the converters' DC side (converter C_{DC} in Appendix 1 + half cable), while R and L are the series electrical parameters

of the DC line (R_{DC} and L_{DC} in Appendix 2, multiplied by the cable length). The transfer function $G_{PI}(s) = K_p \cdot \left(1 + \frac{1}{sT_i}\right)$ represents the DC voltage controller.

By assuming $\Delta V_{DC,ref} = 0$ and progressively reducing the system, the following overall transfer function can be derived with simple mathematical manipulations (Laplace operator neglected for brevity):

$$G_{DC} = \frac{G_C^2 G_L G_{PI}}{1 + G_C G_{PI} + G_C G_L (2 + G_C G_{PI})} \tag{133}$$

Such transfer function can then be used in Eq. (42) to generate the $G_{ACT}(s)$, which is then plugged into the open loop transfer function for assessment of the closed loop stability.

Appendix 5 Additional figures

Additional figures for Chapter 4

Section 4.3.2(b) – Effect of export cable length for basic Option 1

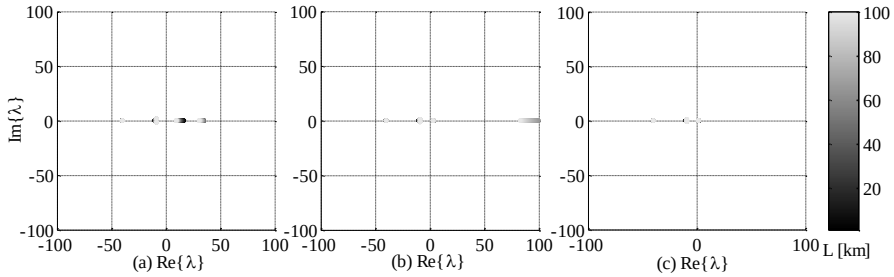

Figure 127 - Option 1: Effect of export cable length on system eigenvalues with default voltage control parameters: (a) P = 300 MW, (b) P = 600 MW and (c) P = 1000 MW.

Section 4.3.2(d) – Sensitivity analysis for Option 2

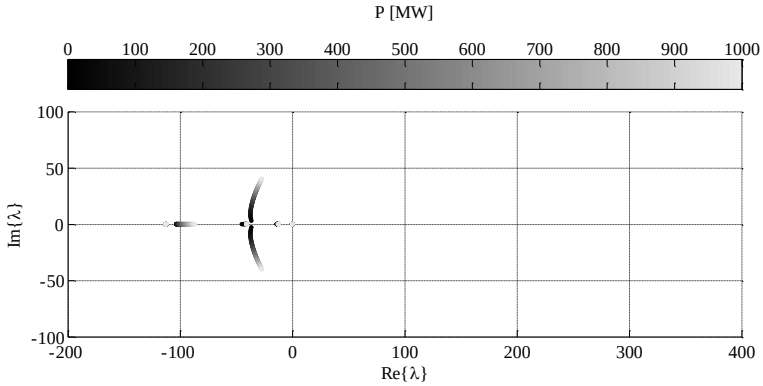

Figure 128 - Option 2: Effect of WPP active power production on system eigenvalues.

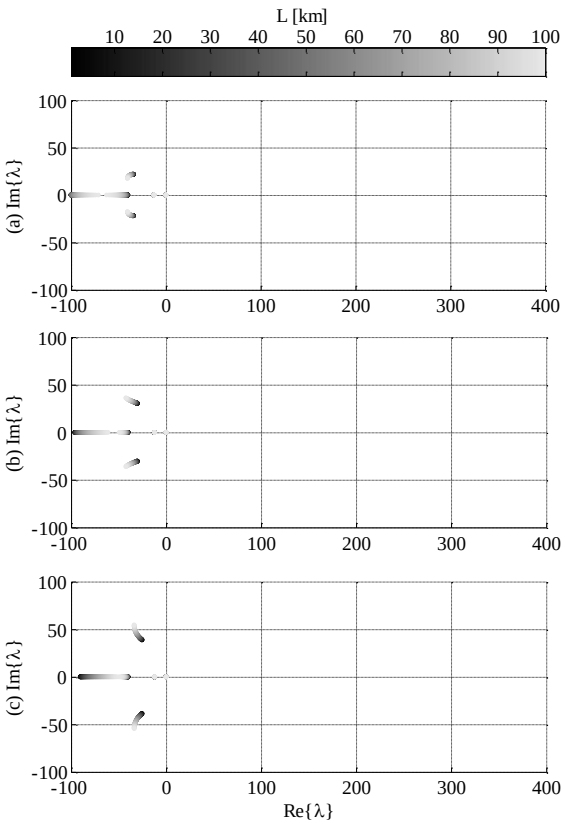

Figure 129 - Option 2: Effect of export cable length on system eigenvalues: (a) P = 300 MW, (b) P = 600 MW and (c) P = 1000 MW.

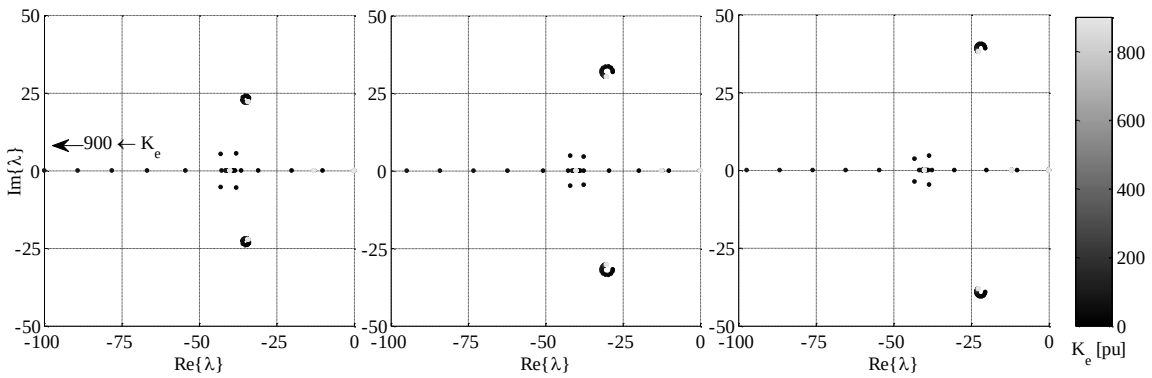

Figure 130 - Option 2: Effect of voltage control gain K_e on system eigenvalues: (a) P = 300 MW, (b) P = 600 MW and (c) P = 1000 MW.

Section 4.3.2(f) – Linear analysis of Option 2 with power-frequency droop

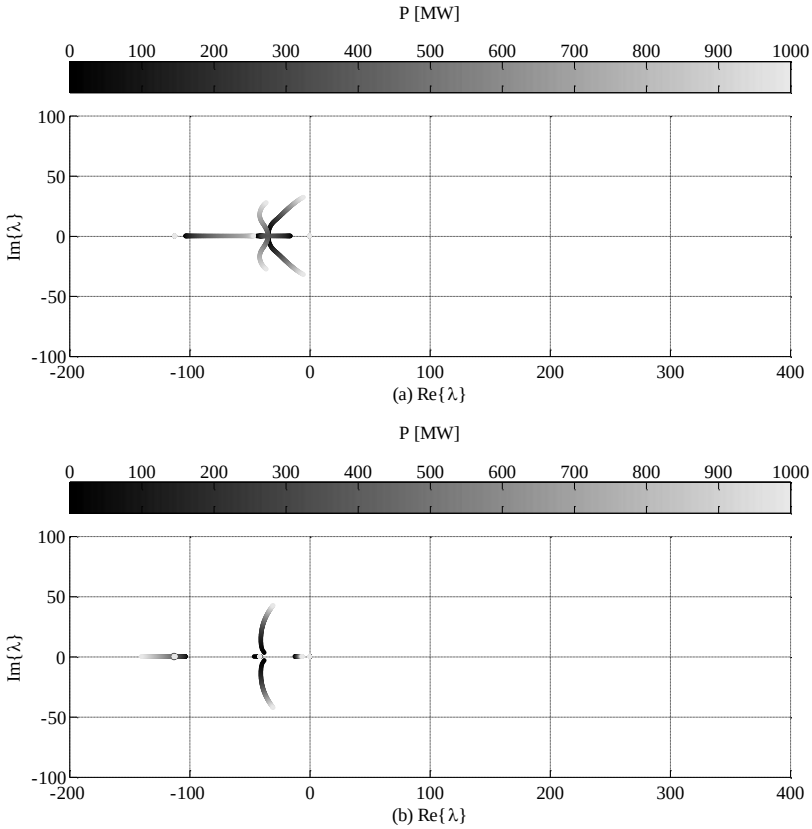

Figure 131 - Option 2: Effect of WPP active power production on system eigenvalues with power-frequency droop with (a) K_{PS} = 100 pu/s and (b) K_{PS} = -100 pu/s.

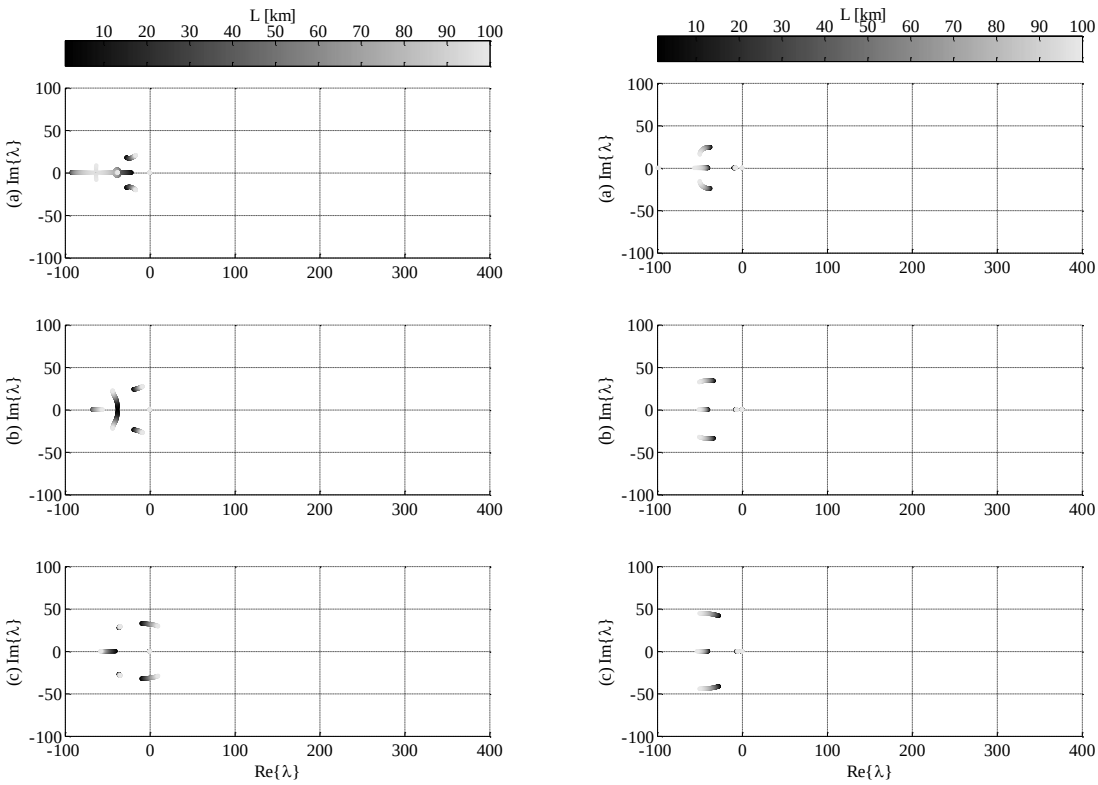

Figure 132 - Option 2: Effect of export cable length on system eigenvalues with power-frequency droop: (a) P = 300 MW, (b) P = 600 MW and (c) P = 1000 MW. Left: K_{PS} = 100 pu/s. Right: K_{PS} = -100 pu/s.

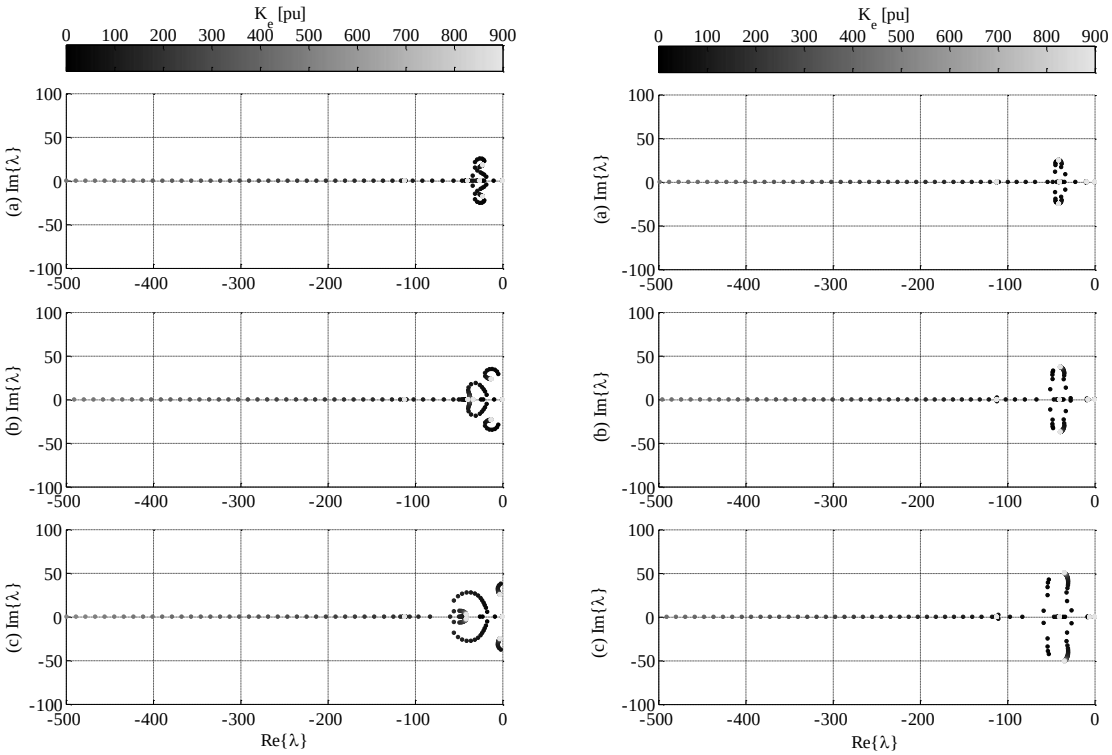

Figure 133 - Option 2: Effect of voltage control gain K_e on system eigenvalues with power-frequency droop: (a) P = 300 MW, (b) P = 600 MW and (c) P = 1000 MW. Left: K_{PS} = 100 pu/s. Right: K_{PS} = -100 pu/s.

Section 4.3.3 – Time domain simulation of Option 2 with power-frequency droop

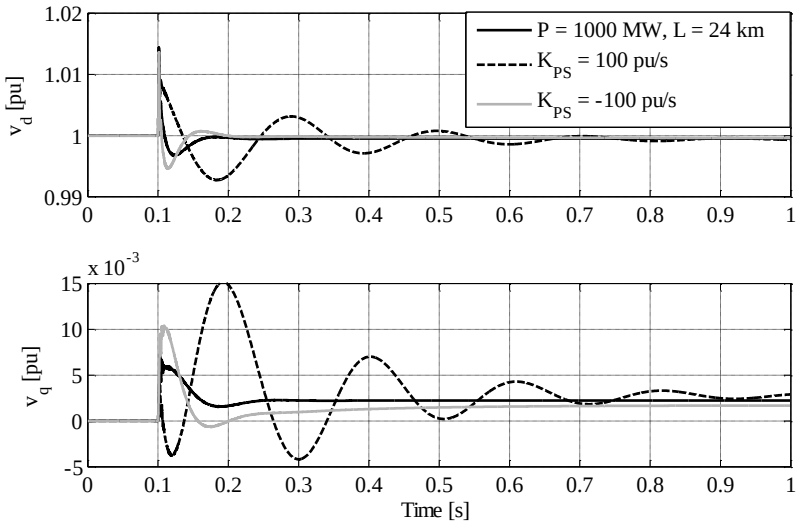

Figure 134 - Time domain verification of linear analysis for Option 2 with power-frequency droop. Black solid plot: P = 1000 MW and L = 24 km. Dashed: K_{PS} = 100 pu/s. Grey: K_{PS} = -100 pu/s.

Section 4.4.3 – Time domain simulations of system with multiple HVDC

Lower proportional gain with Case A

Case A was repeated by halving the voltage control proportional gain: K_{pV} = 1 pu. The results are shown in Figure 135. It is noticed that with a slower control action oscillations tend to institute more easily. This highlights the need for high control gains and therefore control scheduling when utilising Option 1. An alternative could be the use of feed-forward of the transformer currents, as for example executed in [120]. However, the feed-forward seemed to bring about instability and was not included here. Future work could add it.

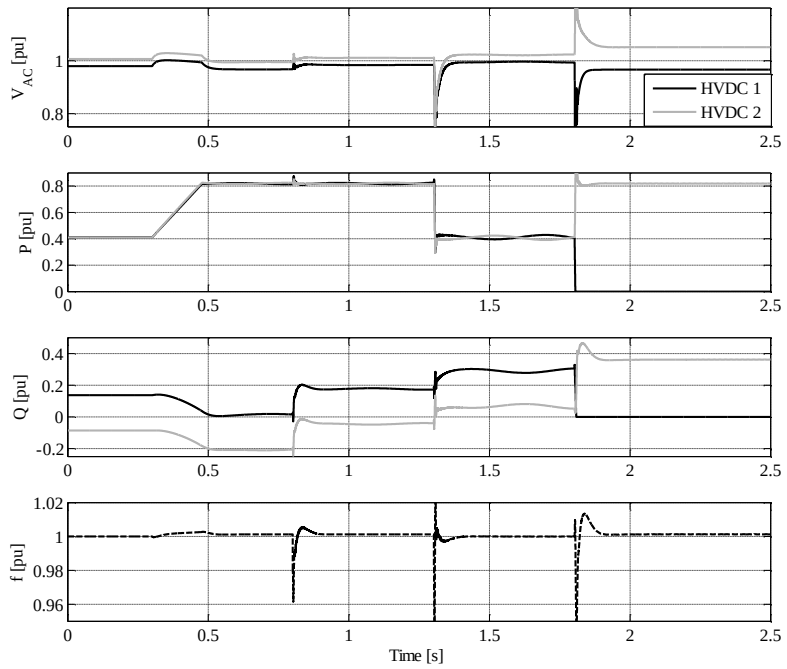

Figure 135 - Case A with K_{pV} = 1.0 pu.

Halved converter transformer impedance

The second sensitivity analysis that was conducted was a reduction of the converter transformer impedance, which halves the electrical separation between the voltage controlled terminals. The results are depicted in Figure 136 and Figure 137 for Case A and B respectively. It can be seen that reducing the electrical distance appears disadvantageous, particularly for Case A, where a potentially unstable phenomenon happens after the load rejection and is neutralised by the HVDC converter outage. This happens quite expectedly, as the interaction between converters is greater when their controlled nodes lie closer to one another. Case B performance, though slightly worse than in the base case, remains reasonable unaffected by the significant change in impedance. Adding the derivative part of the reactive power droop with K_{dV} = 0.001 pu, T_{dV} = 0.01 s and T_{fV} = 0.002 s improves the performance for Case A, as illustrated by Figure 138.

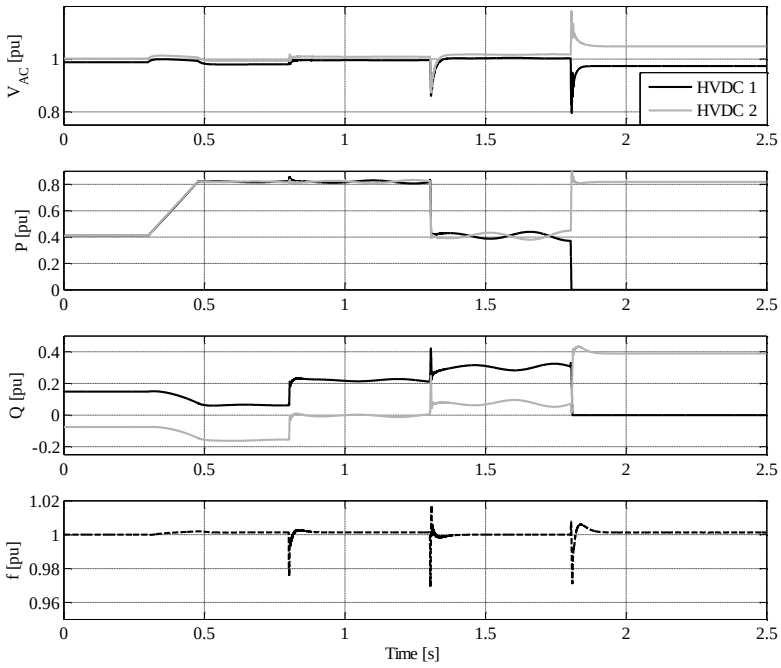

Figure 136 - Case A with halved converter transformer impedance.

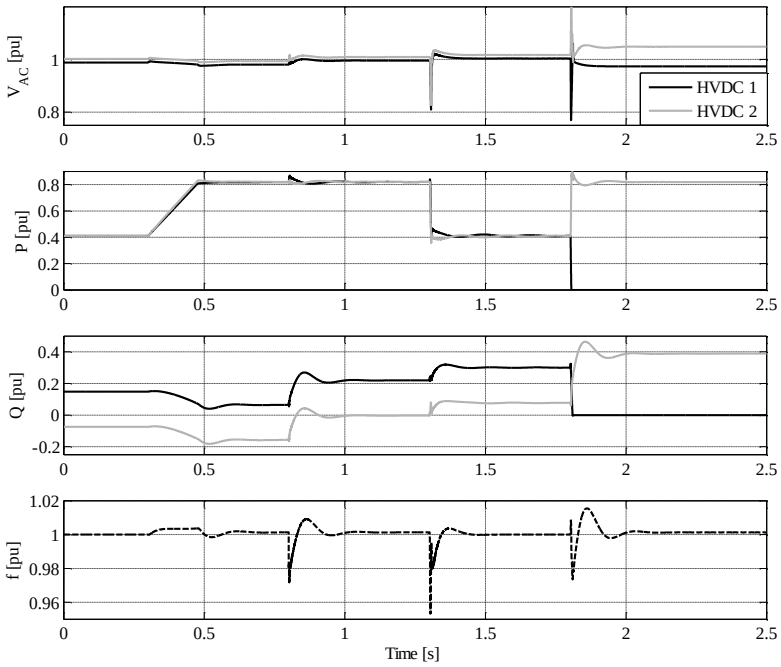

Figure 137 - Case B with halved converter transformer impedance.

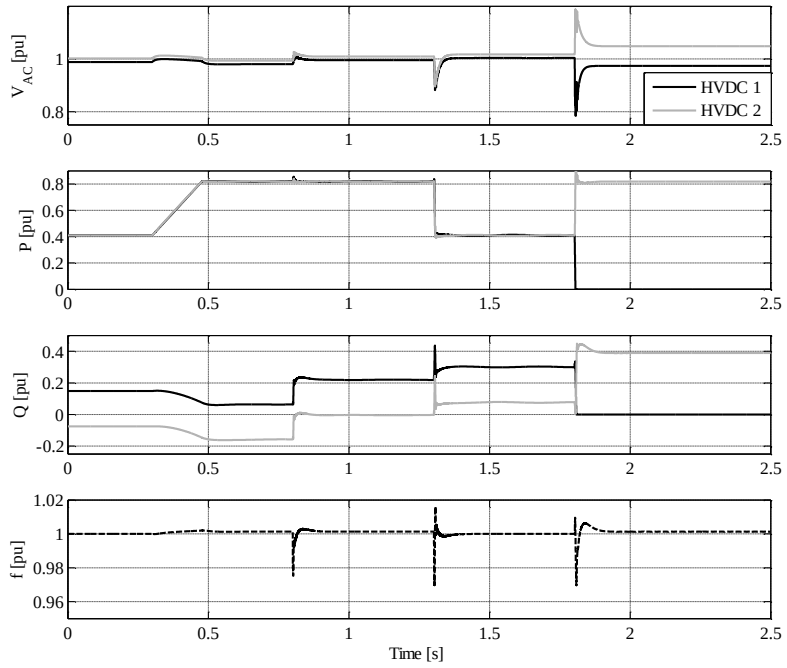

Figure 138 - Case A with halved converter transformer impedance and additional derivative droop.

Augmented interlink length

The interlink length was then increased from L = 0.5 km to L = 20 km and the behaviour of Case A and B against such variation is shown in Figure 139 and Figure 140 respectively.

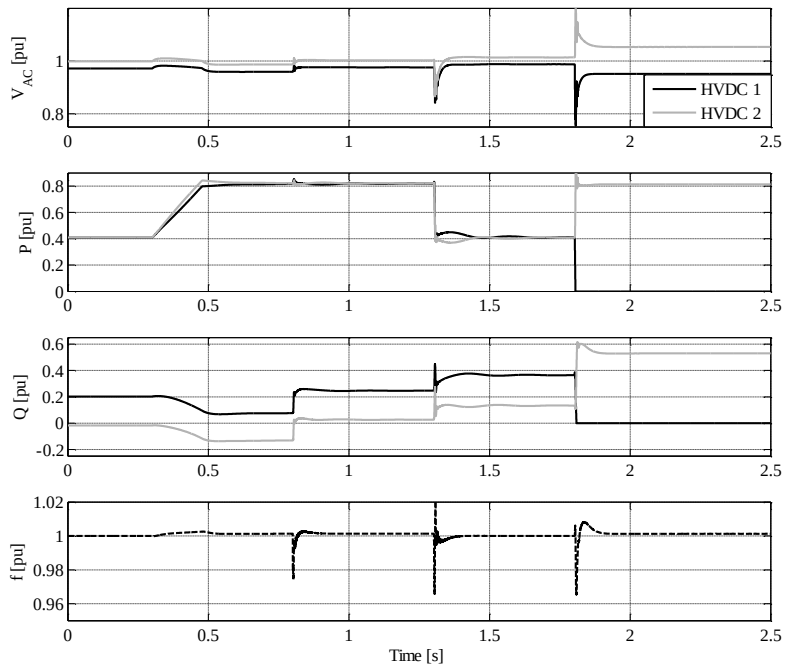

Figure 139 - Case A with longer interlink cable (L = 20km).

Considering the relatively large value of the transformer impedances with respect to the interlink cable, the results are understandably similar to the base case.

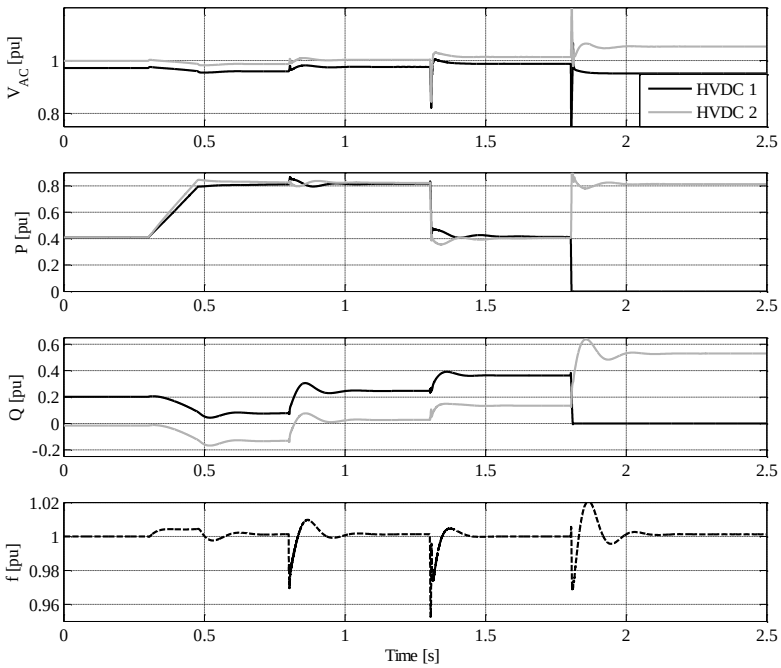

Figure 140 - Case B with longer interlink cable (L = 20km).

<u>Different active and reactive power sharing between HVDC stations</u>

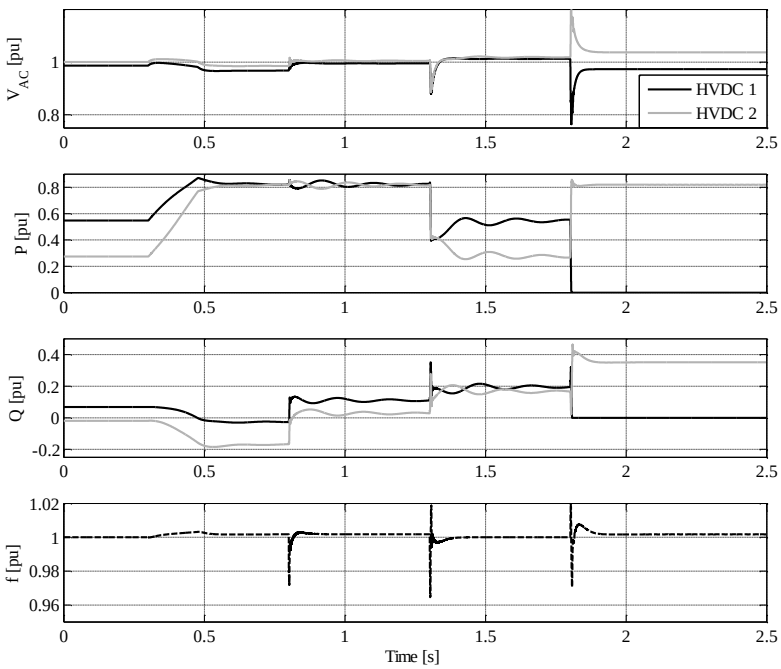

Figure 141 - Case A with different power sharing.

Finally, a different power sharing between HVDC stations is tested. HVDC 2 is programmed to take up two thirds of the WPP's P-Q variations, while HVDC 1 shoulders the rest. This is done by properly selecting the active and reactive power droop gains, maintaining their sum equal to those reported in Table 10 but redistributing them according to the above objective. The results are shown in Figure 141 and Figure 142. Once again, Case A shows a slightly larger sensitivity to variations in the operational scenario and this goes to the advantage of Case B (Option 2).

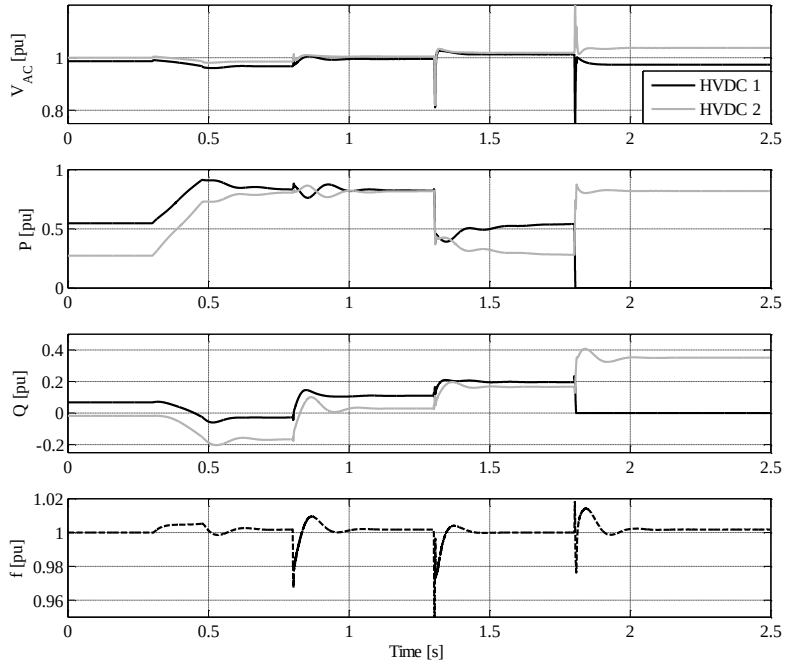

Figure 142 - Case B with different power sharing.

Additional figures for Chapter 8

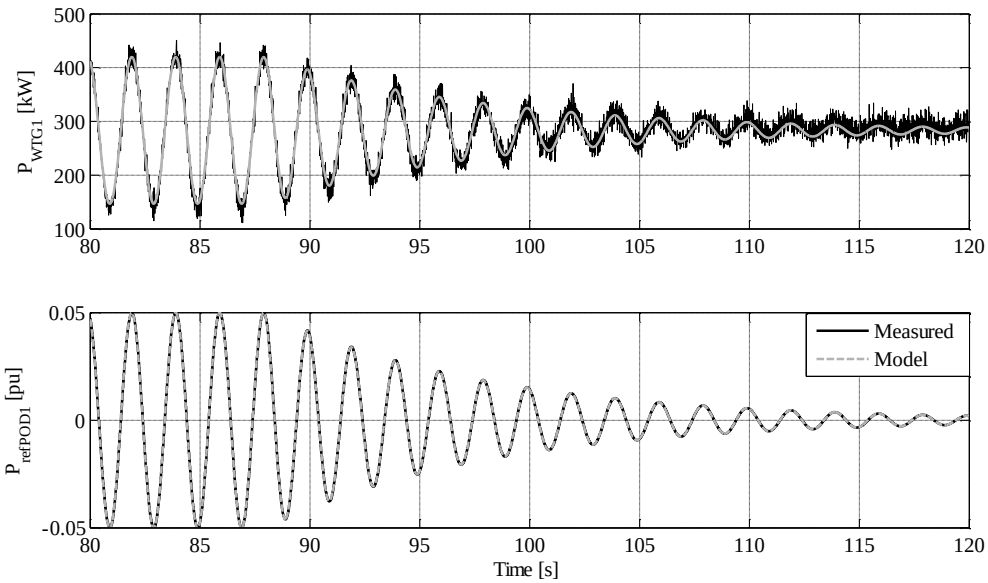

Figure 143 - Validation of 500 mHz POD emulation for WPPC 1.

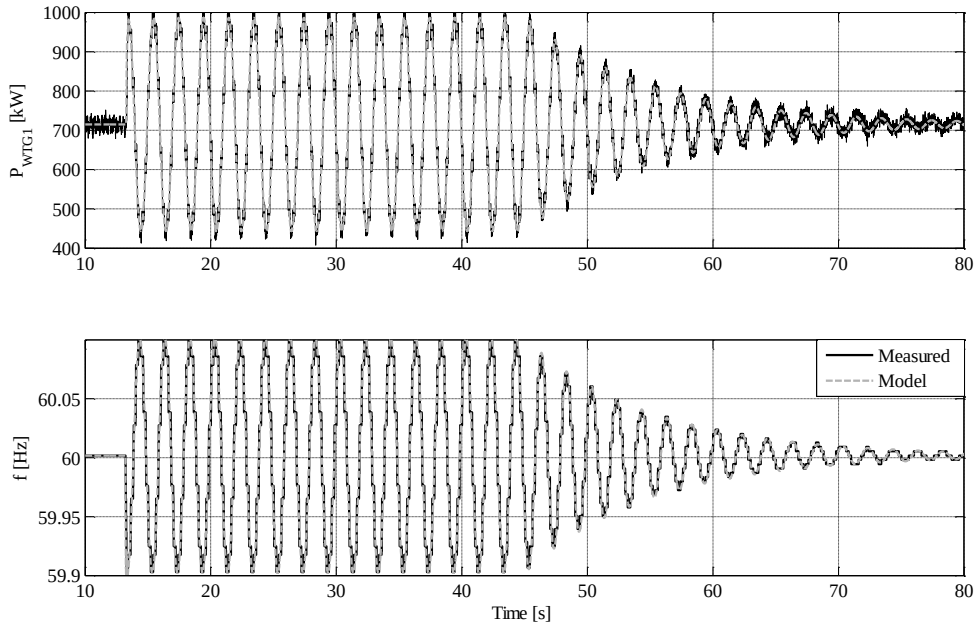

Figure 144 - Validation of 500 MhZ POD emulation, generated with frequency modulation, for WPPC 1.

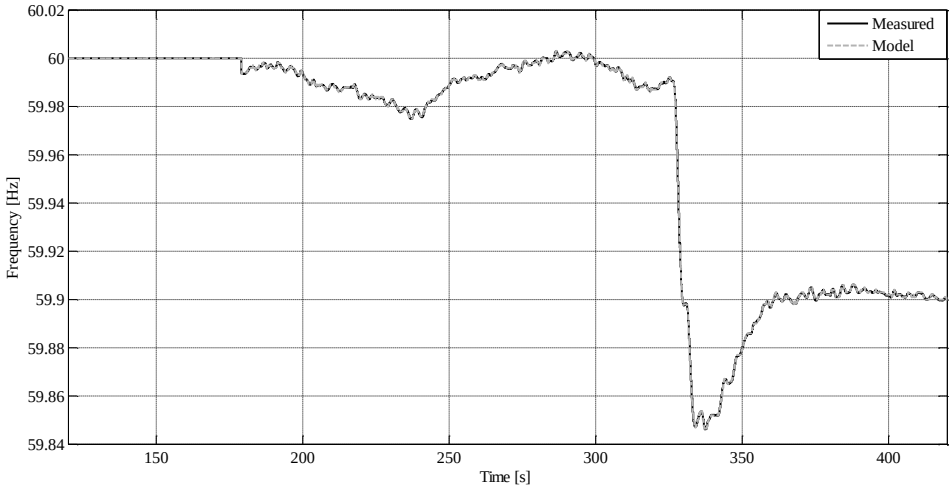

Figure 145 - Validation of frequency control event for WPPC 2 and CC: frequency.

Appendix 6 Experimental setup: data

NOTE: for WTG models the parameter nomenclature is exactly according to IEC standard 61400-27-1. However, in the case of WPPCs the parameters are not named according to IEC standard 61400-27-1 Annex D, since final models will be published in the standard IEC 61400-27-2 and some of the models used here employ additional functionalities.

Table 34 - Modbus communication parameters.

Parameter	Value
Sample rate	1 s
Resolution for power signals	100 kW (4.35%)
Signals CC → WPPC 2	P_{ref}
Signals WPPC 2 → CC	P_{ref}, P_{meas}, P_{av}

Table 35 - WTG 1 parameters – nomenclature according to IEC standard model for Type 4A [22].

Parameter	Value	Unit
T_{ufilt}	0.01	s
dp_{maxp}	10	pu/s
T_{pordp}	0.04	s
i_{pmax}	1	pu

Table 36 - WTG 2 parameters – nomenclature according to IEC standard model for Type 4B [22].

Parameter	Value	Unit
T_{ufilt}	0.01	s
dp_{maxp}	0.217	pu/s
T_{pordp}	0.03	s
T_{paero}	6	s
i_{pmax}	1	pu

Table 37 - WPPC 1 active power control parameters.

Parameter	Value	Unit	Parameter	Value	Unit	Parameter	Value	Unit
dP_{MAX}	0.1	pu/s	f_{DB}	±0.0005	pu	F_{FFf}	0	-
dP_{min}	-0.1	pu/s	K_{ppcf}	20	pu	T_{zPOD}	0	s
K_{ppcP}	1	pu	T_{ppcf}	2	s	T_{pPOD}	0	s
K_{ppcI}	1	pu/s	T_{zC}	-0.025	s	F_{fPOD}	0	-
T_{ppcP}	0.01	s	T_{pC}	0.025	s	K_{POD}	1	pu
P_{MAX}	1	pu	V_{DB}	0	pu	K_{ppcDC}	0	pu
P_{min}	0	pu	T_{ppcDC}	0.01	s			

Table 38 - WPPC 2 active power control parameters.

Parameter	Value	Unit	Parameter	Value	Unit
dP_{MAX}	0.217	pu/s	f_{DB}	±0.015	pu
dP_{min}	-0.217	pu/s	K_{ppcf}	0	pu
dP_{refMAX}	10	pu/s	T_{ppcf}	2	s
dP_{refmin}	-10	pu/s	T_{zC}	-0.1	s
K_{ppcP}	0.5	pu	T_{pC}	0.1	s
K_{ppcI}	5	pu/s	F_{FFf}	0	-
T_{ppcP}	0.5	s	P_{MAX}	1	pu
			P_{min}	0	pu

Table 39 - Time delay for communication channels models.

Parameter	Value	Unit
T_{d1}	0.01	s
T_{d2}	1.6	s

Table 40 - Parameters for CC.

Parameter	Value	Unit	Parameter	Value	Unit	Parameter	Value	Unit
T_{ccf}	2	s	K_{FC1}	1	pu	$K_{c,POD1}$	1	pu
f_{DB}	0	pu	$K_{c,FC1}$	1	pu	T_{zPOD1}	0	s
K_{ccf}	80	pu/s	T_{zFC1}	0	s	T_{pPOD1}	0	s
K_{POD}	0	pu	T_{pFC1}	0	s	K_{POD2}	1	pu
F_{POD}	0	-	K_{FC2}	1	pu	$K_{c,POD2}$	0.5148	pu
F_{PPOD}	1	-	$K_{c,FC2}$	1	pu	T_{zPOD2}	3.842	s
F_{Pfc}	0	-	T_{zFC2}	0	s	T_{pPOD2}	0.6592	s
F_{PPC1}	1	-	T_{pFC2}	0	s	K_{ref1}	1	pu
F_{PPC2}	0	-	K_{POD1}	1	pu	K_{ref2}	1	pu

Table 41 - Parameters varied for frequency control with cluster.

Element	Parameter	Value	Unit
CC	f_{DB}	0.0005	pu
WPPC 1	K_{ppcf}	0	pu/s

Table 42 - Parameters varied for POD with cluster.

Element	Parameter	Value	Unit
WPPC 1	K_{ppcf}	10	pu/s

Department of Wind Energy

Technical University of Denmark

Frederiksborgvej 399

4000, Roskilde, Denmark

www.vindenergi.dtu.dk

+45 46 77 50 24

Technical University
of Denmark